# Regorafenib Amorphous Solid Dispersions: Formulations, Properties and Biopharmaceutical Performance

Inaugural-Dissertation

zur Erlangung des Doktorgrades
der Mathematisch-Naturwissenschaftlichen Fakultät
der Heinrich-Heine-Universität Düsseldorf

vorgelegt von

**Martin Günter Müller**
aus Biberach/Riss

Düsseldorf, Oktober 2020

aus dem Institut für Pharmazeutische Technologie und Biopharmazie
der Heinrich-Heine-Universität Düsseldorf

Gedruckt mit der Genehmigung der
Mathematisch-Naturwissenschaftlichen Fakultät der
Heinrich-Heine-Universität Düsseldorf

Referent: Prof. Dr. Jörg Breitkreutz
Korreferent: Prof. Dr. Dr. h.c. Peter Kleinebudde

Tag der mündlichen Prüfung: 16.02.2021

# Table of content

*The absence of a special marking or a corresponding reference to a trademark, utility model, or patent does not allow the conclusion that the items specified in this work can be freely accessed.*

# Publications

Parts of this thesis have already been published in a patent application and at conferences or are to be published in peer-reviewed journals.

## Patent application

European Patent Office, no. EP20156003.4, application date 2020-02-07

The invention was made by Martin Müller and Werner Hoheisel. The individual contributions are listed in Table *Evaluation of authorship I.* The study design was mainly developed by Martin Müller. Martin Müller performed all experimental work and was supported in results evaluation by Werner Hoheisel. The technical parts of the patent manuscript were written by Martin Müller, the remaining parts by Anke Stroyer and Markus Albers.

**Evaluation of authorship I:** ***Patent EP20156003.4.*** **Parts of contribution in %.**

| Author | Invention | Study design | Experimental | Evaluation | Manuscript |
|---|---|---|---|---|---|
| Martin Müller | 80 | 90 | 100 | 80 | 50 |
| Werner Hoheisel | 20 | 10 | 0 | 20 | 0 |
| Anke Stroyer | 0 | 0 | 0 | 0 | 20 |
| Markus Albers | 0 | 0 | 0 | 0 | 30 |

## Research articles

**Article 1:**

Müller M., Platten F., Fischer B., Dulle M., Hoheisel W., Serno P., Egelhaaf S., Breitkreutz J.: *Precipitation from Amorphous Solid Dispersion at Biorelevant Dissolution: The Polymorphism of Regorafenib*. Manuscript submitted. Target Journal: Int. J. Pharm.

The manuscript resulted from a collaboration, the individual contributions are listed in Table *Evaluation of authorship II.* The idea was mainly defined by Peter Serno and Jörg Breitkreutz. Martin Müller contributed to the study design development, performed most experimental work and was supported in results evaluation by the other authors. The manuscript was written by Martin Müller and Florian Platten with equal shares and revised by Björn Fischer, Martin Dulle, Stefan Egelhaaf, and Jörg Breitkreutz.

**Evaluation of authorship II:** ***Precipitation from Amorphous Solid Dispersion at Biorelevant Dissolution: The Polymorphism of Regorafenib.*** **Parts of contribution in %.**

| Author | Idea | Study design | Experimental | Evaluation | Manuscript |
|---|---|---|---|---|---|
| Martin Müller | 20 | 40 | 80 | 45 | 40 |
| Florian Platten | 0 | 20 | 10 | 15 | 40 |
| Björn Fischer | 0 | 0 | 5 | 5 | 5 |
| Martin Dulle | 0 | 0 | 5 | 5 | 5 |
| Werner Hoheisel | 0 | 10 | 0 | 10 | 0 |
| Peter Serno | 50 | 10 | 0 | 5 | 0 |
| Stefan Egelhaaf | 0 | 10 | 0 | 5 | 5 |
| Jörg Breitkreutz | 30 | 10 | 0 | 10 | 5 |

**Article 2:**

Müller M., Wiedey R., Hoheisel W., Serno P., Breitkreutz J.: *The Impact of HPMCAS Co-administration on the Biopharmaceutical Performance of Regorafenib Amorphous Solid Dispersion.* Manuscript in process. Target Journal: Eur. J. Pharm. Biopharm.

The manuscript resulted from a collaboration, the individual contributions are listed in Table *Evaluation of authorship III.* The idea was defined by Martin Müller, Werner

Hoheisel, Peter Serno, and Jörg Breitkreutz. Martin Müller contributed to the study design development, performed all experimental work and was supported in results evaluation by Raphael Wiedey, Werner Hoheisel, and Jörg Breitkreutz. The manuscript was written by Martin Müller and Raphael Wiedey with equal shares and revised by Jörg Breitkreutz.

**Evaluation of authorship III:** ***The Impact of HPMCAS Co-administration on the Biopharmaceutical Performance of Regorafenib Amorphous Solid Dispersion.*** **Parts of contribution in %.**

| Author | Idea | Study design | Experimental | Evaluation | Manuscript |
|---|---|---|---|---|---|
| Martin Müller | 60 | 80 | 100 | 70 | 45 |
| Raphael Wiedey | 0 | 0 | 0 | 10 | 45 |
| Werner Hoheisel | 10 | 0 | 0 | 10 | 0 |
| Peter Serno | 15 | 0 | 0 | 0 | 0 |
| Jörg Breitkreutz | 15 | 20 | 0 | 10 | 10 |

## Conference contributions

Müller M., Hoheisel W., Serno P., Breitkreutz J.: *Impact of Stabilizer Co-administration for Improved Bioavailability of Regorafenib Amorphous Solid Dispersion*. 13th World Meeting on Pharmaceutics, Biopharmaceutics and Pharmaceutical Technology, Wien (2021), accepted.

Müller M., Serno P., Breitkreutz J.: *Dissolution Behavior of Regorafenib Amorphous Solid Dispersion under Biorelevant Conditions*. 3rd European Conference on Pharmaceutics, Bologna (2019).

Müller M., Serno P., Breitkreutz J.: *Development and Characterization of a Regorafenib Amorphous Solid Dispersion.* 12th World Meeting on Pharmaceutics, Biopharmaceutics and Pharmaceutical Technology, Granada (2018).

# Abbreviations

## Measurements and Discussion

| Abbreviation | Explanation |
|---|---|
| $\Delta$ H | Change in enthalpy |
| ALPS | Amorphous-liquid phase separation |
| API | Active pharmaceutical ingredient |
| ASD | Amorphous solid dispersion |
| AUC | Area under the curve |
| BA | Bioavailability |
| BCS | Biopharmaceutics Classification System |
| CCD | Charge-coupled device |
| CMC | Critical micelle concentration |
| cP | Centipoise |
| CPA | Computed particle analysis |
| CRM | Confocal Raman microscopy |
| $C_t$ | Concentration at time *t* |
| $C_s$, $C_{eq}$ | Equilibrium solubility |
| CV | Coefficient of variation or relative standard deviation |
| DLS | Dynamic light scattering |
| DS | Degree of supersaturation |
| DSC | Dynamic scanning calorimetry |
| et al. | et alii |
| etc. | et cetera |
| $E_{cav}$ | Cavitation formation energy |
| $E_{pack}$ | Crystal packaging energy |
| $E_{solv}$ | Solvation energy |
| f | RGF dose factor |
| FDA | Food and Drug Administration, USA |
| Fig. | Figure |
| FZJ | Forschungszentrum Jülich, Jülich, Germany |
| GIT | Gastrointestinal tract |
| HHU | Heinrich Heine University, Düsseldorf, Germany |

| | |
|---|---|
| HME | Hot-melt extrusion |
| HPLC | High performance liquid chromatography |
| I (q) | Intensity over scattering vector |
| ITC | Isothermal titration calorimetry |
| IVIVC | In-vitro-in-vivo-correlation |
| LC/MS | Coupled liquid chromatography and mass spectroscopy |
| LOD | Limit of detection |
| LOQ | Limit of quantification |
| MHz | Megahertz |
| NCE | New chemical entity |
| Ph. Eur. | European Pharmacopoeia 10 |
| PK | Pharmacokinetic |
| PLM | Polarized light microscopy |
| PP | Polypropylene |
| PSD | Particle size distribution |
| q | Scattering vector |
| rpm | Revolutions per minute |
| s, SD | Standard deviation |
| SAXS | Small angle X-ray scattering |
| SEM | Scanning electron microscopy |
| $T_g$ | Glass transition temperature |
| $T_m$ | Melting temperature, melting point |
| $t_x$ | Sample drawn at time point *x* min |
| UV | Ultraviolet light |
| WAXS | Wide angle X-ray scattering |
| XµCT | X-ray microcomputed tomography |
| XRD | X-ray diffraction |
| XRPD | X-ray powder diffraction |

## Substances

| Abbreviation | Explanation |
|---|---|
| bPMMA | Basic butylated methacrylate copolymer (Ph. Eur.), Eudragit E |
| BSA | Bovine serum albumin |
| EPO, EUD | Eudragit E PO, powdered bPMMA |
| Eudragit RL | Ammonio methacrylate copolymer Type A (Ph. Eur.) |
| FaSSGF | Fasted state simulated gastric fluid |
| FaSSIF | Fasted state simulated intestinal fluid |
| $FaSSIF_{conc.}$ | Concentrated fasted state simulated intestinal fluid |
| $FaSSIF_{rat}$ | Modified fasted state simulated intestinal fluid to mimic rat conditions |
| $FaSSIF_{rat, conc.}$ | Concentrated modified fasted state simulated intestinal fluid |
| FeSSIF | Fed state simulated intestinal fluid |
| HPMC | Hypromellose (Ph. Eur.), Hydroxypropyl methylcellulose |
| HPMCAS | Hypromellose acetate succinate (type 716, unless specified otherwise) |
| MCC | Cellulose, microcrystalline (Ph. Eur.) |
| MgSt | Magnesium stearate (Ph. Eur.) |
| Na-CMCx | Croscarmellose sodium, sodium carboxymethyl cellulose (Ph. Eur.) |
| NaCl | Sodium chloride |
| PS-80 | Polysorbate 80 (Ph. Eur.) |
| PVA | Polyvinyl alcohol |
| PVP | Povidone (Ph. Eur.), polyvinylpyrrolidone (type K25, unless specified otherwise) |
| RGF | Regorafenib anhydrous |
| RGF MH | Regorafenib monohydrate |
| RGF Mod. *x* | Regorafenib modification *x* |
| SDS | Sodium dodecyl sulfate (Ph. Eur.) |

# 1 Introduction

## 1.1 Amorphous solid dispersions for poorly water-soluble drugs

### 1.1.1 Today's challenges in drug development: Focus on BCS II compounds

Today, the poor water solubility of new chemical entities (NCEs) is a major hurdle in the development of new drugs in the pharmaceutical world (Baghel et al. 2016). It has been reported that 40 % of the marketed drug substances can be characterized as poorly water-soluble, according to the Biopharmaceutics Classification System (BCS). Regarding new drug candidates under development, this is even more pronounced, as 90 % of the NCEs in pharmaceutical pipelines show the limitation of poor water solubility (Loftsson and Brewster 2010). The BCS was introduced to classify a molecule by its solubility and permeability properties towards *in-vitro-in-vivo-correlation* (IVIVC), the four classes are listed in Table 1 (Amidon et al. 1995). The Food and Drug Administration (FDA) defines a drug substance to be *highly soluble* when the highest labelled dose is soluble at pH 1 to pH 6.8 in max. 250 mL of various aqueous media at 37 °C, mimicking the conditions within the gastrointestinal tract (GIT). Likewise, the substance is considered as *highly permeable* when the systemic bioavailability (BA) or the extent of absorption of the total dose in humans is at least 85 % (FDA Guidance for Industry, 2000). The BCS system was developed further by subdividing BCS class II into IIa (dissolution limited) and IIb (solubility limited) classes and proposing a Developability Classification System with a focus on the formulation development rather than on the API itself (Butler and Dressman 2010).

**Table 1. Biopharmaceutics Classification System.**

| BCS Class | Solubility | Permeability | Sub-classification |
|---|---|---|---|
| I | High | High | |
| II | Low | High | IIa: dissolution limited<br>IIb: solubility limited |
| III | High | Low | |
| IV | Low | Low | |

Nowadays, the majority of drug substances under development can be categorized as BCS II or BCS IV compounds. By assigning an API to one of the BCS classes different

formulation strategies are promising for the formulation scientist (Baghel et al. 2016; Hallouarda et al. 2016).

The connection between solubility and dissolution rate was mathematically expressed by Noyes and Whitney (1897) and has been further modified by Nernst (1904) and Brunner (1904):

$$\frac{dc}{dt} = \frac{D\,S}{V\,h}(C_s - C_t) \qquad \text{Equation 1}$$

where *dc/dt* is the change in concentration over time, *D* the diffusion coefficient, *S* the accessible surface, *V* the dissolution media volume, *h* the diffusion layer thickness, $C_s$ the equilibrium concentration and $C_t$ the dissolved concentration at time *t*. The diffusion coefficient is dependent on further parameters, described by the Stokes-Einstein equation (Edward 1970):

$$D = \frac{R\,T}{N_A\,6\,\pi\,\eta\,r} \qquad \text{Equation 2}$$

Here, *R* is the universal gas constant, *T* the absolute temperature, $N_A$ the Avogadro constant, *r* the molecular radius, and $\eta$ is the dynamic viscosity of the dissolution medium.

Especially for life-threatening diseases, i.e. cancer, therapy efficacy is of high importance. For peroral small-molecule anticancer drugs, poor dissolution can result in low BA and high variability in plasma concentrations, leading to suboptimal or even failing drug therapy (Sawicki et al. 2016).

The oral route is still the preferred way of drug administration for several reasons. For the patients, the ease of oral administration leads to higher compliance and severe diseases can be treated in a domestic setting, rather than by hospitalization. From a manufacturer's perspective, a solid dosage form offers many advantages over a liquid formulation such as high physicochemical stability, cost-effectiveness and reduced microbial constraints (Baghel et al. 2016; Hallouarda et al. 2016).

In 2016, three anticancer drugs were marketed which are formulated as an amorphous solid dispersion (ASD), i.e. everolimus, vemurafenib, and regorafenib. Because of the numerous advantages of oral solid dosage forms over parenteral formulations, an 'intravenous-to-oral switch trend' has been claimed (Sawicki et al. 2016) and will be a strong driver for pharmaceutical companies towards *enabling formulation* strategies in the near future (Aulton and Taylor 2017; Sawicki et al. 2016).

### 1.1.2 Enabling formulations

#### 1.1.2.1 General

Standard approaches to overcome the BA limitations of poorly water-soluble drugs include pH adjustment, salt formation, formation of co-crystals and reduction of particle size. However, all these methods have their specific limitations. For instance, chemical modification to weak acids or bases may not always be practical and salt formation of neutral compounds is hardly feasible. Moreover, the salts that are formed may convert back to their original acid or base forms and lead to aggregation and precipitation within the GIT. Particle size reduction may not be desirable in situations where handling difficulties and poor wettability are experienced for very fine powders (Buckley et al. 2013; Rahman et al. 2013; Serajuddin 1999). These drawbacks forced the raise of new formulation techniques, so-called *enabling formulations*, including physicochemical modifications (particle size reduction down to the nanoscale, use of polymorphs) or the use of co-solvents, surfactants or solubilizing vehicles that can also be combined. These formulation strategies lead to solubilizing effects in the GIT fluids. Also carrier systems can be applied, such as complex formers (e.g. cyclodextrins), micelle forming solubilizers, emulsions or liposomes, solid crystal suspensions, or embedding an amorphous API into a polymeric carrier matrix, also known as amorphous solid dispersion (ASD) (Baghel et al. 2018b; Hallouarda et al. 2016; Stegemann et al. 2007; Thommes et al. 2011).

In recent years, so-called *supersaturating drug delivery systems* have gained interest (Brouwers et al. 2009; Buckley et al. 2013). Supersaturating drug delivery systems lead to a supersaturated state of molecularly dispersed API within the surrounding liquid and were proven to overcome solubility-limited BA underperformance (Schittny et al. 2020). The typical dissolution profile has been named *spring and parachute*, as the potential free energy of the amorphous API can be visualized as a mechanistic spring, leading to a fast dissolution of the API in dissolution media (Guzman et al. 2007).

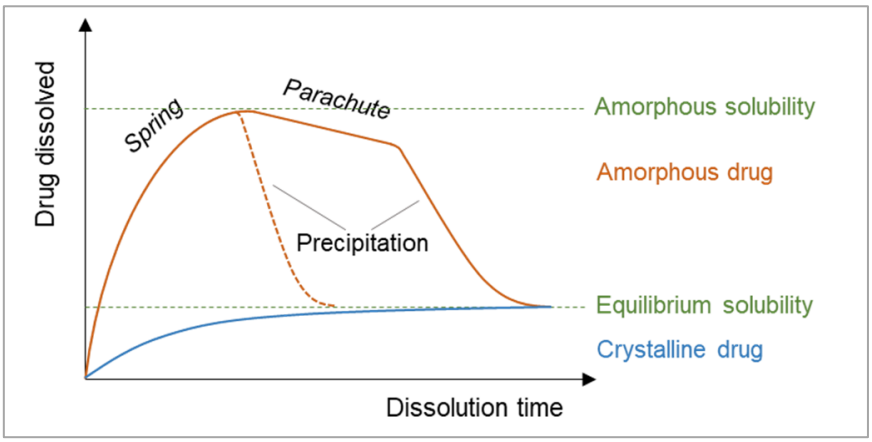


**Figure 1. Schematic illustration of dissolution profiles for amorphous and crystalline drugs.**

Figure 1 illustrates schematic dissolution profiles of amorphous compared to crystalline materials. After the rapid initial *spring* which can reach the amorphous solubility, either precipitation or a *parachute* phase follows, meaning the supersaturation stabilization for the duration of gastrointestinal transit. In contrast, crystalline substances dissolve over time until the thermodynamic equilibrium concentration is reached. The complex mechanistic interplay of ASD dissolution, supersaturation, drug permeation, and precipitation will be explained in more detail in the following sections.

In the last decades, the concept of ASD formulation has been investigated with increasing interest, the numbers of patents and research articles were observed to follow an exponential increase (Zhang et al. 2018). From 2007 to 2017, the FDA has approved 19 new commercial ASD products (Jermain et al. 2018). Hereby, the major difference to solubilizing excipients, e.g. cyclodextrins or lipid vehicles, is that the increase in apparent solubility does not result in reduced permeability, which will be further discussed later (Miller et al. 2012). In this work, the formulation concept of ASD has been investigated, as it is considered to be the most promising formulation technique overcoming drug solubility-related challenges (Haser and Zhang 2018).

#### 1.1.2.2 (Amorphous) Solid Dispersions

The principle of solid dispersions as a technique for BA enhancement was first published in 1961, as the authors introduced eutectic mixtures of sulfathiazole for solubility enhancement (Sekiguchi and Obi 1961). By this technique, very fine crystals were obtained which showed superior drug release kinetics mediated by the carrier and enhanced absorption rates compared to the 'conventional' drug. Further investigations by Goldberg et al. lead to the assumption that these effects become even pronounced if the API is dissolved on a molecular basis within the carrier, forming a *solid solution* (Goldberg et al. 1965, 1966a, b, c). By their definition, a solid solution consists of two components forming a homogeneous phase. These solid solutions exhibit a mixed molecular structure, either interstitial, i.e. the molecules of one component reside in the interstitial spaces of the other component, or substitutional if one component replaces a molecule of the other component in its crystal lattice. By the authors, the benefits in dissolution behavior were attributed to an increase in surface by particle size reduction, where an amorphous dispersion was seen as the maximum in particle size reduction, whereas today's understanding of the underlying mechanisms will be discussed in Section 1.1.2.3.

In literature, several schemes for the categorization of (amorphous) solid dispersions can be found (Schittny et al. 2020). In this work, the definitions will be used as shown in Table 2 (Breitenbach and Mägerlein 2003; Chiou and Riegelman 1971). It is important to note that solid dispersions do not necessarily match only one definition, several types can be present in one solid dispersion.

**Table 2. Definitions of solid dispersion types.**

| Phases | Term | API | Carrier |
|---|---|---|---|
| 1 | glass solution or amorphous solid dispersion | molecularly dispersed | amorphous |
| | solid solution | molecularly dispersed | crystalline |
| 2 | eutectic mixture | crystalline | crystalline |
| | glass suspension | amorphous or crystalline | amorphous |
| | amorphous precipitation | amorphous | crystalline |

Besides the infinite reduction of the API in particle size, a different explanation for the better performance of ASD systems to traditional formulations in dissolution kinetics and apparent solubility was provided from an enthalpy perspective (Brough and Williams 2013;

Lipinski et al. 1997). Three energies are governing the solubility *S* of a compound in a solvent:

$$S = S(E) \quad \text{with } E = E_{pack} + E_{cav} + E_{solv} \qquad \text{Equation 3}$$

where $E_{pack}$ is the crystal packing energy, $E_{cav}$ is the cavitation formation energy and $E_{solv}$ is the solvation energy. The crystal packing energy reflects the energy required for breaking the crystal lattice and to remove a single molecule. The cavitation energy is needed to form a cavity within the solvent to host the dissolving molecule and the solvation energy is released if the solvent and the dissolved molecule form favorable molecular interactions.

For poorly water-soluble compounds, the crystal packing energy is much higher than the solvation energy, therefore the equilibrium solubility is low. In an ASD, the API does not exhibit a crystal lattice, so the crystal packing energy in Equation 3 is minimized and the equilibrium solubility ($C_s$) by that is temporarily increased. In terms of the Nernst-Brunner equation, given as Equation 1, the strong increase in $C_s$ will drastically accelerate the dissolution kinetics of the API.

In contrast to the solubility exposed by crystalline materials in aqueous media, amorphous materials can show strongly enhanced transient solubility. From a thermodynamic perspective, the generated supersaturation is metastable, i.e. not forming a thermodynamic equilibrium, and it exists between the amorphous material and its solution in the absence of any crystalline material. Basically, every concentration of an API dissolved in a solvent above the equilibrium concentration of its most thermodynamically stable polymorph can be considered as supersaturation (Taylor and Zhang 2016). Supersaturation must be distinguished from solubilization, which refers to an increase in thermodynamic equilibrium solubility by e.g. adding functional excipients or dissolution media components. During the dissolution of ASDs, these states are difficult to be considered separately (Frank et al. 2012b). Therefore, the maximum concentration, which can be reached from amorphous compounds as a combination of solubilization by dissolution media components and elevated amorphous solubility, can also be referred to as ‘apparent solubility’, which is to be distinguished from ‘true supersaturation’ (Brouwers et al. 2009; Frank et al. 2012a).

To allow for quantification of generated supersaturation and comparison between different drug formulations, the degree of supersaturation (DS) can be calculated:

$$DS = \frac{C_t}{C_{eq}} \qquad \text{Equation 4}$$

In Equation 4, $C_t$ is the concentration at time point $t$ and $C_{eq}$ the equilibrium solubility in the liquid medium.

#### 1.1.2.3 States of dissolved ASD

Special emphasis should be given to the phenomenon of amorphous-liquid phase separation (ALPS) during the dissolution of ASD formulations. Although several terms are used in literature, such as glass-liquid phase separation and liquid-liquid phase separation, in this work the term ALPS will be used comprising both, as proposed recently (Schittny et al. 2020). For many APIs, once the amorphous solubility of the API is reached during dissolution, ALPS can be observed by the formation of a drug-rich phase, a precursor for drug precipitation (Indulkar et al. 2017). During ALPS, the formation of complex systems was described, consisting of colloidal polymer, drug-rich nanoparticles, amorphous droplets, micelles, and others (Frank et al. 2014; Kanzer et al. 2010; Ueda et al. 2019). In this work, the whole range of observed dissolution states will be referred to as the 'colloidal system' during dissolution.

Studies on ritonavir and povidone (PVP) based ASDs showed that there is a maximum of drug supersaturation by advanced drug delivery systems and ALPS is the precursor for drug precipitation (Ilevbare and Taylor 2013). More specifically, during ALPS of slowly crystallizing drugs, the concentration of molecularly dissolved API in the dissolution media is equal to its amorphous solubility. A further increase in drug concentration level leads to the increased formation of amorphous drug-rich droplets during ALPS, that were found to act as a drug reservoir within permeation studies (Indulkar et al. 2016).

The formation of ALPS has been shown to be dependent on the combination of API and polymer (Purohit and Taylor 2015). If the polymers in ASD formulations are highly hydrophilic, the ASD rapidly dissolves to a certain supersaturation and leads to the formation of ALPS, whereas the polymer is not substantially mixed with the drug droplets (Li and Taylor 2018). In a different study, hypromellose acetate succinate (HPMCAS), a polymer with intermediate hydrophilic-hydrophobic properties, was found to be dispersed

in the drug-rich phase during ALPS, thus leading to a strong stabilization of the supersaturation (Wang et al. 2018b).

The typical *spring and parachute* dissolution profile was introduced in Figure 1. The effectiveness of available precipitation inhibitors to prolong the *parachute* phase was shown to vary strongly (Curatolo et al. 2009). The reasons behind can be found in the different mechanisms governing precipitation inhibition, such as (1) changes in solution properties, e.g. increase in viscosity or solubilization, (2) polymer adsorption on crystal surfaces leading to reduced API diffusion, (3) steric hindrance and elimination of growth sites and (4) molecular interactions, such as hydrogen bonds or hydrophobic interactions, showing best results for intermediate hydrophobic polymers with higher polymer rigidity and molecular weight (Warren et al. 2010; Xu and Dai 2013). These interactions can be either specific for substituents (Kojima et al. 2012) or unspecific binding effects (Baghel et al. 2018b). Khan et al. (2016c) found that intermediate hydrophilicity/hydrophobicity properties lead to superior supersaturation stabilization, as the ability of a polymer to be distributed in drug-rich droplets during ALPS depends on its hydrophobicity. These findings were underlined and linked to the strong crystallization inhibition of HPMCAS (Chen et al. 2016; Ueda et al. 2017).

#### 1.1.2.4 ASD dissolution mechanisms

The dissolution rate was claimed to be influenced by the interactions between carrier polymer and API, however, the published literature is inconsistent in this matter (Schittny et al. 2020). The mechanisms of drug release from ASDs were described by Craig (2002) to be either carrier- or drug-controlled. In case the polymer does not dissolve and forms a gel layer covering the ASD particles, the overall drug release is polymer-controlled. If the polymer does dissolve and drug particles get directly into contact with dissolution medium, the ASD drug release is governed by drug dissolution properties. Both processes were also found to be co-existent (Vo et al. 2013). Sun and Lee (2015c) investigated drug release from media-soluble and -insoluble carriers and found dissolution- and diffusion-controlled drug release, respectively. Further, the authors found higher dissolution rates to pronounce rapid drug crystallization, in their words: ‘haste makes waste’ (Sun and Lee 2015b). For diffusion-controlled release, which can be also considered as carrier-controlled release, the ASD particles might be seen as a drug reservoir within the dissolution system, avoiding too high drug supersaturation. Especially in the context of a critical drug concentration above

which crystallization is promoted, the drug release kinetics should be considered carefully during formulation development (Baghel et al. 2016; Han and Lee 2017).

Schittny et al. (2020) summarized recent literature to the following ASD dissolution mechanisms: (1) Carrier-controlled release, where water penetrates into the polymer and forms a gel layer, through which the API has to diffuse. This is connected to slower drug release and the formation of drug-rich particles via ALPS once the amorphous solubility has been exceeded. (2) Dissolution-controlled release, here polymer and API dissolve simultaneously and quick, achieving high supersaturation levels. (3) Drug-controlled release, at which the polymer dissolves faster and the remaining API forms drug-rich particles in absence of the polymer.

#### 1.1.2.5 Absorption from dissolved ASD

In a published meta-analysis, ASD formulations show an overall positive statistical effect on bioavailability (Fong et al. 2017). On the basis of an immediate-release solid dosage form, different processes will occur before the drug is at the physiological site of action. After intake, the solid dosage form undergoes disintegration in the mouth, the esophagus or the stomach into smaller particles that subsequently dissolve in the gastrointestinal fluids. The absorption process by crossing the intestinal wall can occur either passively by diffusion or actively by transporters. The absorbed drug molecules will be distributed systemically via the bloodstream and hence can trigger the desired pharmacological effect. This concept is different for gastro-resistant dosage forms, here drug liberation from the dosage form should occur in the intestinal sections of the GIT (Aulton and Taylor 2017).

Since the API used in this work, Regorafenib (RGF), is categorized as a BCS II compound, intestinal absorption of dissolved RGF is not the limiting factor regarding bioavailability, as further discussed in Section 1.1.3.1.

These considerations have to be extended for API being formulated as an ASD. Upon contact with digestion fluids, spontaneous dissolution up to completely molecular dispersion may occur. Besides, for dissolved ASDs further states of dissolved API are known, forming the colloidal system introduced above. But not all variants which are present in supersaturation state contribute to an enhanced bioavailability, solely an increase in molecularly dissolved drug was observed to enhance permeation rate (Jacobsen et al. 2019). Drug-rich droplets formed during ALPS were found to act as a drug reservoir in permeation studies (Indulkar et al. 2016).

The concepts of ASD dissolution, supersaturation phenomena, and drug absorption cannot be considered separately, as these processes are overlapping *in-vivo*. From a solid ASD, dissolution leads to the already discussed equilibrium of molecularly dissolved API at a maximum amorphous solubility, the formation of the colloidal system, and eventually precipitation. By passive diffusion, constant drug absorption over the human intestinal membrane removes molecularly dissolved API molecules from the GI compartment over time and therefore affects the overall system. Several studies hinted for a generally non-active drug absorption process from drug supersaturation, except for API specific active transport (Schittny et al. 2020).

Bevernage et al. (2012a) observed reduced crystallization in an absorptive environment compared to a non-absorptive environment. The consistent drop in API concentration was linked to drug permeation. Hence, the effect of crystallization inhibiting polymers was reduced in the absorptive environment.

The effect of supersaturation is terminated by the formation of stable nuclei and subsequent crystal growth to visible particles, leading to a reduced concentration of molecularly dissolved drug and therefore reduced drug absorption (Bevernage et al. 2012a). The precipitation process from the supersaturated state is lined out in more detail in 1.1.2.3.

#### 1.1.2.6 ASD stability during storage

The amorphous state of the API in an ASD also rises challenges for drug stability over shelf life, as the system is thermodynamically metastable. To reduce free enthalpy, the ASD system tends to revert to its crystalline form (Haser and Zhang 2018). A continuous decrease in dissolution kinetics, solubility, and subsequently *in-vivo* drug performance would be the consequence. The process of nucleation and crystal growth in solid ASDs has been extensively studied (Baird and Taylor 2012; Bhugra et al. 2006; Van den Mooter et al. 2001).

The presence of water molecules as moisture within the solid drug formulation or the surrounding gas phase can promote drug crystallization by increasing the molecular mobility, especially when hygroscopic carrier polymers are employed, which might pronounce this phenomenon. The effective steps in re-crystallization are phase separation, crystal growth, or physicochemical transitions from a metastable to a more stable crystalline modification (Brough and Williams 2013). To overcome these limitations of

ASDs, careful consideration in polymer selection and storage conditions must be undertaken.

#### 1.1.2.7 ASD formulation strategies

The general strategy in polymer selection for ASD formulation has to cover two aspects: First, the physical stability is of importance to ensure sufficient shelf-life. It has been reported that the $T_g$ of the ASD matrix should be 50 °C higher than the maximum storage temperature for kinetic stabilization (Hancock et al. 1995). The polymer can further stabilize the amorphous state of the API by molecular interactions, such as hydrogen bonding or Van der Waals forces. By these interactions, the necessity of a well-chosen matrix polymer with high glass-transition temperature ($T_g$) may be reduced (Chokshi et al. 2008). For most ASDs, a combination of kinetic and thermodynamic mechanisms will ensure stabilization. Typical strategies besides proper polymer selection are drug load optimization and appropriate primary packaging to prevent the ASD from moisture (Brough and Williams 2013).

Second, emphasis is given to the drug release kinetics and supersaturation stabilization to achieve the desired BA enhancement. In the pharmaceutical industry, the standard procedure is the use of dissolution assays for polymer screening (He and Ho 2015). Many ASD formulation strategies have been published in recent years. Most of the investigated ASD carrier polymers also stabilize the supersaturated state (Alonzo et al. 2011). The already discussed binary systems comprising API and one polymer were further developed to include surfactants or additional polymers, forming ternary systems (Haser and Zhang 2018). These drug-polymer-polymer systems showed superior dissolution performance and allowed for drug release tailoring (Ilevbare et al. 2012; Knopp et al. 2016; Xie and Taylor 2016a, b). Incorporation of hydrophilic additives or surfactants into the ASD matrix further improved the dissolution results (Franca et al. 2018; Lang et al. 2016; Sun and Lee 2013). However, it has to be evaluated on a case-to-case basis whether the surfactants adversely affect the physical stability and dissolution performance by promoting crystallization (Baghel et al. 2018a). A different approach was presented by Dereymaker et al. (2017), who combined the hydrophilic polymer PVP and insoluble but swellable Ammonio methacrylate copolymer Type A (Eudragit RL) to optimize supersaturation levels and avoid early drug precipitation during dissolution.

Pre-dissolved polymers were described to be less effective for supersaturation maintenance than matrix-embedded polymers (Surwase et al. 2015). Sun and Lee concluded that besides the extent of supersaturation, also the rate of supersaturation seems to be a driving force for drug precipitation; the authors state ‘do not push too far too fast’ (Sun and Lee 2015b).
Xie and Taylor found a novel formulation approach for celecoxib ASDs with hypromellose (HPMC) or HPMCAS as polymeric matrix formers. In their work, celecoxib was embedded into a fast-release ASD matrix, which did not show sufficient supersaturation stabilization itself. The polymers HPMC or HPMCAS were pre-dissolved in dissolution medium and hence ensured satisfying supersaturation. Interestingly, incorporation of these stabilizing polymers into the ASD matrix was not beneficial, as the drug release dropped drastically (Xie and Taylor 2016a).
Some publications classify solid dispersions into ‘generations’, most commonly by their composition, see also Table 2 (Hallouarda et al. 2016). For first-generation solid dispersions, crystalline carriers were used, forming eutectic mixtures or solid solutions. For second-generation solid dispersions, amorphous carriers, mostly polymers, were used, resulting in glass solutions (ASDs) or glass suspensions or a mixture thereof. Additives like surfactants or emulsifiers combined with amorphous solid dispersions were named the third generation. Two new aspects were considered as the fourth generation of ASDs, first tailored polymeric carrier development of polymers with surfactant or complexing properties, second the concept of controlled-release ASDs.

#### 1.1.2.8 ASD preparation techniques: melt-based and solvent-based

Various ASD production methods have been employed, such as spray drying, hot-melt extrusion (HME), mechanical forces, supercritical fluid technology, and electrospinning (Mendonsa et al. 2020). Each technique possesses individual opportunities and limitations, the selection of these methods depends on the API to be processed.
Sekiguchi and Obi were the first to propose the fusion method (Sekiguchi and Obi 1961). A physical mixture of API and excipient is heated to a melt and subsequently cooled under stirring, followed by particle size reduction through crushing and sieving. HME is the modern advanced version of this fusion technique with several improvements. High shearing in the kneading zones of an extruder produces thoroughly mixed products with a uniform particle distribution in the extrudate or ASD (Repka et al. 2007). As HME is a solvent-free process, no subsequent drying is necessary, which makes it a cost-efficient

process and useful for implementation into a continuous manufacturing processes (Vasconcelos et al. 2016). A further advantage is the potential to shape the melt into the final drug dosage forms (Patil et al. 2016). For both fusion-based techniques, drug and polymer have to be thermally stable to avoid degradation during the process. Complete miscibility of polymer and API in the molten state is required, too (Baghel et al. 2016). A novel approach for fusion-based ASD preparation is the Kinetisol technology. By combination of shear force and friction, a melt is generated without external heating. The high energy in the systems enables process times below 30 s (Ellenberger et al. 2018). Although many case studies have been published, this technology is not yet established in the production-scale in pharmaceutical industry (Mendonsa et al. 2020).

The second category of ASD production techniques are solvent-based methods. The drug and the excipients are dissolved in one solvent or a solvent mixture followed by solvent removal. As no or only little heating is required, thermal degradation of the substances may be prevented. Since the process of solvent evaporation is very quick, this causes an increase in fluid viscosity leading to entrapment of the API molecules in the polymer matrix (Araújo et al. 2010). Due to different physicochemical properties of drug and polymer(s), in some cases a solvent mixture has to be used, pronouncing the issue of phase separation during the drying step. Typically, vacuum drying, or as a faster option, rotary evaporation is used. One major challenge in solvent-based techniques is the complete removal of residual solvents, as these can show adverse effects in patients (Baghel et al. 2016). Spray drying has become the most popular solvent-based production method since it offers great control over product properties and manufacturing advantages like ease of scale-up and short process times (Srinarong et al. 2011).

### 1.1.3 Compounds used in this work

#### 1.1.3.1 Regorafenib monohydrate

For this study, the poorly water-soluble API regorafenib monohydrate (RGF MH) was chosen as a representative for the class of orally administered small-molecule kinase inhibitors. The chemical structure of RGF is shown in Figure 2. RGF is a multikinase inhibitor targeting multiple receptor tyrosine kinases and has been approved for the treatment of metastatic colorectal cancer by the FDA in 2012 (Goel 2018). Its therapeutic targets comprise angiogenetic (VEGFR 1-3, TIE-2), oncogenic (c-KIT, RET), and stromal (PDGFR-B, FGFR-1) receptor tyrosine kinases and intracellular signaling kinases

(c-RAF/RAF-1, BRAF, $BRAF^{V600E}$). Clinical studies revealed a dose of 160 mg administered once daily to be tolerated by patients and providing antitumor activity in a therapy treatment cycle of 21 days on and 7 days off (Mross et al. 2012; Strumberg et al. 2012). A clinical phase III study was conducted and confirmed RGF to be the first oral small-molecule multikinase inhibitor with survival benefits at the treatment of metastatic colorectal cancer (Grothey et al. 2013). RGF MH is marketed by the company *Bayer* and branded as *Stivarga* with a dose of 40 mg RGF per tablet. The therapeutic single dose is 160 mg RGF, hence four tablets are administered as single dose daily.

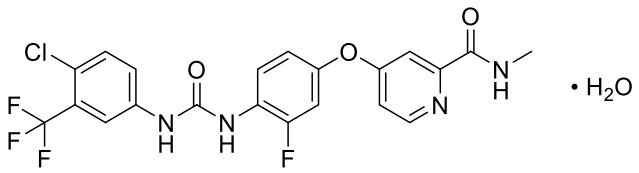


**Figure 2. Chemical structure of Regorafenib monohydrate (RGF MH)**

*Stivarga* is based on an ASD formulation comprising RGF and PVP K25 with a drug load of 20 % within the ASD.

One downside of *Stivarga* is the reported high pharmacokinetic (PK) variability in patients. In a phase III clinical trial, for RGF and its metabolites, high coefficients of variation (CV) values are reported in $AUC_{0\text{-}24h}$. For RGF, a CV of 43 % and for the pharmacodynamically active metabolites M-2 and M-5, CV values of 69 % and 83 % were found, respectively (Mross et al. 2012). In a recent study, these variations were confirmed (de Man et al. 2019). Here, for RGF, M-2, and M-5 CV, $AUC_{0\text{-}24h}$ values were calculated to be 40 %, 71 %, and 103 %, respectively. It should be mentioned that these data were obtained from highly controlled clinical trials, therefore higher PK variability can be assumed in practice.

In Section 1.1.1 the link between bioavailability variability and therapeutic effectiveness is lined out.

Sorafenib is an anticancer drug with a quite similar molecular structure to RGF. For sorafenib, a BCS II compound, the link between poor water solubility and wide intersubject variability was specifically described, however, it is not formulated as an ASD (Gala et al. 2020).

The physicochemical properties of different RGF modifications are not published, though described by *Bayer* internally to some extent. Regorafenib is stable at ambient conditions in different (pseudo-) modifications. For most studies, the monohydrate pseudo-polymorph

and formulations thereof were used. The RGF modifications I, II, and III are described to exist, further, an amorphous form can exist at ambient conditions, although this amorphous form tends to recrystallize rapidly. In principle, all RGF modifications can be distinguished due to their physicochemical properties using different analytical techniques. The reference spectra for available RGF modifications are provided in the respective sections. In this work, the pure RGF modifications Mod. I and the monohydrate could be used as reference substances. The modifications Mod. II and Mod. III could not be prepared successfully.
SEM images of RGF MH and RGF Mod. I are presented in Section 3.1. RGF MH is a white to pink solid substance with needle-shaped crystals, RGF Mod. I appears to be a white to brown powder and does not exhibit the characteristic needle shape of the monohydrate.
Between pH 13 and pH 1, RGF MH is reported to be practically insoluble in water, as the described equilibrium solubility ranges from 5 ng/mL to 103 ng/mL. The UV absorption maximum was found to be 262 nm in aqueous media and methanol. RGF does not exhibit a strong acidic or basic character, the reported calculated $pK_a$ values are 1.3 for the protonation of pyridine sub-structure as base and 12.0 for the deprotonation of the urea part as an acid (*Bayer* internal communication).

For RGF, applying the *Lipinski rule of five* leads to 3 H-bond donors (expressed as the sum of OHs and NHs), 9 H-bond acceptors, the molecular weight of RGF 482.8 g/mol and a calculated LogP of 4.85 (Lipinski et al. 1997). No parameter exceeds the *rule of five* limits, though all parameters are close to the limits. From this perspective, a sufficient permeation of RGF can be expected. These considerations are strengthened, as RGF was found to bind to lipid membranes and intercalate into their lipid-water bilayers. Therefore, a passive absorption mechanism *in-vivo* is assumed (Haralampiev et al. 2016).

### 1.1.3.2 Excipients used in this work

For the preparation of binary and ternary ASD formulations, the following excipients were used, further specification can be found in Table 23 (Materials and Methods).

- Polymers: PVP K25, HPMCAS (types 716, 126, 912), HPMC, Eudragit E PO
- Surfactants: Polysorbate 80, Sodium dodecyl sulfate

The chemical structures are shown in Figure 3. In this section, only a brief overview of the applied excipients will be provided, more detailed information is provided in the respective chapters.

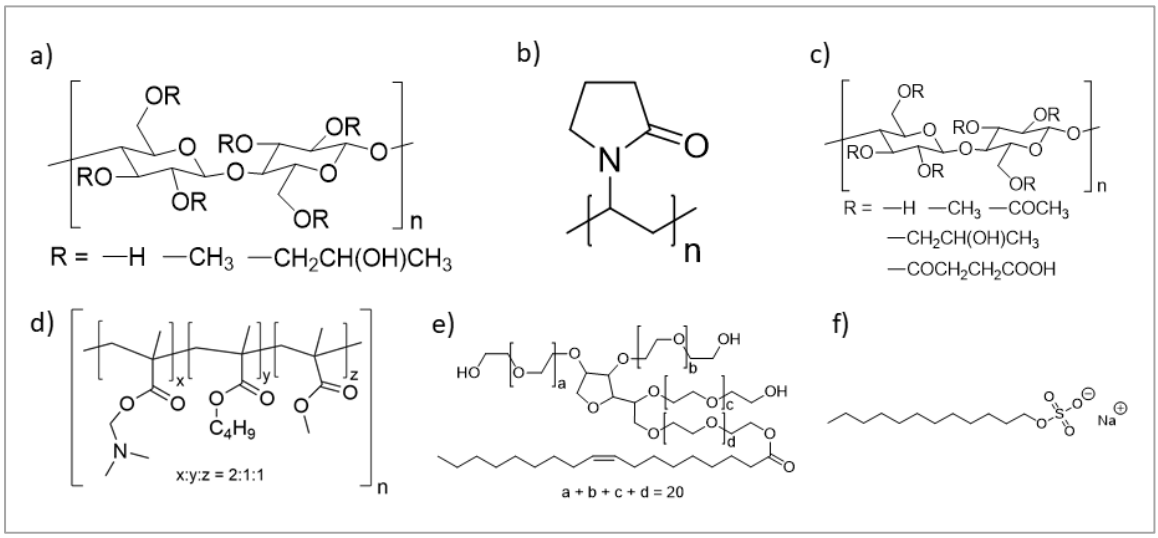


**Figure 3. Chemical structures of the excipients used for regorafenib ASD formulations. a) Hypromellose (HPMC); b) Povidone (PVP); c) Hypromellose acetate succinate (HPMCAS); d) bPMMA (EPO); e) Polysorbate 80 (PS-80); f) Sodium lauryl sulfate (SDS)**

The marketed RGF formulation, *Stivarga*, is based on an ASD composed from RGF in PVP K25, so this formulation can be considered as the control or reference formulation. PVP offers the advantages of a high $T_g$ and high solubility in both, water and organic solvents, which is favorable for drug preparation. Therefore PVP is frequently used as an ASD matrix former in literature and industrial practice (Baghel et al. 2016; Liu et al. 2015). The absence of an acidic functional substituent grants solubility over the entire pH range.

For an alternative formulation approach, HPMCAS has been chosen, since it is a commonly used polymer in commercial ASD formulations (Wang et al. 2018b). In literature, superior supersaturation stabilization by HPMCAS has been reported, compared to PVP (Jackson et al. 2016). HPMCAS is a cellulose-based polymer with high $T_g$ and good solubility in organic solvents. Due to the carboxylic groups with a $pK_a$ of 5, HPMCAS is sparingly

soluble at pH values below 5, dispersing by forming colloidal solutions at approximately pH ca. 5-6. Therefore, HPMCAS is predominantly colloidal at intestinal pH values. In partially ionized state, i.e. above pH 5, the charge on the polymer minimizes polymer aggregates and enables the formation of drug-polymer aggregates. This amphiphilic character of the polymer promotes interactions with hydrophobic drugs, whereas the hydrophilic regions of HPMCAS stabilize colloids in aqueous solution (Friesen et al. 2008). The different HPMCAS grades are compared in Table 3.

**Table 3. Specifications of different HPMCAS types, data obtained from supplier. Mass percentage values are provided.**

| HPMCAS type | 716 | 912 | 126 |
|---|---|---|---|
| Hydroxypropyl content | 5.0 – 9.0 % | 5.0 – 9.0 % | 5.0 – 9.0 % |
| Methoxyl content | 20.0 – 24.0 % | 21.0 – 25.0 % | 22.0 – 26.0 % |
| Dynamic viscosity (2% solution in NaOH)[§] | 2.4 – 3.6 cP | 2.4 – 3.6 cP | 2.4 – 3.6 cP |
| Acetate substitution level | 5.0 – 9.0 % | 7.0 – 11.0 % | 10.0 – 14.0 % |
| Succinate substitution level | 14.0 – 18.0 % | 10.0 – 14.0 % | 4.0 – 8.0 % |
| Mean molecular weight [g/mol][*] | 134,145 | 130,458 | 281,463 |

[*] Supplier refers to publication from Chen et al. 2011.

[§] Supplier does not provide further information about pH of NaOH solution.

bPMMA (Eudragit E PO, EPO) was chosen as third matrix polymer, as the tertiary amine function reveals basic properties. Therefore, a different dissolution behavior for ASDs comprising RGF and EPO has been expected. EPO was investigated intensively as a stabilizing agent for drug supersaturation and is frequently used in ASD formulations (Dereymaker et al. 2017; Kojima et al. 2012; Xie et al. 2017).

During the last decades, numerous publications compared the different types of ASD excipients towards their dissolution and supersaturation performance. Especially, PVP and cellulose-based polymers were intensively investigated and compared, however, general conclusions or a ranking for any API of interest has not been made, so case-by-case evaluation of drug-polymer systems has still to be performed (Xu and Dai 2013).

## 1.2 Physiological conditions and their experimental simulation

### 1.2.1 Gastrointestinal tract

The human gastrointestinal tract (GIT) can be subdivided into segments with different peristaltic movements, composition of fluids, and absorption properties. For all specific values given in this overview, the high inter- and intra-individual variability has to be considered (Clarysse et al. 2009). Ageing and maturation of children may give even higher variations (Batchelor et al. 2014). Besides physiological differences, the amount and type of food consumption and medical preconditions can alter the *in-vivo* situation for the drugs (Dressman et al. 1993). A general overview of physiological parameters regarding the GIT transit is shown in Table 4, adapted from Mudie and co-workers (2010).

**Table 4. Physiological parameters in the gastrointestinal tract, adapted from Mudie et al. (2010). Mean and median values are labeled as stated in references. Deviations, if provided, are one standard deviation.**

| Physiological parameter | Stomach | | Small intestine | |
|---|---|---|---|---|
| | Fasted state | Fed state | Fasted state | Fed state |
| Fluid volume [mL] | 45 ± 18 [1 §] | 800 – 900 [2 *] | 105 ± 72 [1 §] | 900 – 1000 [2 *] |
| Flow rate [mL/min] | 1 [3] | 10 – 50 [3] | 0.3 – 0.7 [4 §] | 2.4 – 3.0 [4 §] |
| Transit time [h] | 1 – 2 [5,6] | 1.4 – 4.0 [5] (16 h) [3] | 3.6 [5], 4.5 [8] | 3.8 [5] |
| pH value | 1.5 – 2 [3]<br>1.4 ± 0.4 [5 §] | 3 – 7 [3] | 6.5–7.2 [5,6 §] | 5.1 – 7.5 [6] |
| Buffer capacity [mmol/L*Δ pH] | 7 – 18 [7 #] | 14–28 [7 #] | 5.6 [7 #] | 18 – 30 [7 #] |
| Osmolality [mOsm/kg] | 98 – 140 [7 #] | 217 – 559 [7 #] | 178 – 271 [7 #] | 287 [7 +] |

[1] Schiller et al. 2005
[2] Custodio et al. 2008
[3] Versantvoort et al. 2004
[4] Kerlin et al. 1982
[5] Ibekwe et al. 2008
[6] Dressman et al. 1998
[7] Kalantzi et al. 2006
[8] Curatolo 1998
[*] including volume of ingested meal
[#] median
[§] mean
[+] measured after 210 min, earlier high fluctuations

The mucosa of the stomach consists of an epithelium, covered by mucus. The tight intracellular junctions in the epithelium do not allow passive absorption of drugs, therefore the gastric compartment is not a typical absorption compartment (Wilson and Crowley 2011). Secretion from gastric glands and ingested food get mixed by muscular contractions within the stomach to form chyme, a semifluid mixture of solutes, emulsion droplets, and

suspended material. The chyme is transferred to the small intestine via the pylorus (DeSesso and Jacobson 2001).

The small intestine is the major absorption site for drug substances and nutrients (Berben et al. 2018). It can be further distinguished into duodenum, jejunum, and ileum. Most absorption occurs in duodenum and proximal jejunum by passive diffusion, facilitated diffusion, active transport, pinocytosis, and solvent drag (DeSesso and Jacobson 2001).

The mucosa in the small intestine presents a surface of up to 200 m² for absorption through convolutions including the Kerckring folds, villi, and microvilli, which lead to a 600-fold increase in intestinal surface (Mudie et al. 2010). Regarding the absorption of drugs, the colon plays a minor role, as the mucosal surface in the colon is reduced and many active carriers are absent. Described non-gastrointestinal absorption sites are the stomach, however, not on a relevant scale, for non-ionized, lipophilic molecules and further sublingual and buccal absorption are also known (DeSesso and Jacobson 2001), but not in the focus of this work, as *Stivarga* is a film-coated tablet for oral administration which releases RGF after dissolving of the film.

The gastric emptying time, which is the time needed for the transport of a solid dosage form through the stomach to the small intestine, is reported to be highly variable. In fasted state, the mechanism behind gastric emptying can be found in peristaltic muscular contractions every 90 min to 120 min which are named the *interdigestive motility complex* (Code 1979). Depending on the motility phase and ingested liquid volume, gastric emptying can be up to 2 h (Dressman et al. 1998; Oberle et al. 1990). Specifically, this is the case for solid dosage forms greater than 1-2 mm, as smaller particles can pass the pylorus significantly faster since the pylorus is not tightly closed (Hunter et al. 1982; Meyer et al. 1988; Park et al. 1984). However, Grimm and coworkers (2017) found the 'Magenstrasse' mechanism to be relevant for fast gastric emptying in the postprandial state. The kinetics of gastric emptying is different for the nutritional state. Whereas in fasted state fluids are emptied by first-order kinetics, in fed state solid meals are emptied by zero-order kinetics. For heavy meals, complete gastric emptying was reported to take up to 16 h (Versantvoort et al. 2004). Special emphasis should be given to the pH increase by later GIT segments. The pH dependency on solubility is known for many APIs, so early drug precipitation of weak acids under the acidic conditions in the stomach might lead to re-dissolution at elevated pH in the intestinal sections (Van Den Abeele et al. 2016). For weak bases, high solubility in gastric fluids leads to supersaturation and precipitation in the small intestine (Berlin et al. 2014). Further, the nutrition state in patients is of high importance for the dissolution

behavior of APIs, as significant differences were found in human gastrointestinal media at fasted and fed states, e.g. affecting pH, enzyme secretion, transit times, or media composition (Kalantzi et al. 2006). An overview of the physiological conditions of the GIT is provided in Table 4. These alterations of *in-vivo* dissolution conditions might impact the supersaturation-permeation interplay and therefore must be carefully considered for overall drug performance of ASDs in humans, since the drug to be formulated should be robust to these variations.

### 1.2.2 Biorelevant dissolution

#### 1.2.2.1 From compendial to biorelevant dissolution models

Traditional dissolution testing using the USP and Ph. Eur. standardized apparatuses 1 and 2 is normally utilized to assess product quality and to predict changes in drug release that may impact *in-vivo* drug performance of oral products. This has not radically changed since the 1970s (Kostewicz et al. 2014). Typically, dissolution media volumes of 500 mL to 1000 mL are applied at sink conditions to ensure full drug release from the dosage form. However, gastric volume in the fasted state is considered to not exceed 250 mL, even if the drug is administered with a glass of water (Schiller et al. 2005). The high *in-vitro* media volumes can lead to false predictions towards *in-vivo* drug performance, and thus distort *in-vitro-in-vivo-correlation* (IVIVC). The reciprocating cylinder apparatus, monographed as dissolution apparatus 3 in USP and Ph. Eur., allows the dosage unit to be dissolved in a subsequent series of vessels at individual media conditions, which is suitable for non-disintegrating dosage forms only. The flow-through cell apparatus, USP and Ph. Eur. apparatus 4, offers the advantage of medium change during dissolution experiments, which makes it ideal for modified release dosage forms. Although it was used for solid dispersion biorelevant dissolution, it does not meet the criteria of this work since a system in which ASD particles and precipitates are in spatial proximity was sought (Kostewicz et al. 2014). More advanced dissolution models were proposed to better reflect the *in-vivo* situation, such as a two-compartment gastric-intestinal transfer model (Kostewicz et al. 2004), a three-compartment model including a reservoir (Psachoulias et al. 2012) or dissolution stress test device (Garbacz et al. 2010; Garbacz et al. 2008), just to name a few. Eventually, sophisticated multi-compartment simulators to mimic the main mechanical and chemical functions were invented, e.g. the artificial stomach-duodenal model (Carino et al. 2010), the fed stomach model (Koziolek et al. 2014), the dynamic gastric model (Vardakou et al.

2011) and the TIM-1 / TIM-2 system (Blanquet et al. 2004; Minekus et al. 1999). To date, none of the available test devices has the capability to simulate all aspects of the GIT, however, for some cases good IVIVC was found (Kostewicz et al. 2014).

#### 1.2.2.2 Biorelevant media

To bridge the gap between quality control and development of predictive dissolution test methods, the importance of using biorelevant media was first proposed in 1998 (Dressman et al. 1998). Especially for investigating supersaturation inducing formulations, fasted state simulated gastric fluid (FaSSGF) and fasted state simulated intestinal fluid (FaSSIF) showed good predictions compared to human intestinal fluid (Bevernage et al. 2013). Relevant parameters in FaSSIF development were the adjustment of pH, osmolality, surface tension, buffer capacity, and concentrations of bile salts and lecithin. For FaSSGF, pH, osmolality, surface tension, and bile salt levels caused by reflux were reflected (Klein 2016; Pedersen et al. 2013). The full composition of biorelevant media types applied in this work is provided in Table 5.

**Table 5. Composition of biorelevant dissolution media, according to supplier information.**

| Component | FaSSGF | FaSSIF | FeSSIF |
|---|---|---|---|
| Sodium taurocholate [mM] | 0.08 | 3.0 | 15 |
| Lecithin [mM] | 0.02 | 0.75 | 3.75 |
| NaCl [mM] | 34 | 106 | 203 |
| HCl [mM] | ~ 25 | / | / |
| Sodium hydroxide [mM] | / | 9 | 101 |
| $NaH_2PO_4$ [mM] | / | 28 | / |
| Acetic acid [mM] | / | / | 144 |
| pH | 1.6 | 6.5 | 5.0 |
| Osmolarity [mOsm/kg] | ca. 120 | ca. 270 | ca. 670 |

The components from biorelevant media were shown to influence drug solubility and dissolution. Furthermore, bile salts were shown to inhibit drug crystallization from supersaturation (Chen et al. 2015b; Lu et al. 2017). Besides the effect of bile salts, also the impact of ionic strength was shown, especially in the presence of surfactants (Fong et al. 2016). Today, several types and advancements are known, e.g. FaSSIF versions 2 and 3 (Fuchs et al. 2015). Recently, a different FaSSIF composition based on bicarbonate buffer

was proposed which showed higher predictive power towards an *in-vivo* rat study for weakly basic poorly water-soluble compounds stabilized by HPMCAS co-administration (Jede et al. 2019). Nevertheless, the high *in-vivo* variability of GIT parameters affecting dissolution also in the fasted state has to be kept in mind, as these variabilities can be the source of BA issues (Klein 2019). In a recent review, Schittny et al. (2020) conclude that investigation of dissolution behavior in biorelevant media is indispensable for the prediction of *in-vivo* results.

#### 1.2.2.3 Biorelevant dissolution setup choice

For this work, a biorelevant dissolution system was sought to enable transfer dissolution studies while avoiding unnecessary mechanic stress and different surfaces for RGF in the supersaturated state. From earlier internal studies, the precipitation tendency of RGF supersaturation on surfaces, e.g. while pipetting, was well-known. Ph. Eur. dissolution apparatus 3 and 4 were considered not to be suitable for the purpose of this work, as described above. Therefore, a dissolution setup similar to the two-chamber model of Kostewicz et al. (2004) was applied. To achieve biorelevant conditions, Klein (2010) proposed 250 mL FaSSGF and 500 mL FaSSIF to mimic gastric and intestinal conditions, respectively. The dissolution time was set to 120 min for the stomach compartment and 360 min for the intestinal compartment, by taking into account some inter-individual variability, in accordance to literature (Curatolo 1998; Ibekwe et al. 2008). The impact of stirring speed on the dissolution rate of solids is known. To allow for discriminative power and reduce coning effects in the dissolution vessels, a stirring rate of 75 rpm was chosen, as suggested by Kostewicz et al. (2014).

### 1.2.3 Permeation: *In-vivo* vs. *in-vitro* models

For better prediction of *in-vivo* drug performance in humans, drug absorption during dissolution has to be taken into account (Takano et al. 2012) for the reasons discussed in Section 1.1.2.5. Many studies were performed evaluating different methods for dissolution-permeation coupling by implementing an absorption compartment, e.g. separated by a simple filter (Gu et al. 2005) or by a Caco-2 cell monolayer (Motz et al. 2007; Sugawara et al. 2005). A different approach is the use of simpler biphasic dissolution systems (Jankovic et al. 2019).

These *in-vitro* approaches offer the ethical and financial benefit of reduced animal sacrifice. Simplification to an *in-vitro* approach inherently leads to disadvantages by simplification, to mention the inter-individual differences between test subjects exemplarily, that will not be observed in a standardized *in-vitro* setup (Nunes et al. 2015). Although animal PK studies are a valuable source of information, differences in GIT conditions between the animal model and humans have to be considered (Griffin et al. 2014). Those differences were examined and are well described, although huge differences in the GIT situation in rat population were found in the literature (DeSesso and Jacobson 2001; Grignard et al. 2017). To investigate dissolution related differences in drug absorption, artificial cell-free permeation setups are useful. To date, the most common approaches are the parallel artificial membrane permeation assay (PAMPA), the phospholipid vesicle based permeation assay (PVPA), PermeaPad, and the artificial membrane insert (AMI) (Berben et al. 2018). The advantage of PermeaPad over the other methods is its commercial availability, thus reduced laboratory workload and high consistency of the membranes. In contrast to PAMPA or PVPA, PermeaPad membranes can be stored at 25 °C under light protection, therefore fresh preparation before the permeation experiment is not necessary. PermeaPad membranes consist of a phospholipid biomimetic membrane and showed good agreement with Caco-2 cell assays (di Cagno et al. 2015). A more simplified version is PermeaPlain that consists of a cellulose membrane with a mean pore size of 33 ± 20 nm, according to personal correspondence with the supplier. For these arguments, an *in-vivo* PK study and the *in-vitro* permeation membranes PermeaPad and PermeaPlain were included in this work.

## 1.3 Precipitation

### 1.3.1 The physicochemical properties of precipitates

The phenomenon of ALPS during ASD dissolution was introduced in Section 1.1.2.3. Precipitation of a drug substance from supersaturated state is the phase separation and nucleation of solid cores from a supersaturated system and is a function of drug concentration and temperature at constant pressure (Price et al. 2019). A supersaturated state is a prerequisite and the driving force for precipitation (Lindfors et al. 2008). In many cases, drug precipitation is linked to decreased bioavailability (Arnold et al. 2011; Bevernage et al. 2012a; Brouwers et al. 2009), assuming re-dissolution of precipitated drug does not occur. There are several mechanisms leading to drug supersaturation, as for example dissolution of amorphous formulations as described above, digestion of excipients or the pH shift during gastric transit, changing the solubilizing acidic environment for weakly basic drugs to the more neutral conditions of the small intestine (Khan et al. 2016c). In literature, the precipitates collected after dissolution experiments have been found to be crystalline, amorphous, or partly amorphous. The precipitation behavior is described to be dependent from the polymer matrix and its interactions with the drug (Boetker et al. 2012; Dereymaker et al. 2017; Elkhabaz et al. 2018; Raina et al. 2015; Sassene et al. 2015). In the case of amorphous precipitation, the solid state of the API is of higher energy than in crystalline material, so re-dissolution and absorption at further digestion *in-vivo* might be assumed (Khan et al. 2016b). The higher re-dissolution rate of precipitated amorphous material was demonstrated, compared to its reference crystalline form (Augustijns and Brewster 2012; Sassene et al. 2010; Stillhart et al. 2014). A proper selection of the polymer excipients is important, as indomethacin-Eudragit RL ASD was described to form crystalline precipitates in the presence of PVP and amorphous precipitates in its absence (Dereymaker et al. 2017). Wang and coworkers found intermediate hydrophilic-lipophilic polymers to directly stabilize the drug-rich phase during ALPS, eventually leading to amorphous co-precipitates (Wang et al. 2018b). Besides the formulation aspects, the precipitation environment was shown to influence the physicochemical properties of formed precipitates (Yamashita et al. 2017).

Further, the co-precipitation of different indomethacin polymorphs was described, dependent on the crystallization rate (Sun and Lee 2013). The crystallization from supersaturation not necessarily directly leads to the most stable polymorph, Raina et al. found nifedipine precipitates to undergo polymorphic transitions *in-situ* (Raina et al. 2014).

Price et al. (2019) state that precipitation inhibiting polymeric excipients were found to adsorb on crystal surfaces, leading to the formation of metastable polymorphs which further transform to the thermodynamically most stable modification over 'sufficient time'.
The simplification of the complex GIT environment in humans to biorelevant dissolution was shown to compromise the experimental predictive power. Psachoulias et al. found *in-vivo* different polymorphs or pseudo-polymorphs compared to *in-vitro* experiments (Psachoulias et al. 2012; Psachoulias et al. 2011).
Brouwers and coworkers (2017) published an *in-vivo* study, comparing the performance of an itraconazole-cyclodextrin inclusion complex to an ASD formulation with HPMC. For the ASD formulation, strong precipitation, hence little supersaturation, was observed in aspirated gastric and duodenal fluids. Since itraconazole is a weak base, the observed supersaturation in the stomach was higher than in the small intestine. The obtained dissolved fraction over time in aspirates correlated with the observed itraconazole plasma concentration, therefore *in-vivo* precipitation was shown to be critical for ASD performance in humans.

### 1.3.2 Methods for precipitate characterization

#### 1.3.2.1 General notes

Typically, the precipitates resulting from the dissolution of supersaturating drug delivery systems are investigated by off-line measurements, i.e. after sample collection, centrifugation, and drying. However, these processes might alter the physicochemical state of the precipitates, from this perspective, *in-situ* analytics seem to better capture the 'true' nature of the precipitates. Additionally, extra information can be gained about precipitation kinetics, e.g. by isothermal calorimetry, as introduced in Section 1.3.2.5. However, analytical limits have to be considered. As one example, Alonzo et al. described that *in-situ* API concentration via UV was limited by the formation of nano species in the dissolution system (Alonzo et al. 2011). NMR studies revealed insights into molecular interactions during supersaturation, but simple buffer media (Coombes et al. 2014; Ueda et al. 2017) or organic solvents (Baghel et al. 2018b) were used by the authors instead of biorelevant media, limiting the predictive power. Promising techniques for *in-situ* investigation of the polymorphic state were shown to be Raman spectroscopy (Alonzo et al. 2010) and *in-situ* X-ray scattering techniques (Chen et al. 2015c; Khan et al. 2016a; Van Eerdenbrugh et al. 2014). All the proposed methods have shown benefits and drawbacks in the published

literature, e.g. lacking sensitivity for certain APIs or falsified signals by APIs or excipients under study.

#### 1.3.2.2 Differential scanning calorimetry (DSC)

The basic principle of the DSC technique is the controlled heating and cooling of sample materials placed in a pan along with a reference pan which might be empty or loaded with solid control. The instrumental output is the electrical power difference to maintain sample and reference cells at the chosen temperature ramp (Paudel et al. 2014). Via DSC measurements, the heat change of a sample can be detected as a function of the temperature profile. The obtained heat flow signal can be linked to thermal events, such as glass transition, melting, evaporation, crystallization, or degradation (Ma and Williams 2019). It is reported that slower and faster heat rates can lead to different results by allowing kinetic processes to happen in the sample (Paudel et al. 2014), therefore in this work all samples were investigated at various heating rates. Since different modifications of the same material can exhibit different thermal behavior, these polymorphs can be distinguished via DSC. Further, the amorphous distribution of an API in an ASD can be confirmed by the absence of the respective melting peak above the detection limit (LOD) and presence and temperature of glass transition (Dereymaker et al. 2017).

DSC is the most commonly used technique to determine the glass transition temperature (Baird and Taylor 2012). Molecularly dispersed mixtures exhibit a single glass transition, depending on the interactions of polymer and API (Paudel et al. 2014). This glass transition was expressed to be dependent on the volume ratio of both components (Gordon and Taylor 1952), therefore a single glass transition in an ASD can be considered as a marker for a single phase mixed system.

#### 1.3.2.3 X-ray diffraction (XRD)

Crystals consist of an ordered arrangement of atoms. If X-rays impinge on a crystal, they are diffracted. The regular distances between the crystalline atoms give rise to diffraction peaks occurring at specific diffraction angles. Such continuous Debye rings can be azimuthally averaged and displayed in a specific diffractogram (Ma and Williams 2019; Paudel et al. 2014). The relationship of diffraction order $n$, incident X-ray wavelength $\lambda$, spacing between lattice planes $d$ and the angle of incident radiation $\Theta$ is given by Bragg's law:

$$n\lambda = 2\,d\sin\theta \qquad \text{Equation 5}$$

XRD based experiments are a common analytical tool in ASD development (Engers et al. 2010). The amorphous state of embedded API was confirmed by the absence of characteristic patterns of API crystals in several works (Al-Obaidi et al. 2013; Moes et al. 2013; Zhao et al. 2014). In principle, different polymorphs and pseudo-polymorphs are distinguishable by XRD and information about the crystal lattice can be gained (Chauhan 2014). In this work, XRD based techniques were used for confirmation of successful ASD preparation but also for precipitate analysis. For powder samples, an off-line setup was used, as described in Section 6.2.3.4.2. Zhu et al. (2013) investigated the re-crystallization from ASDs in solid state by a combination of small-angle and wide-angle X-ray scattering (SAXS/WAXS). The adjustment of the distance from sample to detector allows different scattering vector ranges to be investigated from the same sample. A more sophisticated technique is *in-situ* SAXS/WAXS, which was shown to allow measurement of water dispersed samples, e.g. in biorelevant media (Boetker et al. 2016; Boetker et al. 2012; Raina et al. 2015). Chen and coworkers (2015c) demonstrated the feasibility to investigate the kinetics of gold nanoparticle formation from precursor reaction with subsequent nucleation and particle growth. For clarity, in this work wide-angle X-ray diffraction from dry powder samples obtained at HHU Düsseldorf is named XRPD, whereas the wide angle X-ray scattering experiments conducted at the FZ Jülich beamline are named WAXS.

#### 1.3.2.4 Raman spectroscopy, Raman mapping, and confocal Raman microscopy (CRM)

The phenomenon of inelastic scattering of light by matter was first proven experimentally by Sir Chandrasekhara Venkata Raman, who was later awarded the Nobel prize in physics for his work on the scattering of light and the discovery of the effect named after him (Raman and Krishnan 1928). The mechanism for Raman scattering lies in the change of the rotational or vibrational quantum states of molecules being illuminated. Most of the incoming light on a sample is scattered elastically without energetic transitions, i.e. the wavelength λ is not altered. This effect is named Rayleigh scattering. However, a small proportion of the incident photons is scattered inelastically. By changes in the rotational or vibrational modes of sample molecules, energy is transferred to or received from the sample

causing a change in the energy, and therefore λ of the scattered light. For the scattering effects with shifts in λ, two cases can be differentiated: scattered light with shorter λ is named Anti-Stokes scattering, scattered light with greater λ is named Stokes scattering. In this work, only Stokes scattering was detected from the applied analytical devices and used for analytical investigations due to the higher intensities at ambient temperature.
The scattered photons are collected over a defined exposure time by the detector as a function of their frequency shift. The resulting graphs show the collected scattered photons as arbitrary units over the relative frequency shift in $cm^{-1}$. As the Raman effect is sensitive towards molecular functional groups and its vibrational states, unique spectra for molecules and its polymorphs can be obtained in the 'fingerprint region', typically <1800 $cm^{-1}$ for organic compounds (Camp Jr. et al. 2014). Further, distinct molecular structures can be identified by characteristic Raman bonds, as such the symmetric aromatic ring breathing mode at about 990 $cm^{-1}$ to 1000 $cm^{-1}$ (Krasser et al. 1983). In this work, this bond was used as a marker for aromatic compounds in the analyzed sample. As RGF was the only aromatic compound used in dissolution experiments, it was expected to be observed in all samples containing RGF to avoid analytical artifacts. It should be noted that aromatic RGF degradation products cannot be differentiated by the aromatic marker bond, so only the presence or absence of aromatic compounds in the sample can be proven.

Confocal Raman microscopy (CRM) is a modern approach using the principles of Raman scattering. Here, the excitation laser light is focused on the sample leading to a well-defined and very small measurement spot, typically in the order of 1 µm. Via the implemented light microscope, a suitable measurement position can be identified and subsequently analyzed in Raman mode. CRM can be operated in two different modes. First, single spectra can be acquired to provide chemical information on the sample composition in one exact spot. Second, multiple measurements of a defined area can be clustered to form a so-called *Raman map* or *chemical image*. Raman mapping was shown to reveal the distribution and its physicochemical properties of different compounds (Scoutaris et al. 2014), to study dissolution processes (Haaser et al. 2011), distribution of crystalline and amorphous API within the same sample (Nakamoto et al. 2013), recrystallization of amorphous API during stability testing (Sinclair et al. 2011) and kinetics thereof (Ueda et al. 2014).
The procedure of Raman mapping is the following: Raman spectra are obtained from different points of the sample or a region of interest. The Raman spectra can be processed by univariate or multivariate approaches. Univariate approaches are used whenever

possible, as this method is the simplest way. If the compounds do not offer characteristic signals or in case of overlapping signals, a more advanced data analysis such as multivariate analysis is preferred (Scoutaris et al. 2014; Vajna et al. 2011).

#### 1.3.2.5 Isothermal titration calorimetry (ITC)

Almost every physicochemical process or chemical reaction is accompanied by a change in heat (O'Neill and Gaisford 2011), energy can be released (exothermic) or consumed (endothermic). Isothermal titration calorimetry (ITC) measures this energy: during the process or reaction, the sample is kept at a constant temperature (isothermal) and power is supplied in order to compensate for the change in heat. Hence, the energetics of the process or reaction can be inferred from the temporal evolution of the power signal. Besides the thermodynamic data, also the rate of change in heat signal is detected. Therefore, the method provides insights in both, reaction kinetics and thermodynamics (Freyer and Lewis 2008). In literature, this method was extensively used to explore thermodynamics of polymer binding interactions, enzyme activity, but also for small molecules, i.e. ligand binding, chemical reaction constants or adsorption processes (Freyer and Lewis 2008; Fujisawaa et al. 1990; Prozeller et al. 2019; Rodgers and Jackson 2017).

In this work, the precipitation of RGF from the supersaturated state is of interest. As during crystallization the enthalpy ($\Delta H$) of the system becomes reduced, a monitoring of this process via ITC is expected to be feasible. The approach of precipitation monitoring via ITC for a pharmaceutical small-molecule drug is already described in the literature for the precipitation process of pseudoephedrine (Pudipeddi et al. 1995). ITC experiments have to be designed carefully to avoid overlapping in heat signals from different processes, such as dissolution or dilution. In this work, the ITC injection device was not used, as the formulation of interest was applied together with biorelevant dissolution media at the beginning of the ITC experiment, generating RGF supersaturation through the concept of ASD dissolution. In literature, this method was not used so far for precipitation monitoring of an API from the supersaturated state, generated by the dissolution of an ASD formulation.

# 2 Aims and Objectives of the thesis

For regorafenib (RGF), significant inter-individual variability in bioavailability is known, which might be linked to insufficient drug performance during *in-vivo* dissolution after oral administration. This hypothesis shall be investigated by gaining insights into the interplay of dissolution, precipitation, and absorption for different RGF ASD formulations. As a second aim, the physicochemical properties of resulting RGF precipitates are to be investigated with a focus on polymorph solid-state characterization. As the suggested methodologies in the literature often show lacking sensitivity or potential artefacts, a complementary analytical approach should be applied.

The main objectives for this work are:

(1) Method development for physicochemical off-line and *in-situ* characterization of RGF polymorphs
(2) Preparation of new ASD formulations with RGF via solvent evaporation
(3) Development of a biorelevant dissolution system mimicking gastric and intestinal conditions, including method development for concentration determination of RGF in biorelevant media
(4) Investigating the fate of RGF during *in-vitro* dissolution, after precipitation and its manipulation behavior under biorelevant conditions
(5) Proof-of-concept of a new formulation approach using *in-vitro* dissolution and permeation studies and an *in-vivo* pharmacokinetic study in rodents

These questions will be answered by a combined strategy of formulation development and complementary analytical investigations at simulated *in-vivo* conditions by biorelevant dissolution techniques.
The knowledge gained from this research shall contribute to a better understanding in the formulation of poorly water-soluble drugs as ASD since RGF is a typical class II compound according to the Biopharmaceutics Classification System (BCS).

# 3 Results and Discussion

## 3.1 ASD characterization

Preamble

*The experimental results and discussions in the following section are partly based on a collaboration with external partners. Dr. Björn Fischer (HHU, Fischer Raman Service) was supporting in acquisition and evaluation of Raman spectra.*

*Essential contents of this chapter are based on the patent application "EP20156003.4" (European Patent Office) by Martin Müller, Werner Hoheisel, Anke Stroyer, Markus Albers.*

*Essential contents of this chapter are based on the research article manuscript "The Impact of HPMCAS Co-administration on the Biopharmaceutical Performance of Regorafenib Amorphous Solid Dispersion" (Target Journal Eur. J. Pharm. Biopharm.) by Martin Müller, Raphael Wiedey, Werner Hoheisel, Peter Serno, and Jörg Breitkreutz.*

*Essential contents of this chapter are based on the research article manuscript "Precipitation from Amorphous Solid Dispersion at Biorelevant Dissolution: The Polymorphism of Regorafenib" (Target Journal Int. J. Pharm.) by Martin Müller, Florian Platten, Björn Fischer, Martin Dulle, Werner Hoheisel, Peter Serno, Stefan Egelhaaf, and Jörg Breitkreutz.*

Different binary and ternary ASDs formulations with RGF were prepared as described in Section 6.2.2.1. There, also the formulation codes used in the following sections are defined. In these binary and ternary formulations, RGF was dispersed in one or two matrix polymers, respectively. To get a deeper understanding of the supersaturation and precipitation behavior of RGF, different types of polymers were chosen for ASD formulation, as was introduced in Section 1.1.3.2. The marketed RGF formulation from *Bayer*, branded as *Stivarga*, is based on a formulation with PVP as matrix polymer with a drug load of 20 %, which will be seen as a reference during formulation development. To allow for better comparability between the formulations, the drug load was kept constant in the majority of new formulations. In literature, HPMCAS is commonly used as a matrix polymer for ASD formulations. The main difference of PVP apart from the polymer backbone is the absence of carboxylic substituents. Whereas PVP molecules are not ionized at FaSSIF conditions at pH 6.5, the carboxylic groups of HPMCAS will be deprotonated to some extent leading to a negative charge on HPMCAS molecules. Also, Eudragit E is often used as a matrix former, the molecular structure is a basic butylated methacrylate copolymer, making it a chemically basic molecule. In this section, emphasis is given to binary ASD formulations, the characterization of ternary ASDs preparation is discussed in later sections.

The obtained ASDs were investigated for their amorphous state via SEM, XRPD, DSC, and CRM. Further, a collection of photographic images of API, prepared ASD formulations, and resulting precipitates are presented in Figure 82 of the Appendix.

Figure 4 shows the SEM images of investigated ASDs and reference materials, the method is described in Section 6.2.3.4.7. Whereas RGF monohydrate (RGF MH) particles are needle-shaped, RGF Mod. I particles exhibit a brick-like shape. Both the structures could not be found in the prepared ASDs. This was also the case for the polymers used in these experiments, PVP, HPMCAS, and EPO. By the solvent evaporation process, a new morphology of the ASDs was created, exhibiting a smooth surface. Although the SEM images do not allow confirmation of the amorphous nature of RGF, the clear change in morphology probably indicates a successful ASD preparation process, especially when comparing the ASD RGF_PVP to its respective physical mixture RGF-PVP. Due to the preparation process, the ASD formulations differed in particle size distribution, which was further investigated in this section.

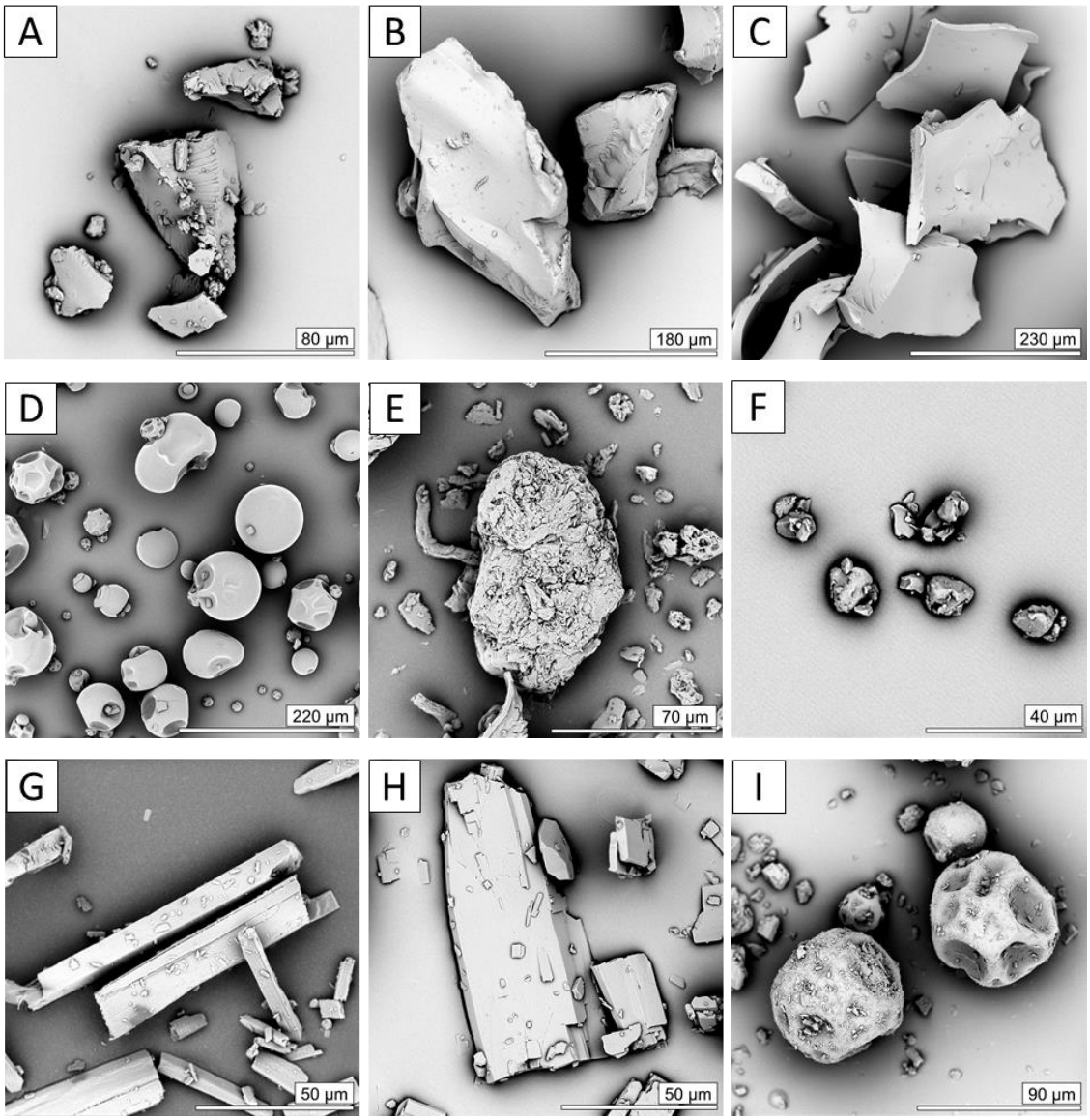


**Figure 4. SEM images of prepared ASDs and pure components: RGF_PVP (A), RGF_HPMCAS (B), RGF_EPO (C), PVP K25 (D), HPMCAS 716 (E), Eudragit E PO (F), RGF MH (G), RGF Mod. I (H), Physical mixture RGF-PVP (I).**

The results from XRPD measurements are shown in Figure 5, the method is described in Section 6.2.3.4.2. As described in the introduction (1.3.2.3), the absence of peaks in X-ray diffraction patterns indicate the lack of crystalline structures in the sample, although quantitative data and proof for complete absence of crystals cannot be obtained. RGF MH exhibited intense and sharp signals at characteristic $2\Theta$ values, which confirmed the monohydrate pseudo-polymorphic state (Sun et al. 2016). In contrast, the polymers PVP, HPMCAS, or EUD did not show diffraction peaks from 10° to 50°. These so-called *halo* signals are typical for polymers and indicate their amorphous state by the absence of distinct X-ray scattering (Alhayali et al. 2017). Halo signals were found for all prepared

ASDs, therefore, the amorphous state of RGF in the polymer matrix could be confirmed. Physical mixtures of RGF MH in PVP were prepared as calibration samples to determine the limit of detection. As shown in Figure 81 of the Appendix, XRPD detection of RGF MH crystals in PVP was possible to < 5 % (m/m) RGF MH content. Regarding the prepared ASDs with a drug load of 20 %, the 5 % diffractogram was equivalent to an ASD with a ratio of 3:1 of amorphous to crystalline RGF, limiting the XRPD technique in detection of small residual crystalline contents. Therefore, a combination of multiple analysis techniques must be applied to prove the amorphous state of RGF.

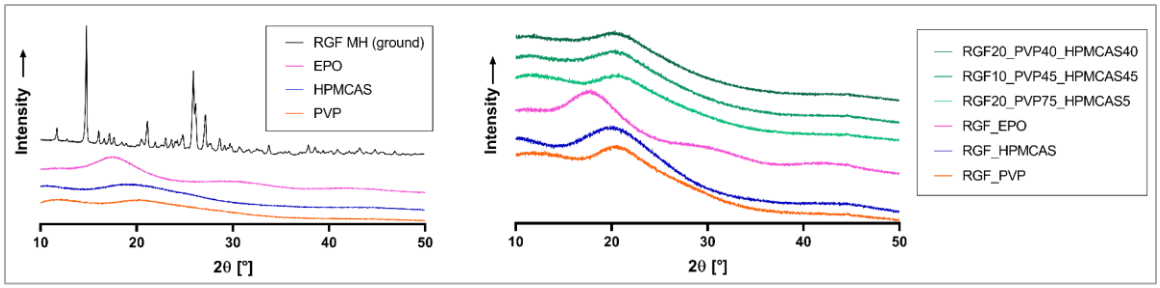


Figure 5. XRPD diffractograms of the single components (left) and prepared ASDs (right).

The single components and prepared ASDs were further investigated by DSC, the method is described in Section 6.2.3.4.6 and results are shown in Figure 6. An overview of DSC thermograms for all investigated materials is provided in Figure 78 and Figure 79 of the Appendix.

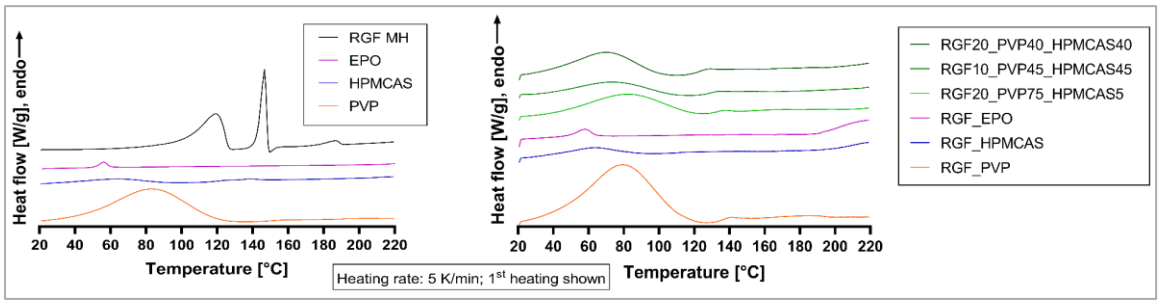


Figure 6. DSC thermograms of the single substances (left) and prepared ASDs (right).

For clarity purpose, not all heating cycles are shown in the Results section but are provided in the aforementioned figures in the Appendix. Amorphous RGF is described by *Bayer* to exist at ambient temperature, so only first heating curves are shown since, at second heating curves, characteristic RGF melting events were not present. The thermograms obtained

from polymer and ASD measurements mostly exhibited a similar profile. After water evaporation to ca. 130 °C, a glass transition could be observed for amorphous samples at a system-specific glass transition temperature ($T_g$). For RGF_EPO, the endothermic event at 58 °C was caused by the polymer and not by crystalline RGF.

Since all prepared ASD formulations exhibited one glass transition event, the API is assumed to be homogeneously dissolved in the polymer (Ma and Williams 2019). The respective Tg values are listed in Table 6, however, for RGF_EPO a clear glass transition was not detected.

**Table 6. Characteristic glass transition temperatures (Tg) of prepared ASD formulation determined via DSC. Onset temperatures are provided.**

| ASD formulation | Tg [°C] |
|---|---|
| RGF_PVP | 133 |
| RGF_HPMCAS | 94 |
| RGF_EPO | not detectable |
| RGF20_PVP40_HPMCAS40 | 117 |
| RGF10_PVP45_HPMCAS45 | 124 |
| RGF20_PVP75_HPMCAS5 | 128 |

As expected, only RGF MH exhibited distinct melting peaks and its profile can be explained as follows: After removal of the water bound into the monohydrate, RGF Mod. III starts melting at 144 °C, directly followed by an exothermic event, presumably a solid-liquid-solid phase transformation or re-crystallization process leading to some extent of RGF Mod. I. Eventually, at 184 °C, Mod. I melting occurs. The melting behavior of RGF is presented in more detail in Table 30 (Appendix).

For LOD determination of DSC experiments, the physical mixtures (PMs) already used for XRPD LOD determination were measured, the results are shown in Figure 80 (Appendix). The endothermal removal of the monohydrate water molecules was detectable for all PM concentrations, but the more broadened melting signals were only detectable for PMs with a RGF MH content of greater than 5 %.

The formulations RGF_PVP and RGF_HPMCAS were additionally investigated by confocal Raman microscopy (CRM, see Section 6.2.3.4.5) since these are the major formulations to be investigated in this work. In Figure 7, the Raman spectra of the ASDs and their single components are illustrated. For both ASD formulations, every signal can

be referred to as one of their components, more specifically to amorphous RGF or the respective matrix polymer. The absence of shifted peaks or additional signals in the ASD Raman spectra is a confirmation of the amorphous embedding of RGF in the polymer matrix.

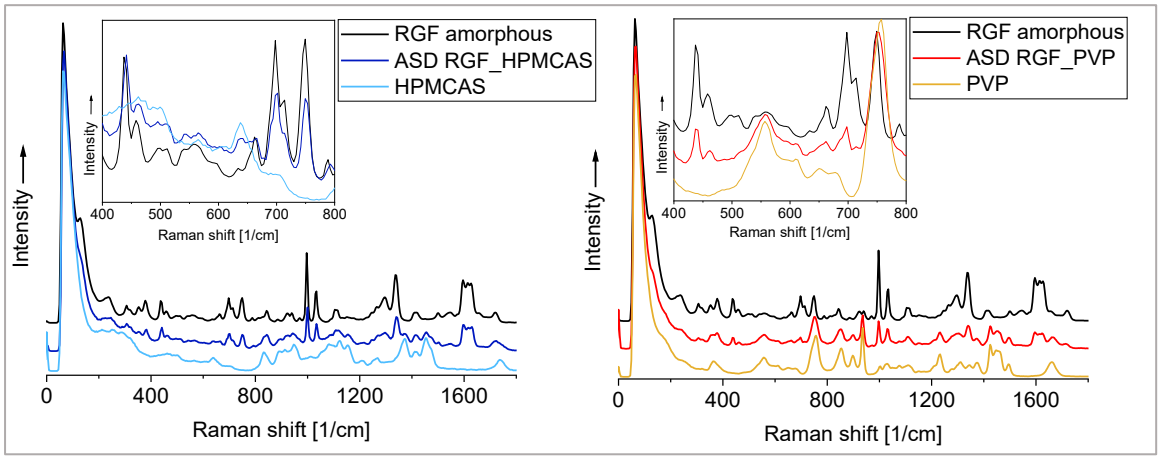


**Figure 7. Raman spectra of RGF_PVP and RGF_HPMCAS and its corresponding single components acquired by confocal Raman microscope. Insets show the 'region of interest'.**

All prepared ASD formulations were manually ground in a mortar and sieved to achieve narrow particle size distribution (DSP) in order to reduce the impact of particle sizes in further dissolution studies. This approach was feasible for all ASD formulations, except for RGF_HPMCAS. During particle size reduction of RGF_HPMCAS, electrostatic charge of the material led to massive loss of ASD, therefore only gentle grinding without sieving could be performed.

The differences in PSD were determined via CPA for RGF_PVP and RGF_HPMCAS. The resulting curves are shown in Figure 8 and Table 7.

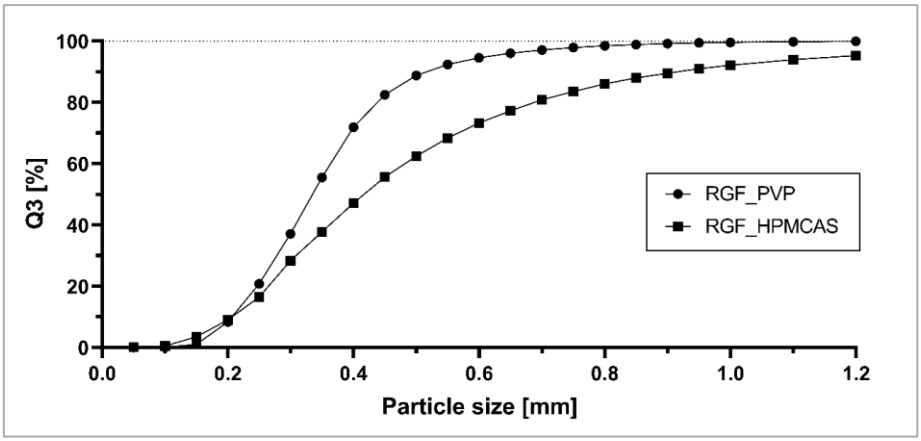


**Figure 8. Particle size volume distributions of the ASD formulations RGF_PVP and RGF_HPMCAS. Characteristic values are provided in Table 7.**

RGF_PVP particles were generally smaller and showed a more narrow PSD than RGF_HPMCAS particles. This can be expressed by comparison of the $d_{50}$ and $d_{90}$ values of Q3 distribution. These differences had to be considered for the dissolution studies, as the specific surface of RGF_PVP was increased compared to RGF_HPMCAS.

**Table 7. Particle size distribution of ASDs measured by CPA.**

| ASD formulation | Q3 $d_{50}$ [mm] | Q3 $d_{90}$ [mm] |
|---|---|---|
| RGF_PVP | 0.334 | 0.514 |
| RGF_HPMCAS | 0.414 | 0.913 |

The amorphous state of embedded RGF in the polymer matrices was confirmed for all prepared ASD formulations. Since the three independent analytical methods XRPD, DSC, and CRM confirmed the amorphous embedding or RGF, these ASDs were pursued for further investigations. All preparations were re-analyzed during storage for re-crystallization on a regular basis, however, re-crystallization was not detected for either of the formulations.

## 3.2 Biorelevant dissolution

Preamble

*Essential contents of this chapter are based on the patent application "EP20156003.4" (European Patent Office) by Martin Müller, Werner Hoheisel, Anke Stroyer, Markus Albers.*

*Essential contents of this chapter are based on the research article manuscript "The Impact of HPMCAS Co-administration on the Biopharmaceutical Performance of Regorafenib Amorphous Solid Dispersion" (Target Journal Eur. J. Pharm. Biopharm.) by Martin Müller, Raphael Wiedey, Werner Hoheisel, Peter Serno, and Jörg Breitkreutz.*

#### 3.2.1.1 Solubility of RGF in biorelevant media

The solubility of RGF in FaSSIF medium in the absence and presence of matrix polymers was measured by HPLC/UV as described in Section 6.2.3.1.3. The solubility of pure RGF in FaSSGF could not be determined since the sensitivity of the analytical method was insufficient for this concentration range. The polymer concentration in solubility studies was chosen to reflect the situation of complete ASD dissolution in FaSSIF.

As given in Table 8, the addition of PVP did not exhibit a solubilizing effect on RGF in FaSSIF. Interestingly, the equilibrium solubility of RGF in FaSSIF was even lowered in the presence of PVP. In contrast, for HPMCAS, a solubilizing effect could be observed, as the addition of HPMCAS led to an increased solubility of RGF in FaSSIF. Two-sided t-test analysis proves these results to be statistically significant with p = 0.048 and p = 0.00088 for PVP and HPMCAS, respectively.

**Table 8. Solubility of RGF in FaSSIF and influence of main ASD polymers used (mean ± CV, n = 3)**

| Samples in FaSSIF | RGF solubility [µg/mL] |
|---|---|
| RGF MH | 0.778 ± 9.8 % |
| RGF MH + PVP K25 | 0.619 ± 9.8 % |
| RGF MH + HPMCAS 716 | 3.177 ± 14.5 % |

From these results, the 'amorphous solubility advantage' was calculated, as proposed by Alonzo et al. (2011). According to the Hoffman equation (1958), the free energy difference between crystalline and amorphous forms was calculated based on the melting enthalpies determined by DSC. Since RGF MH undergoes solid-liquid-solid transformation between two different melting events, RGF Mod. I was chosen for these calculations with a reported melting point of 206 °C and a melting enthalpy of 92 J/g. This is reasonable because *Bayer* describes Mod. I to be the thermodynamically most stable RGF modification. In Equation 7, $\sigma^{amorph}/\sigma^{crystal}$ represents the ratio of the solubility of the amorphous form to the solubility of the stable crystalline form. $R$ is the universal gas constant, $T$ the temperature in Kelvin. The free energy difference $\Delta G$ is estimated from the enthalpy of fusion $\Delta H_f$, the experimental temperature $T$, and the melting point $T_m$.

$$\Delta G = \frac{\Delta H_f \cdot \Delta T \cdot T}{T_m^2} \qquad \text{Equation 6}$$

$$\frac{\sigma^{amorph}}{\sigma^{crystal}} = e^{\frac{\Delta G}{RT}}$$ Equation 7

As a result, the expected solubility advantage is a factor of 51.1. Hence, for amorphous RGF MH, RGF_PVP and RGF_HPMCAS dissolution studies in FaSSIF, a maximum supersaturation of 39.7 µg/mL, 31.6 µg/mL and 162.2 µg/mL can be expected, respectively.

### 3.2.2 Biorelevant dissolution setup development

To investigate the impact of different ASD formulations on RGF supersaturation and precipitation behavior, a biorelevant dissolution system was developed. As mentioned in Section 1.2.2.3, many different systems are published in the literature, each with specific advantages and disadvantages regarding the effects to be investigated.

One aim of the work was to investigate the supersaturation behavior of RGF at biorelevant conditions. Therefore, an experimental system with higher biorelevant significance than pharmacopoeial dissolution systems was sought, although, experimental complexity should not be too high. For this work, a system was used similar to the one described by Kostewicz et al. (2004), which comprises of a gastric compartment that is transferred over time an intestinal compartment. In contrast to their work, a simplified transfer was preferred instead of defined pumping rate, also called *dumping approach*, meaning the instant change of dissolution media from simulated gastric to intestinal conditions (Kambayashi et al. 2016). The immediate change of dissolution thus supersaturation environment was expected to lead to more clearly detectable differences in the dissolution profiles. The alternative, a gradual transfer of FaSSGF into a concentrated FaSSIF medium, would lead to a change in dissolution medium composition over time, possibly overlaying the RGF purely time-dependent supersaturation or precipitation effects. Additionally, for *in-situ* analytics, which will be discussed in a later chapter, the background signal is stable after dumping the FaSSGF conditions to FaSSIF conditions.

Although *in-situ* concentration analytics is preferable due to reduced sample preparation work, which might lead to greater analytical deviations, this approach seems challenging for supersaturated systems. Alonzo et al. (2011) observed the formation of submicron particles in the range of 200 – 400 nm during dissolution which lead to erroneous results at *in-situ* UV absorption measurements. Therefore, sample filtration is crucial to avoid falsified results by re-dissolution of precipitated drug during HPLC sample preparation. To

avoid RGF loss during sample preparation, a filter adsorption test was performed to investigate potential RGF adsorption on applied syringe filter membranes. For PP syringe filters with a max. pore size of 0.2 µm, the results are shown in Figure 9 for two independent samplings from biorelevant dissolution experiments at different levels of RGF supersaturation. A sample of 10 mL was filtrated in steps of 0.5 mL into HPLC vials and analyzed for RGF concentration. A plateau was reached after ca. 6 mL of the dissolution suspension has passed the filter, indicating complete filter saturation. The decrease in RGF concentration at 8 mL might be explained by the temperature decrease of the supersaturated dissolution suspension in the syringe, leading to precipitation of RGF. Based on these results, a pre-filtration step of minimum 9 mL was performed in all experiments directly before filtration into the HPLC vials, to cover possible variation of filters and RGF concentrations.

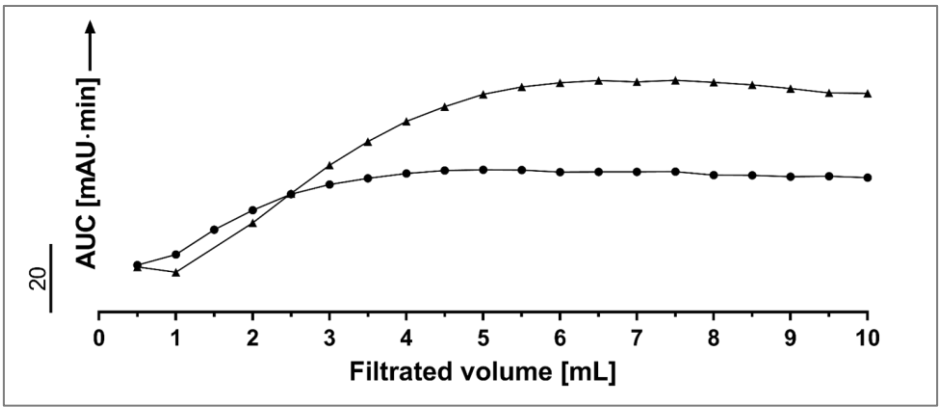


**Figure 9. Filter adsorption effects of RGF on PP 0.2 µm syringe filters. Two independent supersaturated samples, drawn at different time points during biorelevant dissolution experiments, are shown as examples. One experimental value at 1.5 mL is missing due to sampling error.**

A syringe pump was implemented into the sampling process to avoid variation in temperature drop of supersaturated samples by manual handling and to ensure higher experimental reproducibility. Since multiple dilution and pipetting steps were avoided, the supersaturated samples were solely in physical contact with the inner surface of the syringe, cannula, filter membrane, and vials. Moreover, the constant filtration rate and a similar time delay between sampling and filtration into the HPLC vials for all experiments led to decreased variability in dissolution results.

### 3.2.3 Biorelevant dissolution at simulated intestinal conditions

#### 3.2.3.1 Binary ASD formulations: The impact of matrix polymers

The binary ASD formulations RGF_PVP, RGF_HPMCAS, and RGF_EPO were investigated for their biorelevant dissolution behavior at simulated intestinal conditions. The applied method is described in Section 6.2.3.2.1 (one-compartment dissolution).

One physical mixture (PM RGF_PVP) was used as a negative control sample to demonstrate the potential of ASD formulation for RGF. Since the API was in the crystalline state within the PM, no supersaturation effects were expected to be observed. For these dissolution studies, an ASD dose of 200 mg was chosen, which is equivalent to one *Stivarga* tablet.

The dissolution graphs are presented in Figure 10. Characteristic data points are summarized in Table 9. The investigated RGF formulations exhibited very different release profiles and supersaturation behavior. The highly reproducible dissolution curves of RGF_PVP and RGF_HPMCAS allow the presentation of single curves in the diagrams, so it can be distinguished between each dissolution run.

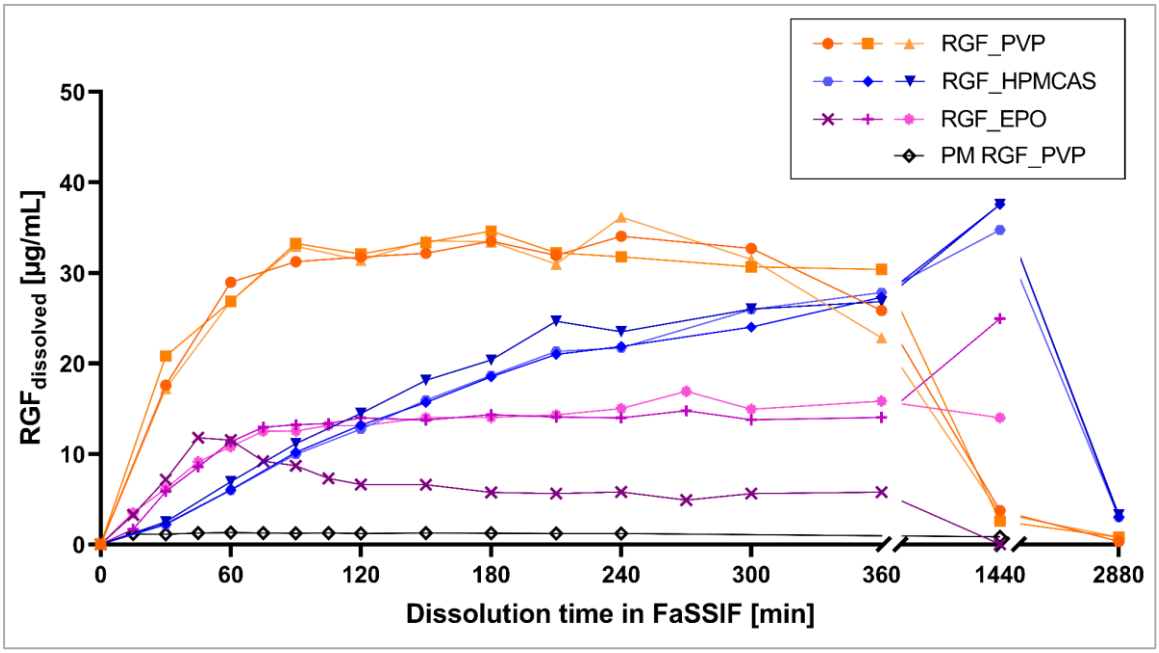


**Figure 10. Biorelevant dissolution behavior of different ASD formulations in FaSSIF (750 mL, 37 °C, 75 rpm). The dissolved dose is equivalent to one *Stivarga* tablet (40 mg RGF). Single curves are shown.**

The formulation RGF_PVP exhibited a rapid dissolution profile, reaching an RGF supersaturation plateau after 90 min. RGF supersaturation was detected for 360 min, although, the RGF concentration in one of three dissolution replicates began to decrease at

240 min dissolution time, indicating precipitation. The achieved maximum supersaturation was 36.2 µg/mL at 240 min and almost meets the calculated amorphous solubility of 31.6 µg/mL. After 24 h (1440 min) dissolution time, only very little supersaturation was observed due to precipitation of the API from the supersaturated state. Comparison of the dissolution graphs of the ASD RGF_PVP and its corresponding PM allows concluding that the ASD approach for RGF is a suitable technique to improve its dissolution performance. In contrast to the dissolution of RGF_PVP, the dissolution profile of RGF_HPMCAS showed a steady increase in RGF concentration. Interestingly, the maximum RGF concentration could be found after 1440 min, indicating a strong supersaturation stabilization. Both the different RGF release profiles, the fast-release profile from RGF_PVP and the prolonged-release profile from RGF_HPMCAS, could be explained by stronger molecular interactions between the polymers and RGF in the solid-state. This hypothesis is supported by a study of Li and Taylor (2018), who have determined that the strength of polymer-API interactions lead to a 'solubility suppression' of the drug during dissolution studies.

**Table 9. Maximum achieved RGF concentrations ($c_{max}$), degrees of supersaturation (DS) and the ratio of $c_{max}$ to hypothetical complete dissolution (% $dissolved_{max}$) in biorelevant dissolution testing at FaSSIF conditions for investigated ASD formulations.**

| Formulation | $c_{max,\ 0\text{-}360\ min}$ [µg/mL] | $DS_{max,}$: 0-360 min | $c_{max}$ [µg/mL] | $DS_{max}$ total | % $dissolved_{max}$ * |
|---|---|---|---|---|---|
| RGF_PVP | 36.2 | 67 | 36.2 | 67 | 68 % |
| RGF_HPMCAS | 27.8 | 9 | 37.6 | 12 | 71 % |
| RGF_EPO | 15.8 | - | 15.8 | - | 30 % |

* maximum RGF concentration is 53.3 µg/mL

In Figure 8, the PSD differences between RGF_HPMCAS and RGF_PVP have been given. Since the RGF_HPMCAS particles are larger, thus offer smaller specific surface for dissolution media, particle sizes might also contribute to the different RGF release kinetics. The observed $c_{max}$ values do not meet the calculated amorphous solubility advantage. The higher $C_s$ of RGF in presence of HPMCAS was explained by solubilization effects of the polymer, which may not be extrapolated as assumed by the use of Equation 7. This consideration is strengthened as the maximum supersaturation of RGF_HPMCAS dissolution in FaSSIF was 37.6 µg/mL which is close to the $c_{max}$ achieved by RGF_PVP.

The dissolution profiles obtained from RGF_EPO did not show reproducible results and lower RGF supersaturation over the full dissolution time. Whereas two of three curves matched satisfyingly for 360 min dissolution time, one replicate differed from 30 min dissolution time. It can be concluded that the ability of RGF supersaturation stabilization by EPO is reduced compared to PVP and HPMCAS.

It should be mentioned that the high reproducibility of different release kinetics is a quality parameter for the developed dissolution method, which was proven to be suitable for these investigations. Therefore, the variability within and amongst the formulations can be considered as 'true' effects which allow to draw conclusions about the role of polymer choice in ASD formulations with RGF.

Comparing RGF_PVP and RGF_HPMCAS, each formulation offers specific advantages and disadvantages. Since a fast drug release is favorable, the RGF_PVP formulation concept seems beneficial. The $c_{max}$ achieved by RGF_HPMCAS was higher than by other formulations, however, the maximum RGF concentration was observed after 24 h. At physiological conditions, intestinal transit times of ca. 4.5 h were reported, as mentioned in Section 1.2.1, so the maximum RGF concentration would be reached after the site of absorption was passed.
A more detailed discussion about the underlying mechanisms leading to different supersaturation stabilization and precipitation inhibition is provided in Section 3.4.2.8.
Since RGF_PVP and RGF_HPMCAS exhibited very different drug release and supersaturation profiles, these formulations were investigated further. The concept of RGF_EPO was not further pursued due to unsatisfying results obtained in this section.

#### 3.2.3.2 Dose effects of binary ASDs

The therapeutic daily dose of *Stivarga* consists of four tablets of 40 mg RGF each, administered together once daily. Hence, the RGF release profiles obtained from the dissolution of an ASD dose equivalent to one tablet *Stivarga* might not sufficiently reflect the *in-vivo* drug performance in patients. Therefore, dissolution experiments were performed with the daily RGF dose, which is a fourfold increase in ASD dose. The resulting graphs are shown in Figure 11.

As for the ASD dose equivalent to one tablet *Stivarga*, RGF release from RGF_PVP was faster than from RGF_HPMCAS and both formulations led to comparable maximum RGF concentrations of 46.0 µg/mL and 45.6 µg/mL, respectively. For both formulations, the higher applied ASD dose led to faster drug release and increased RGF supersaturation, however, not proportional to the dose. For RGF_PVP, the achieved supersaturation was not stable for 360 min for all replicates. In contrast, RGF_HPMCAS led to a stabilized RGF supersaturation for over 360 min, and only one of three replicates showed a decrease in concentration after 24 h. Interestingly, the calculated amorphous solubility was exceeded, which might be explained either by an increase in equilibrium solubility through a higher concentration of dissolved polymer or the formation of ALPS droplets smaller than the pore size of the syringe filters used for sampling.

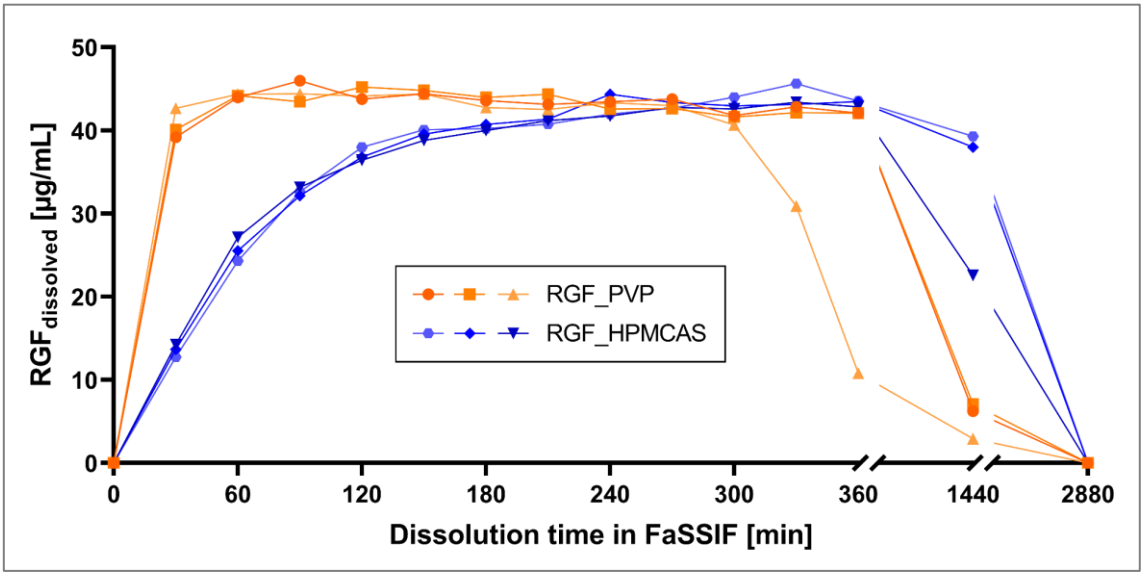


**Figure 11. Biorelevant dissolution testing in FaSSIF (750 mL, 37 °C, 75 rpm). The dissolved dose is equivalent to four *Stivarga* tablets (160 mg RGF), which is the therapeutic single dose. Single curves are shown.**

An increase in administered dose seemed to be beneficial under simulated intestinal dissolution conditions regarding drug release and maximum RGF concentration. However, these benefits bear the risk to promote crystallization from supersaturated systems, as the rate of supersaturation generation was described to be a driver for drug precipitation (Sun and Lee 2015b).

### 3.2.4 Biorelevant transfer dissolution: From gastric to intestinal conditions

#### 3.2.4.1 Experimental setup

At physiological conditions, the administered ASD formulations first enter the stomach before being transferred to the small intestine. To better mimic this *in-vivo* situation, the impact of simulated gastric transfer towards RGF dissolution was investigated. As described in Section 1.2.1, reported gastric passage times for oral drug formulations range from some minutes to many hours, depending on the nutrition state. To detect its relevance for RGF formulations, gastric transfer times of 30 min and 120 min at simulated fasted conditions were chosen. The experiments were performed as described in the Methods section 6.2.3.2.2. Because of limitations regarding the analytical limit of quantification (LOQ) of the applied HPLC/UV method for RGF concentration determination, the first data points were acquired immediately after media change to FaSSIF conditions (0 min).

#### 3.2.4.2 The impact of gastric transit time

The transfer dissolution curves for RGF_PVP and RGF_HPMCAS for 30 min and 120 min gastric passage time are presented in Figure 12 and Figure 13, respectively. RGF_PVP dissolution in FaSSGF led to rapid crystallization in the dissolution vessels, clearly visible by the eye by an increase in turbidity.

In the 30 min transfer experiment, no dissolved RGF was measured directly after the media change from FaSSGF to FaSSIF was conducted. After further 30 min, RGF supersaturation reached a plateau concentration, comparable to the concentrations measured at one-compartment intestinal FaSSIF dissolution studies in Section 3.2.3. This fast RGF release could be explained by ASD particle swelling and disintegration during FaSSGF conditions and therefore faster release kinetics after media conversion to FaSSIF conditions.

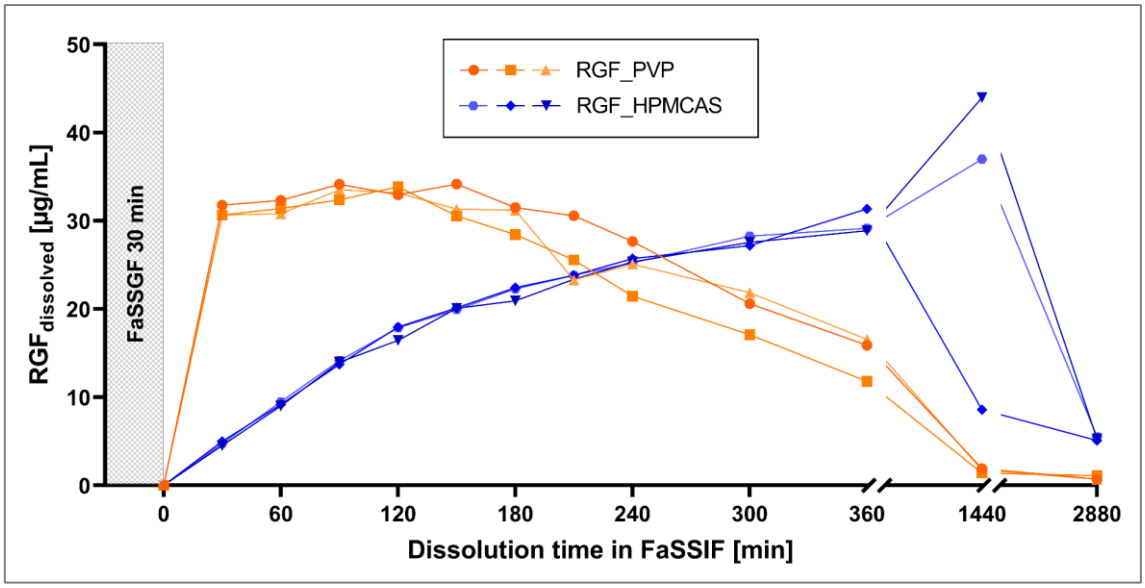


**Figure 12. Biorelevant transfer dissolution testing (37 °C, 75 rpm). ASDs were dissolved in FaSSGF (250 mL) for 30 min prior to addition of FaSSIF$_{conc}$ (500 mL). The dissolved dose is equivalent to one *Stivarga* tablet (40 mg RGF). Single curves are shown.**

The gastric transfer negatively impacted RGF supersaturation stabilization in FaSSIF for RGF_PVP. The supersaturation decreases constantly after approximately 150 min. The mean RGF concentration at 360 min was reduced to 56 % compared to the one-compartment FaSSIF dissolution in Figure 10.

The interplay of dissolution, ALPS, and precipitation during ASD dissolution was discussed in Sections 1.1.2.3 and 1.3.1. Accordingly, RGF crystals, formed under FaSSGF conditions, could act as nucleation seeds and by that have led to rapid desupersaturation of the system by RGF crystal growth.

As described in Section 1.1.3.2, the polymer HPMCAS is insoluble at gastric, thus acidic, conditions. As a consequence, RGF release from this formulation was not affected by the pre-treatment in FaSSGF and immediately took place after FaSSIF conversion. The release kinetics was similar to FaSSIF dissolution with a calculated similarity factor f2 = 73.5, whereas a value greater than 50 indicates equivalent dissolution profiles (Moore and Flanner 1996; Xie et al. 2015).

Embedding amorphous RGF into a FaSSGF-insoluble matrix polymer seemed to preserve the amorphous state of the API from early precipitation and led to a drug release in FaSSIF similar to the one-compartment dissolution studies.

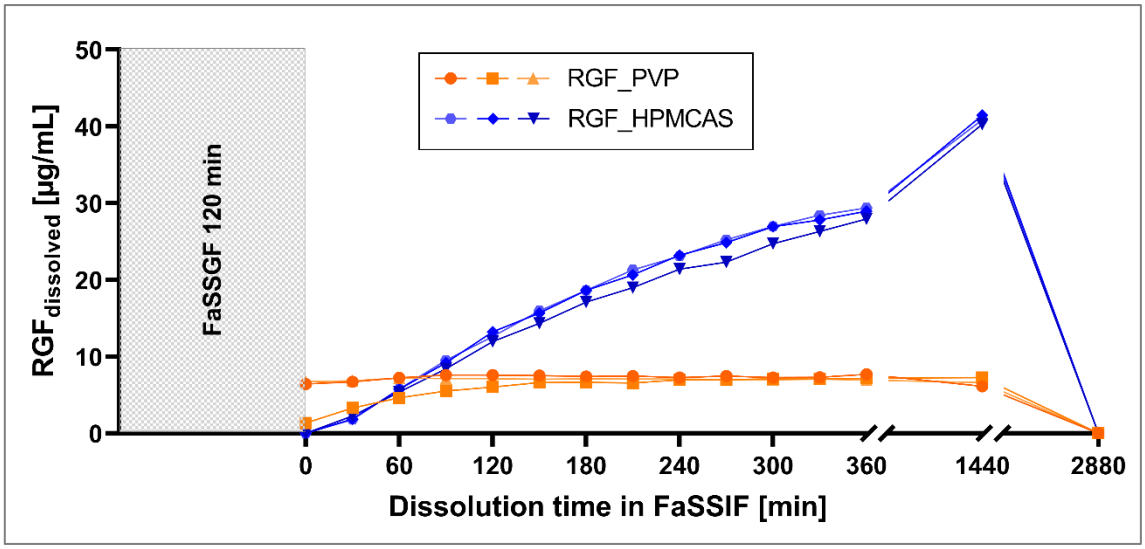


**Figure 13. Biorelevant transfer dissolution testing (37 °C, 75 rpm). ASDs were dissolved in FaSSGF (250 mL) for 120 min prior to addition of FaSSIF$_{conc}$ (500 mL). The dissolved dose is equivalent to one *Stivarga* tablet (40 mg RGF). Single curves are shown.**

To reflect the *in-vivo* observed variability in gastric transit time in fasted state of 1-2 h (see Table 4), in a second experiment, the simulated gastric transit time was increased to 120 min. The described effects were even more pronounced, as can be seen in Figure 13.
For RGF_PVP formulation, the increase in FaSSGF residence time to 120 min drastically affected the level of generated RGF supersaturation. The maximum RGF concentration was 7.59 µg/mL, the respective DS is 14. Interestingly, this concentration plateau was found to be constant for more than 24 h after media change. The same dissolution behavior as described above can be observed: under acidic conditions in FaSSGF, re-crystallization of amorphous RGF occurred, reducing the amount of amorphous API and subsequently reducing supersaturation after FaSSIF conversion.
As expected, the extension of gastric transit time from 30 min to 120 min did not affect RGF release from the formulation RGF_HPMCAS. The similarity factor f2 = 86.6 was calculated to compare the dissolution profiles obtained from FaSSIF dissolution without and with 120 min gastric transfer, indicating high similarity and therefore little variation in RGF release kinetics. These results demonstrate the capability of HPMCAS to preserve the amorphous state of incorporated RGF from early re-crystallization.

To conclude, for RGF_PVP, time-dependent precipitation at simulated gastric conditions was observed, strongly affecting the following RGF release at FaSSIF conditions. At 30 min transfer time, a *spring and parachute* profile was still achieved, but this effect

completely vanished by increasing the FaSSGF transit time to 120 min. These findings can be linked to reported BA fluctuations in the patient population. The highly variable physiological conditions and in particular unpredictable gastric transit times might lead to poor drug release and limited supersaturation for some patients, which could lead to insufficient plasma levels and eventually therapy failure.

As discussed in Section 1.1.2, from a formulator's perspective, a fast *spring* (drug release) and long-lasting *parachute* (supersaturated state) are both desirable. For RGF_PVP a fast spring was observed, but overall drug performance was limited due to precipitation under acidic conditions. The formulation RGF_HPMCAS led to more reproducible drug release kinetics exhibiting long RGF supersaturation, not affected by acidic conditions, but a small slope (slow *spring)*. So far, none of the RGF formulations investigated including the marketed drug formulation meets the optimal drug release properties. One approach often proposed in the literature is the formulation of ternary ASDs, comprising the API and either two matrix polymers or one polymer and a surfactant. Both approaches will be investigated in Section 3.3.

### 3.2.5 Small-scale dissolution development

The high experimental effort of the biorelevant vessel-based dissolution experiments is disadvantageous for time- and cost-efficient formulation studies. To enable for time-efficient but still meaningful results, a small-scale dissolution method was newly developed, the exact method is described in Section 6.2.3.2.3. The aim of this development was to investigate multiple formulations or impacts on dissolution profile with three to four characteristic data points per dissolution testing. A total of 50 mL FaSSIF was used per run, whereas the ratio ASD to FaSSIF media was kept constant for all dissolution models used in this work for better comparability of the dissolution results.

The geometries of the glass cylinders are different from those of the USP vessels, which is expected to influence dissolution kinetics, as hydrodynamics are linked to drug release and precipitation rate from supersaturation (Bevernage et al. 2013; Carlert et al. 2010). Different from the vessel-based dissolution method, a higher stirring rate was chosen to avoid sedimentation of the ASD particles, leading to a reduction of the diffusion layer thickness around dissolving ASD particles. In Equation 1, the influence of the diffusion layer thickness $h$ and the exposed surface $S$ on the dissolution rate are stated. As the vessel-based dissolution method was stirred by a USP 2 paddle stirring device, for the small-scale

dissolution approach a magnetic stirrer at the bottom of the dissolution glass was applied. By applying mechanical stress to the ASD particles by direct impaction, particle size reduction with might occur, which could accelerate ASD dissolution by the creation of additional surfaces, hence the exposed surface *S* would be increased. Since RGF_HPMCAS particles were shown to be larger than RGF_PVP particles, this effect is expected to be pronounced for RGF_HPMCAS dissolution.

For both formulations, representative sampling time points were chosen to simultaneously provide information about drug release (faster or slower), supersaturation plateau concentration (higher or lower) and a control data point after 24 h, see Table 10. The sampling time points were not always identical among all small-scale dissolution studies, but in all cases within the experimental triplicates for each formulation.

**Table 10. Representative sampling time points in small-scale biorelevant dissolution studies**

| Formulation | RGF_PVP | RGF_HPMCAS | Evaluation |
|---|---|---|---|
| 1st sampling: RGF release *(spring)* | 90 min | 90 min | faster or slower |
| 2nd sampling: $c_{max}$ *(parachute)* | 210 min | 300 min | higher or lower |
| 3rd sampling: after precipitation | 1440 min | 1440 min | control |

The comparability of both applied dissolution methods was evaluated. The results from biorelevant small-scale dissolution of RGF_PVP and RGF_HPMCAS are shown in Figure 14 and compared to the results obtained by the biorelevant vessel-based dissolution in Table 11. The results clearly demonstrate the comparability between both dissolution setups in regards to dissolution kinetics profiles of both formulations. For RGF_PVP, high supersaturation was measured after 90 min. For the data points at 210 min, the high standard deviation can be explained by precipitation in one of three replicates, indicating a faster dissolution-precipitation process than observed in the vessel-based studies. After 1440 min dissolution time, no supersaturation could be observed anymore.

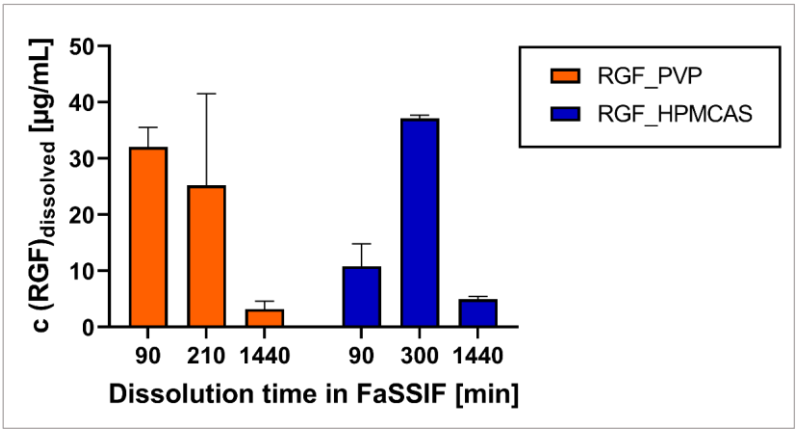


**Figure 14. Small-scale dissolution testing of ASD formulations (mean ± s, n = 3). Dissolution was performed in 50 mL FaSSIF at 37 °C, the dissolved RGF dose (2.7 mg) is equivalent to one *Stivarga* tablet (40 mg RGF) in 750 mL.**

The same statements can be made for RGF_HPMCAS dissolution behavior. The general dissolution profile matched the scheme from the vessel-based dissolution results. Interestingly, no strong supersaturation was observed at the 1440 min sample, as above, indicating faster precipitation caused by the higher fluid dynamics and stirrer impaction. Comparison of the absolute RGF concentrations proved that both methods led to similar RGF concentrations (Table 11), although the shift to faster drug release and precipitation kinetics has to be considered.

**Table 11. Comparison of small-scale dissolution and vessel-based dissolution setups for biorelevant RGF ASD dissolution in FaSSIF (mean ± s, n = 3). The respective dissolution graphs are depicted in Figure 10 and Figure 14.**

| Formulation / Dissolution time [min] | RGF_PVP [µg/mL] | | RGF_HPMCAS [µg/mL] | |
|---|---|---|---|---|
| | Vessel | Small-scale | Vessel | Small-scale |
| 90 | 32.47 ± 1.1 | 32.03 ± 3.5 | 10.42 ± 0.6 | 10.82 ± 4.0 |
| 210 | 31.70 ± 0.7 | 25.18 ± 16.4 | / | / |
| 300 | / | / | 25.31 ± 1.1 | 37.10 ± 0.6 |
| 1440 | 3.23 ± 0.6 | 3.21 ± 1.4 | 36.61 ± 1.6 | 4.96 ± 0.5 |

## 3.3 Formulation development of improved ASD matrices

Preamble

*Essential contents of this chapter are based on the patent application "EP20156003.4" (European Patent Office) by Martin Müller, Werner Hoheisel, Anke Stroyer, Markus Albers.*

*Essential contents of this chapter are based on the research article manuscript "The Impact of HPMCAS Co-administration on the Biopharmaceutical Performance of Regorafenib Amorphous Solid Dispersion" (Target Journal Eur. J. Pharm. Biopharm.) by Martin Müller, Raphael Wiedey, Werner Hoheisel, Peter Serno, and Jörg Breitkreutz.*

### 3.3.1 Ternary ASDs with two matrix polymers

#### 3.3.1.1 Concept

As mentioned in Section 1.1.2.7, one strategy to improve supersaturation stability and drug release is the use of polymer combinations as ASD matrix. Xie and Taylor (2016b) presented an alternative ASD formulation approach by the combination of one polymer with rapid release properties and a second polymer selected for its crystallization inhibitory properties. To follow this concept, ternary ASD formulations of RGF with a polymer combination of PVP and HPMCAS were prepared. This approach seems to be promising since the fast release properties of PVP and strong supersaturation stabilization of HPMCAS were found during previous dissolution studies. Therefore, ternary ASD formulations with variations in drug load and HPMCAS content were investigated for their dissolution performance by use of the biorelevant small-scale dissolution method.

#### 3.3.1.2 Preparation of ternary matrix ASDs

Ternary ASD of RGF and the polymers PVP and HPMCAS were prepared by solvent evaporation and manually ground. The amorphous state of RGF in prepared ASDs was confirmed by the absence of X-ray diffraction in XRPD experiments and the absence of a characteristic melting event in DSC analytics, as shown in Figure 5 and Figure 6, respectively. Figure 15 shows the acquired SEM images of the prepared formulations. Ternary ASDs were prepared according to Section 6.2.2.1 and the nomenclature of the presented formulations is provided in Table 24.

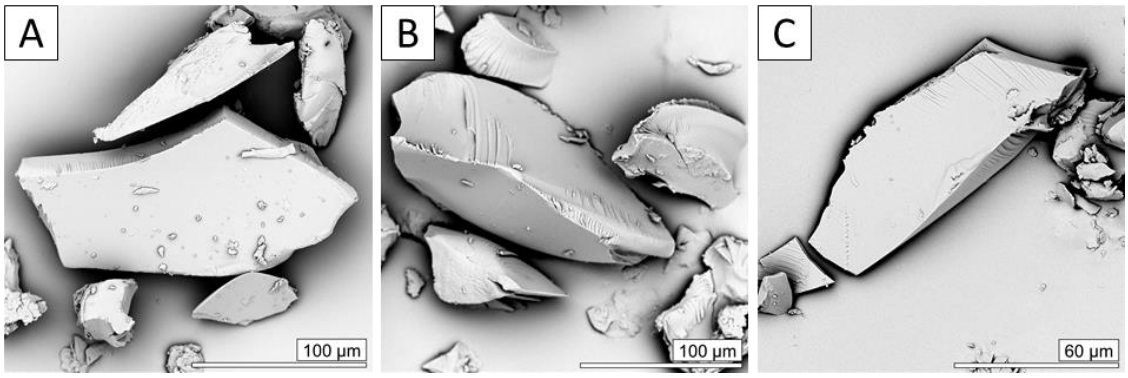


**Figure 15. SEM images of ternary ASD formulations RGF10_PVP45_HPMCAS45 (A), RGF20_PVP40_HPMCAS40 (B) and RGF20_PVP75_HPMCAS5 (C).**

#### 3.3.1.3 Biorelevant dissolution at FaSSIF conditions

For RGF10_PVP45_HPMCAS45, twice the ASD dose was dissolved to keep the absolute RGF dose equal for all formulations for a better comparison of observed effects.

Surprisingly, all formulations showed a dissolution profile similar to RGF_HPMCAS. Even the formulation RGF_20_PVP75_HPMCAS5 with an HPMCAS content of only 5 % exhibited a dissolution profile, which seemed to be dominated by the incorporated HPMCAS, as shown in Figure 14. Direct comparison of the formulations of 10 % and 20 % drug load raise the assumption that lower drug load might be beneficial. This finding is in accordance with the literature for other APIs (Tres et al. 2018) and can be explained by a higher specific surface and the different ratio of polymer to RGF in the supersaturated state, which is twice as high for the formulation with 10 % drug load.

#### 3.3.1.4 Transfer dissolution

Biorelevant transfer dissolution studies of the formulation RGF_HPMCAS in Section 3.2.4.2 revealed its robustness against the simulated gastric transfer. The investigated ternary ASD formulations all contained HPMCAS as matrix polymer in different ratios, which is insoluble at FaSSGF conditions and therefore might be protective regarding the maintenance of the amorphous nature of embedded RGF. A small-scale transfer dissolution study was performed as described in Section 6.2.3.2.3., the results are illustrated in Figure 17. For evaluation regarding the impact of simulated gastric transfer on dissolution performance of ternary formulations, Figure 16 and Figure 17 should be compared.

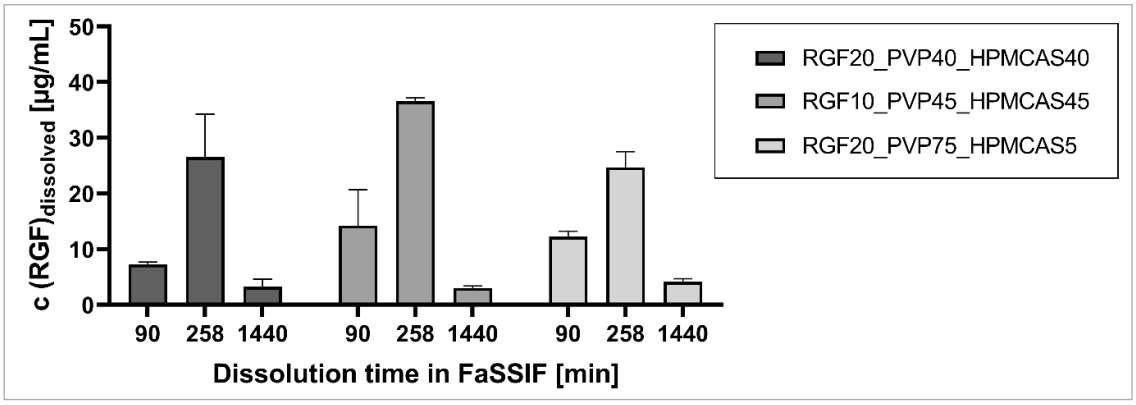


**Figure 16. Small-scale dissolution testing of ternary ASD formulations (mean ± s, n = 3). Dissolution was performed in 50 mL FaSSIF at 37 °C, the dissolved RGF dose (2.7 mg) is equivalent to one *Stivarga* tablet (40 mg RGF) in 750 mL.**

All three formulations are negatively affected regarding the achieved RGF supersaturation in FaSSIF by the pre-dissolution in FaSSGF prior to FaSSIF conversion. The RGF release profiles are different from those without transfer by means of the time point of maximum RGF concentration ($t_{max}$), except for RGF20_PVP75_HPMCAS5, albeit for this formulation the difference in RGF concentration between $t_{90min}$ and $t_{258min}$ is probably too small to be of importance.

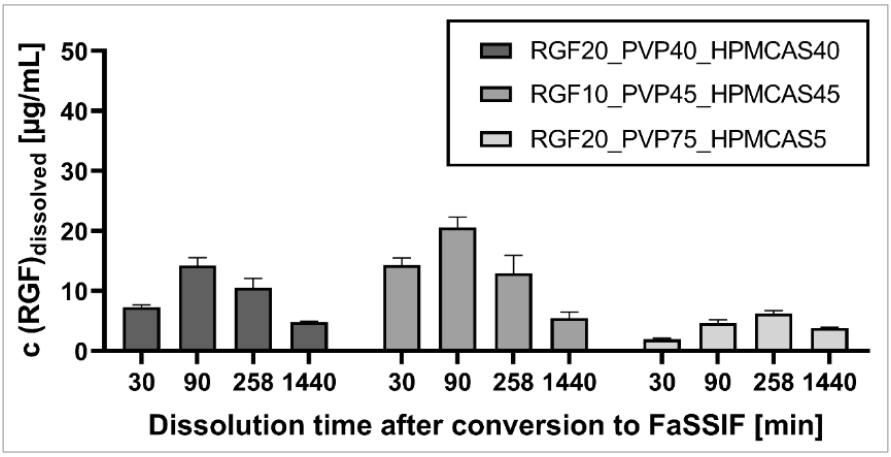


**Figure 17. Small-scale transfer dissolution testing of ternary ASD formulations (mean ± s, n = 3). Dissolution was performed at 37 °C in 20 mL FaSSGF for 120 min prior to addition of 40 mL $FaSSIF_{conc.}$, the dissolved RGF dose (3.2 mg) is equivalent to one *Stivarga* tablet (40 mg RGF) in 750 mL.**

RGF20_PVP75_HPMCAS5 showed a dissolution behavior similar to RGF_PVP vessel-based transfer dissolution (see Figure 13). The obtained $c_{max}$ values of 6.2 µg/mL and 7.3 µg/mL, for RGF20_PVP75_HPMCAS5 and RGF_PVP respectively, were in the same concentration range.

For the formulations RGF20_PVP40_HPMCAS40 and RGF10_PVP45_HPMCAS45, superior dissolution performance can be stated compared to RGF_PVP, which is the formulation concept behind *Stivarga*. For RGF10_PVP45_HPMCAS45 and RGF20_PVP40_HPMCAS40, after gastric transfer, a faster drug release at $t_{90min}$ was detected. During FaSSGF dissolution, the PVP dominated parts of the ASD might have been swollen by water uptake and dissolution, enabling a faster drug release from the HPMCAS dominated ASD sites after media change.

#### 3.3.1.5 Discussion

As outlined above for binary ASD formulations, the use of HPMCAS led to stronger RGF supersaturation stabilization compared to PVP. From a molecular perspective, this could be achieved by stronger interactions between the polymer and API in the supersaturated state. The same mechanism might be an explanation for the dissolution profiles of the investigated ternary ASDs. During preparation, RGF and HPMCAS form the stronger conjugates, decreasing the number of available interaction sites for RGF and PVP. Consequently, only a small proportion of embedded RGF is bound to PVP, hence leading to dissolution kinetics governed by RGF_HPMCAS.

However, a faster RGF release was observed from the formulation with 10 % RGF and the reduced drug load showed best supersaturation in the transfer dissolution experiment. As expected, not only the type of the stabilizing polymer, but also the ratio of RGF to polymeric excipients in the ASD seemed to enhance the supersaturation stabilization.

However, in transfer dissolution experiments, the possible maximum supersaturation of RGF in FaSSIF was not achieved, indicating precipitation during the simulated gastric transit which affected subsequent RGF supersaturation in FaSSIF by the formation of crystal seeds and subsequent crystal growth.

To conclude, the formulation concept of ternary ASDs comprising RGF, PVP, and HPMCAS was beneficial towards RGF_PVP in transfer dissolution studies, but overall performance was not satisfying since drug release was similar to RGF_HPMCAS, probably caused by strong, thus dominant interactions of RGF with HPMCAS.

### 3.3.2 Ternary ASDs: Surfactant-containing ASDs[1]

#### 3.3.2.1 Concept

In this section, the incorporation of surfactants into the ASD system RGF_PVP was investigated with regards to its dissolution performance. Two structurally different surfactants were chosen, the molecular structures are depicted in Section 1.1.3.2. The concept of surfactant-containing ASDs, already mentioned in Section 1.1.2, is to achieve faster drug release kinetics and to stabilize drug supersaturation in a thermodynamic way by incorporation into micelles, therefore, reducing the fraction of molecularly dissolved drug as the driving force for crystallization (Feng et al. 2018). A more detailed systematic investigation about the role of surfactants below and above its critical micelle concentration (CMC) by Zhang et al. (2019) highlighted the necessity of dissolution screening, as the results were varying. Since RGF_PVP reflects the marketed formulation of *Stivarga*, the impact of surfactant incorporation was investigated in this formulation. Polysorbate 80 (PS-80) and sodium dodecyl sulfate (SDS) were chosen as surfactants because of their different physicochemical properties. SDS exhibits a strong solubilization potential in aqueous media and incorporation into an ASD can be challenging due to its negatively charged nature in contrast to PS-80, which is a neutral surfactant (Patel and Joshi 2008; Sjökvist et al. 1992). The critical micelle concentrations are reported to be 8 mmol/L for SDS and 13-25 mg/L for PS-80 (Curatolo 1998; Rahman and Brown 1983).

The different formulations contained 2 % and 10 % surfactant in the ASD matrix since these concentrations were assumed to be feasible towards incorporation into the *Stivarga* granules, which was not investigated in detail. The final surfactant concentrations in the dissolution system at complete ASD dissolution were 0.019 mmol/L to 0.093 mmol/L for SDS and 5.3 mg/L to 27 mg/L for PS-80. Therefore, only the formulation RGF_PVP-PS10% exceeded the CMC, hence micelle formation could be expected. On the other hand, FaSSIF media already contains micelles, so surfactant concentrations below CMC might alter the existing micelles in FaSSIF, impacting the RGF dissolution-supersaturation-precipitation interplay.

[1] These results were partly generated during an internship (WPP) with support of Isra Atalla and Pinar Bozkurt.

### 3.3.2.2 Preparation of surfactant-containing ASDs

Surfactant-containing ASD formulations were prepared as described in Section 6.2.2.1 and investigated for the amorphous state of embedded RGF. In Figure 18, the absence of the RGF melting peaks proved the amorphous state of RGF in the ASDs and enabled for further dissolution studies.

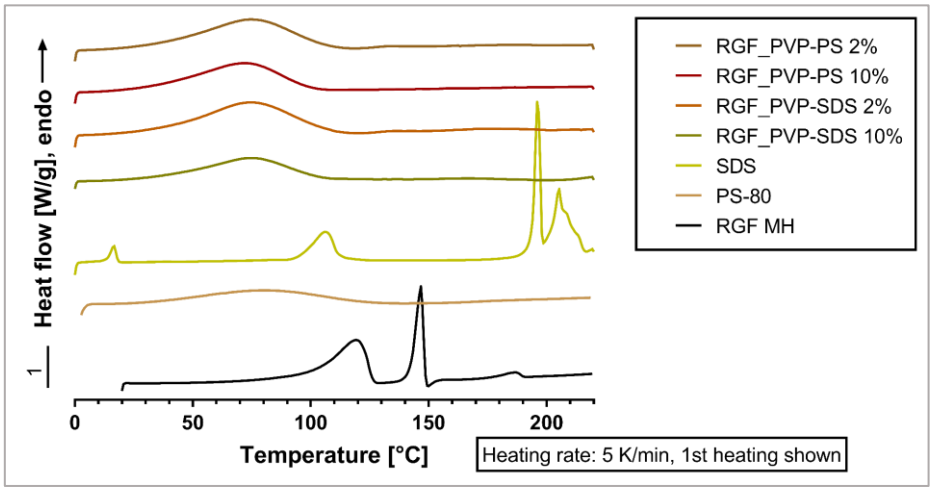


Figure 18. DSC of surfactant-containing ASD formulations and reference materials.

Additionally, the characteristic melting events of crystalline SDS were not detectable in the prepared formulations, confirming the molecular dispersion of SDS in the ASD.

### 3.3.2.3 Solubility in FaSSIF in presence of surfactants

To allow DS calculation and detect possible RGF solubilization effects of the surfactants, solubility studies were executed as described in Section 6.2.3.1.3. The amount of surfactants in solubility studies was calculated to reflect the situation of complete ASD dissolution.

The results are shown in Table 12. The solubility of RGF in FaSSIF, without any additives, was determined to be 0.778 µg/mL ± 9.8 % (see Table 8). Incorporation of 2 % SDS did not show a solubilization effect, whereas the formulation containing 10 % SDS led to an increase in RGF solubility. For PS-80, the different amounts in the ASD formulations did not lead to relevant differences between the formulations, for both formulations, negligible RGF solubilization was observed.

Table 12. Solubility of RGF in FaSSIF in presence of surfactants (mean ± s, n = 3).

| Polymer addition to FaSSIF respectively to % in ASD formulation | RGF solubility [µg/mL] |
|---|---|
| SDS 2 % | 0.77 ± 3.6 % |
| SDS 10 % | 1.15 ± 7.9 % |
| PS 2 % | 1.14 ± 5.7 % |
| PS 10 % | 0.99 ± 9.4 % |

#### 3.3.2.4 Biorelevant dissolution at FaSSIF conditions

The surfactant-containing ASDs were investigated by biorelevant one-compartment dissolution in FaSSIF, as described in Section 6.2.3.2.1. The resulting graphs are shown in Figure 19 and characteristic dissolution values are provided in Table 13.

All formulations showed superior dissolution results compared to their respective physical mixtures. As expected, fast drug dissolution was observed for surfactant-containing ASDs, however, strong deviations between dissolution replicates were found as indicated by the high CV values in Table 13. As a consequence, the achieved RGF supersaturations were considered to be less stabilized in presence of surfactants than the respective binary formulation RGF_PVP. Solely formulation RGF_PVP-PS 10% showed smaller fluctuations during the first 120 min of dissolution, which might be explained by micelle formation of PS-80, as this is the only formulation that exceeds the CMC of the incorporated surfactant. Through micelle formation and RGF solubilization, the degree of supersaturation as a driving force for precipitation is decreased by an elevation of the thermodynamic stable equilibrium concentration of RGF (Equation 4). Furthermore, through API partitioning into micelles, the fraction of molecularly dissolved API, the 'true supersaturation', is reduced, hence the driving force for precipitation is reduced (Feng et al. 2018).

These findings are in accordance with published literature, as SDS and PS-80 were shown to promote crystallization from drug supersaturation (Chen et al. 2015a). Therefore, the previously reported positive effects of SDS incorporation on ASD dissolution in biorelevant media (Franca et al. 2018) cannot be confirmed for the present ASDs. Ueda et al. (2017) found SDS to destabilize the drug-rich phase formed during ALPS and demonstrated the *in-vivo* relevance of this experimental finding in dogs, as the BA was decreased to 30% compared to the formulation not containing SDS.

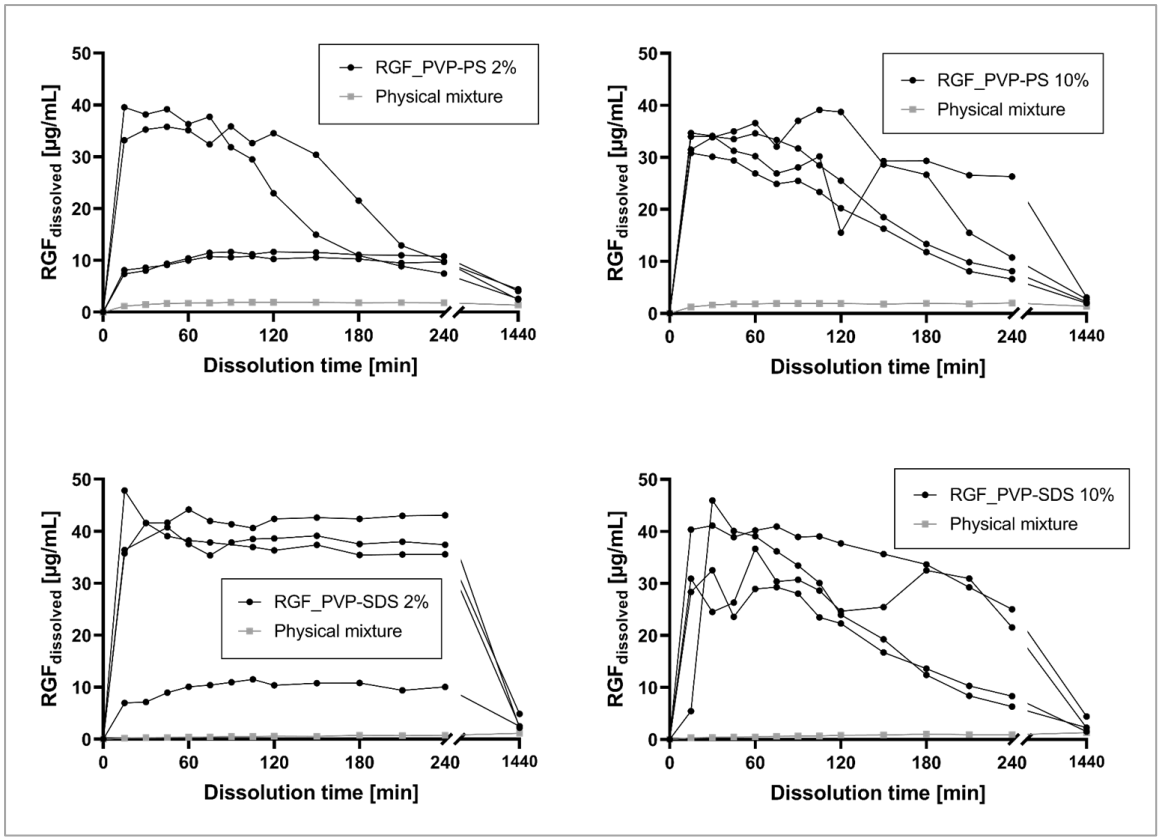


**Figure 19. Biorelevant one-compartment dissolution testing of surfactant-containing ASDs versus the corresponding PMs in FaSSIF (750 mL, 37 °C, 75 rpm). The dissolved dose is equivalent to one *Stivarga* tablet (40 mg RGF). Single curves are shown (n = 4).**

From a biopharmaceutical perspective, this formulation concept would probably lead to strong precipitation *in-vivo* thus undesired BA fluctuations. Therefore, this concept was concluded to be not suitable for the investigated RGF_PVP systems.

**Table 13. Characteristic data from surfactant-containing ASD dissolution in FaSSIF presented in Figure 19 (n = 4, mean ± s). Mean maximum achieved RGF concentrations ($c_{max, mean}$), mean maximum degrees of supersaturation ($DS_{max, mean}$) and the ratio of $c_{max, mean}$ to hypothetical complete dissolution (% $dissolved_{max, mean}$).**

| Formulation | $c_{max, mean}$ [µg/mL] | $DS_{max, mean}$ | % $dissolved_{max, mean}$* |
|---|---|---|---|
| RGF_PVP-PS 2% | 24.46 ± 62.8 % | 21 | 45.9 % |
| RGF_PVP-PS 10% | 34.78 ± 9.7 % | 35 | 65.2 % |
| RGF_PVP-SDS 2% | 35.42 ± 45.9 % | 46 | 66.4 % |
| RGF_PVP-SDS 10% | 39.04 ± 14.8 % | 34 | 73.2 % |

* maximum RGF concentration is 53.3 µg/mL

## 3.4 Formulation development: External supersaturation stabilization

Preamble

*Essential contents of this chapter are based on the patent application "EP20156003.4" (European Patent Office) by Martin Müller, Werner Hoheisel, Anke Stroyer, Markus Albers.*

*Essential contents of this chapter are based on the research article manuscript "The Impact of HPMCAS Co-administration on the Biopharmaceutical Performance of Regorafenib Amorphous Solid Dispersion" (Target Journal Eur. J. Pharm. Biopharm.) by Martin Müller, Raphael Wiedey, Werner Hoheisel, Peter Serno, and Jörg Breitkreutz.*

### 3.4.1 Prolonged-release of RGF_PVP: Lipid extrusion

#### 3.4.1.1 Concept

In literature, fast ASD dissolution kinetics were reported to impair subsequent supersaturation (Sun and Lee 2015b). A recent approach in ASD formulation development is the engineering of prolonged-release formulations by swellable but insoluble ASD matrices, leading to a diffusion-governed drug release, which showed some promising results (Dereymaker et al. 2017; Sun and Lee 2015a).

In this work, the fast-release formulation RGF_PVP was modified to a prolonged-release modification via incorporation into a hard fat (Witocan 42/44) matrix. This concept for an ASD has not been published so far. By this, after the initial dissolution of RGF_PVP particles on the extrudate surface, drug release was expected to be controlled by softening of the extrudate and release of RGF_PVP particles over time. No additional water-soluble components were introduced into the dissolution system, which allows better comparability to previous dissolution studies. Witocan 42/44 is powdered hard fat according to Ph. Eur. and exhibits a low melting range from 42 °C to 44 °C, which was desired for extrusion at room temperature to avoid recrystallization of RGF. It is worth to note that Witocan is commonly used in food industries for the formulation of their products and hardly in pharmaceutical products (Breitkreutz et al. 2003). Pharmaceutical coated granules containing sodium benzoate as active substance have been on the market, branded as *Prohippur* by *Lucane Pharma*.

The extrusion process is described in Section 6.2.2.2. Two formulations were extruded, which differed in the ratio RGF_PVP to hard fat, either 50/50 or 80/20 percent by weight, respectively. The total drug load of the extrudates was therefore reduced by this ratio to 10 % and 16 %. A photographic image of the resulting extrudate is provided as Figure 20.

**Figure 20. Extrudate RGF_PVP-Witocan 20/80 after extrusion and cooling. The scale bar is in steps of 1 mm.**

Additionally, SEM images of the extrudates were recorded. As shown in Figure 21, the extrudates are characterized by a smooth and homogeneous surface. Between both formulations, no morphological differences were found.

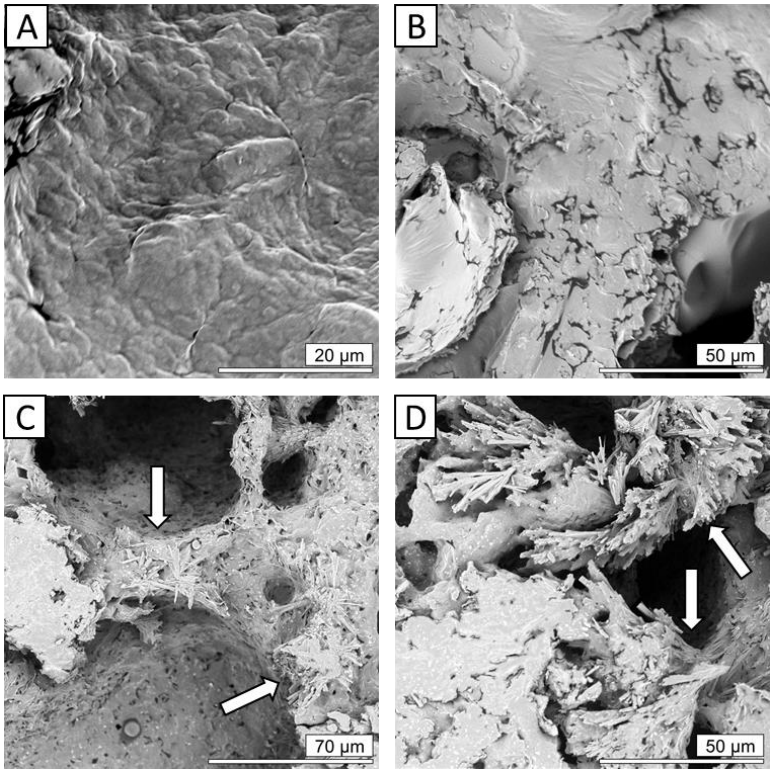


**Figure 21. SEM images of RGF_PVP-Witocan extrudates before (A, B) and after (C, D) dissolution in FaSSIF. Arrows indicate precipitated RGF.**

The prepared extrudate RGF_PVP-Witocan was analyzed by DSC to verify that no recrystallization of RGF during the hot-melt extrusion process occurred. Physical mixtures comprising RGF, PVP, and hard fat did not exhibit the typical RGF patterns in XRPD measurements in transmission mode, indicating an insufficient LOD regarding RGF MH diffractions. Therefore this method was not suitable to investigate the RGF polymorphic state in the prepared extrudates. In Figure 22, the DSC curves of pure hard fat and the extrudate RGF_PVP-Witocan 50/50 are shown exemplarily. In the extrudate sample, the characteristic peak of hard fat was not shifted, although the peak became broader, hinting for either a restructuring or a polymorphic transition of hard fat or an interaction with the embedded system RGF_PVP. Since no characteristic RGF peaks were observed, the amorphous state of RGF_PVP was assumed to have been preserved.

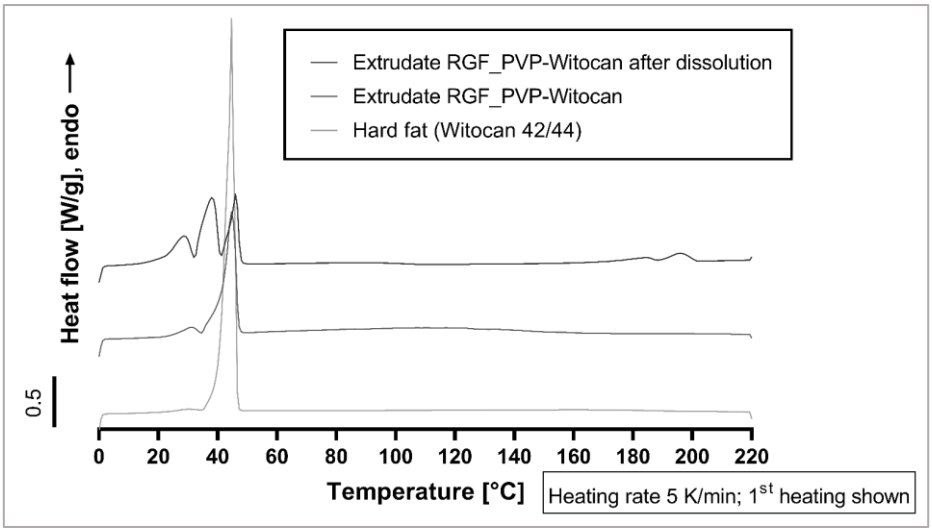


**Figure 22. DSC profiles of the extruded RGF_PVP-Witocan formulation before and after biorelevant dissolution in FaSSIF and pure hard fat (Witocan 42/44).**

### 3.4.1.2 Biorelevant dissolution at FaSSIF conditions

The prepared extrudates were investigated towards their dissolution behavior in FaSSIF, as described in Section 6.2.3.2.1. To allow for comparability between both extrusion formulations and to RGF_PVP powder, the ratio RGF to FaSSIF was kept constant by an increase in applied sample dose.

For the formulation RGF_PVP-Witocan 50/50, no dissolved RGF was detected in the dissolution runs for 24 h. This result might be explained by several hypotheses. The embedding of RGF_PVP particles into the water-insoluble hard fat matrix might have led to complete encapsulation, thus preventing the ASD from being dissolved. Alternatively, RGF could have dissolved into the hard fat matrix during the extrusion process. Further, since no re-crystallization during the extrusion process was detected, precipitation within the extrudate system during the dissolution experiments could be hypothesized. In the next step, the ratio of hard fat to RGF_PVP was shifted towards RGF_PVP, resulting in the formulation of RGF_PVP-Witocan 80/20. This modified formulation was investigated for dissolution in FaSSIF, as described above, the results are shown in Figure 23.

A steady increase in RGF concentration was observed over the dissolution experiment. The achieved supersaturation was quite low with $c_{max}$ of 1.9 µg/mL at 1440 min which is a DS of 3.1, calculated to the solubility of RGF MH in FaSSIF with pre-dissolved PVP.

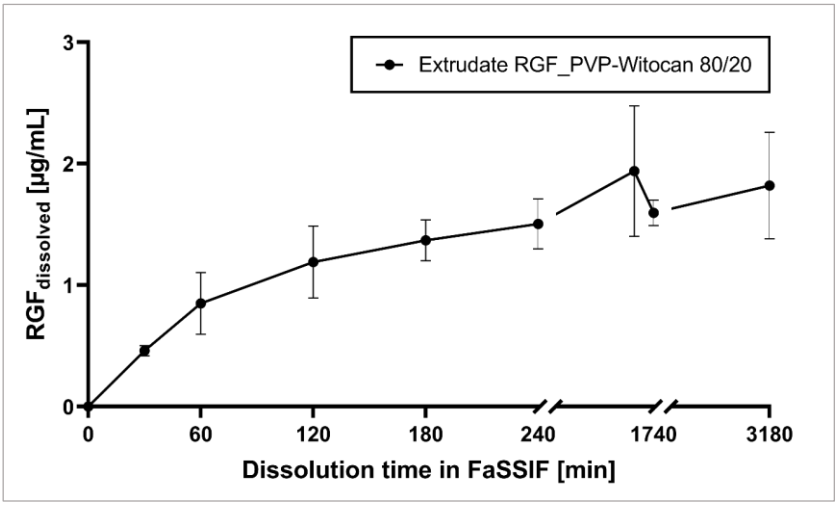


**Figure 23. Biorelevant dissolution testing of RGF_PVP-Witocan 80/20 extrudate in FaSSIF (750 mL, 37 °C, 75 rpm). The dissolved RGF dose is equivalent to one *Stivarga* tablet (40 mg RGF) (n = 2, mean ± s).**

The small extent of dissolved RGF might be explained by kinetic or thermodynamic processes. Although 20 % of hard fat is not expected to completely cover RGF_PVP particles from physical contact with FaSSIF, the hydrophobic and water-insoluble environment might lead to a strongly reduced dissolution rate through limited accessible surfaces. The impact of a material's accessible surface on its dissolution rate was shown in Equation 1. Also, the extrudates did not soften to a relevant extent or even disintegrate which would have liberated RGF_PVP particles to the dissolution system.

These hypotheses are strengthened by the RGF supersaturation which was still present after 3180 min, indicating a strongly decelerated drug release rate and/or parallel processes of ASD dissolution and RGF precipitation. Since a highly lipophilic compound is present at the site of maximum supersaturation, which is the water layer around dissolving ASD particles, RGF precipitation can be assumed to be limiting the dissolution rate, which is further investigated in the following section.

#### 3.4.1.3 Precipitation on hard fat matrix

The extrudates were collected from the dissolution baskets, dried at ambient condition and DSC measurements were conducted. The results are shown in Figure 22. The extrudates after dissolution exhibited endothermic signals at 172 °C and 189 °C onset, which cannot be linked to hard fat or PVP. Therefore, crystalline RGF precipitation on the extrudates during dissolution can be assumed. For further discussion about the physicochemical state of precipitate RGF, the reader is referred to Section 3.5.2.5. SEM images of the extrudates after dissolution were recorded and compared to extrudates before dissolution, as shown in

Figure 21. As mentioned above, before dissolution, the extrudates exhibited a smooth and homogeneous surface (images A and B). After the dissolution studies, the surface of the extrudates were different, as cavities have formed during dissolution. Next to the cavities, various needle stacks could be seen, highlighted by the arrows. As this morphological structure cannot be linked to hard fat, it must be precipitated RGF. From a thermodynamic perspective, this can be explained as follows: Hard fat is a strongly lipophilic substance. Once FaSSIF gets into direct contact with RGF_PVP within the extrudate, the dissolution process starts immediately. The maximum supersaturation during ASD dissolution is expected directly at the site of dissolving ASD particles (Sun and Lee 2015b). Regarding the extruded formulation, the highest RGF supersaturation takes place in direct contact with the lipophilic surface of hard fat, which forced supersaturated RGF to precipitate. Although PVP was proven to stabilize RGF supersaturation, the stabilizing capability was obviously too weak compared to the free enthalpy gain of RGF crystallization onto the hard fat matrix.

By evaluation of the dissolution data, the concept of embedding a fast-release ASD formulation into hard fat to achieve a reduced dissolution rate and ensure longer supersaturation was not successful. Precipitation of RGF on the hard fat surface during dissolution was limiting the supersaturation during dissolution, making BA enhancement improbable. Aside from the dissolution results, the results from these experiments allow insights into the biopharmaceutical difficulties in the formulation of poorly soluble APIs. As discussed in Section 1.2.1, the *in-vivo* situation in the human GIT is quite complex and highly individual. Food effects are known to drastically influence drug bioavailability. For *Stivarga*, the German patient leaflet demands an intake of the

> ‘prescribed dose together with a light, low-fat meal. A light (low-fat) meal consists, for example, of 1 portion of muesli (about 30 g), 1 glass of skimmed milk, 1 slice of toast with jam, 1 glass of apple juice and 1 cup of coffee or tea (520 calories, 2 g fat)’ (Stivarga 40 mg Filmtabletten Gebrauchsinformation 2019).

Since one treatment cycle comprises three weeks of *Stivarga* intake followed by one week without medication, it might be assumed that not the entire patient population will strictly follow the proposed meal scheme every day on treatment. If a more fatty meal is consumed by the patient, or the food scheme is not followed, the therapeutic effect of RGF might be impacted negatively, since RGF was shown to likely precipitate on the lipophilic surface of hard fat. Additionally, RGF bioavailability might be affected towards higher variability, if the fat content during *Stivarga* intake is varying over the medication phase, or to generally

lower RGF plasma levels, if the nutritional state in the GIT shows a high level in fat concentration.

### 3.4.2 Supersaturation stabilization and seeding experiments

#### 3.4.2.1 Concept

The physiological situation in humans is by far more complex than mimicked by dissolution testing using biorelevant media and shows high variations amongst individuals. For instance, the secretion of bile salts or pH of gastric and duodenal fluids can vary within patient population, which is discussed in more detail in the introduction section of this work. Since RGF is approved for the treatment of colon carcinoma, a severe illness, co-medication could further influence the gastrointestinal situation by either co-administration of different crystalline APIs or altering gastric or intestinal propulsions and pH. Additionally, food intake is prone to have an impact on drug bioavailability. The precipitation tendency of supersaturated RGF solutions on the lipophilic surface of hard fat was demonstrated in Section 3.4.1.3. Although hard fat is used in chocolate candies, in this work it shall be rather considered as a surrogate for lipophilic, water-insoluble food components. Co-medication and food effects are just exemplarily chosen factors, highlighting the inter-individual variability of gastrointestinal environment for RGF supersaturation and could be one reason for the observed variability in bioavailability of RGF in the patient population.

The importance of a reliable and sufficient supersaturation for ASD formulations was outlined in previous chapters. However, residual crystalline material in an amorphous formulation, resulting from the manufacturing process or formed during storage, has significant impact on the extent and duration of supersaturation and therefore on BA in patients (Ilevbare et al. 2013). To date, only few research papers are published about stress resistance or supersaturation robustness of generated supersaturation towards manually applied crystal seeds. Alonzo et al. (2012) attributed the presence of crystal seeds a large impact on the degree of supersaturation, even in the presence of a precipitation inhibitor. However, from a practical perspective it may not be possible to always produce ASDs that are completely free of residual crystallinity (Que et al. 2018). This might be due to insufficient process control abilities and limitations in LOD of the crystalline (or re-crystallized) API in quality control departments. The ASD formulations investigated in this work mainly consisted either of polymers or surfactants and RGF, whereas a

pharmaceutical solid drug product is composed of a variety of excipients, some of them in crystalline state. This sample matrix of crystalline excipients is impeding the analytical detection of crystalline or re-crystallized API, especially for contents below 1% drug load (Wanapun et al. 2010).

To evaluate the impact of residual crystals in ASD formulation on the dissolution behavior, seeding dissolution studies were conducted. In this work, RGF MH, the raw material for ASD preparation, and hard fat, which was shown to promote RGF re-crystallization, were used as seeding components. An SEM image of RGF MH is provided in Figure 4 (G).Que et al. (2018) found the available growth area and the interface structure of different crystal seeds to be more relevant for precipitation than the mass of applied seeds. To allow for better comparison, in all seeding dissolution studies the same mass of seeded components was used.

If not stated otherwise, all seeding dissolution studies were performed as described in Section 6.2.3.2.3 in the biorelevant small-scale apparatus.

#### 3.4.2.2 Seeding dissolution studies: The need for a robust supersaturation

The impact of seeding on RGF ASD dissolution was investigated to evaluate the supersaturation stability achieved by different formulations. Small-scale dissolution studies of RGF_PVP and RGF_HPMCAS were conducted to investigate the role of polymer choice for RGF supersaturation stabilization, in comparison to the non-seeded dissolution study results in Section 3.2.5.

At first it was investigated if the co-administration of assumed de-stabilizing substances (e.g. crystal seeds) generally leads to different dissolution results. As such, crystalline RGF MH was chosen since it is the raw material for ASD preparation, and hard fat, which provides a lipophilic surface leading to RGF precipitation, as described in Section 3.4.1.3. The results are shown in Figure 24. For RGF_PVP dissolution without seeding, fast RGF dissolution and unstable supersaturation were observed, indicated by the high standard deviation at $t_{210min}$. The seeding of RGF MH led to a reduced RGF *spring* concentration at $t_{90min,}$ but a drastic decrease of the *parachute* at $t_{210min}$. Also, the de-stabilizing effect of hard fat could be confirmed by comparison of the RGF supersaturation in the *parachute* phase at $t_{210min}$. However, the small number of replicates (n = 3) limits the significance of the experimental results, so the experimental results must not be overinterpreted. On the contrary, RGF_HPMCAS generated RGF supersaturation did not seem to be

affected by RGF MH seeding in the same magnitude as RGF_PVP and the addition of hard fat did not lead to a decrease in RGF supersaturation.

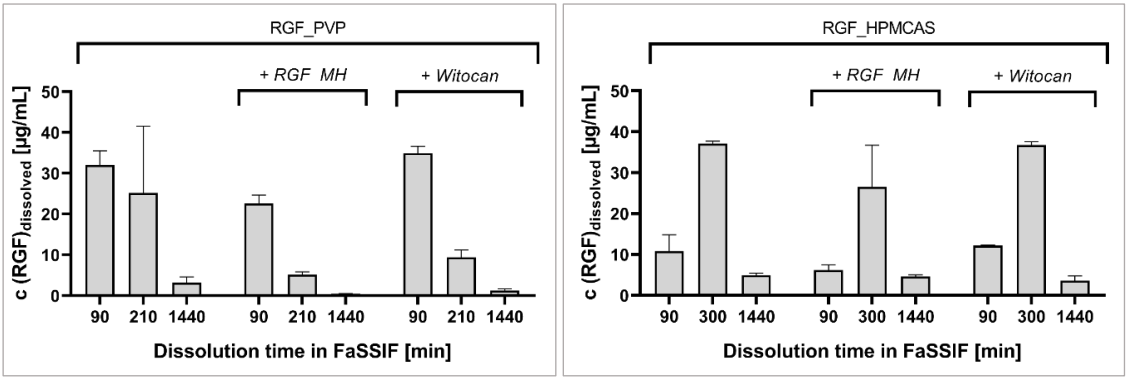


**Figure 24. Influence of RGF MH and hard fat (Witocan) seeding on dissolution behavior of ASDs RGF_PVP and RGF_HPMCAS. Biorelevant small-scale dissolution studies were performed (50 mL, 37 °C), the dissolved RGF dose (2.7 mg) is equivalent to one *Stivarga* tablet (40 mg RGF) in 750 mL. Seeded substances are named in *italic* (n = 3, mean ± s).**

It was not only the general drug release profile which was influenced by the matrix polymer, as expected from the dissolution studies in Section 3.2.3, but also the maintenance of the supersaturated RGF in solution in the presence of crystal seeds. Both observations can be explained and connected by the strength of molecular interactions between polymer and API, such as π-electron interaction or hydrogen bonding. The stronger the molecular interactions between both components, the lower is the dissolution rate to be expected, as these interactions have to be broken during the dissolution process. Accordingly, in the supersaturated state, stronger interactions could provide a more stable and robust supersaturation towards seeded crystalline API. These findings are in accordance with dissolution studies of ternary ASDs, comprising two polymers and RGF. As described in Section 3.3.1.3, even a small quantity of 5% HPCMAS in the ASD matrix drastically reduced RGF release, probably due to inhomogeneous RGF distribution, thus an RGF enrichment at HPMCAS polymer chains, caused during preparation by thermodynamically more stable interactions between RGF and HPMCAS than between RGF and PVP.

#### 3.4.2.3 Stabilizing polymer co-administration and seeding of hydrophilic non-soluble substances

The influence of hard fat seeding on RGF superstation was shown, although hard fat is insoluble in aqueous media and solely offers its lipophilic surface as a favorable site for precipitation. As a negative control for hard fat seeding, barium sulfate ($BaSO_4$) was used,

as it is also an insoluble compound, but as an ionic salt compound providing a hydrophilic surface to the supersaturated system (Hua et al. 2014). Additionally, the impact of co-administration of PVP or HPMCAS for RGF_HPMCAS and RGF_PVP, respectively, was investigated. Previous experiments demonstrated the superior RGF supersaturation stabilization of HPMCAS compared to PVP. As discussed in Section 3.3.1.3, embedding HPMCAS into the ASD polymer matrix led to a decreased release rate, but high supersaturation.

The results are shown in Figure 25. The percentage values for polymer addition are calculated to the polymer mass in RGF_PVP, specific information is provided in Section 6.2.2.1. Regarding the impact of $BaSO_4$ to the dissolution performance of ASDs with RGF, no clear effect could be observed for both formulations. As expected, $BaSO_4$, as a hydrophilic but insoluble compound, did not influence the dissolution-supersaturation-precipitation interplay of RGF, in contrast to hard fat.

For RGF_HPMCAS, co-administration of PVP powder did not affect the dissolution results, however, HPMCAS powder co-administration to RGF_PVP led to remarkable dissolution results. The dissolution results of RGF_PVP + 100% HPMCAS showed a fast release, as expected for RGF_PVP, but also high supersaturation at $t_{231min}$. Comparison to the reference dissolution of RGF_PVP dissolution in the same experiment without additional HPMCAS demonstrates the superior dissolution performance in the *parachute* phase by co-administration of HPMCAS powder.

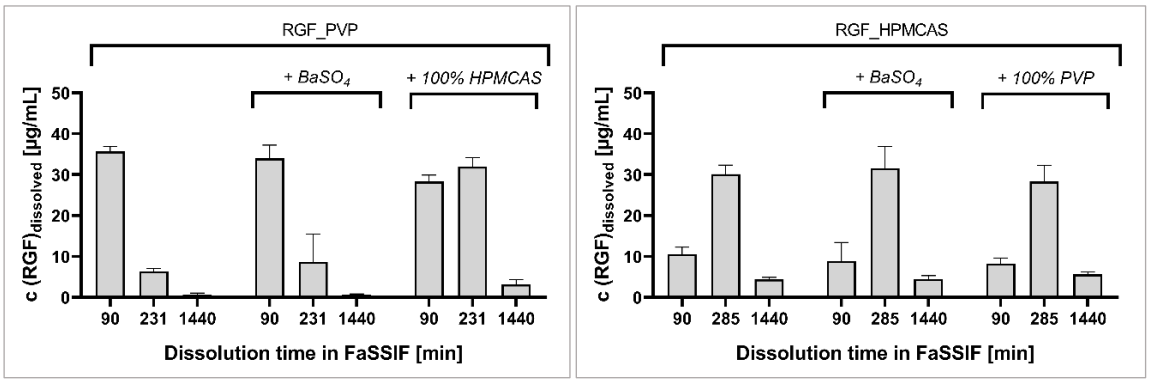


**Figure 25. Influence of barium sulfate (BaSO4) and PVP or HPMCAS seeding on dissolution behavior of ASDs RGF_PVP and RGF_HPMCAS. The percentage numbers reflect polymer addition calculated to the polymer mass in the ASD. Biorelevant small-scale dissolution studies were performed (50 mL, 37 °C), the dissolved RGF dose (2.7 mg) is equivalent to one *Stivarga* tablet (40 mg RGF) in 750 mL. Seeded substances are named in *italic* (n = 3, mean ± s).**

The mechanism behind the stabilization is to be further explored in the following sections. So far, the system RGF_PVP + 100% HPMCAS shows superior dissolution results in FaSSIF, compared to all formulation strategies discussed above, as it provides the desired dissolution profile of fast release *(spring)* and a long-lasting and high supersaturation *(parachute)*.

#### 3.4.2.4 *Stivarga* excipients seeding

In a further experiment, the formulation excipients from *Stivarga* were investigated for stabilizing or destabilizing effects towards RGF_PVP generated RGF supersaturation. The excipients used in *Stivarga* tablet core formulation are microcrystalline cellulose (MCC), cross-linked sodium carboxymethyl cellulose (Na-CMCx), magnesium stearate (MgSt), PVP, and colloidal anhydrous silica (Stivarga product monograph, 2020).

For the excipient screening, MCC, Na-CMCx, and MgSt were chosen to be investigated. MCC is known to be partly crystalline and therefore might promote RGF crystallization on crystalline sites (Suzuki and Nakagami 1998). Na-CMCx was chosen since during manufacturing RGF_PVP is spray-dried together with Na-CMCx, so an intimate contact during dissolution is given. Na-CMCx and MCC are not water-soluble but swellable, so possible effects would be caused by surface interactions, as observed for hard fat.

The ratio of seeded excipients to ASD was equal to the ratio of the components in the *Stivarga* tablet (*Bayer* internal data). The lubricant MgSt is a lipophilic substance and typically used in low concentration. According to the supplier, particle sizes determined by laser diffraction are reported to be $\geq 1$ µm, 3 – 7 µm, and $\leq 20$ µm for $d_{10}$, $d_{50}$, and $d_{90}$, respectively. To more clearly observe any possible effects and for weighing precision, the MgSt concentration was increased tenfold. The results are presented in Figure 26.

For MCC and Na-CMCx, neither a stabilizing nor a de-stabilizing effect was observed. Only the lipophilic MgSt showed a decrease of RGF supersaturation, which is in accordance with the results obtained from hard fat seeding, but the 10-fold increase in concentration has to be taken into consideration. It can be concluded that the *Stivarga* excipients investigated do not influence RGF supersaturation in a stabilizing or de-stabilizing manner in the chosen experimental setup.

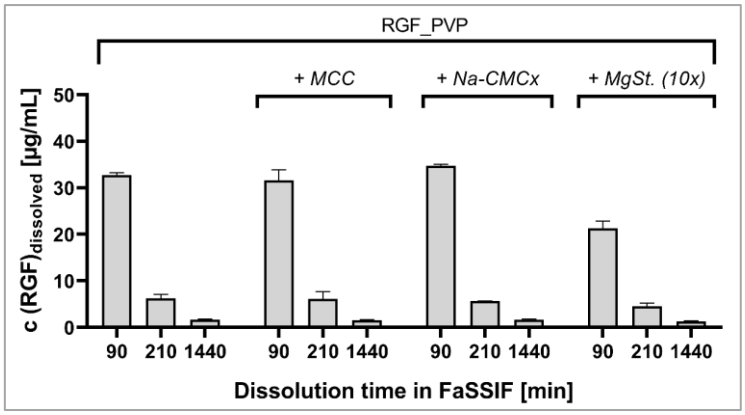


**Figure 26. Influence of seeded *Stivarga* excipients on RGF_PVP dissolution performance. Biorelevant small-scale dissolution studies were performed (50 mL, 37 °C), the dissolved RGF dose (2.7 mg) is equivalent to one *Stivarga* tablet (40 mg RGF) in 750 mL. Seeded substances are named in *italic* (n = 3, mean ± s).**

### 3.4.2.5 HPMCAS co-administration: Stabilization of RGF_PVP generated RGF supersaturation

The advantages of co-administration of HPMCAS powder with RGF_PVP were shown in Figure 25. However, the total mass of stabilizing polymers was doubled in that study. To distinguish between an effect caused just by elevated polymer concentration and specific HPMCAS-related effect, the supersaturation stabilization abilities of PVP and HPMCAS were compared, both co-administered to RGF_PVP in the same mass ratio. For better differentiation regarding RGF supersaturation stabilization, the de-stabilizing compounds RGF MH and hard fat were applied as seeding for both test groups to stress the RGF supersaturation.

The results are presented in Figure 27. For the formulation RGF_PVP + 100% PVP, no benefit in co-administration of PVP could be observed. Analogous to the dissolution results from Section 3.4.2.2, seeding of RGF MH or hard fat led to RGF precipitation, whereas the effect was more pronounced for RGF MH seeding. However, under seeding with RGF MH and hard fat, the system RGF_PVP + 100% HPMCAS still exhibited the desired dissolution profile, as such fast release *(spring)* and high and robust supersaturation *(parachute)*.

As mentioned above, residual crystallinity in ASD products cannot be always detected analytically, hence prevented. It can be assumed from this *in-vitro* data that for the formulation concept RGF_PVP + 100% HPMCAS, residual RGF crystals would possibly not impede the BA in patients as this would be the case for the *Stivarga* formulation RGF_PVP. Nevertheless, the predictability is limited from these results since the robustness was proven against RGF MH as the bulk material and not against precipitated

RGF from biorelevant dissolution experiments, which leads to different RGF modifications, as described in Section 3.5. Different modifications of crystal seeds were shown in literature to impair drug supersaturation differently. Exemplarily for paclitaxel, the available growth area and interface structure of different crystal seeds were found to be more relevant for drug precipitation from supersaturation rather than the mass of crystal seeds (Que et al. 2018).

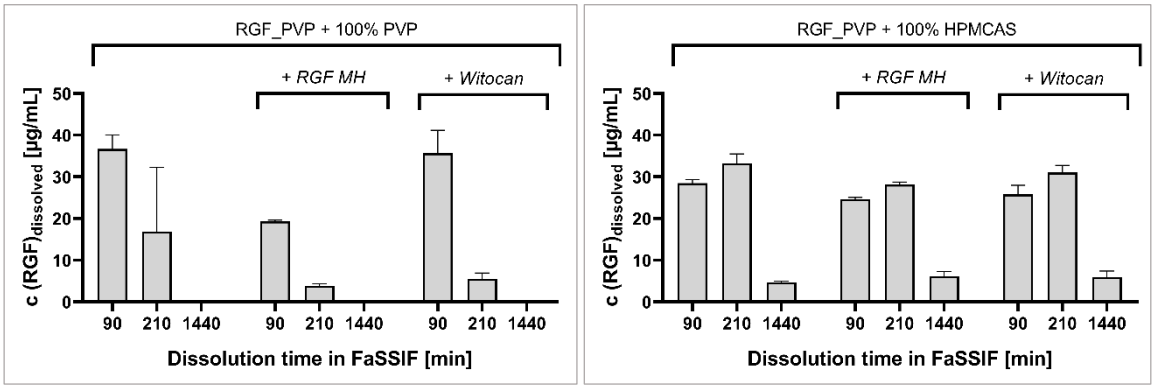


**Figure 27. Influence of RGF MH and hard fat (Witocan) seeding on dissolution behavior of RGF_PVP, co-administered with stabilizing polymer. The percentage numbers reflect polymer addition calculated to the polymer mass in the ASD. Biorelevant small-scale dissolution studies were performed (50 mL, 37 °C), the dissolved RGF dose (2.7 mg) is equivalent to one *Stivarga* tablet (40 mg RGF) in 750 mL. Seeded substances are named in *italic* (n = 3, mean ± s).**

The presented formulation concept of embedding the API into a fast-release ASD matrix together with a co-administered stabilizing polymer was first proposed by Xie and Taylor (2016a) for celecoxib with PVP K12 as matrix polymer and small amounts of HPMC or HPMCAS as crystallization inhibitors, added as a separate component from the ASD matrix. However, in the present study a practical relevance for an existing, marketed drug product is shown for the first time.

#### 3.4.2.6 HPMCAS co-administration: Concentration study

HPMCAS was a suitable precipitation inhibitor for RGF_PVP co-administration, as the formulation approach RGF_PVP + 100% HPMCAS combined fast drug release kinetics with a high and robust supersaturation. As a next step, the necessary amount of HPMCAS co-administration was investigated. The results are presented in Figure 28. The amount of HPMCAS was reduced down to 5 % of the incorporated PVP in RGF_PVP. For all HPMCAS amounts, a strong supersaturation at $t_{258min}$ was observed. One-way ANOVA analysis for means ± SD confirms that at $t_{258min}$ the differences in RGF concentration were not significantly different (p=0.1412). For $t_{90min}$ data points, only 20 % HPMCAS co-

administration differed significantly from the remaining values, which might be explained by experimental variation, likewise for the $t_{1440min}$ values.

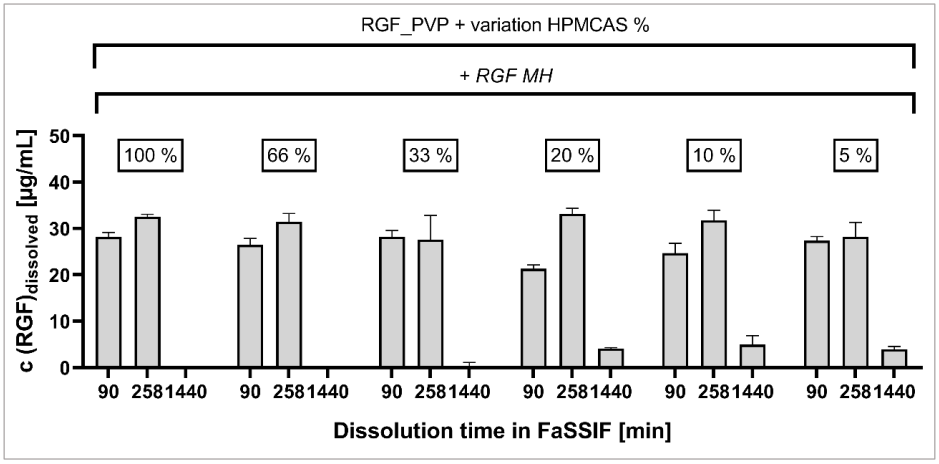


**Figure 28. Influence of amount co-administered HPMCAS to stabilize RGF supersaturation under RGF MH seeding (n = 3, mean ± s). The percentage numbers reflect HPMCAS addition in % to the polymer mass in the ASD. Biorelevant small-scale dissolution studies were performed (50 mL, 37 °C), the dissolved RGF dose (2.7 mg) is equivalent to one *Stivarga* tablet (40 mg RGF) in 750 mL.**

For RGF_PVP + 5 % HPMCAS, the co-administered HPMCAS results in an HPMCAS concentration in FaSSIF of 10.7 µg/mL, which is comparable to the results obtained by Xie and Taylor (2016a), who found ca. 5 µg/mL HPMCAS sufficient for celecoxib supersaturation stabilization. Since co-administration of 5 % did not show reduced stability against RGF MH seeding compared to higher HPMCAS amounts, a further decrease in the amount of co-administered HPMCAS might be possible. These results indicate that even small quantities of HPMCAS allow for successful RGF supersaturation stabilization, even at RGF MH seeding. For a single *Stivarga* tablet, a co-administration of 8 mg HPMCAS would be sufficient, which could be realized in practice by incorporation of HPMCAS into the powder blend with other excipients.

#### 3.4.2.7 HPMCAS co-administration: Grade comparison

Several grades of HPMCAS are marketed in Europe. For this work, the commercially available HPMCAS grades Affinisol AS 716G, 126G, and 912G were compared regarding their RGF supersaturation stabilization potential. Up to this section, HPMCAS 716 was used exclusively for formulation studies and should be compared to related grades. As discussed in Section 1.1.3.2, these grades differ mainly in acetate and succinate substitution levels and chain length and therefore in physicochemical properties, for example, the

minimum pH for solubility. More importantly, the tendency of the polymer to form molecular interactions with RGF might be affected by the different substitution grades, since the substituents introduce hydrogen bonding sites or π-electrons via the $sp^2$-hybridized carbon and the oxygen. Therefore, the most suitable partner for RGF had to be found experimentally. In Figure 29, the different types of HPMCAS are compared under seeding of RGF MH.

The results show the superior RGF stabilization by HPMCAS 716, as at $t_{90min}$ and $t_{258min}$ the dissolved RGF concentration was higher compared to HPMCAS 912 and HPMCAS 126. Although HPMCAS 126 co-administration led to higher RGF supersaturation at $t_{1440min}$, HPMCAS 716 is favorable because of the higher reproducibility and faster drug release. However, careful data interpretation is adequate to avoid overinterpretation, since a small number of replicates (n = 3) was chosen. As described in Section 1.2.1, the major absorption site in humans is the small intestine, therefore the generated supersaturation at 24 h after drug intake is not of relevance since the drug will have passed the absorption window.

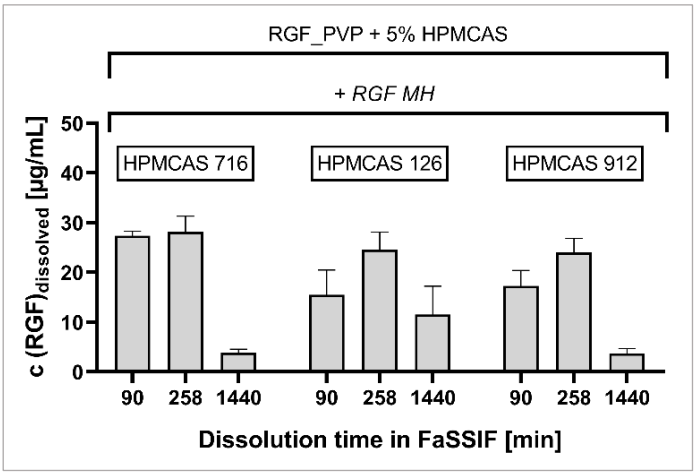


**Figure 29. Influence of co-administered HPMCAS type to stabilize RGF supersaturation. The percentage number reflects polymer addition calculated to the polymer mass in the ASD. Biorelevant small-scale dissolution studies were performed (50 mL, 37 °C), the dissolved RGF dose (2.7 mg) is equivalent to one *Stivarga* tablet (40 mg RGF) in 750 mL. Seeded substances are named in *italic* (n = 3, mean ± s).**

Based on these results, the formulation concept of RGF_PVP and HPMCAS 716 co-administration was proven to be superior regarding the dissolution performance in FaSSIF compared to all formulation approaches presented in this work. HPMCAS 716 is characterized by the highest succinate substitution level of all investigated HPMCAS grades. Thus, the stronger RGF supersaturation stabilization might be attributed to either a

direct interaction of RGF and the succinate groups, such as π-electrons or H-bondings, or an ionic interaction, since HPMCAS 716 is expected to exhibit the greatest number of negatively charged sites of all HPMCAS grades. For all further dissolution studies, the formulation strategy RGF_PVP + HPMCAS 716 was chosen, with polymer co-administration of 5 % or 10 %.

#### 3.4.2.8 HPMCAS co-administration: Mechanistic understanding

The mechanistic reasons behind the stronger interactions between RGF and HPMCAS compared to RGF and PVP will be outlined in this section.

In some formulation studies before, HPMCAS resulted in better API supersaturation stabilization compared to PVP, e.g. Raina et al. (2015) compared the crystallization inhibitory potential of several commonly used polymers for six drugs of the dihydropyridine class. In their study, polymers with intermediate hydrophobicity-hydrophilicity (e.g. HPMCAS) clearly outperformed strongly hydrophilic or hydrophobic polymers (e.g. PVP) by stabilization of both phases, the aqueous supersaturation and the droplet phase formed during ALPS. These findings are in full alignment with a study by Khan et al. (2016c).The authors conclude that stabilization of the hydrophobic drug-rich phase and the aqueous phase is a prerequisite for supersaturation stabilization and demonstrated the superiority of intermediate hydrophobic-hydrophilic polymers. The mechanism behind the stabilization of drug-rich droplets by HPMCAS was attributed to the incorporation of HPMCAS into these hydrophobic structures (Wang et al. 2018b). In addition, specific interactions of the stabilizing polymer and the API play an important role. Chen and coworkers reported specific H-bonding interactions for PVP with a lipophilic, poorly soluble compound which were shown to be ‘water-vulnerable’, as water moles are competing for the binding sites. In contrast, unspecific hydrophobic, yet ‘water-resistant’ interactions were described for HPMCAS and the drug, leading to superior crystallization inhibition (Chen et al. 2018).

These findings can be underlined by the results of this work, as the more hydrophilic PVP showed less RGF supersaturation stabilization compared to HPMCAS. Since RGF is a highly lipophilic molecule and possesses secondary amine (–NH) and carboxylic structures, unspecific lipophilic interactions and specific H-bonding are expected to occur.

However, deeper insights into the mechanism of drug supersaturation stabilization can be provided by direct *in-situ* determination in solution, but common methods are not feasible in this experimental setup (Price et al. 2019). The experiments had to be performed in FaSSIF which exhibits a diverse analytical matrix, composed of bile salts. The interplay of dissolution, supersaturation, ALPS, interaction polymer-API, micelle formation, and precipitation was discussed in the introduction section, hence investigation solely in water could yield some results, but would not reflect the situation present in *in-vitro* dissolution experiments, not to mention the more complex situation *in-vivo*. Further, FaSSIF was necessary since the crystalline solubility of RGF in distilled water is below the LOQ of the applied HPLC/UV technique and would require HPLC-MS coupling (mass spectroscopy detection), which was not available for this study, to gain information about the observed interactions over the dissolution time. The addition of solubilizing detergents or organic solvents could influence the interactions of polymer and API, thus limit the prediction for the *in-vivo* situation.

The molecular constitution of HPMCAS in aqueous solutions at different pH was discussed in Section 1.1.3.2. In short, HPMCAS forms colloidal structures in water at intestinal pH together with the API. Here, the hydrophobic nature of the substituents promotes interactions between the polymer and the API whereas the negatively charged carboxylic substituents keep these nanostructures stable (Chavan et al. 2019). However, HPMC does not possess acetate and succinate substituents, still providing sufficient supersaturation stabilization properties comparable to HPMCAS (Bevernage et al. 2011; Xu and Dai 2013). To evaluate the role of hydrophobic and negatively charged carboxylic substituents in HPMCAS, HPMC was chosen as a co-administered stabilizing agent for comparison to HPMCAS. For a better comparison between HPMC and HPMCAS, a similar HPMC grade to HPMCAS 716G was provided by the supplier, the characteristics are listed in Table 14. The exact molecular weight of both materials was not provided, so the dynamic viscosity of a 2 % aqueous solution will serve as an indicator for comparison (Rowe 1980).

**Table 14. Comparison of applied HPMC and HPMCAS grades.**

| Material / Substituents | HPMCAS: Affinisol AS 716 | HPMC: Methocel E3 Premium LV HP |
|---|---|---|
| Methoxyl [%] | 20.0 – 24.0 | 28 – 30 |
| Hydroxypropyl [%] | 5.0 – 9.0 | 7 – 12 |
| Viscosity, 2.0 % in water [mPa·s] | 2.4 – 3.6 | 2.4 – 3.6 |
| Molecular weight | 134,400 * | not published by supplier |

* Supplier refers to publication from Chen et al. 2011.

A biorelevant dissolution study was performed to compare RGF supersaturation stabilization ability of HPMC to HPMCAS under RGF MH seeding conditions, the results are shown in Figure 30. As expected from the previous experiments, HPMCAS co-administration led to fast RGF release and high supersaturation for at least 258 min. Interestingly, also HPMC showed stabilizing properties, even more pronounced than HPMCAS. From these results, it can be concluded that the dominant mechanism of RGF supersaturation stabilization by HPMCAS is not caused by the acetate and succinate functional groups, hence different types of cellulosic polymers might be suitable as stabilizing agents.

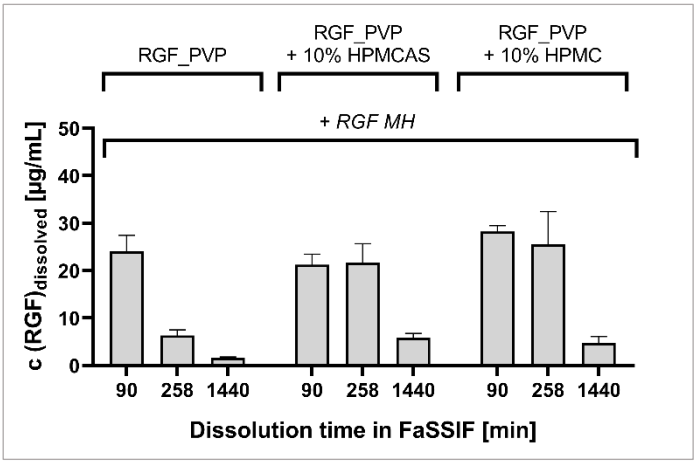


**Figure 30. Comparison of co-administered HPMCAS to HPMC to stabilize RGF supersaturation. Biorelevant small-scale dissolution studies were performed (50 mL, 37 °C), the dissolved RGF dose (2.7 mg) is equivalent to one *Stivarga* tablet (40 mg RGF) in 750 mL. The percentage numbers reflect polymer addition calculated to the polymer mass in the ASD. Seeded substances are named in *italic* (n = 3, mean ± s).**

To conclude, the dominant mechanism of the interaction HPMCAS – RGF cannot be explained by π-electrons from the acetate or succinate groups. As described above, the

formation of micellar structures of supersaturated drug with the polymer is assumed to be the dominant effect for RGF supersaturation stabilization by HPMC and HPMCAS.

#### 3.4.2.9 Reproducibility: The role of HPMCAS on RGF ASD formulations

To ensure the validity of the findings regarding the influence of HPMCAS on RGF dissolution and supersaturation behavior, a reproducibility experiment was performed. In Figure 31, the formulation concepts of RGF_PVP as the starting point of formulation development, the developed formulation RGF_PVP + HPMCAS, and the ternary ASD formulation comprising both polymers inside the ASD matrix were compared. To allow comparison between different formulation concepts, the same amount of HPMCAS was used for co-administration and incorporation into the ASD matrix, hence the stabilizing polymer was either externally administered or embedded into the ASD matrix. To mimic a stress situation for RGF supersaturation, RGF MH seeding conditions were chosen.

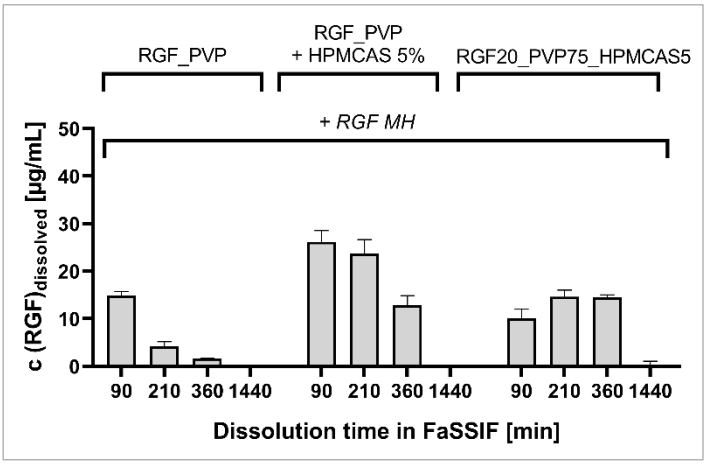


**Figure 31. Comparison of ternary ASD formulation and co-administration of HPMCAS regarding RGF supersaturation. Formulation codes are explained in the text. Biorelevant small-scale dissolution studies were performed (50 mL, 37 °C), the dissolved RGF dose (2.7 mg) is equivalent to one *Stivarga* tablet (40 mg RGF) in 750 mL. Seeded substances are named in *italic* (n = 3, mean ± s).**

The resulting dissolution graph confirms the previous findings and considerations. As expected, the binary formulation RGF_PVP shows strong precipitation of supersaturated RGF in presence of RGF MH seeds. The ternary formulation RGF20_PVP75_HPMCAS5 exhibits slower drug release and precipitation of supersaturated RGF. Exclusively the new formulation approach RGF_PVP + 5% HPMCAS shows the target dissolution profile of fast RGF release kinetics *(spring)* followed by a robust and high supersaturation *(parachute)*, although some RGF precipitation from $t_{210min}$ to $t_{360min}$ could be observed. As

mentioned earlier, the small number of replicates has to be considered to avoid overinterpretation of the experimental results.

### 3.4.3 Viscosity

An increase in dissolution media viscosity was described to cause precipitation inhibition from supersaturated systems (Chavan et al. 2019; Xu and Dai 2013). This can be explained by the Stokes-Einstein equation (Equation 2) by which the diffusion coefficient $D$ is inversively correlated with dynamic viscosity $\eta$. Further, the dissolution rate $dc/dt$, described by the Noyes-Whitney and Nernst-Brunner equation (Equation 1) is dependent on $D$ and high $dc/dt$ was described to be a driver for drug precipitation (Sun and Lee 2015b). Therefore, the role of PVP and HPMCAS towards a possible increase in dynamic viscosity was investigated. Both polymers were dissolved in FaSSIF, the concentrations chosen were calculated to mimic the situation in dissolution experiments after full ASD dissolution, as such 0.21 mg/mL PVP and 10.7 µg/mL HPMCAS were chosen, to mimic the formulation RGF_PVP + 5% HPMCAS. The experimental setup is described in detail in Section 6.2.3.4.9, the resulting viscosities are graphed in Figure 32. No significant differences in viscosities were found, so the stabilization of RGF supersaturation must be caused by intermolecular interactions rather than the physical effect of viscosity enhancement.

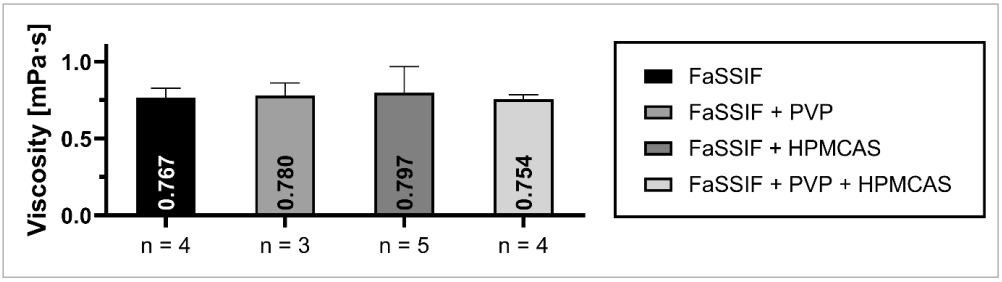


**Figure 32. Viscosity measurements of biorelevant dissolution medium with pre-dissolved polymers at 37 °C (mean ± s). The number of experimental repetitions is given below each bar.**

### 3.4.4 The need for gastric fluid protection by enteric coating

In this chapter, a new formulation approach for ASDs with RGF was developed and proven to show superior results in FaSSIF dissolution, even under seeding conditions.

This approach is based on the formulation RGF_PVP, which did not show satisfying robustness in biorelevant simulated transfer dissolution studies, described in

Section 3.2.4.2. Co-administration of HPMC and HPMCAS was demonstrated to stabilize RGF supersaturation at RGF MH seeding conditions, by increasing supersaturation robustness. Since HPMCAS is not soluble in gastric pH, it was not expected to have a stabilizing effect during the simulated gastric transfer. However, different HPMCAS grades were included in this study, as the different substitutions lead to differences in pH-dependent solubility (Chavan et al. 2019; Friesen et al. 2008).

The results are presented in Figure 33. Within this dissolution experiment, different formulations were compared in simulated stress scenarios, comprising 120 min gastric transfer with or without RGF MH seeding. The dissolution performance of RGF_PVP (A) after conversion to FaSSIF conditions was poor, as expected from previous experiments. The resulting RGF concentration was even lower when RGF MH seeds were present (C). The stabilizing agent HPMCAS did only work as such to a small extent in FaSSGF media, as HPMCAS is insoluble at low pH, so only a very small proportion will be dissolved thus providing crystallization inhibition. Therefore, the dissolution profiles of RGF_PVP with (B) or without (A) co-administered HPMCAS were found to be similar, although with slightly higher RGF concentration in presence of HPMCAS. Further, seeding of RGF MH showed little effect in presence of HPMCAS (D vs. B). None of the investigated HPMCAS grades (D, E, F) could prevent RGF_PVP from precipitation during FaSSGF transfer, but HPMCAS 716 showed best results by means of highest RGF concentrations and smallest standard deviations, however, the results from this study are not satisfying for practical use.

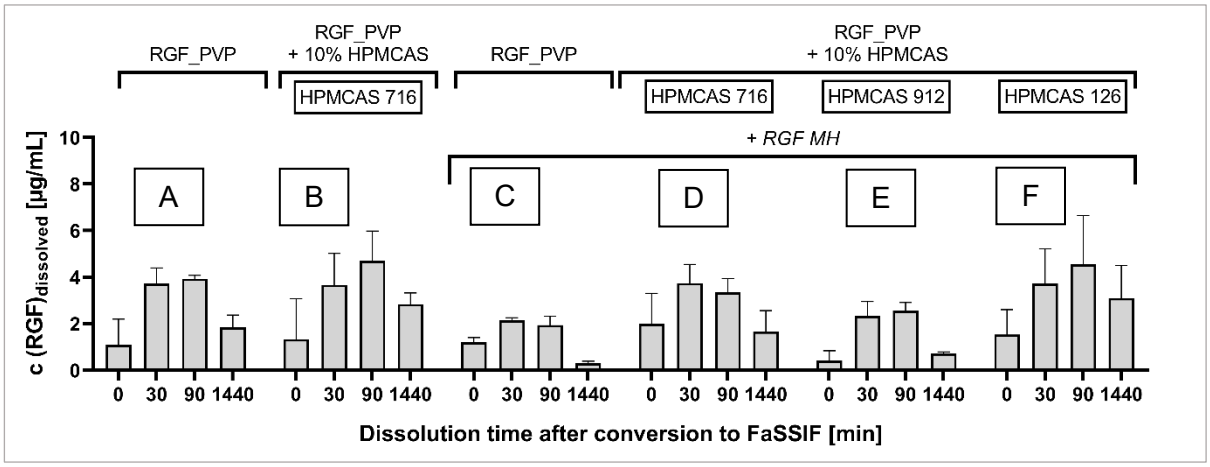


**Figure 33. Small-scale transfer dissolution studies with 120 min simulated gastric conditions. The percentage numbers reflect polymer addition calculated to the polymer mass in the ASD. Dissolution was performed at 37 °C in 20 mL FaSSGF prior to addition of 40 mL FaSSIF$_{conc.}$, the dissolved RGF dose (3.2 mg) is equivalent to one *Stivarga* tablet (40 mg RGF) in 750 mL. Seeded substances are named in *italic* (n = 3, mean ± s).**

From these results, it can be concluded that gastric fluid protection of the system RGF_PVP in humans could increase the *in-vivo* performance of ASDs with RGF by reducing the inter-patient variability, which will be further investigated in the following section.

### 3.4.5 New formulation approach: HPMCAS coating of *Stivarga* tablets

#### 3.4.5.1 Concept

The most common strategy to prevent drug release from a solid dosage form before it reaches the small intestine is a so-called *enteric coating*, at which a polymer with pH-dependent solubility forms an outer film layer around the tablet core. Once the dosage form has reached the small intestine, the polymer film dissolves and tablet core disintegration followed by dissolution will occur. This concept has been widely applied to protect a drug from dissolution in the stomach (Maderuelo et al. 2019; Singh et al. 2012).

Bevernage et al. (2012b) stated supersaturation stability of the drugs loviride, glibenclamide, danazol, itraconazole, and etravirine in human gastric fluids to be in general inferior compared to intestinal fluids, hence drug supersaturation should be targeted to the intestine. In this work, the approach of an enteric coating with HPMCAS was chosen. This concept is based on a dual function of HPMCAS. First, by coating of HPMCAS 716 on a *Stivarga* tablet, dissolution of the film and subsequently of the tablet will occur after media change to FaSSIF. Regarding the *in-vivo* situation, after the tablet has left the stomach by passing the pylorus, dissolution of the HPMCAS film will enable the *Stivarga* tablet to disintegrate, thus release RGF, at the small intestine which is the site of absorption. Therefore, the dissolution of the HPMCAS film, tablet disintegration, and RGF release will occur at the same site in the human gastrointestinal tract which ensures the spatial proximity between the dissolved API and HPMCAS. In this case, HPMCAS could additionally act as a stabilizing agent for the RGF supersaturation, generated by the dissolution of RGF_PVP, which is the basis formulation of *Stivarga*. This dual function of HPMCAS could increase *Stivarga* stability during gastric transfer and lead to the desired dissolution profile of a fast dissolution *(spring)* with stable supersaturation *(parachute)* in the small intestine. The ability of HPMCAS to act as a film former for enteric coating was shown for tablets containing theophylline and sulfapyridine (Tanno et al. 2008).

*Stivarga* tablets are film-coated tablets, containing polyvinyl alcohol (PVA) as film-forming polymer (Stivarga product monograph, 2020). Marketed *Stivarga* tablets were coated as described in Section 6.2.2.3 and process parameters during coating were

recorded, as listed in Table 32 (Appendix). The additional HPMCAS coating will form a second coating on the PVA film.

A coating mass per tablet of 20.14 mg was achieved, so the formulation can be considered as RGF_PVP + 12.6 % HPMCAS. As shown in Section 3.4.2.6, the stabilizing effect of HPMCAS was given over a large range of concentrations, so the difference between 10 % and 12.6 % can be considered negligible.

The coated tablets were dried overnight to ensure complete solvent evaporation. In Figure 34 an original *Stivarga* tablet and an HPMCAS coated tablet are presented. The general appearance did not change during the coating process, although the additional coating was visible as an opaque film. In the following, HPMCAS coated *Stivarga* tablets will be named 'Stivarga_HPMCAS'.


**Figure 34. Left: original *Stivarga* tablet. Right: HPMCAS coated *Stivarga* tablet. Tablet core size is 16 x 7 mm.**

### 3.4.5.2 Coating integrity

The HPMCAS film coating was investigated via X-ray micro-computed tomography (µCT) and disintegration according to Ph. Eur. 10, which is described below. The procedure of µCT measurements is specified in Section 6.2.3.4.8. From the obtained data, no defects in HPMCAS film coating could be found by manual scrolling through the image stack. The coating thickness was calculated and compared to an original *Stivarga* tablet, which did not undergo a second coating process to ensure that no change in the original film has occurred. An exemplary µCT image of a *Stivarga* tablet is shown in Figure 35 and of Stivarga_HPMCAS in Figure 36. The determination of PVA coating thickness in original *Stivarga* tablets revealed considerable variations in coating thickness. At the exemplary measurement in Figure 35, a PVA film thickness of 36.8 µm was determined.

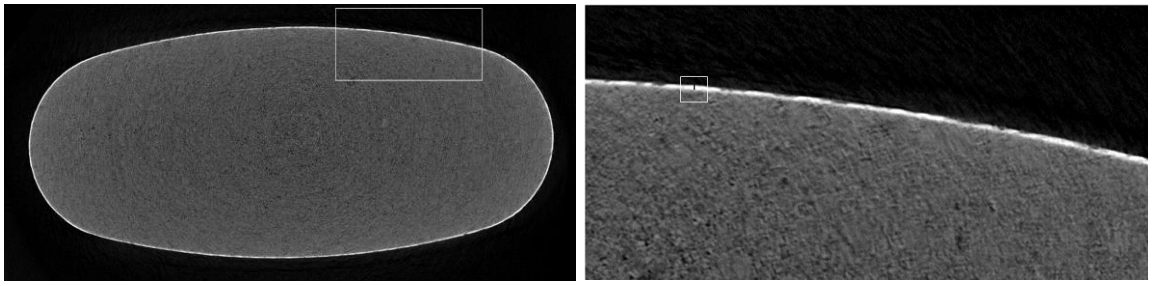

**Figure 35. Exemplary µCT images of a *Stivarga* tablet. Left: Cross-sectional view through a *Stivarga* tablet. The frame indicates the magnified section on the right. Right: Coating thickness measurement position is indicated by a frame and measured pixels are shown as black bars. Tablet core size is 16 x 7 mm.**

For Stivarga_HPMCAS, four measurement positions are shown in Figure 36. The PVA film thickness was determined to range from ca. 15 µm to 44.7 µm and the HPMCAS film thickness was from 34.0 µm to 50.2 µm.

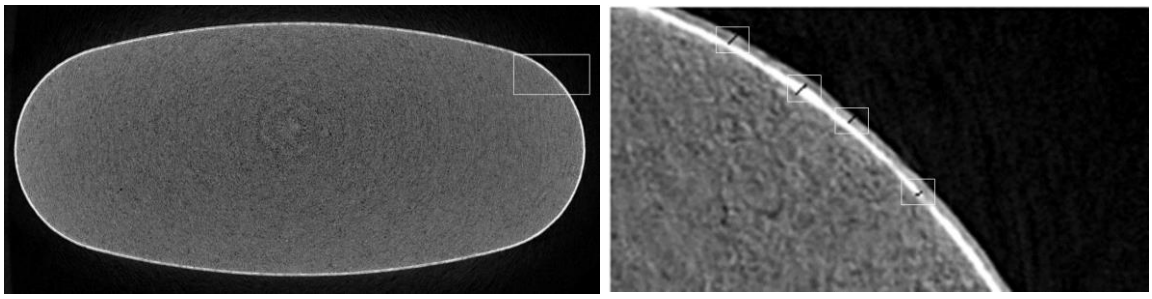

**Figure 36. Exemplary µCT images of Stivarga_HPMCAS tablet. Left: Cross-sectional view of the tablet. The frame indicates the magnified section on the right. Right: Coating thickness measurement positions are indicated by the black bars in the frames and measured pixels are shown as black bars. Tablet core size is 16 x 7 mm.**

µCT analysis of HPMCAS coating on *Stivarga* tablets revealed a consistent HPMCAS film on the tablets. Although some fluctuations in PVA film thickness were detected, it can be anticipated that these small variations would not lead to *in-vivo* implications, as e.g. different disintegration behavior, because PVA possesses good solubility in aqueous media and is usually applied for light and moisture protection during storage (Teckoe et al. 2013).

#### 3.4.5.3 Disintegration test of HPMCAS coated tablets

The produced Stivarga_HPMCAS tablets were investigated for disintegration time according to Ph. Eur. 10 (monograph 2.9.1). As the HPMCAS coating is considered to achieve enteric coating functionality, the test specimen for enteric-coated dosage form was chosen, as explained in Section 6.2.3.4.12. Figure 37 shows the tablets between media change from 0.1 M HCl to phosphate buffer pH 6.8. To pass the test requirements of gastric-resistant tablets according to Ph. Eur., no disintegration in acidic media must be

detectable that could allow the API to be released from the dosage form. Further, no cracks in the tablet coating must be visible. In the performed test, no particle liberation from the tablet cores during 120 min in 0.1 M HCl was observed, as the disintegration media was clear after media transfer. Nevertheless, the tablets exhibited considerable cracks and therefore did not pass Ph. Eur. test requirements. However, the formulation Stivarga_HPMCAS was not developed as a gastric-resistant tablet. The HPMCAS coating successfully prevented the tablet cores from disintegration at acidic conditions during the disintegration test. The effect of coating cracks, possibly leading to water ingress and subsequently RGF precipitation in gastric fluids, will be evaluated in transfer dissolution studies in the following section. The disintegration behavior of HPMCAS coated tablets at higher pH was not investigated.


**Figure 37. Stivarga_HPMCAS tablets at disintegration test before media change.**

For this batch, quite a little amount of coating material was used to allow comparability of dissolution results to formulation RGF_PVP + 10% HPMCAS. If gastric resistance is required, increasing the coating mass to form a thicker film should be feasible.

#### 3.4.5.4 Biorelevant transfer dissolution

An *in-vitro* proof-of-concept study was performed to examine the impact of HPMCAS coating on *Stivarga* tablets. In a biorelevant transfer dissolution setup, as explained in Section 6.2.3.2.2, the HPMCAS coated Stivarga tablets were compared to original *Stivarga* tablets, the results are shown in Figure 38.

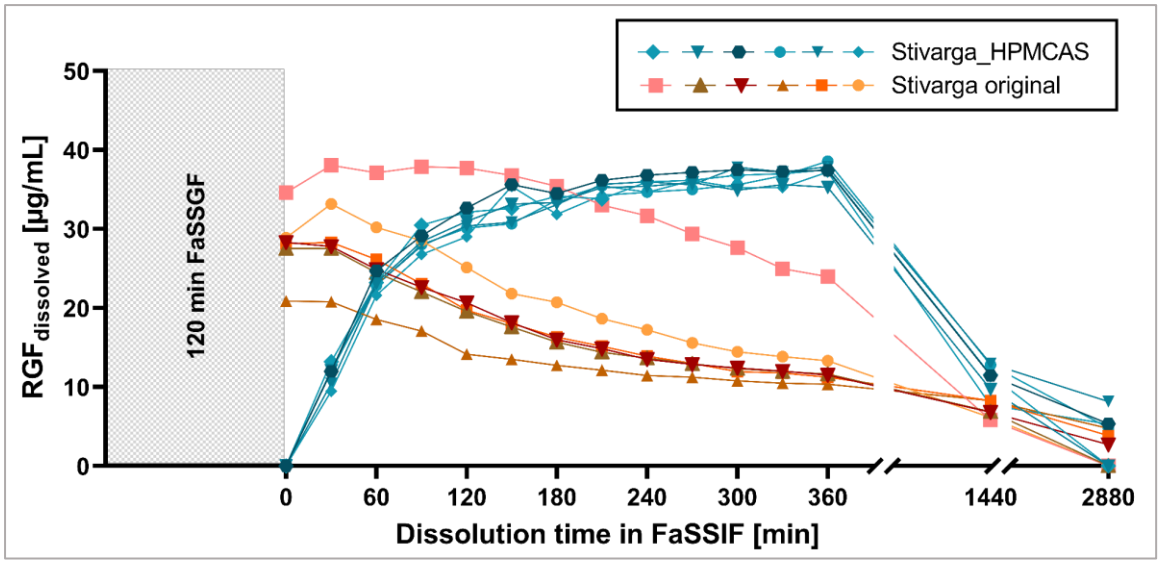


**Figure 38 Biorelevant transfer dissolution testing (37 °C, 75 rpm) of *Stivarga* and Stivarga_HPMCAS (40 mg RGF each). Tablets were dissolved in FaSSGF (250 mL) for 120 min prior to addition of $FaSSIF_{conc}$ (500 mL). Single curves are shown.**

The dissolution profiles obtained from original *Stivarga* tablets show strong variability in RGF concentrations immediately after media conversion to FaSSIF conditions. The PVA coating of *Stivarga* tablets is soluble in FaSSGF media, so dissolution and precipitation are expected to occur during the 120 min simulated gastric phase. In this experiment and in contrast to the ASD dissolution experiments described in above chapters, tablets were used for dissolution, so the processes of disintegration and dissolution were overlapping. Therefore, not the entire quantity of RGF in *Stivarga* tablets precipitated during FaSSGF phase, in contrast to the dissolution of the pure RGF_PVP particles, as described in Section 3.2.4.2. It should be mentioned that PVA was not investigated for its possible RGF supersaturation stabilizing ability. Nevertheless, the dissolution of *Stivarga* tablets did not lead to reproducible results in FaSSIF, which might be one reason for the reported *in-vivo* variability in patients.

For Stivarga_HPMCAS, neither dissolution nor tablet core disintegration was detected during the FaSSGF phase. After media conversion to FaSSIF conditions, fast and highly reproducible RGF dissolution occurred as expected from the results of RGF_PVP in Section 3.3.1.3. The resulting RGF supersaturation was stable for 360 min, whereas the precipitation process has begun until $t_{1440min}$.

The high similarity of single dissolution kinetics and the strong supersaturation indicate that coating cracks during FaSSGF dissolution (see Figure 37) led to no or only negligible RGF re-crystallization. To conclude the performed tablet dissolution studies, the newly

developed formulation concept Stivarga_HPMCAS showed clear superiority by means of reproducibility and RGF concentration profile compared to original *Stivarga* tablets at simulated biorelevant transfer conditions.

### 3.4.6 Conclusion formulation development

A new formulation concept for ASDs with RGF is proposed by a combination of a fast-release ASD formulation with co-administration of a supersaturation stabilizing agent. It was found in systematic experiments that the investigated stabilizing polymer HPMCAS must not be incorporated into the ASD matrix. HPMC was found to be another potential precipitation inhibitor. Since RGF tends to precipitate in RGF_PVP dissolution under acidic conditions, an enteric coating formulation is strongly recommended. Therefore, a final dosage form comprising RGF_PVP for satisfying RGF drug release and a stabilizing agent might be formulated as:

- Enteric-coated tablets, with
    - RGF_PVP in the tablet core plus an HPMCAS coating, as was demonstrated with Stivarga_HPMCAS
    - a blend of RGF_PVP and HPMC or HPMCAS in the tablet core plus one enteric coating, e.g. Eudragit S/L
- Enteric-coated pellets or minitablets, similar to enteric-coated tablets

Through these formulation approaches, a more robust RGF drug release *in-vivo* would be expected, leading to a reduced impact of nutritional states or co-medication. Eventually, therapy effectiveness could be increased by reducing the reported inter-patient variability. However, the predictability of *in-vivo* drug performance from *in-vitro* data is still limited and can be proven only by a clinical study in humans.

## 3.5 Precipitate analysis

Preamble

*The experimental results in the following section are based on collaborations with the external partners Dr. Martin Dulle (Forschungszentrum Jülich), Dr. Florian Platten (Department of Physics, HHU) and Dr. Björn Fischer (Fischer Raman Service).*
*The SAXS/WAXS experiments were conceived, performed, analyzed, and interpreted together with Dr. Dulle and Dr. Platten; the ITC experiments with Dr. Platten.*
*The CRM experiments were conceived, performed, analyzed, and interpreted together with Dr. Fischer.*

*Essential contents of this chapter are based on the research article manuscript "Precipitation from Amorphous Solid Dispersion at Biorelevant Dissolution: The Polymorphism of Regorafenib" (Target Journal Int. J. Pharm.) by Martin Müller, Florian Platten, Björn Fischer, Martin Dulle, Werner Hoheisel, Peter Serno, Stefan Egelhaaf and Jörg Breitkreutz.*

### 3.5.1 Introduction

One aim of the work was the investigation of physicochemical and morphological properties of precipitated RGF from different ASD formulations. In this section, RGF precipitates derived after dissolution experiments at various conditions were collected, prepared if necessary, and analyzed. By the combination of the results from different analytical tools, a deeper understanding of the physicochemical properties of precipitated RGF was gained. General considerations about off-line and *in-situ* analysis of precipitates are discussed in Section 1.3.2.1. In Section 3.5.2, dried RGF precipitates were analyzed by off-line techniques and in Section 3.5.3, *in-situ* analytical techniques were used to elucidate RGF precipitation during biorelevant dissolution experiments. The investigated freeze-dried precipitates are labelled by indicating the ASD formulation and the dissolution medium. The following precipitates were examined:

- RGF_PVP / FaSSIF
- RGF_PVP / FaSSGF
- RGF_HPMCAS / FaSSIF
- RGF_PVP + co-administered HPMCAS / FaSSIF

Since HPMCAS is insoluble in acidic FaSSGF media, all formulations containing HPMCAS were exclusively investigated in FaSSIF.

### 3.5.2 Off-line analysis of dried RGF precipitates

#### 3.5.2.1 General notes

Concentrated biorelevant dissolution studies were conducted and the resulting RGF precipitates were collected, as described in Section 6.2.3.4.1. The freeze-dried precipitates were investigated regarding their physicochemical behavior by a complementary analytical approach to reveal the RGF modification within the precipitates.

RGF and FaSSIF reference samples were prepared as described in Section 6.2.3.4.1. It should be noted, that only RGF MH and RGF Mod. I could be used as reference materials, as explained in Section 1.1.3.1.

### 3.5.2.2 Scanning electron microscopy

The SEM images showed morphological differences between the precipitates from the dissolution experiments, in Figure 39 some typical morphologies are illustrated. Except for the precipitate RGF_HPMCAS / FaSSIF, for all other investigated precipitates PVP was present in the dissolution medium when RGF precipitation from supersaturated state occurred. These RGF precipitates share a common morphology. The spherical cluster structures were based on needle-shaped particles, most likely RGF, because solely this substance was expected to form solid precipitates during the dissolution experiments. For the precipitate RGF_HPMCAS / FaSSIF, spherical agglomerates of needle-shaped particles co-existed with a leaf-like structure with a smooth surface similar to the RGF_PVP platelets shown in Figure 4.

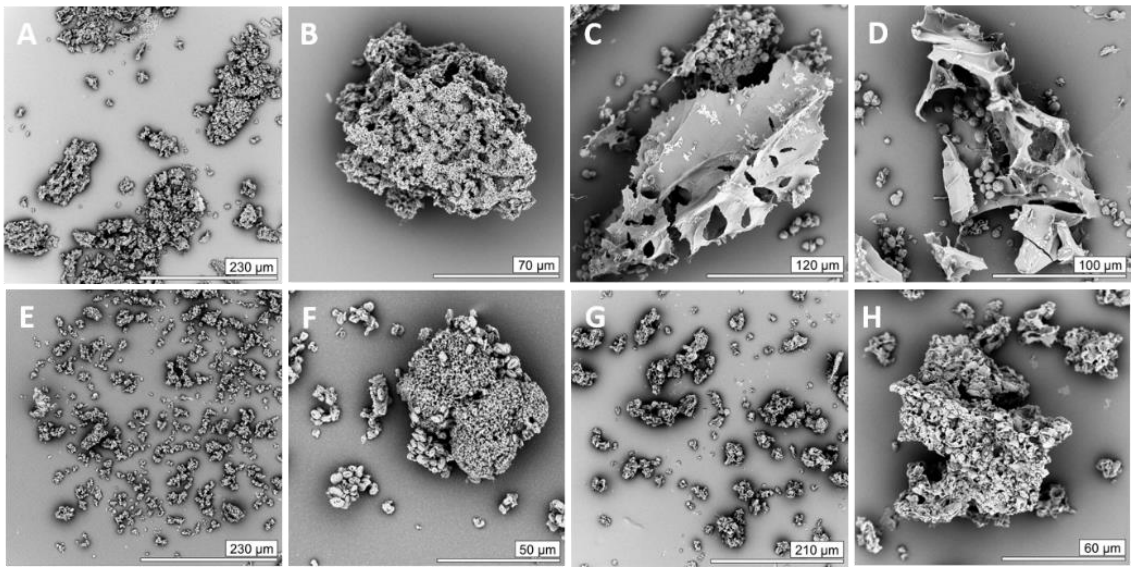


**Figure 39. SEM images of freeze-dried precipitates RGF_PVP / FaSSIF (A+B), RGF_HPMCAS / FaSSIF (C+D), RGF_PVP + 10% HPMCAS / FaSSIF (E+F) and RGF_PVP / FaSSGF (G+H).**

### 3.5.2.3 RGF content determination

The RGF content in the precipitates was measured by HPLC/UV, as described in Section 6.2.3.3.2. The results are listed in Table 15. RGF was found in all precipitates, the small SD in drug content indicated a uniform distribution within the precipitates. All precipitates contained further substances, as the RGF content was below 100 %, as such biorelevant media components or the ASD formulation polymers. The RGF content of the precipitate from RGF_HPMCAS dissolution in FaSSIF was drastically lower than those of the other samples. Interestingly, the drug load was not that low for the precipitate

RGF_PVP + 10% HPMCAS / FaSSIF. The reduced RGF content in the precipitate RGF_HPMCAS / FaSSIF might be caused by co-precipitation with the ASD polymer in absence of PVP, however, direct determination of the HPMCAS content by HPLC/UV was not possible. Usually, an evaporative light scattering detector is used for this approach, which was not available (Chen et al. 2015d; Wang et al. 2018a).

**Table 15. RGF content in freeze-dried precipitates after biorelevant dissolution (n = 3, mean ± s).**

| ASD formulation / precipitation media | RGF content in % (m/m) |
|---|---|
| RGF_PVP / FaSSIF | 88.8 ± 0.3 |
| RGF_HPMCAS / FaSSIF | 41.3 ± 0.3 |
| RGF_PVP + 10% HPMCAS / FaSSIF | 75.5 ± 0.2 |
| RGF_PVP / FaSSGF | 76.9 ± 0.5 |

The molecular ratio of RGF to HPMCAS can be calculated. Assuming that the difference to 100 % RGF content is co-precipitated HPMCAS results in a ratio of 193 molecules RGF per molecule HPMCAS. Assuming that the content of co-precipitated is the difference to 76 %, which is the RGF content in RGF_PVP + 10% HPMCAS / FaSSIF, and the leftover 24 % are media components and/or humidity, the resulting ratio of RGF molecules to one HPMCAS molecule is 325.

#### 3.5.2.4 X-ray powder diffraction (XRPD)

The precipitates from biorelevant dissolution studies were examined by XRPD as described in Section 6.2.3.4.2. Diffractograms with Bragg peaks are depicted in Figure 40. For clarity, those of amorphous materials, i.e., the polymers and amorphous RGF, exhibiting only a non-characteristic halo signal are not shown.

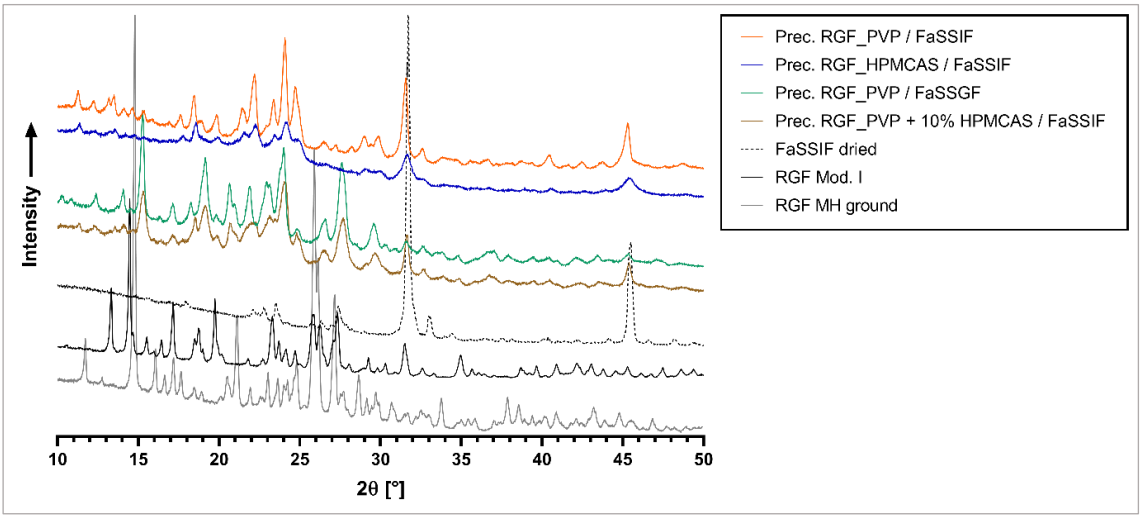


**Figure 40. XRPD spectra of freeze-dried ASD precipitates, dried biorelevant media, and reference substances. RGF MH was ground to reduce preferred orientation effects. Spectra have been vertically offset for clarity.**

The RGF precipitates exhibit diffraction peaks, indicating the presence of crystalline structures. As the precipitated material was not washed to remove FaSSIF components in order to avoid sample altering, the dominant FaSSIF signals at 31.7° and 45.5° were found in the diffraction pattern of all precipitates. This confirms the presence of biorelevant media components in the precipitates and explains why the drug load of the precipitates was below 100 % (Table 15). The diffraction patterns of the pure RGF modifications were strikingly different from those of the precipitates regarding the signal positions. However, two characteristic diffraction patterns were found for the precipitates. The signals from RGF_HPMCAS / FaSSIF and RGF_PVP / FaSSIF exhibited the same characteristic pattern, and hence the crystalline RGF modifications in both samples were assumed to be identical. The reduced XRPD intensity of RGF_HPMCAS / FaSSIF compared to RGF_PVP / FaSSIF indicates reduced crystallinity within the sample, likely due to less crystalline RGF precipitates or reduced RGF content. The XRPD spectra from the precipitates RGF_PVP + 10% HPMCAS / FaSSIF and RGF_PVP / FaSSGF were different from the previous ones, but albeit minor variations, quite similar to each other. The major differences are likely due to the variations in the pH value and bile salt concentration for FaSSGF and FaSSIF, which might have impacted the crystal formation during RGF precipitation.

### 3.5.2.5 Differential scanning calorimetry (DSC)

DSC experiments were performed for the precipitates to investigate the thermal properties, the method is described in Section 6.2.3.4.6. The DSC thermograms of the precipitates and reference materials are shown in Figure 41 and the respective values and explanations of observed events are listed in Table 31 (Annex). The *Bayer* internally reported thermoanalytical behavior of different RGF modifications in DSC experiments is provided in Table 30 (Annex). Interestingly, for RGF Mod. I and RGF MH, two different DSC profiles are reported, which is outlined in more detail on page 203 (Annex).

The number of RGF modifications and different thermoanalytical profiles reported for the same modifications raise the challenge of assigning the RGF precipitates to one modification. In case of co-existence of multiple modifications in one precipitate, to distinguish the modifications might be difficult and complementary analytical information is necessary.

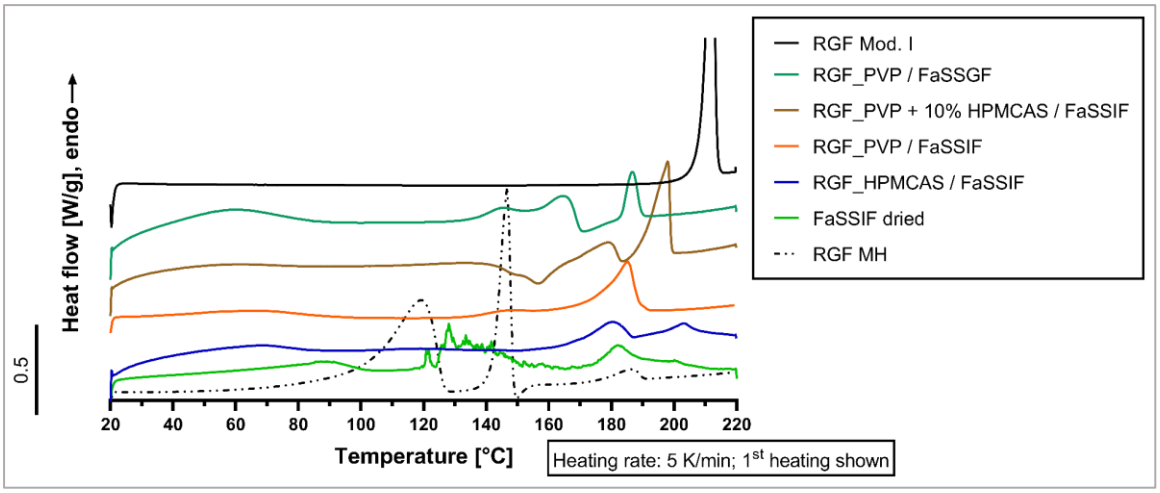


**Figure 41. DSC thermograms of freeze-dried RGF precipitates from biorelevant dissolution and references. For illustration reasons the RGF Mod. I signal is divided by 5. The scale bar on the left is equivalent to 0.5 W/g.**

The characteristic melting events of the pure RGF modifications were not found in the precipitates. Hence, a different crystalline RGF species has formed in the precipitates, which is in accordance with the XRPD results. Interestingly, the thermograms of the samples RGF_PVP / FaSSIF and RGF_HPMCAS / FaSSIF differ in their temperatures of the endothermal event around 180 °C and in the presence of a second endothermal event for RGF_HPMCAS / FaSSIF. This might be attributed to a different amount of incorporated FaSSIF or polymer or to a non-homogeneous dispersion of the RGF crystallites in the co-precipitated material, leading to melting event broadening by different

local melting temperatures (Paudel et al. 2014). Since the XRPD spectra did not reveal differences in the crystalline structures in both the precipitates, the endothermal event at 192 °C onset is likely related to an amorphous structure.

The DSC curves of the samples RGF_PVP / FaSSGF and RGF_PVP + 10% HPMCAS / FaSSIF show different thermoanalytical behavior in terms of specific endothermal or exothermal events. This is in contrast to the XRPD results which indicated high similarity in the crystalline structure of the samples. However, the reason for the discrepancy between DSC and XRPD results remains unknown.

The crystalline precipitates from extrudates RGF_PVP-Witocan after dissolution were examined by DSC (Figure 22). The endothermic events at 172 °C and 189 °C onset could be attributed to melting events of RGF Mod. I. Interestingly, these melting events were similar to those observed from RGF_PVP / FaSSIF and RGF_HPMCAS / FaSSIF, although further differentiation was not possible.

#### 3.5.2.6 Confocal Raman microscopy (CRM)

The principles of Raman scattering and the analytical insights provided by this method are explained in Section 1.3.2.4.

To further study the amorphous precipitate in co-existence with a crystalline form in the sample RGF_HPMCAS / FaSSIF, CRM measurements were performed as described in Section 6.2.3.4.5.

The acquired light microscopic images are shown in Figure 42, the colored crosses indicate the Raman single spot measurement positions. An overview of the number of detected RGF modifications in the investigated samples is provided in Table 16. For clarity, a region of interest was defined from 400 $cm^{-1}$ to 800 $cm^{-1}$, although the full data sets were considered for analysis and comparison.

**Table 16. Number of RGF modifications found in freeze-dried precipitates by confocal Raman microscopy.**

| Precipitate | No. of RGF polymorphs found |
|---|---|
| RGF_PVP / FaSSIF | 1 |
| RGF_PVP / FaSSGF | 1 |
| RGF_HPMCAS / FaSSIF | 2 |
| RGF_PVP + 10% HPMCAS / FaSSIF | 2 |

For the freeze-dried precipitate RGF_PVP / FaSSIF, identical Raman spectra were found at different measurement spots. This was also the case for RGF_PVP / FaSSGF precipitate, both spectra are compared in Figure 43 (left). Significant differences in the Raman signals were observed, indicating that the change in precipitation media leads to different RGF modifications.

For RGF_HPMCAS, two different species were found in the freeze-dried precipitate which is in accordance with SEM results (Figure 39). As depicted in Figure 42 (C and E), CRM revealed 'bubbles' and 'plain glassy' structures, which show different Raman spectra. The plain glassy structures matched the Raman spectrum of amorphous RGF, which confirms the results from DSC and XRPD studies of a co-existence of amorphous and crystalline RGF. The second type of material was highly similar to the spectrum from RGF_PVP / FaSSIF, thus confirming the co-existence of amorphous RGF and a crystalline RGF polymorph.

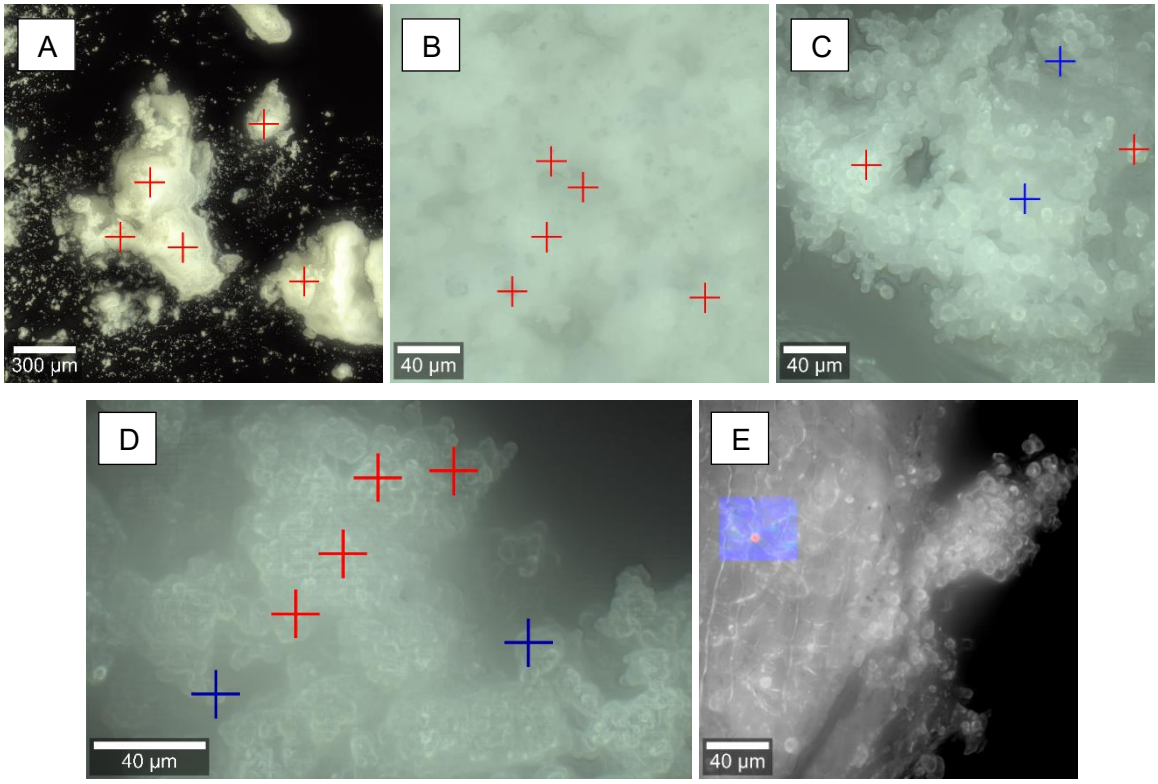


**Figure 42. Light microscopy images obtained from CRM. The measurement spots are indicated by crosses. For each sample, identical Raman spectra are indicated by color-coding. The precipitates RGF_PVP / FaSSIF (A), RGF_PVP / FaSSGF (B), RGF_HPMCAS / FaSSIF (C) and RGF_PVP + 10% HPMCAS / FaSSIF (D) are shown. Raman mapping for RGF_HPMCAS / FaSSIF is shown in (E).**

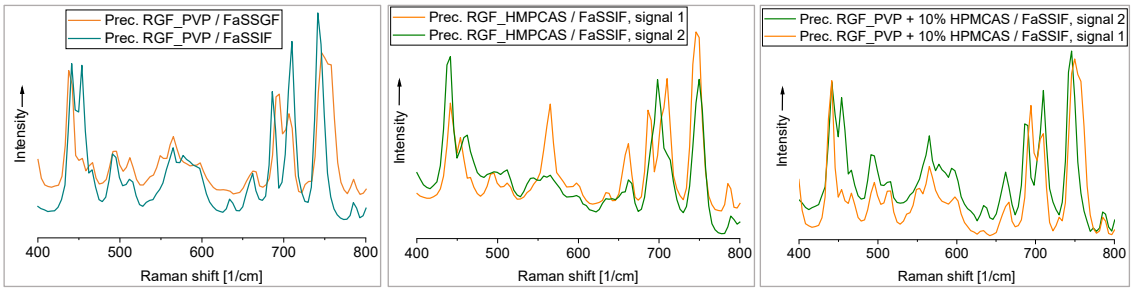


Figure 43. Different Raman spectra within the investigated precipitates.

A co-existence of two RGF species was also found for the freeze-dried precipitate RGF_PVP + 10% HPMCAS / FaSSIF. Although the light microscopic images of RGF_PVP + 10% HPMCAS and RGF_HPMCAS / FaSSIF were similar, only one RGF species was present in both precipitates while the other Raman spectra did not match. For the precipitate RGF_PVP + 10% HPMCAS, no amorphous spots were found, however, the remaining spectrum matched with precipitate RGF_PVP / FaSSGF.

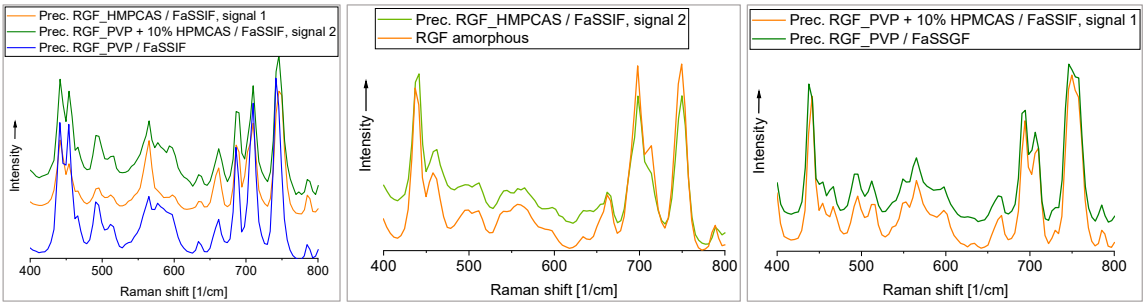


Figure 44. Raman spectra of RGF precipitates. Matching signals are shown for different RGF polymorphs.

### 3.5.2.7 The influence of sample preparation

To preserve the 'natural state' of the investigated precipitates, freeze-drying was chosen to avoid thermal-induced modification transformations during drying which might lead to falsified results. The importance was demonstrated by variation of sample preparation for the precipitates from RGF_HPMCAS and RGF_PVP dissolution in FaSSIF. The precipitates were washed with distilled water to remove water-soluble components and subsequently dried in a vacuum oven at 30 °C. The results are displayed in Figure 45.

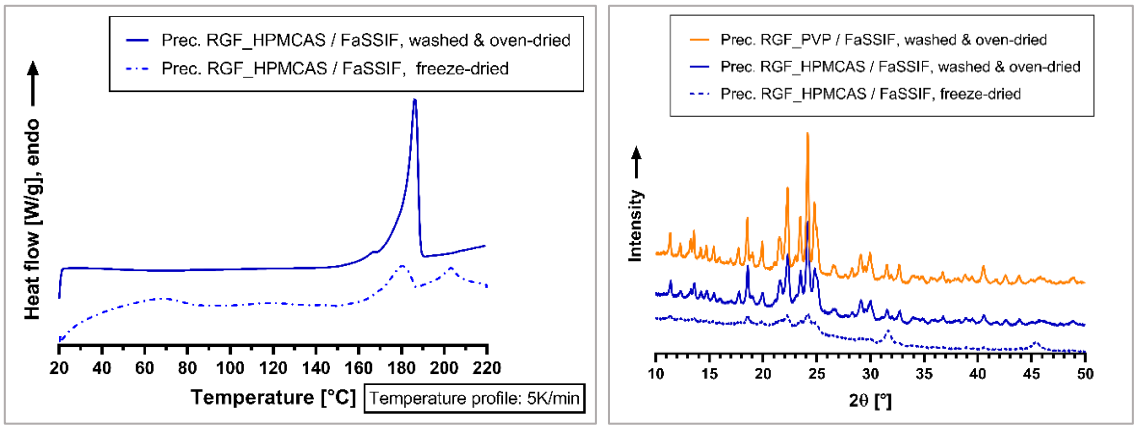


**Figure 45. Influence of sample preparation on amorphous character of collected precipitate from RGF_HPMCAS / FaSSIF.**

Whereas no impact of the applied drying method or sample preparation was found for RGF_PVP / FaSSIF, for RGF_HPMCAS / FaSSIF a vast increase in crystallinity was observed. In DSC experiments, the melting enthalpy of the freeze-dried precipitate was raised from 19 J/g or 35 J/g (single event at 168 °C or sum of both melting events, respectively) to 55 J/g of the oven-dried precipitate. Interestingly, the second endothermic event in DSC has vanished, indicating a polymorphic transition. This increase in crystallinity was supported by greater XRPD diffraction intensities for the oven-dried and washed precipitate.

### 3.5.3 *In-situ* RGF precipitation characterization

#### 3.5.3.1 General considerations

The numerous advantages of *in-situ* analysis over off-line precipitate characterization were outlined in Section 1.3.2 In this section, the RGF precipitates were analyzed by *in-situ* CRM and *in-situ* WAXS to gain a deeper understanding of the RGF precipitation process and about the comparability of off-line results to *in-situ* results. X-ray diffraction was conducted in the two operation modes of wide-angle (WAXS) and small-angle X-ray scattering (SAXS), whereas only WAXS was performed *in-situ*. The experimental SAXS/WAXS setup consisting of a beamline and SAXS/WAXS detector is depicted in Figure 46.

A biorelevant dissolution system, either the vessel-based dissolution system or the small-scale dissolution system, was installed directly next to the analytical device. This setup allowed direct sample analysis without or with only a little time delay.

By the time the SAXS/WAXS experiments were conducted, solely the freeze-dried precipitates RGF_PVP / FaSSIF and RGF_HPMCAS / FaSSIF and its respective ASD formulations were available, therefore a higher number of formulations was investigated by CRM than by SAXS/WAXS.

#### 3.5.3.2 *In-situ* wide-angle (WAXS) and off-line small-angle X-ray scattering (SAXS)

##### 3.5.3.2.1 WAXS results

The comparability of diffraction data derived from the WAXS setup to the XRPD data from Section 3.5.2.4 was proven by the measurements of RGF MH and the freeze-dried precipitates RGF_HPMCAS / FaSSIF and RGF_PVP / FaSSIF. To allow comparison, a transformation of the 2Θ values from XRPD diffractograms to its scattering vector ($q$) was calculated by the following equation:

$$q = \frac{4\pi}{\lambda} \, sin\,(\theta) \qquad \text{Equation 8}$$

where $\lambda$ is the X-ray wavelength of the copper anode of 0.15406 nm and $\Theta$ the single diffraction angle.

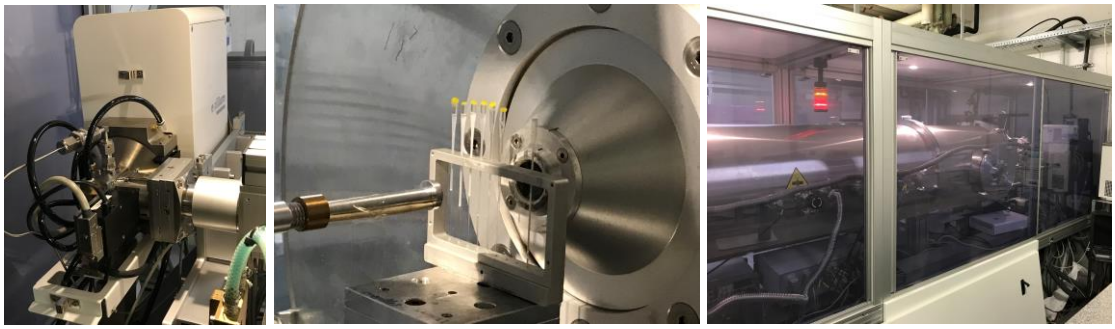

**Figure 46. SAXS/WAXS setup at Forschungszentrum Jülich, consisting of X-ray metal jet source (left), capillary autosampler for dissolution samples (middle), and detector tube (right).**

The range of detected scattering angles was not identical for both setups due to its geometries, hence the overlapping q range from 7 $nm^{-1}$ to 25 $nm^{-1}$ will be compared. The results of setup comparison are shown in Figure 83 for RGF MH and in Figure 84 for the freeze-dried precipitate RGF_PVP / FaSSIF (both Appendix). For all samples with X-ray diffraction above the analytical LOD, the diffraction peaks and relative intensities are matching both. It was concluded that both setups lead to comparable results. The only deviation was found in the freeze-dried precipitate RGF_HPMCAS / FaSSIF sample, as no diffraction signals were found in the WAXS setup. This could be either explained by a difference in analytical LOD for crystalline quantities between both setups or by some variability within freeze-dried RGF_HPMCAS / FaSSIF samples regarding the crystalline content. The non-crystalline samples PVP, HPMCAS, RGF_PVP, and RGF_HPMCAS did not exhibit any X-ray diffraction.

For WAXS measurements of biorelevant dissolution samples, the ASD dose was increased to ensure a sufficient particle density and will be named as the 'ASD dose factor' (*f*). The major downside of this compromise is that the concentration of dissolved polymer will be higher than in dissolution studies, possibly affecting the supersaturation stability and precipitation rate. The results from the following experiments will be discussed, as they led to a deeper understanding of RGF precipitation behavior from supersaturated state in biorelevant media:

**Table 17. WAXS and SAXS experiments from which results are presented. Experiments 1-3 were conducted *in-situ*, experiment 4 with freeze-dried precipitate.**

| No. of experiment | X-ray setup | Formulation | Dissolution medium | ASD dose factors *f* |
|---|---|---|---|---|
| 1 | WAXS | RGF_PVP | FaSSIF | 4, 20, 100 |
| 2 | WAXS | RGF_HPMCAS | FaSSIF | 4, 20, 100 |
| 3 | WAXS | RGF_PVP | FaSSGF | 20 |

| No. of experiment | X-ray setup | Powder sample |
|---|---|---|
| 4 | SAXS | Precipitate RGF_HPMCAS / FaSSIF, freeze-dried |

For RGF_PVP dissolution in FaSSIF (experiment 1), the results are shown from Figure 47 to Figure 52. After 14 h and 24 h, the identical RGF modification was found, independent of the ASD dose factor. These data are in alignment with the freeze-dried RGF_PVP / FaSSIF precipitate, see Figure 48. From RGF_PVP dissolution in FaSSIF a sample was drawn after 3 h and diffractograms were collected over 14 h, the results are depicted in Figure 49.

The results from biorelevant transfer dissolution studies indicated rapid RGF crystallization during FaSSGF conditions (Figure 12 and Figure 13) which was confirmed by WAXS. For RGF_PVP dissolution in FaSSGF (experiment 3), a weak scattering signal was recorded after 2 h, as shown in Figure 47. The low intensity did not allow to assign the signal to a known RGF precipitation diffractogram, though it indicated the crystalline state of the precipitate. Most likely, the particle density of the analyte was not sufficiently high.

The precipitation process of RGF_PVP from FaSSIF was monitored over 14 h. A small-scale dissolution run was performed (*f = 100*) to achieve a sufficient signal-to-noise ratio. After 3 h, a dissolution sample was drawn and transferred into a sample capillary. In the next step, an air bubble was manually inserted into the capillary, so precipitated material enriched in the X-ray beam by sedimentation. Hence, the processes of crystal sedimentation and further precipitation were overlapping. Figure 49 displays the increase in X-ray diffraction of RGF_PVP in FaSSIF over time. Only one diffraction pattern was found to increase over the experiment time, confirming the absence of intermediate crystalline polymorphs above the analytical LOD.

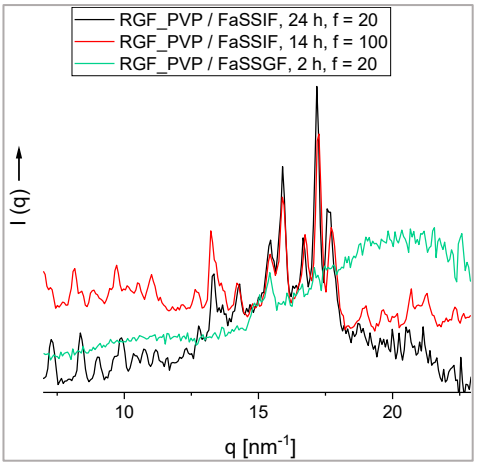


Figure 47. *In-situ* WAXS spectra of precipitates from RGF_PVP dissolution

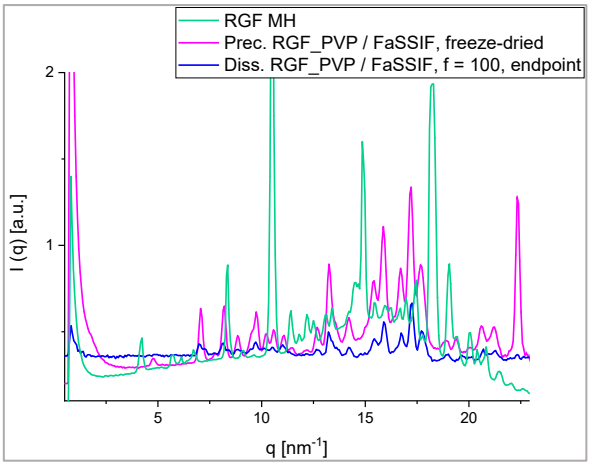


Figure 48. WAXS spectra of RGF precipitates and RGF MH

The time evolution of the scattered intensity of the *in-situ* crystallization process shown in Figure 49 has been analyzed in more detail. Figure 50 shows how the diffraction signals at q = 9.44 $nm^{-1}$, 1.286 $nm^{-1}$, 15.44 $nm^{-1}$, and 16.77 $nm^{-1}$ evolved with time. For each *q*, the intensity has been normalized to the respective maximum value, as obtained from a sigmoidal fit. The experimental data fall on top of each other, indicating that the different diffraction peaks exhibit the same kinetics and reflect the same crystallization process.

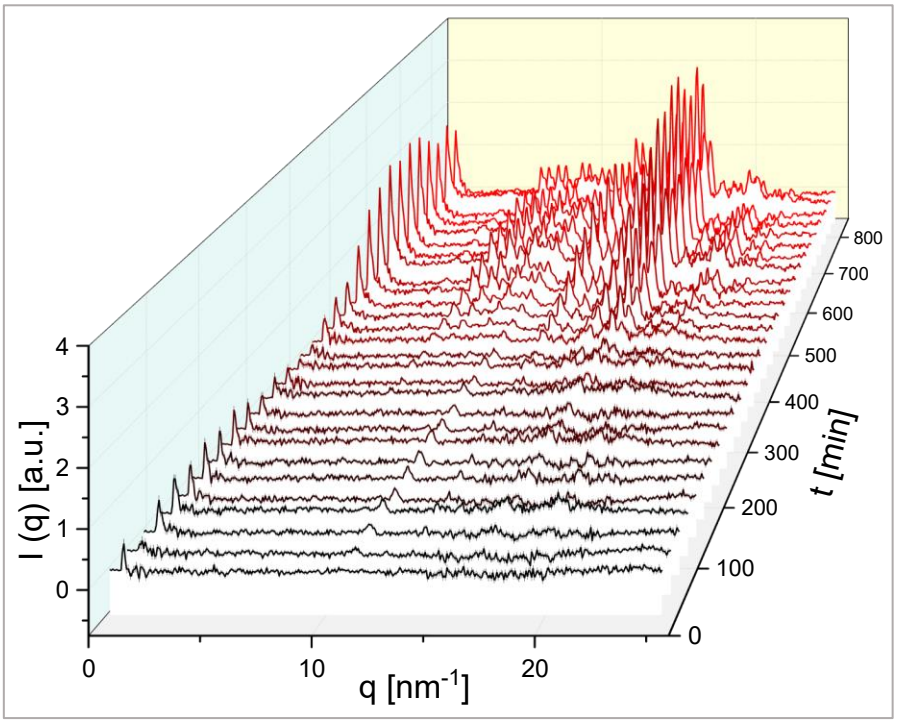


Figure 49. RGF_PVP dissolution in FaSSIF in WAXS capillary, after sampling from small-scale dissolution setup after 3 h.

Since the peak at $q$ = 16.77 nm$^{-1}$ had the highest long-time intensity and thus offered the best statistics, the temporal evolution of its width $\Delta q$ was analyzed. Figure 51 shows the peak data points (symbols) which are described by a Lorentzian fit (line) in order to estimate $\Delta q$. For clarity, data are shown only for selected times as indicated.

In turn, the width of the diffraction peaks of small crystallites is related to their size $L$ via the Scherrer equation (Warren 1990):

$$L = K\frac{2\pi}{\Delta q} \qquad \text{Equation 9}$$

where $K$ is a dimensionless shape factor, which is set to 0.9, and $\Delta q$ is the full width at half peak maximum. Figure 52 shows the time evolution of the crystallite size obtained in this way. First crystallites with a size of ca. 7 ± 2 nm are detected after about 300 min. Then, the crystal size grows linearly over time (power law of 1.1 ± 0.3), reaching a constant value of ca. 23 ± 2 nm at about 600 min.

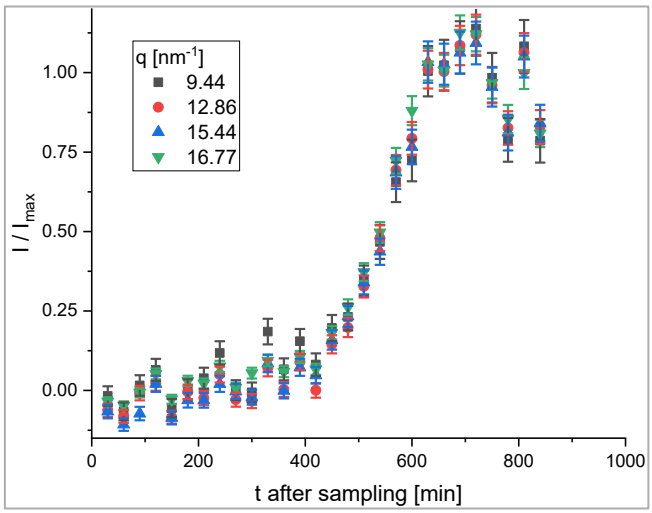


**Figure 50. Relative intensity of characteristic scattering signals during dissolution of RGF_PVP in FaSSIF.**

No RGF MH precipitated during this experiment, as the characteristic diffraction peaks at ca. 10 nm$^{-1}$, 15 nm$^{-1}$, and 18 nm$^{-1}$ were not found.

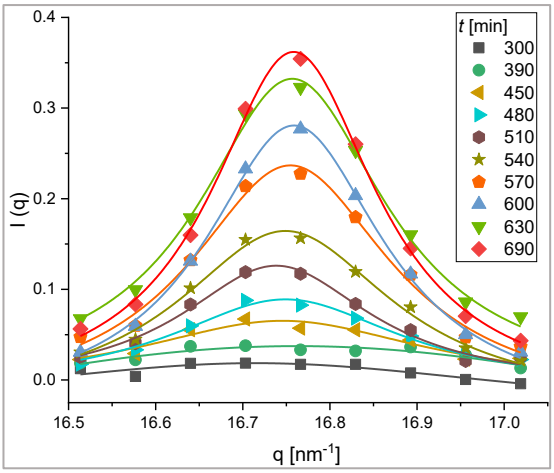


Figure 51. Temporal evolution of Δq for the most prominent signal of RGF_PVP in FaSSIF.

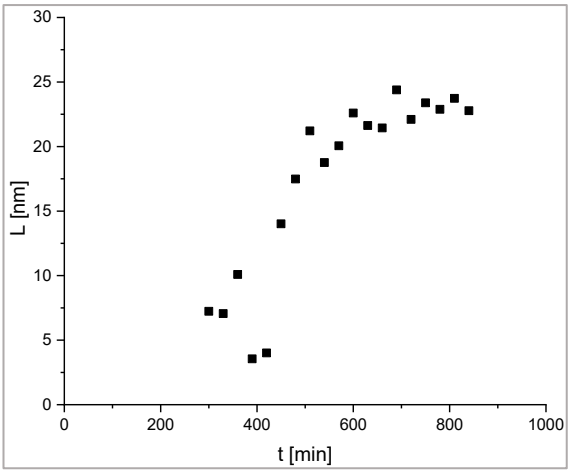


Figure 52. Crystallite size growth of RGF_PVP precipitate in FaSSIF

For RGF_HPMCAS in FaSSIF (experiment 2), no WAXS signal was found, independent from the applied ASD concentration factor or sampling time point. This is in accordance with the findings from the freeze-dried precipitate RGF_HPMCAS / FaSSIF which did not exhibit X-ray scattering in WAXS experiments, too. The reason behind why no X-ray scattering was found for this sample might be that the crystalline content, if present, was below the device-specific analytical LOD. Also, variability within the precipitation process from RGF_HPMCAS dissolution in FaSSIF could lead to different ratio of amorphous to crystalline RGF by chance.

#### 3.5.3.2.2 SAXS results

Interestingly, SAXS signals were detected in the freeze-dried precipitate RGF_HPMCAS / FaSSIF (experiment 4). In contrast to WAXS experiments, also amorphous structures lead to X-ray scattering in SAXS experiments. The scattered intensity *I (q)* is shown in Figure 53. From *I (q)* data an inverse Fourier transformation (IFT) was calculated, resulting in a histogram of pairs of distances within the precipitate, depicted in Figure 53. From the shape of the histogram, the shape of the precipitate subunits can be estimated (Glatter 1980; Koch et al. 2003).

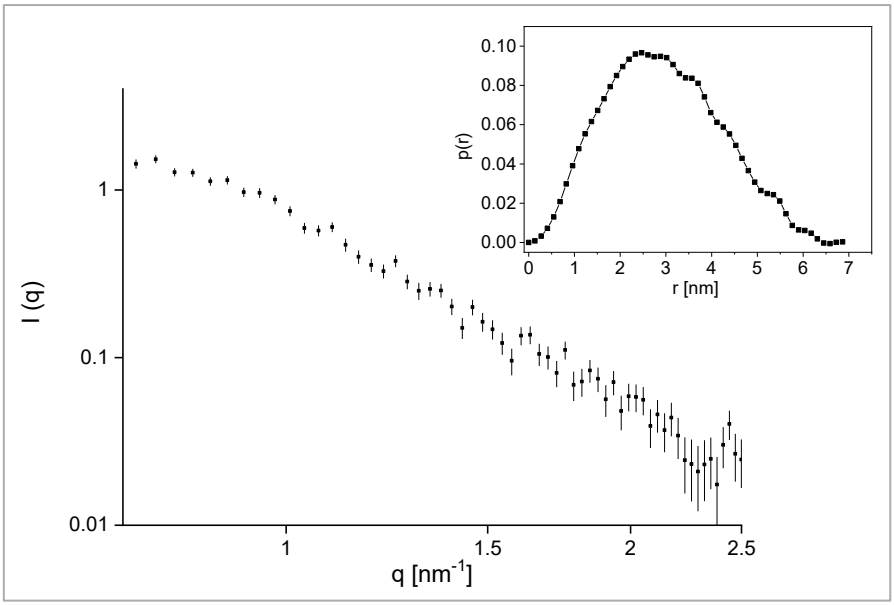


**Figure 53. SAXS intensity of precipitate RGF_HPMCAS / FaSSIF, data points and statistical errors are shown. Inset: Pair distance distribution function *p(r)* of pairs of points within the precipitate.**

To illustrate the connection between a geometrical shape and its distance distribution curve, in Figure 54 a sphere, an elongated particle, a flattened particle, a hollow particle, and a particle with well-defined subunits are presented, reprinted from Svergun and Koch (2003).

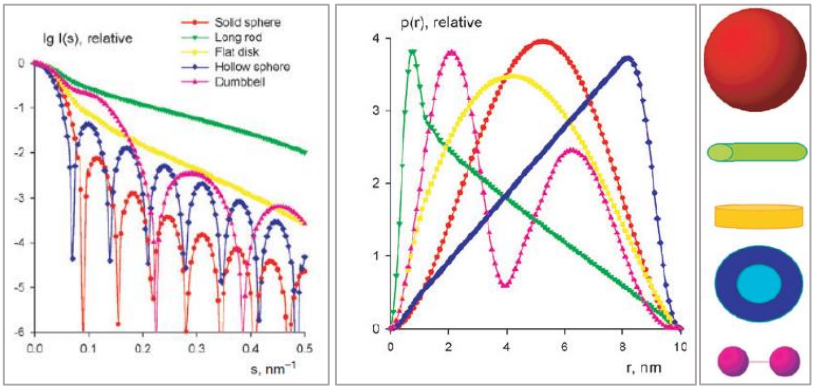


**Figure 54. Scattering intensities and distance distribution functions of geometrical bodies. Depicted from Svergun and Koch (2003) with permission.**

It is important to state that these data are directly obtained from the experimental data and not fitted. By that, globularly shaped particles are present in the precipitate. The maximum detected distance of around 6 nm within one precipitate subunit can be assumed to be the diameter of these structures. By combination of the results from SAXS and WAXS it can be assumed that the precipitated material from RGF_HPMCAS dissolution in FaSSIF was amorphous and consisted of globularly shaped subunits with a diameter of ca. 6 nm.

### 3.5.3.3 *In-situ* confocal Raman microscopy (CRM)

#### 3.5.3.3.1 General notes

To explore the formed RGF modifications in biorelevant dissolution *in-situ*, confocal Raman microscopy (CRM) studies were conducted. Therefore, a biorelevant vessel-based dissolution as described in Section 6.2.3.2.1 was installed next to the CRM device. The sample preparation procedure is described in Section 6.2.3.4.5. As for the investigation of powder state samples, Raman single spot measurements and Raman mapping was conducted. For the *in-situ* Raman dissolution measurements, it was necessary to wait until a sufficient sample density was formed to achieve a Raman signal which allowed for RGF modification assignment. On overview of the discussed CRM results is provided in Table 18.

**Table 18. *In-situ* CRM experiments which are discussed in the present work.**

| Formulation | Dissolution media | Sampling time [h] |
|---|---|---|
| RGF_PVP | FaSSIF | 48 |
| RGF_HPMCAS | FaSSIF | 48 |
| RGF_PVP + 10% HPMCAS | FaSSIF | 48 |
| RGF_PVP | FaSSGF | 0 – 2, multiple |

To ensure the necessary particle density, and for comparison to the results obtained from the freeze-dried precipitates, the dissolution endpoint 48 h was chosen for most experimental runs. The fast RGF precipitation rate of RGF_PVP dissolution in FaSSGF was known from previous dissolution runs and WAXS experiments which allowed to observe the transition from amorphous RGF in the ASD to crystalline precipitate over 120 min.

### 3.5.3.3.2 RGF_PVP in FaSSIF

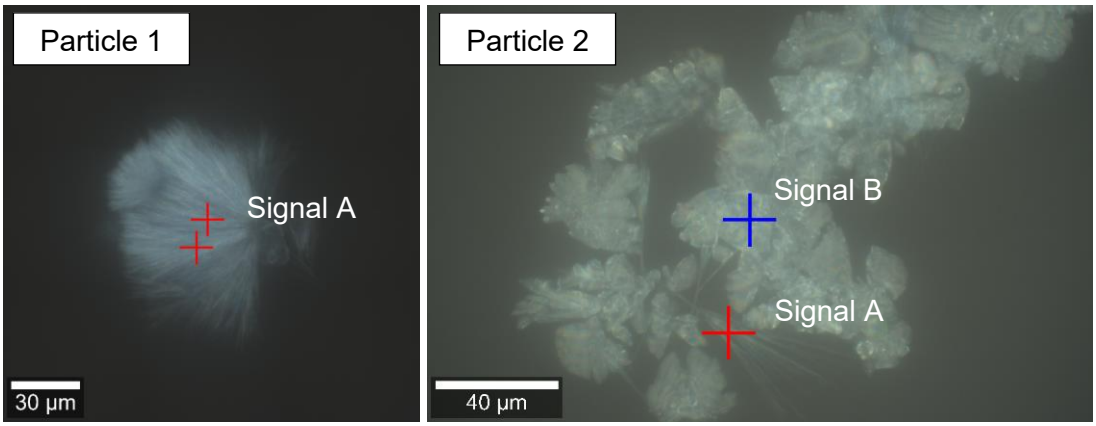


**Figure 55. Light microscopy images of precipitates particles from RGF_PVP dissolution in FaSSIF after 48 h. Raman measurement positions are indicated by the crosses.**

For dissolution of RGF_PVP in FaSSIF, three particles were investigated, thereof particle 1 and particle 2 are presented in Figure 55 and particle 3 in Figure 57. Characteristic particle morphologies exhibited specific Raman spectra, indicating the co-existence of different RGF polymorphs (Figure 56). In particle 1, the Raman spectrum of the needle stack was matched with RGF MH. The morphology of particle 2 was different, besides the needles, a flake precipitate was found. Whereas the needles (Signal A) were found to be RGF MH, the flakes (Signal B) showed Raman signal from the freeze-dried precipitate RGF_PVP / FaSSIF which could not be assigned to a RGF polymorph.

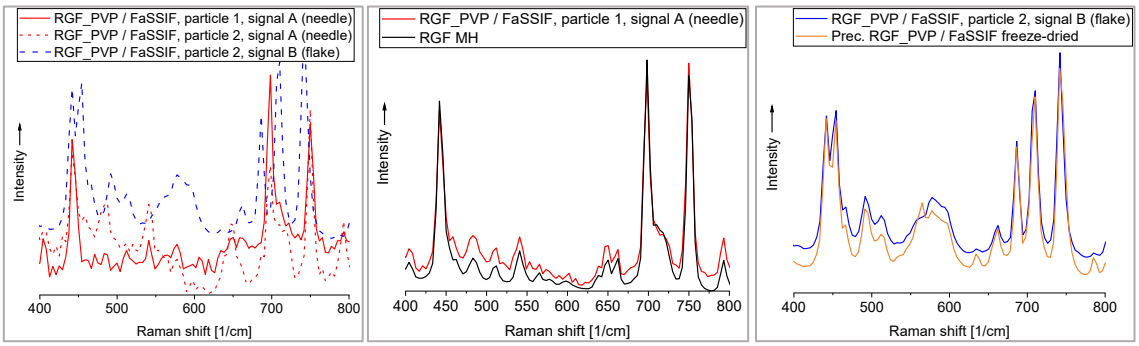


**Figure 56. Raman spectra obtained from particles 1 and 2 shown in Figure 55.**

In contrast to these *in-situ* results, only one Raman signal was found within the freeze-dried precipitate RGF_PVP / FaSSIF. These findings indicate that by freeze-drying, the

monohydrate water was removed and RGF modification transition to an unknown polymorph occurred.

The correlation of precipitated RGF polymorphs to the morphological properties was illustrated by Raman imaging. In particle 3 (Figure 57), the yellow frame in the light microscopic image represents the area of which the Raman mapping was acquired.

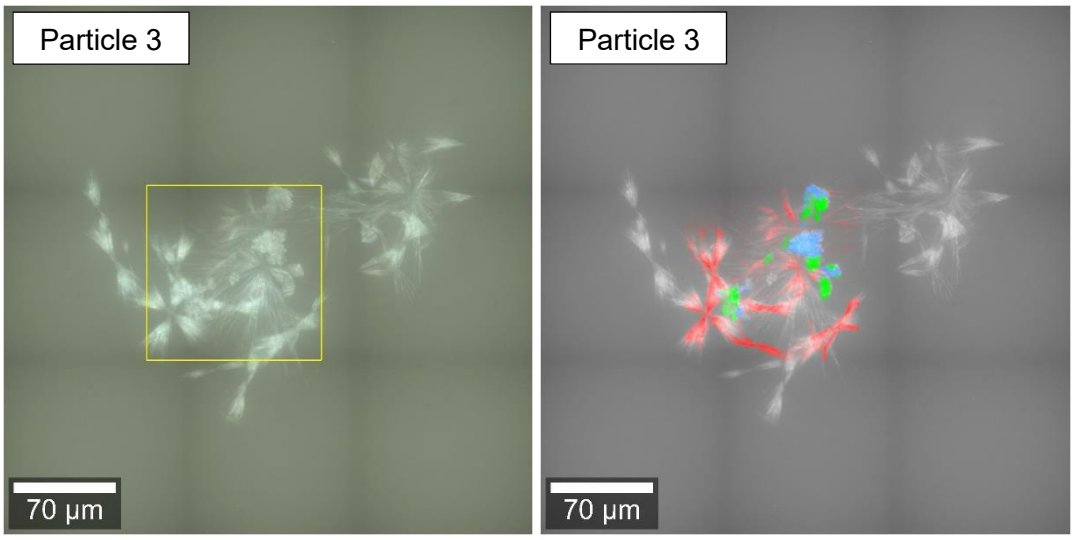


**Figure 57. Light microscopy image of precipitated particles from RGF_PVP dissolution in FaSSIF after 48h without (left) and with (right) Raman mapping. The component spectra for color coding are shown in Figure 85.**

The different Raman signals were color-coded by the implemented software. For Raman mapping, the exposure time and therefore the signal intensities were markedly reduced, leading to a decreased signal-to-noise ratio. As a consequence, only parts of the Raman spectra with sufficient intensity were chosen for evaluation, in this case <150 $cm^{-1}$.

Three different species were found in the investigated area, the respective single spectra are presented in Figure 85 (Annex). As in particle 2, the Raman signal from needle-shaped precipitates matched with RGF MH and the Raman signal from flake-shaped precipitate matched with those from the respective freeze-dried precipitate. For the third identified species, colored in green, no match with a reference was found. However, this cannot be considered without doubts as a different RGF modification, due to the low signal signal-to-noise ratio.

#### 3.5.3.3.3 RGF_HPMCAS in FaSSIF

For RGF_HPMCAS dissolution in FaSSIF, two particles were analyzed. The measurement spots on particle 1 are shown in Figure 58. Three different Raman signals were recorded, as presented in Figure 59.

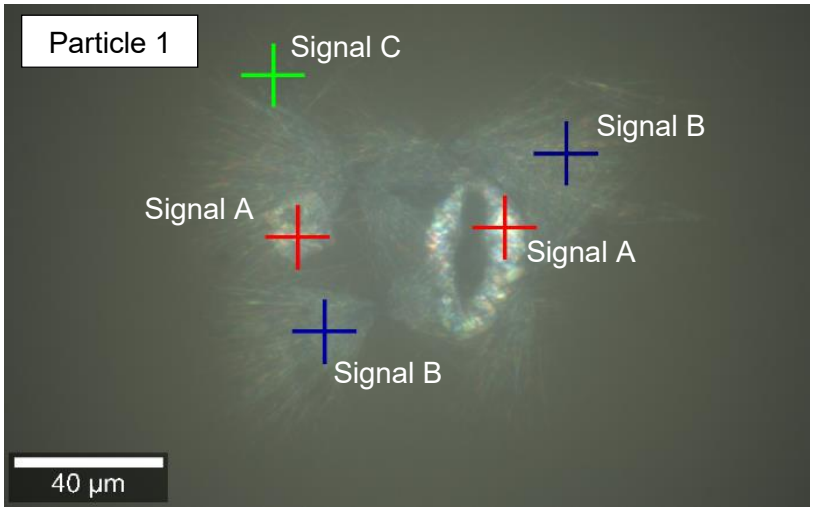


**Figure 58. Light microscopy images of precipitated particles from RGF_HPMCAS dissolution in FaSSIF after 48 h. Raman measurement positions are indicated by the crosses.**

The signals derived from the needle-shaped precipitates (Signal B), unlike for RGF_PVP, matched with reference substance RGF Mod. I. Signal A showed similarities, though significant differences, compared to RGF Mod. I. Signal C showed similarities to the Component 3 from RGF_PVP / FaSSIF dissolution, although comparison in the region of 400 $cm^{-1}$ to 800 $cm^{-1}$ was difficult, as explained above.

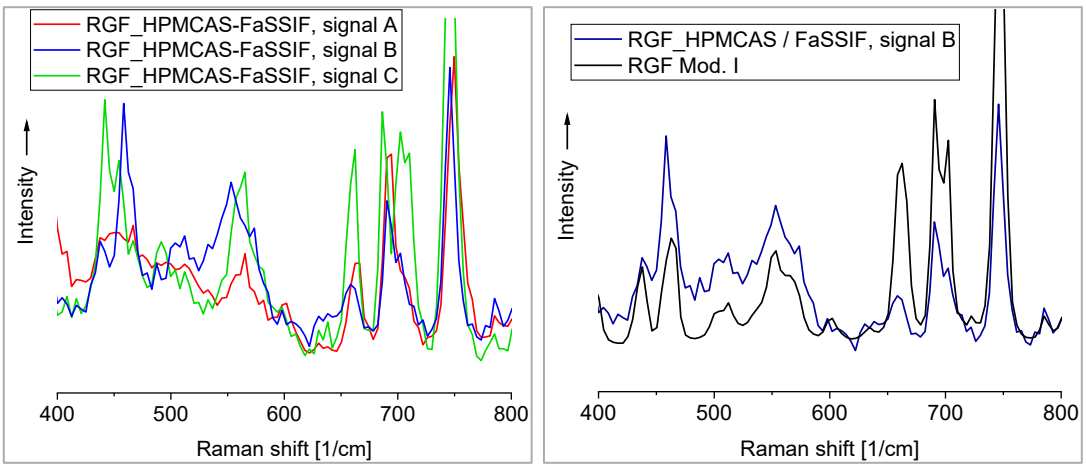


**Figure 59. Raman spectra recorded for particle 1, shown in Figure 58.**

For particle 2, a Raman mapping was performed, shown in Figure 60. As for RGF_PVP / FaSSIF results, the difference in precipitate morphology was also found in different Raman spectra. The single-component spectra are provided in Figure 88 (Appendix). Again, since the acquired Raman spectra were less intense compared to single spot measurements, a clear RGF modification assignment cannot be provided. Though, the co-existence of different RGF modifications can be confirmed given the different morphologies with characteristic Raman signals matching the morphological structures.

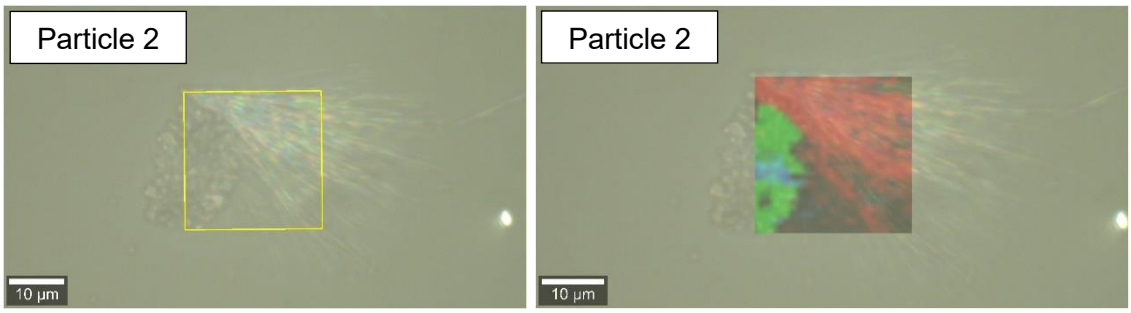


**Figure 60. Light microscopy image of precipitates from RGF_HPMCAS dissolution in FaSSIF after 48 h without (left) and with (right) Raman mapping. The component spectra for color coding are shown in Figure 86 (Appendix).**

Interestingly, amorphous RGF was not found in the investigated particles. Since only visible particles in the light microscope were investigated, the particle size of the amorphous precipitate might be too small for CRM *in-situ* analysis.

#### 3.5.3.3.4 RGF_PVP + 10% HPMCAS in FaSSIF

For RGF_PVP dissolution in FaSSIF with co-administered HPMCAS, also two different Raman signals were found, as presented in Figure 61. Here, no morphological differences in the precipitates could be seen, although the spectra showed clear differences, as shown in Figure 62.

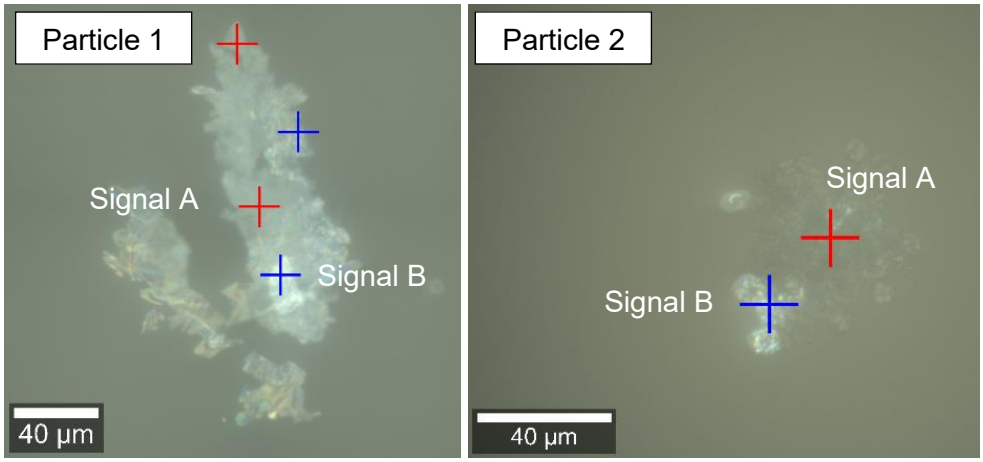


**Figure 61. Light microscopy images of precipitated particles from RGF_PVP + 10% HPMCAS dissolution in FaSSIF after 48 h. Raman measurement positions are indicated by the crosses.**

The obtained spectra A and B matched the signals from freeze-dried precipitates RGF_PVP / FaSSIF and RGF_PVP + 10% HPMCAS, respectively. Accordingly to the findings from the above *in-situ* CRM studies, RGF tended to precipitate in different modifications or pseudo-modifications during biorelevant dissolution studies.

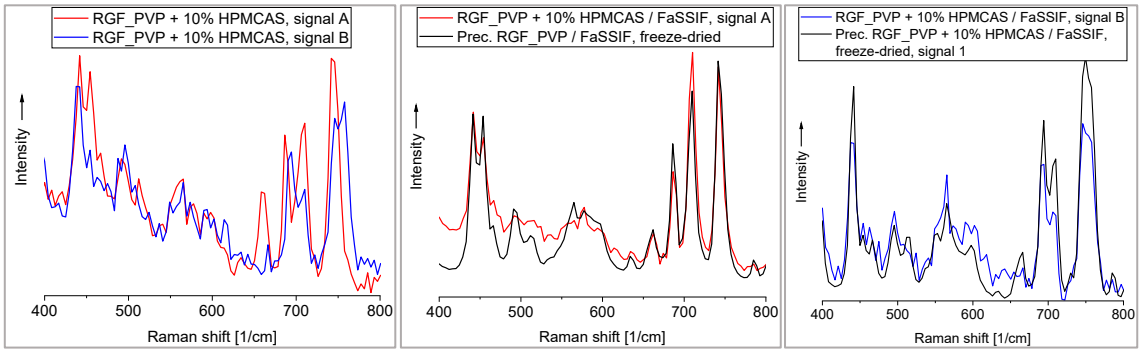


**Figure 62. Raman spectra acquired from both investigated precipitated particles from RGF_PVP + 10% HPCMAS dissolution in FaSSIF, shown in Figure 61.**

#### 3.5.3.3.5 RGF_PVP in FaSSGF

For RGF_PVP in FaSSGF dissolution, samples were drawn for 120 min and analyzed, according to the biorelevant transfer dissolution protocol applied in this work. Previous dissolution study results showed the fast RGF crystallization from RGF_PVP dissolution in FaSSGF (Figure 12 and Figure 13). Therefore, a dissolution study was performed for 120 min in FaSSGF and samples were drawn at 0, 15, 30, 77, and 120 min. The light microscopy images with single spot Raman measurements are shown in Figure 63, the acquired Raman signals and reference spectra are shown in Figure 64 and Figure 65.

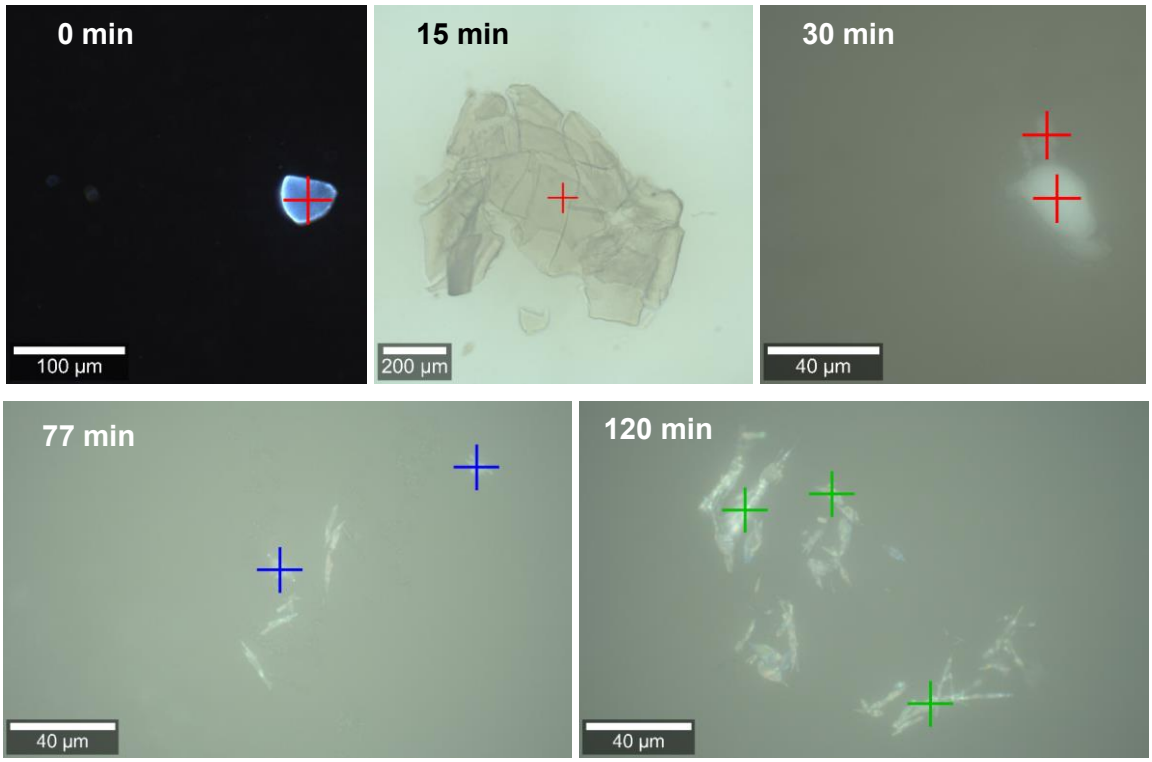


**Figure 63. Light microscopy images of RGF_PVP dissolution and precipitation in FaSSGF. Raman measurement positions are indicated by the crosses, the colors represent matching signals. The image at 0 min was acquired in dark field mode for better visibility.**

The ASD platelets underwent dissolution for 30 min, the particles became more transparent and the characteristic edges vanished. Raman spectra were recorded and showed full alignment to the Raman spectrum of the ASD RGF_PVP. After 30 min, no more ASD platelets were found. The first crystals with particle sizes allowing Raman measurement were found after 77 min, after 120 min the number of precipitates was vastly increased.

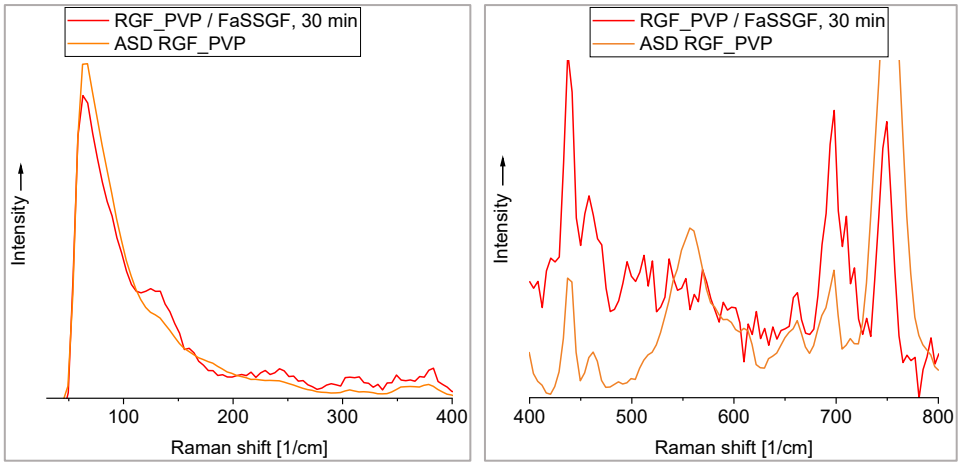


**Figure 64. Raman spectra of RGF_PVP platelets in FaSSGF. Different spectra excerpts are shown for better visualization.**

The Raman spectra from $t_{77min}$ and $t_{120min}$ showed clear differences, therefore the precipitated RGF is assumed to undergo further modification transitions. Whereas for RGF precipitates at $t_{120min}$ no match with a reference RGF modification was found, the precipitates measured at $t_{77min}$ were matching the signal of the freeze-dried precipitate.

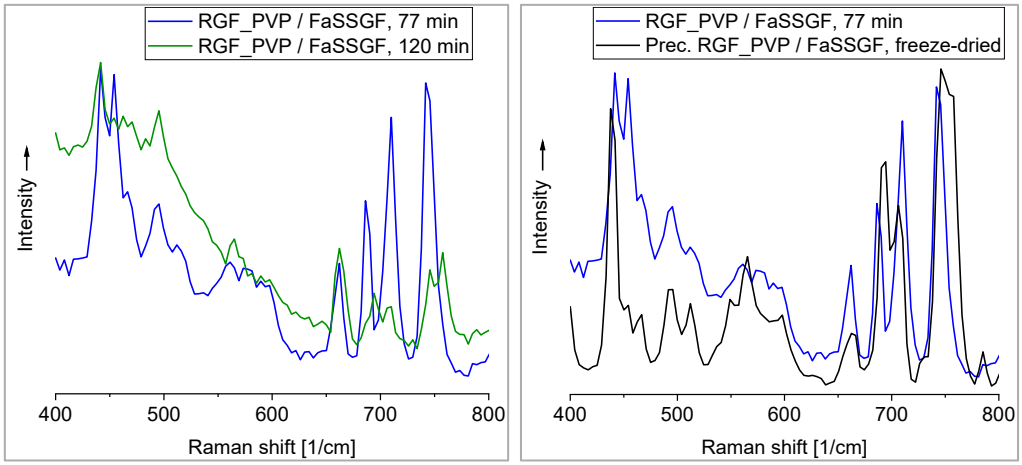


**Figure 65. Raman spectra of needle-shaped precipitates during dissolution of RGF_PVP in FaSSGF.**

### 3.5.3.4 Isothermal titration calorimetry (ITC)

To investigate the precipitation kinetics and enthalpies of different RGF formulations, ITC experiments were carried out. The technique of ITC was introduced in Section 1.3.2.5 and the experiments were executed as described in Section 6.2.3.4.10. Due to the 40 min of equilibration time of the ITC device after dissolution has started, all dissolution studies were carried out in FaSSIF. Since RGF precipitation from RGF_PVP in FaSSGF is faster, this would not allow a stable baseline before signal recording. It should be mentioned that only successful ITC runs were included in this work, resulting in an unequal number of replicates. From the results in Section 3.2.5, the influence of hydrodynamic situation on the *in-vitro* drug release from RGF_PVP is known. The geometry of the ITC sample cell and the stirring rate are different from the applied biorelevant dissolution systems, so the dissolution profiles obtained from the ITC device cannot be directly compared regarding the concentration-time profiles.

ITC experiments were conducted to monitor the precipitation process by measuring the change in heat over time. The obtained ITC graphs are presented in Figure 66. After equilibration, exothermal events were observed, which were regarded as precipitation signals. The resulting precipitation enthalpy $\Delta H$ and the time of maximum precipitation rate ($t_{max}$) which is equal to the time of minimum ITC power consumption are listed in Table 19. These values showed significant variability, i.e. relatively large CV, for RGF_PVP as well as slower precipitation kinetics and less scattering values for RGF_HPMCAS. It is thus conceivable that RGF supersaturation stabilized by PVP is less reproducible than the supersaturation using HPMCAS, indicating a less (HPMCAS-) stabilized RGF supersaturation in the presence of PVP.

**Table 19. ITC results: Precipitation enthalpy (ΔH) and time of maximum ITC signal ($t_{max}$) for different ASD formulations with RGF during biorelevant dissolution in ITC setup in FaSSIF.**

| Formulation | $t_{max}$ [h] | | $-\Delta H$ [kJ/mol$_{RGF}$] | |
|---|---|---|---|---|
| | Mean | CV [%] | Mean | CV [%] |
| RGF_PVP | 10.2 | 51.9 | 112.5 | 21.8 |
| RGF_HPMCAS | 16.4 | 7.4 | 124.9 | 12.6 |
| RGF_PVP +100 % HPMCAS | 9.4 | 47.9 | 100.7 | 13.3 |
| RGF_PVP +10 % HPMCAS | 12.1 | 14.9 | 108.4 | 54.5 |

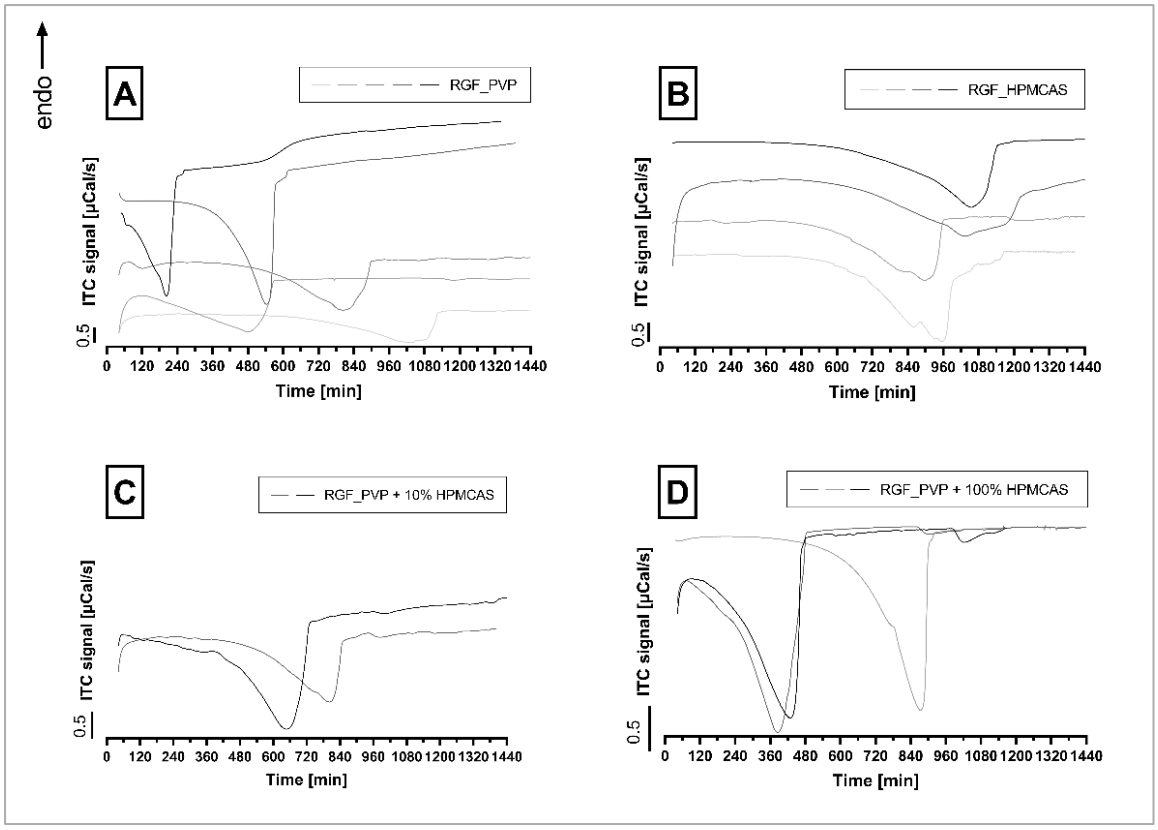


**Figure 66. Isothermal calorimetric investigation of the RGF precipitation from different formulations in FaSSIF. Single runs are shown. Spectra have been vertically offset for clarity.**

The precipitation enthalpies of RGF from different formulations, ranging from -101 kJ/mol to -125 kJ/mol, were compared to available data in literature. A study from Pudipeddi et al. (1995) reported $\Delta H$ for pseudoephedrine precipitation to range from -11 kJ/mol to -24 kJ/mol. For lysozyme crystallization within aqueous solution, -30 kJ/mol to -91 kJ/mol were reported (Schall et al. 1996).

Since RGF is a poorly water-soluble API with a melting temperature $T_m$ of about 200 °C for the thermodynamically most stable modification (RGF Mod. I), higher precipitation enthalpies were expected, compared to pseudoephedrine and lysozyme. Besides the lipophilic character of RGF, the high lattice enthalpy of RGF causes the high $T_m$ and poor water solubility in contrast to pseudoephedrine and lysozyme. The reported $T_m$ for pseudoephedrine is 117 °C and, for lysozyme crystals, range between 20 – 50 °C and 79 – 94 °C if the crystals are in solution or removed from the mother liquid and covered by oil, respectively (Jacob et al. 1998; Pudipeddi et al. 1995). In accordance, mean precipitation enthalpies of -101 kJ/mol to -113 kJ/mol were found for RGF formulations containing PVP and -125 kJ/mol for RGF_HPMCAS.

For RGF Mod. I, the heat of fusion was reported by *Bayer* to be 92 J/g or 44.4 kJ/mol (see Table 30, Annex). Surprisingly, for all ASD formulations, the mean precipitation enthalpies were more than twofold higher. These results were not expected, since *Bayer* states RGF Mod. I to be the most stable RGF polymorph and dominant precipitate species. One explanation might be simultaneous enthalpic processes during dissolution that have falsified experimental results. Further, highest precipitation enthalpies were measured for the formation of the amorphous precipitate RGF_HPMCAS / FaSSIF, which was not expected. From a thermodynamic perspective, the (partly) amorphous precipitate was expected to exhibit the least precipitation enthalpy, since no or only little crystalline lattice is formed during precipitation.

Based on the ITC signals, the temporal evolution of the RGF concentration of the supernatant was calculated to illustrate the different precipitation kinetics, as was shown for lysozyme earlier (Darcy and Wiencek 1988). Figure 67 shows representative RGF concentration-time plots. For each formulation, the ITC run which exhibited the smoothest profile was chosen.

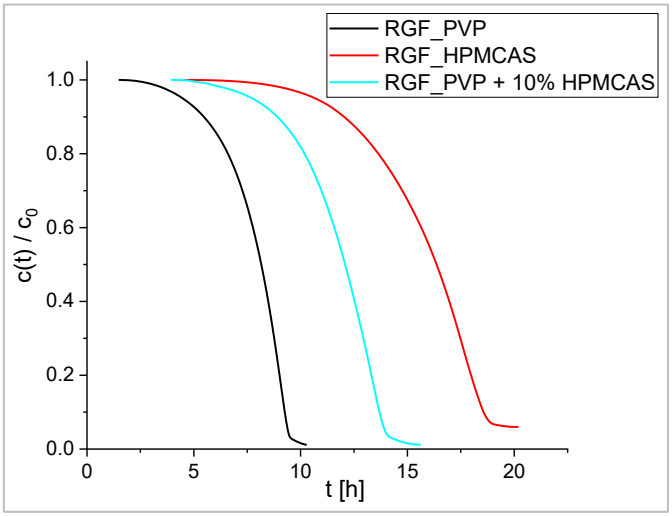


**Figure 67. Precipitation kinetics of RGF from various ASD formulations in FaSSIF at 37 °C.**

For the calculation, the observed change in enthalpy is assumed to be solely due to RGF crystallization since this is the dominant enthalpy process to be expected and no further components are likely to crystallize. This implies that entire RGF material was amorphous or dissolved at the beginning of the experiment. The equilibrium solubility of RGF in FaSSIF in the presence of PVP and HPMCAS was determined in Section 3.2.1.1. For the case, in which both PVP and 10 % HPMCAS were present, the solubility was assumed to

be that in the presence of only PVP. Since the initial concentration $c_0$ is known, the solubility $c_\infty$ measured independently and the whole temporal evolution of the baseline-corrected ITC power signal, *P(t)*, recorded, the concentration of the supernatant at a certain time *t* can be computed as follows:

$$c(t) = c_0 + (c_\infty - c_0)\frac{\int_{t_0}^{t} P(t')dt'}{\int_{t_0}^{t_{\max}} P(t')dt'} \qquad \text{Equation 10}$$

where $t_0$ and $t_{\max}$ indicate the starting and final time of the ITC experiment, respectively.

Once precipitation started, the growth of RGF nuclei and the formation of new RGF nuclei led to an increase in the precipitation rate until the solution was fully depleted and the solubility reached. The exemplarily chosen runs highlight the different precipitation induction times between both formulations and the slower formation of the amorphous co-precipitate of RGF and HPMCAS, compared to crystalline RGF from RGF_PVP dissolution.

These findings underline a different precipitation mechanism for RGF in presence of HPMCAS and absence of PVP.

The hypothesis of different molecular interaction between HPMCAS and RGF in the supersaturated state compared to PVP, leading to precipitates with different physicochemical properties, can be supported by comparison of the precipitation enthalpy $\Delta H$. Whereas $\Delta H$ values are quite similar for RGF_PVP with and without co-administered HPMCAS, the precipitation enthalpy seems to be greater for the precipitation process from RGF_HPMCAS dissolution, albeit the lack of statistical significance. The higher $\Delta H$ for RGF precipitation in absence of PVP leads to the assumption of a more stable precipitation product, therefore the presence of PVP in this system could interfere by molecular interactions and inhibit the formation of the co-amorphous RGF-HPMCAS precipitate. The slower drug release from RGF_HPMCAS already indicated a stronger interaction of RGF to HPMCAS than for PVP (Li and Taylor 2018).

### 3.5.4 Conclusions from precipitate analysis

The different physicochemical nature of investigated precipitates underlines a different precipitation mechanism for RGF in presence of HPMCAS and absence of PVP. It is likely that HPMCAS and RGF form a co-amorphous precipitate parallel to crystalline RGF.

In the RGF_HPMCAS / FaSSIF sample, a high-melting endothermal DSC event (Figure 41), but no additional diffraction peak compared to the RGF_PVP / FaSSIF sample was found (Figure 40). The amorphous state and the morphological separation of crystalline and amorphous parts was also revealed by CRM results (Figure 42 and Figure 44). These findings were indirectly supported by *in-situ* measurements due to the absence of diffraction peaks during *in-situ* WAXS experiments, hence an amorphization process during the freeze-drying is unlikely to have occurred. SAXS measurements revealed the inner structure of the amorphous co-precipitate to be built of spherical units with a maximum diameter of 6 nm (Figure 53).

The presence of PVP was suppressed the amorphous nature of RGF_HPMCAS / FaSSIF precipitates in favor of crystalline polymorphs, as various co-existing morphologies were observed in SEM images (Figure 39). To further study non-amorphous precipitation in the presence of both PVP and HPMCAS, HPMCAS was co-administered to the dissolution of RGF_PVP in FaSSIF. If compared with the reference formulations RGF_PVP / FaSSIF and RGF_HPMCAS / FaSSIF, a new RGF polymorph with different physicochemical behavior was identified in DSC (Figure 41), XRPD (Figure 40), and CRM studies (Figure 42 to Figure 44).

Changing FaSSIF to FaSSGF illustrated the importance of the precipitation environment on the RGF polymorph formation. The reduced amount of bile salts and lower pH from 6.5 to 1.5 altered the precipitate from RGF_PVP dissolution. A transformation of precipitated RGF polymorph over dissolution time was observed in *in-situ* CRM experiments for RGF_PVP dissolution in FaSSGF, whereas the precipitated RGF polymorph from RGF_PVP dissolution in FaSSIF did not change over time in *in-situ* WAXS studies (Figure 47).

The interactions between polymer (HPMCAS and/or PVP) and RGF in the supersaturated state affected the physicochemical properties of the precipitates, as reflected in the precipitation enthalpy. The values of $\Delta H$ were quite similar for RGF_PVP with and without co-administered HPMCAS, but seemed to be larger for the precipitation process from RGF_HPMCAS dissolution (Table 19), however, statistical significance was not reached. The higher $\Delta H$ for RGF precipitation from RGF_HPMCAS in FaSSIF in the absence of

PVP can be ascribed to a more stable precipitation product. Therefore, the presence of PVP could interfere with molecular interactions, inhibiting the formation of the co-amorphous RGF-HPMCAS precipitate. The influence of HPMCAS co-administration to RGF_PVP more strongly affected the shape of the precipitation profile (Figure 66), i.e. the precipitation kinetics, than the characteristic values $t_{max}$ or $\Delta H$, since also a crystalline precipitate formed, but with different precipitation kinetics, presumably by stronger stabilization of supersaturated RGF by HPMCAS.

These new findings support the existing data for different drug substances in literature. Chen et al. (2016) reported an amorphous co-precipitate of posaconazole and HPMCAS with a drug load of 16-18 %, however, in the presence of SDS the precipitates were not amorphous. These findings were explained by strong interactions of HPMCAS and the API and SDS, inhibiting the formation of amorphous co-precipitates by competitive interactions with the stabilizing polymers. This concept might also be applied to the system RGF-HPMCAS-PVP. RGF and HPMCAS formed amorphous co-precipitates in the absence of PVP, while strong interactions between HPMCAS and PVP decreased the availability of HPMCAS for stabilization. In a different study, Elkhabaz and coworkers (2018) reported a strong precipitation inhibition and delay capability of HPMCAS leading to drug precipitates with a partly amorphous character.
The importance of the dissolution medium on the physicochemical properties of the precipitates is in accordance with published literature, as posaconazole was found to form co-precipitates with HPMCAS with a drug load depending on the pH of the dissolution medium and HPMCAS grade (Wang et al. 2018b).
The importance of polymer selection on the physicochemical properties of precipitated API was also described by Dereymaker et al (2017). An indomethacin-Eudragit RL ASD was formed crystalline precipitates in the presence of PVP and amorphous precipitates in its absence, which was explained by different release kinetics. Moreover, the lipophilic and hydrophilic properties of HPMCAS (Friesen et al. 2008) could promote the formation of an amorphous co-precipitate. Wang and coworkers found intermediate hydrophilic-lipophilic polymers to directly stabilize the drug-rich phase during ALPS, eventually leading to amorphous co-precipitates (Wang et al. 2018b).

Since re-dissolution of amorphous precipitates might increase the overall bioavailability of poorly water-soluble drugs, which is outlined in more detail in Section 1.3.1, the generation

of amorphous precipitates *in-vivo* by careful polymer selection might be promising. The formulation strategy of engineered amorphous precipitates might stimulate further research to evaluate the potential of amorphous precipitation *in-vivo* for the oral bioavailability and further improvement of the drug formulation strategy. The proposed complementary analytical approach might serve as a protocol for future investigations of ASDs with poorly water-soluble APIs.

## 3.6 Permeation Studies

### 3.6.1 Introduction

The superior *in-vitro* performance of the formulation concept RGF_PVP + HPMCAS has been demonstrated in dissolution studies. However, the prediction of *in-vivo* drug performance by *in-vitro* dissolution studies is challenging for BCS II compounds, even by applying biorelevant dissolution test devices (Tsume et al. 2018).

For more valid statements, not only dissolution but also permeation testing has to be considered. As RGF MH is a typical representative of BCS II compounds, permeability is expected not to limit bioavailability in humans. On the other hand, the formulation approach developed in this work suggests a combination of fast-release ASD with a stabilizing agent, which might impact drug permeation, e.g. by incorporation into colloidal HPMCAS structures. Cyclodextrins (CDs) are often used in pharmaceutical formulations for solubilization of poorly water-soluble compounds via incorporation of hydrophobic APIs into the CDs' hydrophobic cavities. This effect is also raising difficulties, as the bioavailability can be limited by the incorporation (Loftsson and Brewster 2010).

For HPMCAS, a solubilizing effect for RGF was observed as described in Section 3.2.1.1. Analogous to CDs, RGF might be incorporated into HPMCAS hydrophobic sites thus being prevented from absorption which might impair BA in patients, since only molecularly dissolved API is described to increase drug permeation rate (Buckley et al. 2013). To reveal the impact of RGF incorporation into HPMCAS, *in-vitro* permeation studies were conducted.

### 3.6.2 *In-vitro* permeation model development

The permeation model was mainly designed to answer the following question: Does RGF from its supersaturated HPMCAS-stabilized state still permeate through a membrane or is it 'trapped' in HPMCAS colloids? If this were the case, bioavailability be might even decreased and not increased.

In literature, different methods are published, as discussed in Section 1.2.3. For the specific questions of the present work, the permeation model was determined to comprise of:

- a biomimetic barrier membrane
- RGF sink conditions in acceptor media to avoid precipitation and reflux

- comparable dissolution conditions as in the small-scale dissolution method, e.g. stirring and temperature
- avoidance of unnecessary surfaces (tubes, glasses), as this might lead to deviations from dissolution results by RGF adsorption and precipitation on these materials

For the reasons described in Section 1.2.3, it was decided to acquire the artificial membranes PermeaPlain and PermeaPad. For PermeaPad similar results were obtained compared to PAMPA and Caco-2 setups in several comparative studies (Bibi et al. 2016; di Cagno et al. 2015). PermeaPad consists of two cellulose backing layers stabilizing a phospholipidic membrane in between. Since the membrane is not perforated, no media exchange is expected to occur across the barrier. The design of PermeaPlain is a more basic approach, here only the described cellulose backing sheet is used as a membrane with a maximum pore size of 33 ± 20 nm, according to personal correspondence with the supplier. Both barrier types are described to be compatible with FaSSIF media according to the respective manual (InnoME, 2018). For PermeaPlain, clear separation of donor and acceptor media is not given, so special care must be undertaken to avoid re-flux of already permeated RGF to the donor compartment.

The exact experimental setup and procedure are given in Section 6.2.4.2. A self-assembled dissolution-permeation chamber was used, as shown in Figure 77 and Table 29. The lower donor compartment was stirred with a magnetic stirring bar at 200 rpm, similar to the small-scale dissolution method used in this work, but gentle enough to avoid membrane damage. A lid with a hole was used to fixate the membrane in the inner glass cylinder. The diameter of the lid hole was 7.55 mm, so the membrane surface for permeation was 179.1 mm². A hole was drilled through the upper end of the inner glass cylinder to allow the autosampler tube to gently circulate the acceptor media, to avoid a concentration gradient within the acceptor compartment. The ability of poorly soluble drug molecules to permeate across membranes is greatly affected by plasma protein binding, as after absorption, the drug typically exists in a protein-bound form that ensures sink conditions in the blood stream (Buckley et al. 2012). This was also found for RGF and its major metabolites in humans (Zopf et al. 2016). Typically, a 4 % BSA solution is used for *in-vitro* permeation studies to achieve sink conditions (Buckley et al. 2012). Prior to injection into HPLC, RGF has to be released from BSA, e.g. by precipitation of BSA through the addition of organic solvents (Taevernier et al. 2015). Although, after sample preparation, to some extent the API might

be still bound to precipitated BSA or be encapsulated within the precipitate. But since this procedure is a common approach, the methodical limitations are considered to be neglectable.

The PermeaPad and PermeaPlain barriers were found to be retentive to BSA. As shown in Table 20, a 4 % BSA solution was tested for permeation across a PermeaPlain membrane which is also part of the PermeaPad membrane system. After 24 h, no BSA was detected in the acceptor compartment in a triplicate approach. This is a necessary prerequisite for permeation studies, as the dissolution media at the donor side must not be affected by the acceptor media. However, FaSSIF components are expected to permeate across PermeaPlain membranes, contrary to PermeaPad membranes. As a consequence, 4 % BSA in FaSSIF was used as acceptor medium when PermeaPlain membranes were used to avoid a flux of FaSSIF components to the acceptor medium over time.

**Table 20. DLS results of BSA permeability across PermeaPlain barrier after 24 h. A solution of 4 % BSA and distilled water were used as acceptor compartment or donor compartment media, respectively.**

| | Measurement 1 | Measurement 2 | Measurement 3 |
|---|---|---|---|
| | z-average [nm] | | |
| Acceptor compartment | 4.0 | 4.0 | 4.1 |
| Donor compartment | - | - | - |

The determined z-average of BSA in the acceptor compartment was 4.0 nm which is in accordance with literature (Wright and Thompson 1975). In the present setup, only the presence or absence of a detectable z-average in the donor compartment was of interest. Since no light scattering was determined in the donor compartment, a z-average cannot be calculated and no BSA permeation across the PermeaPlain barrier is assumed.

### 3.6.3 RGF solubility in BSA solution

As mentioned in the permeation setup development section above, 4 % BSA in water or FaSSIF solution was used as acceptor medium. Therefore, sufficient RGF solubility is required for sink conditions to avoid RGF precipitation in the acceptor compartment.

The solubility of RGF in 4 % BSA was determined analogously to Method 6.2.3.1.3, the results are stated in Table 21.

Table 21. RGF solubility in permeation acceptor media (n = 3, mean ± CV).

| Acceptor media | RGF concentration |
|---|---|
| 4 % BSA solution | 23.63 µg/mL ± 34.3 % |

From these results, sink conditions in the acceptor compartment are not given. Since 10 mL acceptor medium is used, a total of 236 µg RGF is soluble in the acceptor compartment. However, the applied RGF dose in these experiments was 2.66 mg RGF, exceeding the equilibrium solubility by a factor of 11. An increase in BSA concentration was not successful, as the higher viscosity was impeding the autosampler device. Hence, the acceptor medium was changed regularly in case of borderline RGF concentrations to avoid RGF precipitation or a reduced permeation.

### 3.6.4 *In-vitro* permeation through artificial membranes

The ASD formulations RGF_PVP and RGF_HPMCAS were investigated regarding their RGF permeation potential by the dissolution-permeation setup described above. In a first attempt, PermeaPad membranes were used, as higher biopredictive potential was expected. Unfortunately, for all four PermeaPad dissolution-permeation setups no RGF was found in the acceptor compartment. This would indicate that from neither formulation, RGF_PVP or RGF_HPMCAS, permeation across the PermeaPad membrane occurred. Since *Stivarga* is based on RGF_PVP and permeation definitely was observed in animal and human clinical trials, this experimental setup did not satisfyingly mimic the RGF permeation process.

As mentioned above, the PermeaPad membranes consist of cellulose backing sheets and a phospholipid membrane enclosed. The hydrophobic nature of RGF could have led to either precipitation of dissolved RGF on the membrane, as this effect was observed for hard fat, described in Section 3.4.1.3. Also possible is the accumulation of RGF within the PermeaPad membrane, but this effect was not further investigated. In the dissolution-permeation setup, the membrane type was changed from PermeaPad to PermeaPlain and the experiments were repeated. The resulting are shown in Figure 68. The RGF signal intensities were below the analytical LOQ, so a rather comparative discussion is appropriate.

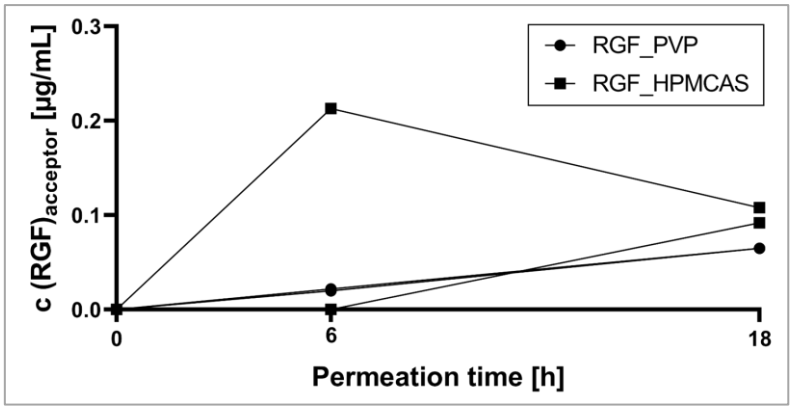


**Figure 68. Permeation of RGF across PermeaPlain barrier (n = 2). Single curves are shown.**

The most important result is obvious: In all samples RGF was detected, hence RGF permeation from both formulation across PermeaPlain barriers appeared. It can be stated for the hypothetical RGF-HPMCAS associates to either have a thermodynamic balance between molecularly dissolved RGF and HPMCAS-associated RGF or the associates were unable to cross the pores in PermeaPlain, e.g. due to their size. Generally, a trend was visible for both formulations, as permeated RGF increased over time. Interestingly, for RGF_HPMCAS in one setup more RGF was detected after 6 h than after 18 h. The generally very low RGF concentrations might be affected by the sample preparation procedure, as mentioned above. A further possible explanation would be a re-flux from acceptor to donor media when the RGF supersaturation was reduced.

To conclude, RGF permeation in the presence and absence of HPMCAS was observed by the use of PermeaPlain barriers. But as colloidal particles and media components can pass the membrane, and RGF re-flux from acceptor to donor compartment cannot be avoided, this system does only provide hints but does not allow predictions for the *in-vivo* situation.

## 3.7 *In-vivo* pharmacokinetic study

Preamble

*The experimental results and discussions in the following section are partly based on a collaboration with external partners. Dr. Jan Stampfuss (Bayer AG) was responsible for the design and execution of the* in-vivo *PK study in rats and provided RGF concentration analysis from plasma samples.*

*Essential contents of this chapter are based on the patent application "EP20156003.4" (European Patent Office) by Martin Müller, Werner Hoheisel, Anke Stroyer, Markus Albers.*

*Essential contents of this chapter are based on the research article manuscript "The Impact of HPMCAS Co-administration on the Biopharmaceutical Performance of Regorafenib Amorphous Solid Dispersion" (Target Journal Eur. J. Pharm. Biopharm.) by Martin Müller, Raphael Wiedey, Werner Hoheisel, Peter Serno, and Jörg Breitkreutz.*

### 3.7.1 Pharmacokinetic study in rats

An *in-vivo* pharmacokinetic (PK) study in rats was performed at *Bayer*. The aim of this study was a proof-of-concept for BA effects of co-administration of the stabilizing agent HPMCAS, which led to superior results at *in-vitro* dissolution experiments, as described in Section 3.4. Furthermore, *in-vitro* dissolution-permeation results hinted that co-administration of the stabilizing agent HPMCAS does not necessarily reduce permeability across a cellulose membrane, shown in Section 3.6.4.

General aspects about *in-vivo* studies are discussed in Section 1.2.3, in short, an *in-vivo* approach is one step closer to the *in-vivo* conditions in humans than biorelevant dissolution tools. The study protocol was predetermined by *Bayer* and in accordance with the relevant ethics committee and authorities. More details about the study protocol are provided in Section 6.3.1. It is important to mention that solely RGF and no pharmacologically active metabolites were detected, so individual metabolism rates in the animals are not reflected. Regulated by the study design, only a suspension could be administered via a stomach tube to the rats. This implicated the formulation approach Stivarga_HPMCAS developed in Section 3.4, as an enteric-coated monolithic tablet could not be administered. In theory, HPMCAS coating of RGF_PVP powder particles would be possible, however, this would lead to an undesired increase in the ratio of HPMCAS to RGF_PVP because of the higher surface of RGF_PVP particles compared to a *Stivarga* tablet. Therefore, this concept was rejected. Hence, the formulation RGF_PVP + 10% HPMCAS was chosen, which superior dissolution performance at simulated intestinal conditions was shown in this work, but re-crystallization of the amorphous API at acidic conditions is expected from the results presented above.

Before application to the rats, the ASD formulations were pre-suspended in tap water. From preliminary studies, the rapid precipitation of RGF_PVP in distilled water is known. This could not be avoided due to the study protocol. However, the effect was assumed to be the same for both formulations and of minor extent since the time span between pre-suspension and application was about 3 min to 5 min. The executing lab technician from *Bayer* stated that the application of suspended ASDs to the rats was difficult, so the applied dose might not be absolutely exact. By the use of a 10 mL syringe, some variability in the applied doses might have occurred.

### 3.7.2 Biorelevant transfer dissolution at rat conditions

The *in-vivo* study in rats was planned to investigate the impact of HPMCAS co-administration on bioavailability. Moreover, the biorelevant transfer dissolution system used in this work was modified to meet the *in-vivo* conditions in rats to evaluate the predictive power of the dissolution results towards the obtained *in-vivo* PK data.

Rats are extensively used as *in-vivo* model in pre-clinical testing, but the gastrointestinal conditions of rats differ to some extent from those of humans which has to be considered, especially if pH-dependent drug formulations are investigated. McConnell et al. (2008) found the pH in the rat stomach to be 3.2 ± 1.0 and 3.9 ± 1.0 in the fed and fasted state, respectively. The intestinal pH was described to range from 5.0 ± 0.3 in the fed state to 5.9 ± 0.3 in the fasted state . The $pK_a$ of HPMCAS succinyl groups is around 5, hence ca. 99 % of the carboxylic substituents of the polymer are not ionized at fasted gastric conditions in rat. At elevated intestinal pH of 5, the polymer becomes negatively charged since 50 % of carboxylic groups are deprotonated, which allows the polymer to dissolve in aqueous media (Friesen et al. 2008). Therefore, the stabilization of RGF_PVP generated RGF supersaturation by dissolved HPMCAS molecules is expected after media conversion to $FaSSIF_{rat}$.

The gastric transfer time in rats might be assumed to be around 15 min to 30 min for liquids, but only limited data is available (Grignard et al. 2017). The pH values and gastric transit time in the dissolution experiment were adapted to mimic the gastrointestinal situation in rat. Moreover, the sampling time points were adapted to those of the planned PK study. For this study, the above-mentioned pH values were considered. To mimic the rat gastric media, FaSSGF was modified to pH 3.2 ($FaSSGF_{rat}$) and for rat intestinal media, pH 5.0 ($FaSSIF_{rat}$) was chosen. In literature different types of rat mimicking biorelevant media are described, however, in this study, only the pH of FaSSGF and FaSSIF were adapted (Jede et al. 2019; Tanaka et al. 2017).

The results of the rat-mimicking biorelevant transfer dissolution studies are shown in Figure 69. The RGF release profiles of RGF_PVP without HPMCAS co-administration followed the same trend, $c_{max}$ was measured at $t_{120min}$ after media conversion. De-supersaturation occurred consistently from $t_{180min}$ to $t_{420min}$ and at $t_{1440min}$ no supersaturation was found. These findings are in accordance with the results obtained by the biorelevant transfer dissolution mimicking the human small intestinal conditions with a transit time of 30 min, as shown in Section 3.2.4.2. Hence, it can be assumed that precipitated RGF during

simulated gastric transfer acted as a seeding crystal and subsequently led to faster precipitation and crystal growth rates during the *parachute* phase.

The co-administration of HPMCAS had a strong impact on the RGF release profile. As already displayed in Figure 25, the addition of HPMCAS led to a decreased drug release in the *spring* phase, whereas the *parachute* effect is strongly pronounced. One sample drawn at $t_{60min}$ seems to be an outlier, this could be caused by filter defects by which small particles might have passed the syringe filter and falsified this specific sample.

Interestingly, the predicted *in-vivo* variability in rats is reduced compared to humans, for whom biorelevant dissolution testing of *Stivarga* predicted the strong fluctuations (Figure 38), which have been reported in literature (see Section 1.1.3.1).

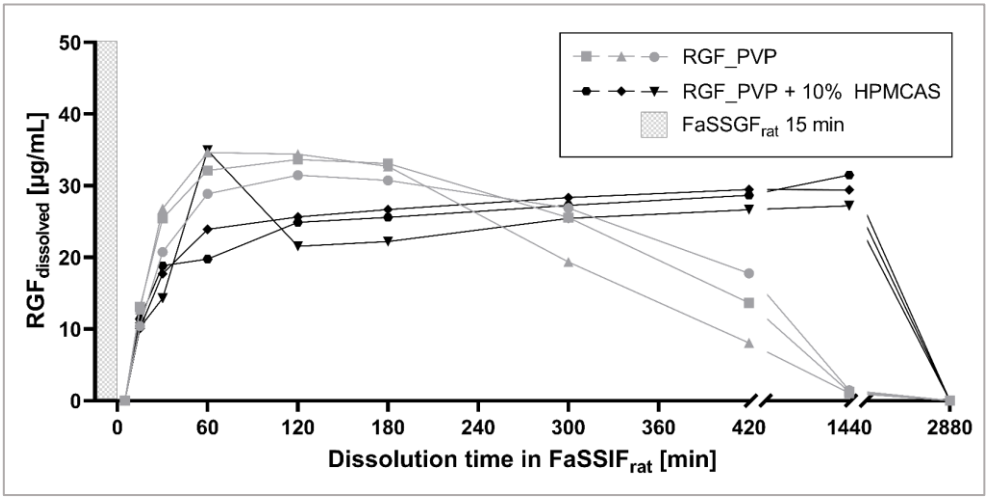


**Figure 69. Biorelevant transfer dissolution testing at simulated rat conditions of RGF_PVP with and without stabilizing agent HPMCAS (37 °C, 75 rpm). Dissolution was performed in 250 mL FaSSGF$_{rat}$ for 15 min prior to addition of 500 mL FaSSIF$_{conc., rat}$. The dissolved dose is dose is equivalent to one *Stivarga* tablet (40 mg RGF). Single curves are shown.**

From these results, the expected impact of HPMCAS co-administration *in-vivo* will come into effect from $t_{420min}$ to $t_{1440min}$ however, the variable gastric emptying in rats must be kept in mind. As the absolute difference in mean RGF concentration between both formulations for the first 300 min is not strongly different, a clear difference in PK data is expected in the best case for the *parachute* phase.

### 3.7.3 Results of PK study

The *in-vivo* study was conducted successfully with eight rats. The RGF plasma level curves for both study groups RGF_PVP (reference group) and RGF_PVP + 10 % HPMCAS (study group) are presented on a linear scale in Figure 70 and on a logarithmic scale in

Figure 71. Selected PK parameters for both study groups are given in Table 22, more detailed information is provided in Table 33 and Table 34 (Annex). Further, the RGF plasma concentrations for both administered formulations are provided in Table 35 and Table 36 (Annex).

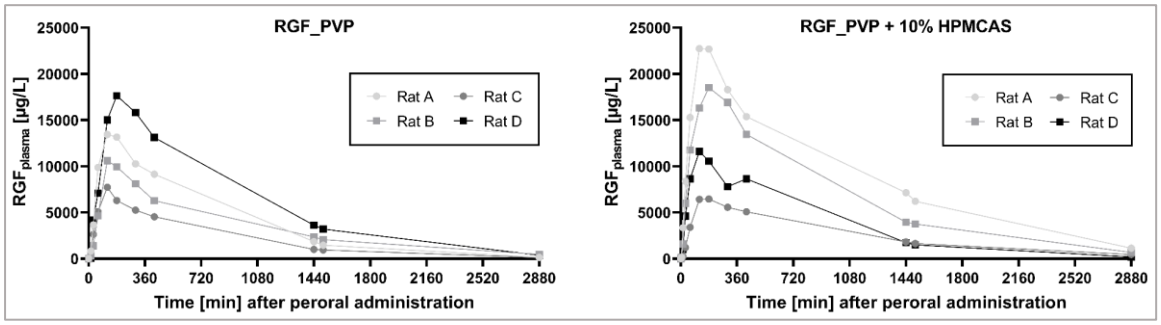


**Figure 70. *In-vivo* RGF plasma levels over time for both study RGF_PVP and RGF_PVP + 10 % HPMCAS on a linear scale.**

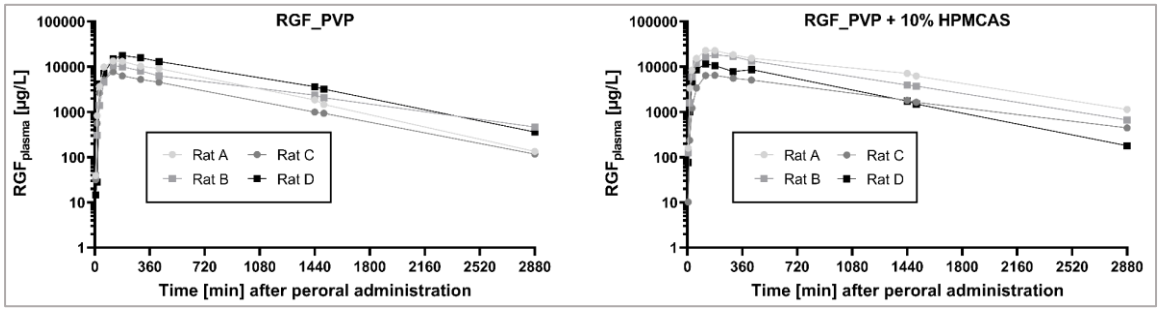


**Figure 71. *In-vivo* RGF plasma levels over time for both study RGF_PVP and RGF_PVP + 10 % HPMCAS on a semi-logarithmic scale.**

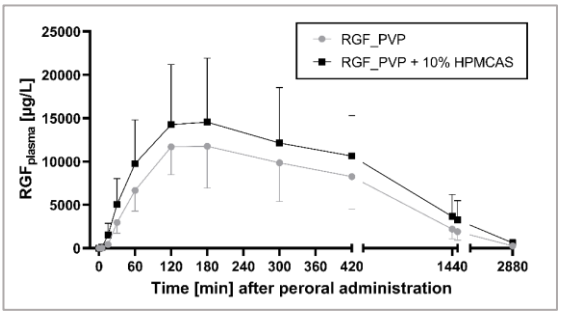


**Figure 72. *In-vivo* RGF plasma levels over time for both study groups. Mean values, linear scale (n = 4, mean ± s).**

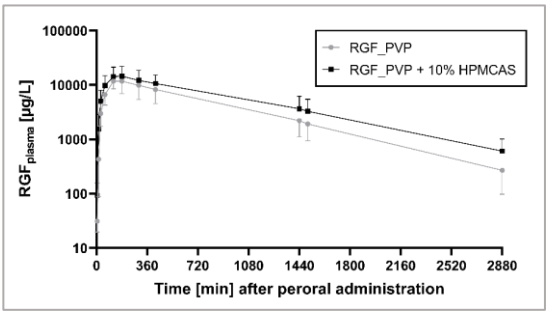


**Figure 73. *In-vivo* RGF plasma levels over time for both study groups. Mean values, semi-logarithmic scale (n = 4, mean ± s).**

The plasma curves from all rats showed the typical plasma profile after oral administration of immediate-release formulations comprising absorption and elimination. In all rats, $t_{max}$ was found to be between 2 h and 3 h after administration and not significantly influenced

by HPMCAS co-administration. In contrast to these quite reproducible data, the absolute RGF $c_p$ values showed strong variations within both study groups. The observed $c_{max}$ values differed by a factor of 2.3 for RGF_PVP and by 3.5 for HPMCAS co-administration.

**Table 22. PK parameters of *in-vivo* study (m ± CV or s). More parameters are listed in Table 33 and Table 34 (Appendix). p values are given for two-tailed (one-tailed) t-test (α = 0.05).**

| PK parameter | RGF_PVP | RGF_PVP + 10% HPMCAS | p-value |
|---|---|---|---|
| $AUC_{total}$ [mg·h/L] | 166.8 (± 42 %) | 241.5 (± 54 %) | 0.35 (0.17) |
| $t_{1/2}$ [h] mean | 8.3 (± 19 %) | 10.0 (± 18 %) | 0.21 (0.10) |
| $c_{max}$ [mg/L] mean | 12.3 (± 34 %) | 14.8 (± 49 %) | 0.58 (0.29) |
| $t_{max}$ [h] mean | 2.25 (± 0.5) | 2.5 (± 0.6) | 0.54 (0.27) |
| $k_e$ [1/h] mean | 0.0858 (± 18 %) | 0.0713 (± 19 %) | 0.21 (0.10) |

The plasma profiles of both study groups can be compared by their mean values which are, as shown in Figure 72, higher for RGF_PVP + 10% HPMCAS at all measured time points, hinting for a generally superior PK performance. However, the high inter-individual variabilities in both study groups lead to statistically not significant differences, thus any observed differences might be arisen by chance. On the other hand, also a decreased absorption in the presence of external stabilizer was deemed plausible due to strong molecular interactions of RGF and HPMCAS. In this study, however, the data do not indicate such a phenomenon.

As mentioned above, an enteric RGF_PVP formulation could not be administered to the rats, limiting the predictive power towards *in-vivo* performance in humans. In humans, precipitation of RGF from RGF_PVP in the human stomach would be avoided by an enteric formulation, as demonstrated *in-vitro* for Stivarga_HPMCAS (Figure 38). Moreover, *Bayer* reports the $c_{max}$ after intake of four *Stivarga* tablets (160 mg RGF) to be 2.53 mg/L ± 43 % and $t_{1/2}$ to be 28.4 ± 58 %, which is strongly different compared to the *in-vivo* data in rats, limiting the predictive power of this *in-vivo* setup (Stivarga product monograph, 2020).

To obtain more solid data about the impact of HPMCAS on RGF BA in rats, the *in-vivo* study would have to be extended to more subjects. These limitations in statistical significance of the conducted rodent study are a common phenomenon for poorly water-soluble APIs (Grabowski et al. 2014; Jede et al. 2019). Consequently, for stronger results

with higher predictability, human subjects in must be chosen in the frame of a controlled clinical study.
The lack of statistical significance also impedes detailed comparison of the biorelevant dissolution at simulated rat conditions (Section 3.7.2) and the *in-vivo* results regarding IVIVC.

To conclude, these *in-vivo* findings do not demonstrate superior PK performance for RGF in the presence of HPMCAS, which was assumed from the promising *in-vitro* biorelevant dissolution results. Since RGF permeation was found to be not statistically different between both study groups, the newly developed formulation concept Stivarga_HPMCAS is not expected to show limited RGF permeation in humans.

# 4 Summary

Today, the poor water solubility of new drug candidates is a major challenge to achieve sufficient bioavailability for orally administered drugs. To overcome this limitation, the formulation technique of amorphous solid dispersions (ASDs) was shown to be promising in the development of poorly water-soluble drug candidates. In literature, various formulation approaches have been published, however, the interplay of dissolution, supersaturation, absorption, and precipitation, all together governing the drug bioavailability, is not fully understood. Further, it is hypothesized that the physicochemical properties of precipitated drug substance can influence the overall bioavailability. For some active pharmaceutical ingredients (APIs), crystalline and amorphous precipitates have been described, depending on the formulation composition.

Regorafenib monohydrate (RGF MH), marketed by *Bayer* under the trademark of *Stivarga*, is a poorly water-soluble API formulated as an ASD, which shows undesired variability in bioavailability. To gain a deeper understanding of the underlying mechanisms and to reduce this variability, the impact of different ASD formulation strategies was investigated. Besides binary compositions of the drug in a matrix of one polymer, ternary formulations comprising the drug, one polymer and one surfactant or one more excipient polymer, were investigated.
In addition to povidone (PVP), which is the ASD matrix former in *Stivarga*, the structurally different polymers hypromellose acetate succinate (HPMCAS) and powdered basic butylated methacrylate copolymer (Eudragit E PO) were successfully used for binary or ternary RGF ASD preparation.

Biorelevant dissolution studies at simulated intestinal conditions revealed strongly different drug release and supersaturation behavior, dependent of the ASD composition. For RGF_PVP, fast drug release and sufficient supersaturation stability for 6 h was found, but for RGF_HPMCAS, a prolonged-release profile and RGF supersaturation for over 24 h were found. Interestingly, the drug release from ASDs comprising PVP and HPMCAS was ruled by the drug release properties of HPMCAS, independent of the polymer ratio. Since RGF_EPO showed strong variability *in-vitro*, this formulation was rejected.

The physiological transit from the stomach to intestinal sections was mimicked by the implementation of a biorelevant transfer dissolution model. Whereas RGF_PVP dissolution performance was strongly affected by the simulated gastric emptying time, RGF_HPMCAS was found to be a robust formulation.
These findings were underlined by seeded dissolution studies, i.e., the co-administration of de-stabilizing compounds, such as crystalline RGF or hard fat. Hypromellose (HPMC) and HPMCAS inhibited RGF crystallization from the supersaturated state stronger than PVP. From these results, a new formulation concept was developed by co-administration of the stabilizing polymers HPMC or HPMCAS to the fast-release formulation RGF_PVP, however, the stabilizing agent must not be comprised in the matrix to avoid undesired slow drug release kinetics.
These different drug release and supersaturation stabilization properties were attributed to molecular interactions of the ASD polymers with RGF in the dry and dissolved states.

To encounter the early re-crystallization which was predicted from *in-vitro* studies to occur during *in-vivo* gastric transit, thus to increase the robustness in drug dissolution performance, the drug product must exhibit a gastro-resistant function. This concept was demonstrated successfully by coating of *Stivarga* tablets with HPMCAS, leading to a dual function of HPMCAS; gastro-resistance of the dosage form and supersaturation stabilization after drug release.

The physicochemical properties of formed precipitates during biorelevant dissolutions of different formulations were explored off-line and *in-situ*. Regorafenib precipitated in different polymorphic states depending on the precipitation environment, as such the ASD polymer(s) and the type of biorelevant media.
For RGF_PVP dissolution in FaSSIF, *in-situ* wide angle X-ray scattering experiments were conducted to monitor RGF crystal growth from ca. 7 nm to 23 nm. Interestingly, an amorphous co-precipitate was found after dissolution of RGF_HPMCAS in FaSSIF, which did not form in presence of PVP. Small angle X-ray scattering measurements indicated globular shaped objects of approximately 6 nm diameter to be the dominant species within the amorphous co-precipitate.
The co-existence of different RGF polymorphs during dissolution in different biorelevant media was demonstrated by *in-situ* confocal Raman microscopy measurements.

Isothermal calorimetric dissolution studies confirmed the stronger stabilization of RGF supersaturation by HPMCAS since higher precipitation enthalpies were found for the amorphous co-precipitate than for crystalline precipitates.

The impact of HPMCAS on RGF permeation was evaluated in an *in-vivo* study in rats. No significant difference in bioavailability was found for RGF_PVP with or without co-administered HPMCAS. However, it was concluded that the strong interactions of RGF and HPMCAS in the dissolved state did not inhibit RGF permeation in rats.

The concept of co-administering of a stabilizing agent to a fast-release ASD seems to be highly promising and its practical relevance for an existing, marketed drug product is shown in this work for the first time.
To date, the concept of a dual function of a single excipient as supersaturation stabilizing agent and simultaneously gastro-resistant coating material has not been published before. This concept provides an elegant future formulation approach by reducing the number of excipients in simplified drug formulations. Here, further research will have to be conducted with structurally different APIs to evaluate its full potential for formulation scientists.

# 5 Zusammenfassung

Die Formulierungsentwicklung von schwer wasserlöslichen Arzneistoffen zu oralen Darreichungsformen mit genügender Bioverfügbarkeit ist eine große Herausforderung in der heutigen Arzneimittelentwicklung. Das Konzept der amorphen festen Lösungen (ASDs) erwies sich hierbei als ein erfolgsversprechender Ansatz.
Trotz intensiver Forschungsarbeit in den vergangenen Jahren und daraus hervorgegangenen modernen Formulierungsstrategien für neue Wirkstoffkandidaten ist das Zusammenspiel von Auflösung, Übersättigung, Absorption und Ausfällung, die alle zusammen die Bioverfügbarkeit von Arzneimitteln bestimmen, nicht vollständig verstanden. Weiterhin wird vermutet, dass die physikalisch-chemischen Eigenschaften des präzipitierten Arzneistoffs dessen Bioverfügbarkeit beeinflussen können. Für einige Arzneistoffe wurden formulierungsabhängig kristalline und amorphe Präzipitate beschrieben.

Regorafenib Monohydrat (RGF MH) ist ein schwer wasserlöslicher Arzneistoff, der von *Bayer* als ASD in *Stivarga* formuliert ist und eine unerwünschte Variabilität der Bioverfügbarkeit aufweist. Um diese Variabilität zu verringern und ein tieferes Verständnis der zugrundeliegenden Mechanismen zu gewinnen wurden verschiedene ASD-Formulierungsstrategien von RGF hergestellt und untersucht. Hierbei wurden neben binären Systemen, bestehend aus Arzneistoff und einem Trägerpolymer, auch ternäre Systeme hergestellt, die ein weiteres Polymer oder Tensid enthalten.
Neben Povidon (PVP), das als Matrixpolymer in *Stivarga* formuliert ist, wurden die strukturell diversen Polymere Hypromellose-Acetat-Succinat (HPMCAS) und gepulvertes basisches butyliertes Methacrylatcopolymer (Eudragit E PO) für die Herstellung alternativer Formulierungen erfolgreich eingesetzt.

Die Freisetzungskinetiken verschiedener ASD Formulierungen wurden zunächst durch biorelevante Freisetzungsstudien bei simulierten intestinalen Bedingungen untersucht. In Abhängigkeit der verwendeten Matrixbildner wurden stark unterschiedliche Freisetzungs- und Übersättigungsverhalten von RGF gefunden. Für RGF_PVP zeigte sich eine rasche Freisetzungskinetik mit ausreichender Übersättigung über 6 h, für RGF_HPMCAS jedoch eine verlangsamte, gleichmäßige Freisetzungskinetik mit anschließender Übersättigung

über mehr als 24 h. In den ternären Formulierungen aus RGF, PVP und HPMCAS wurde das Freisetzungsverhalten unabhängig vom Polymerverhältnis von HPMCAS dominiert. Aufgrund der beobachteten starken *in-vitro* Schwankungen wurde die Formulierung RGF_EPO in weiteren Untersuchungen nicht berücksichtigt.
Um die Aussagekraft der verwendeten Freisetzungsstudien zu erhöhen wurde ein simulierter Magen-Darm Transfer entwickelt. Hier zeigte sich die weniger ausgeprägte Stabilisierung der Regorafenib-Übersättigung durch PVP, im Gegensatz zur Stabilisierung durch HPMCAS. Durch das gezielte Einbringen von Impfkristallen und anderer destabilisierender Zusätze konnte die beachtliche Überlegenheit von HPMCAS und Hypromellose (HPMC) in der Stabilisierung der RGF-Übersättigung gegenüber PVP bestätigt werden.
Abgeleitet aus diesen Ergebnissen konnte ein neues Formulierungskonzept entwickelt werden. Hierbei wird die schnellfreisetzende ASD RGF_PVP gemeinsam mit HPMCAS oder HPMC als Stabilisierungszusatz verabreicht. Um unerwünscht langsame Freisetzungskinetiken zu vermeiden darf jedoch der Stabilisierungszusatz nicht Teil der ASD Matrix sein.
Die unterschiedlichen *in-vitro* Freisetzungskinetiken und Stabilisierungseigenschaften konnten auf direkte Wechselwirkungen zwischen RGF und den Polymeren im festen oder gelösten Zustand zurückgeführt werden.

Um die unerwünschte Rekristallisation von RGF während der *in-vivo* Magenpassage zu vermeiden, die aus *in-vitro* Daten zu erwarten ist, wurde eine magensaftresistente Formulierung entwickelt. Hierbei wurden marktübliche *Stivarga* Tabletten mit HPMCAS lackiert, was zu einer doppelten Funktionalität des HPMCAS führt: einerseits zur Magensaftresistenz der Darreichungsform und nach der Wirkstofffreisetzung zur Stabilisierung der RGF Übersättigung.

Die physikalisch-chemischen Eigenschaften der durch biorelevante Freisetzungsuntersuchungen gewonnenen Präzipitate unterschiedlicher Formulierungen wurden off-line und *in-situ* untersucht. Abhängig von der Präzipitationsumgebung, wie den eingesetzten Polymeren oder der Art der biorelevanten Freisetzungsmedien, zeigte Regorafenib ausgeprägte Polymorphie.
Durch *in-situ* Weitwinkelröntgenstreuung konnte während der Freisetzung von RGF_PVP in FaSSIF das Kristallwachstum von RGF Kristallen von circa 7 nm bis 23 nm verfolgt

werden. Interessanterweise wurde am Ende der Freisetzung der ASD RGF_HPMCAS ein amorphes Co-Präzipitat gefunden, das sich ausschließlich in Abwesenheit von PVP bildete. Mittels Röntgenkleinwinkelstreuung konnte der innere kugelförmige Aufbau mit einem Durchmesser von 6 nm aufgeklärt werden.
Die Koexistenz unterschiedlicher RGF Polymorphe unter biorelevanten Freisetzungsbedingungen wurde mittels *in-situ* konfokaler Raman-Mikroskopie gezeigt.
Die Ergebnisse kalorimetrischer Freisetzungsversuche bestätigten die stärkere Stabilisierung von RGF durch HPMCAS durch höhere Präzipitationsenthalpien für das gefundene amorphe Co-Präzipitat im Vergleich zu kristallinen Präzipitaten.

Der Einfluss von HPMCAS auf die Resorption von RGF wurde *in-vivo* an einem Tiermodell mit Ratten untersucht. Die Zugabe von HPMCAS zu RGF_PVP führte nicht zu statistisch signifikant verschiedenen Ergebnissen im Vergleich zu RGF_PVP ohne HPMCAS Zusatz. Daher konnte festgestellt werden, dass die starken Wechselwirkungen zwischen RGF und HPMCAS im gelösten Zustand die Resorption von RGF nicht negativ beeinflussen.

Das Konzept der Doppelfunktion eines Hilfsstoffes als Übersättigungsstabilisator und magensaftresistente Lackierung ist bisher nicht veröffentlicht und bietet einen neuen Formulierungsansatz unter Vermeidung zusätzlicher Hilfsstoffe. Die Formulierungsstrategie der Kombination eines Stabilisatorpolymers und einer schnellfreisetzenden ASD ist vielversprechend und wurde im Rahmen dieser Arbeit zum ersten Mal für ein auf dem Markt befindliches Arzneimittel gezeigt. Um das Potenzial dieses Formulierungsansatzes abschließend zu bewerten werden weitere Forschungsarbeiten die Übertragbarkeit auf strukturell verschiedene Arzneistoffe zeigen müssen.

# 6 Materials and Methods

## 6.1 Materials and Chemicals

All chemicals and materials used in this work are listed in Table 23.

**Table 23. Chemicals used in this work**

| Substance/ Trade name | Abbreviation/ Synonyme | Supplier | Batch/Lot |
|---|---|---|---|
| Acetone | | VWR Chemicals, France | various |
| Acetonitrile | ACN | VWR Chemicals, France | various |
| Affinisol AS 126 G | HPMCAS 126 | Dow Wolff Cellulosics, Germany | F282H45A01 |
| Affinisol AS 716 G | HPMCAS 716 | Dow Wolff Cellulosics, Germany | F282G3FA01 |
| Affinisol AS 912 G | HPMCAS 912 | Dow Wolff Cellulosics, Germany | F282GA3A01 |
| Albumin, bovine heat stock isolation | BSA | VWR Life Science, USA | 18J2056025 |
| Avicel PH-101 | MCC | FMC Biopolymers, Germany | 61137C1C |
| Demineralized water | aq.demin. | in-house production | |
| di-Sodium hydrogen phosphate dihydrate | $Na_2HPO_4 \cdot 2\ H_2O$ | Carl Roth, Germany | 296245327 |
| Distilled water | aq.dest. | in-house production | |
| Ethanol | EtOH | Merck, Germany | various |
| Eudragit E PO | EPO bPMMA | Evonik, Germany | G150731543 |
| FaSSGF/FaSSIF/FeSSIF buffer concentrate | | Biorelevant.com, UK | various |
| FaSSGF/FaSSIF/FeSSIF powder | SIF powder | Biorelevant.com, UK | various |

| | | | |
|---|---|---|---|
| Hydrochloric acid solution 1 mol/L | HCl 1M | Fisher Chemical, UK | various |
| Kollidon 25 | PVP K25 | BASF, Germany | 53204524U0 |
| Methanol | MeOH | VWR Chemicals, France | various |
| Methocel E3 Premium LV HP | HPMC, Hypromellose | DuPont Specialty Electronic Materials, Switzerland | D011GBEL01 |
| Parteck LUB MST | MgSt, Magnesium stearate | Merck, Germany | 995097581 |
| PermeaPad barrier | | InnoME, Germany | 2019-0010 |
| PermeaPlain barrier | | InnoME, Germany | 2019-0001 |
| Polysorbate 80 | PS-80 | Caelo, Germany | 17064707 |
| Regorafenib monohydrate | RGF MH | Bayer, Germany | BxR3JxC, SV0000HL, BxR6DJG |
| Sodium chloride | NaCl | Carl Roth, Germany | 227258380 |
| Sodium dihydrogen phosphate monohydrate | $NaH_2PO_4 \cdot H_2O$ | Applichem, Germany | 2G001827 |
| Sodium hydroxide pellets | NaOH pellets | Merck, Germany | B1369898 706 |
| Sodium hydroxide 1 mol/L solution | NaOH 1M | Fisher Chemical, UK | various |
| Sodium lauryl sulfate | SDS, SLS | Caelo, Germany | 12153013 |
| Stivarga | Regorafenib coated tablets | Bayer, Germany | BXA7S6B |
| Trifluoroacetic acid | TFA | Acros, USA | A0390881 |
| Vivasol | Croscarmellose sodium | JRS, Germany | 3201062048 |
| Witocan 42/44 | Hard fat | Cremer Oleo, Germany | 911028 |

If no specification is given regarding HPMCAS, Eudragit and PVP types, HPMCAS 716G, Eudragit E PO, and PVP K25 were used for experiments.

## 6.2 Methods

### 6.2.1 Data, graphing and analysis methods

For data evaluation and statistical calculations Excel 2016 (Microsoft, USA) was used. For graphing but also for statistical calculations Prism 8 (GraphPad, USA) and Origin 2019/2020 (OriginLab, USA) were used. Before a t-test was performed, an F-test of the population variances was calculated to check if the assumptions were fulfilled. A significance level $\alpha = 0.05$ was chosen, if not stated otherwise.

In some cases, analytical standard deviations are not shown in graphs, e.g. for dissolution single curve graphs, if the standard deviations from triplicate determination in HPLC are smaller than the data point symbols.

For drawing of chemical structures, the software ChemDraw Professional 16 (PerkinElmer, USA) was applied.

### 6.2.2 ASD preparation

#### 6.2.2.1 Solvent evaporation

For ASD preparation, a rotary evaporator (Büchi, Germany) and Variopro PC3001 vacuum pump (Vacuubrand, Germany) were used for solvent evaporation at 60 °C. The compositions of prepared ASDs are given in Table 24. Regorafenib monohydrate (RGF MH), calculated for the RGF anhydrate mass, and one or more matrix compounds were dissolved in one or more organic solvents and evaporated. For RGF_PVP a mixture of 85/15 (v/v) of butanone/ethanol, for RGF_HPMCAS and RGF_EPO pure acetone, and for ternary ASDs containing PS-80 or SDS a mixture of 80/20 (v/v) of butanone/ethanol was used. Pure methanol was used for the ternary ASD formulations comprising RGF, PVP, and HPMCAS. The precipitate was vacuum dried overnight at room temperature and finally ground by hand in a mortar. The formulations based on RGF_PVP and RGF_EPO were sieved to <350 µm mesh size. This was not possible for formulations containing HPMCAS in the ASD matrix.

For all prepared batches, the amorphous state of RGF was confirmed by DSC and XRPD after preparation and during storage. The formulation codes used in this work regarding co-administration of the stabilizing agents HPMCAS or HPMC to RGF_PVP are explained in Table 25. Physical mixtures were produced by gentle co-grinding of the components in a mortar.

All ASD formulations were stored in tightly closed containers (glass, polyethylene, polypropylene) under light protection at room temperature. For ASD formulations, batch sizes ranged from 2 g to 30 g. The batch size of physical mixtures was 2 g.

**Table 24. Compositions of prepared ASD formulations. Amounts are given in percent by weight.**

| Formulation Code | RGF | PVP K25 | HPMCAS 716 | Eudragit E PO | SDS | PS-80 |
|---|---|---|---|---|---|---|
| RGF_PVP | 20 | 80 | | | | |
| RGF_HPMCAS | 20 | | 80 | | | |
| RGF_EPO | 20 | | | 80 | | |
| RGF20_PVP40_HPMCAS40 | 20 | 40 | 40 | | | |
| RGF20_PVP75_HPMCAS5 | 20 | 75 | 5 | | | |
| RGF10_PVP45_HPMCAS45 | 10 | 45 | 45 | | | |
| RGF_PVP-SDS 2% | 20 | 78 | | | 2 | |
| RGF_PVP-SDS 10% | 20 | 70 | | | | 10 |
| RGF_PVP-PS 2% | 20 | 78 | | | 2 | |
| RGF_PVP-PS 10% | 20 | 70 | | | | 10 |

**Table 25. Compositions of formulations containing the ASD RGF_PVP and co-administered stabilizing agent. The percentage of stabilizing agent is calculated to the PVP mass in RGF_PVP. Amounts are given in percent by weight.**

| Formulation Code | RGF | PVP K25 | Stabilizing agent |
|---|---|---|---|
| | ASD matrix [%] | | Co-administered, not in ASD matrix |
| RGF_PVP + 100% HPMCAS | 20 | 80 | m (HPMCAS) = m (PVP in ASD matrix) |
| RGF_PVP + 66% HPMCAS | 20 | 80 | m (HPMCAS) = m (PVP in ASD matrix) · 0.66 |
| RGF_PVP + 33% HPMCAS | 20 | 80 | m (HPMCAS) = m (PVP in ASD matrix) · 0.33 |
| RGF_PVP + 20% HPMCAS | 20 | 80 | m (HPMCAS) = m (PVP in ASD matrix) · 0.20 |
| RGF_PVP + 10% HPMCAS | 20 | 80 | m (HPMCAS) = m (PVP in ASD matrix) · 0.10 |
| RGF_PVP + 5% HPMCAS | 20 | 80 | m (HPMCAS) = m (PVP in ASD matrix) · 0.05 |
| RGF_PVP + 5% HPMC | 20 | 80 | m (HPMC) = m (PVP in ASD matrix) · 0.05 |

#### 6.2.2.2 Hot-melt extrusion

Extrudates consisting of Witocan 42/44 and ASD RGF_PVP were produced via hot-melt extrusion. Prior to extrusion, the powder mixture was blended in a Turbula mixer (Willy A. Bachofen, Switzerland) for 20 min. A RH 2000 capillary rheometer (Malvern Panalytical, Germany) equipped with a die (2 mm diameter, 2 cm long) was used as a small scale ram extruder and operated at 40 °C. The resulting extrudates were stored for 24 h at

ambient temperatures before further use. Two different formulations were extruded as listed in Table 26. The batch size was 5 g.

All formulations were stored in tightly closed containers (glass, polyethylene, polypropylene) under light protection at room temperature.

**Table 26. Compositions for hot-melt extrusion in percent by weight.**

| Formulation code | RGF_PVP [%] | Witocan 42/44 [%] |
|---|---|---|
| RGF_PVP-Witocan 50/50 | 50 | 50 |
| RGF_PVP-Witocan 80/20 | 80 | 20 |

#### 6.2.2.3 *Stivarga* HPMCAS coating

*Stivarga* tablets, already coated during manufacturing, were coated with an additional HPMCAS layer at *Bayer* site Wuppertal. A total of 100 *Stivarga* tablets were blended with placebo tablets of the same geometry to a batch mass of 1.0 kg and placed in a BFC5 drum coater (L.B. Bohle Maschinen und Verfahren, Germany), using a small divided drum with a maximum volume of 3 L. The coating material HPMCAS 716 was dissolved in acetone and constantly stirred during the coating process. After a warm-up to an exhaust air temperature of 35 °C, spraying was started. Drum rotation speed was 17-19 rpm, airflow was 140-160 $Nm^3/h$ at 40 °C, spraying and forming pressure were set to 0.5 bar and 0.3 bar, respectively, and the spraying angle was 40°. The actual process parameters are listed in Table 32. After spraying, tablets were dried in the coater before unloading and stored at room temperature overnight for solvent evaporation. The target HPMCAS coating mass per tablet was 16 mg to reflect the formulation concept RGF_PVP + 10% HPMCAS. An average mass gain of 20.14 mg HPMCAS or 4.21 % tablet weight was achieved. Therefore, the formulation achieved reflects the formulation RGF_PVP + 12.6 % HPMCAS.

### 6.2.3 Analytical methods

#### 6.2.3.1 Biorelevant dissolution conditions

##### 6.2.3.1.1 Biorelevant media

To obtain biorelevant conditions, fasted state simulated gastric fluid (FaSSGF) and fasted state simulated intestinal fluid (FaSSIF) were used. FaSSIF/FeSSIF/FaSSGF powder was obtained from Biorelevant.com (Biorelevant.com Ltd., UK) and dissolution media were freshly prepared before each experiment, according to the preparation protocol available at the company website *www.biorelevant.com*. For buffer preparation, the commercially available FaSSIF/FeSSIF/FaSSGF buffer concentrate, as well as self-prepared buffers, were used. The compositions of the different biorelevant media types are listed in Table 5.
For 1 L of FaSSIF, 2.240 g FaSSIF/FeSSIF/FaSSGF powder was added to 1000 mL FaSSIF buffer, stirred until dissolved, equilibrated for 2 h, and pH was adjusted to 6.5. To prepare FaSSIF buffer, either 41.65 g FaSSIF buffer concentrate was mixed with 961.1 g aq.dest. Alternatively, FaSSIF buffer preparation was done by dissolving 0.420 g NaOH pellets, 3.438 g sodium dihydrogen phosphate, and 6.168 g NaCl in 1000 mL aq.dest.
For 1 L of FaSSGF, 0.060 g FaSSIF/FeSSIF/FaSSGF powder was added to 1000 mL FaSSGF buffer, stirred until dissolved, and pH was adjusted to 1.6. To prepare FaSSGF buffer, either 36.78 g FaSSGF buffer concentrate was mixed with 961.9 g aq.dest. Manual FaSSGF buffer preparation was done by dissolving 1.999 g NaCl and 29.10 g of 1M HCl in 1000 mL aq.dest.
For transfer dissolution experiments, $FaSSIF_{conc.}$ was used to change media conditions from FaSSGF to FaSSIF. For $FaSSIF_{conc.}$ preparation, the concentrations of FaSSIF components were increased by a factor of 1.5, taking into calculation the amount of NaCl and FaSSIF powder already dissolved in FaSSGF.

##### 6.2.3.1.2 RGF dose

For biorelevant dissolution studies performed in USP 2 dissolution vessels, if not stated otherwise, 200 mg ASD powder, a dose equivalent to one *Stivarga* tablet, was dissolved in 750 mL dissolution media. For PMs, the equal amounts were chosen.
For biorelevant small-scale dissolution experiments, the ratio of ASD to dissolution media was kept constant, therefore the dose was adjusted to 13.3 mg and 16.0 mg for 50 mL or 60 mL, respectively.

For dissolution studies of the extrudate RGF_PVP-Witocan 80/20, 250 mg of the sample was dissolved in 750 mL FaSSIF, a dose equivalent to 40 mg RGF.

#### 6.2.3.1.3 Regorafenib solubility in biorelevant media, influence of additives

The solubility of RGF in different types of biorelevant dissolution media was tested in the presence and absence of the used ASD matrix polymers. The polymer concentration chosen in solubility studies reflected the concentration in biorelevant dissolution experiments, so 0.21 mg/mL polymer were pre-dissolved. An excess of RGF MH was added to 50 mL biorelevant media and dissolved for 48 h at 37 ± 0.5 °C by the use of the small-scale dissolution setup, as described in Section 6.2.3.2.3. Sampling was performed according to Section 6.2.3.2.5. The samples were analyzed by HPLC as described in Section 6.2.3.3. The solubility experiments were performed in triplicate.

### 6.2.3.2 Biorelevant dissolution setups

#### 6.2.3.2.1 One-compartment vessel biorelevant dissolution setup

Dissolution studies were performed in a Ph. Eur. dissolution vessel at 37 ± 0.5 °C under constant stirring (Eurostar 20 digital, IKA-Werke, Germany) at 75 rpm using a paddle apparatus 2 (European Pharmacopoeia 10.0, monograph 2.9.3, 2019). Temperature control was provided by a Julabo MP thermostat (Julabo Labortechnik, Germany). To mimic intestinal conditions, FaSSIF was used as biorelevant dissolution medium.

For dissolution of extrudates, a Ph. Eur. apparatus 1 basket setup was used instead of the paddle setup.

The sampling procedure is described in 6.2.3.2.5. The sampling time points were not consistent for all one-compartment dissolution experiments. The small-scale biorelevant dissolution setup is described in 6.2.3.2.3. The applied ASD and PM doses are described in 6.2.3.1.2. The number of experimental repetitions is stated at the respective figure captions.

#### 6.2.3.2.2 Simulated gastric transit in vessel-based biorelevant dissolution setup

Biorelevant transfer dissolution studies were performed in dissolution vessels according to Ph. Eur. (European Pharmacopoeia 10.0, monograph 2.9.3, 2019), but also at the small-scale apparatus.

Transfer vessel dissolution studies were performed to mimic the transfer from gastric to intestinal conditions by using the dissolution systems described in 6.2.3.2.1. Here, the ASD

was dissolved first in 250 mL FaSSGF for 30 min or 120 min prior to FaSSIF equilibration with 500 mL $FaSSIF_{conc.}$ (concentrated FaSSIF). After adding $FaSSIF_{conc}$, the pH of the dissolution system was measured with a pH-meter (Labor-pH-Meter 766 Calimatic, Knick Elektronische Messgeräte, Germany) and adjusted by addition of NaOH or HCl solution. The sampling procedure is described in 6.2.3.2.5. The sampling time points were not consistent for all vessel-based dissolution experiments. The small-scale biorelevant transfer dissolution setup is described in Section 6.2.3.2.3.

#### 6.2.3.2.3 Small-scale dissolution setup and seeding experiments

Small-scale dissolution studies were performed at 37 ± 0.5 °C in screw-top glass cylinders with an inner diameter of 32 mm, deviating from the Ph. Eur. vessel dissolution conditions in hydrodynamics and ratio of glass surface to media. A volume of 50 mL FaSSIF was used. A magnetic multi-position stirring plate (Ikamag Eoa 9 electronic and ES 5, IKA Labortechnik, Germany) was placed below the dissolution setup to control the stirring bars inside the glass cylinders. The stirring speed was set to level 3 – 4.

Seeding experiments were performed analogous to the small-scale method described above, except for the addition of the additives to be investigated. In case of RGF MH addition, the same amount was added as was incorporated into the ASD formulations, leading to 50 % amorphous RGF and 50 % RGF monohydrate (w/w) at the start of the dissolution experiment. For experiments in 50 mL or 60 mL dissolution media, 2.67 mg or 3.2 mg of seeding material (RGF MH or Witocan) was added, respectively.

For small-scale transfer dissolution experiments, the adjusted dose was dissolved in 20 mL FaSSGF before 40 mL $FaSSIF_{conc.}$ was added and pH was adjusted by the addition of HCl 1M and NaOH 1M solution.

Different sampling time points were chosen for the investigated formulations, as described in 3.2.5. Also, experimental settings (with or without simulated gastric transfer) were considered.

The applied ASD and PM doses are described in 6.2.3.1.2. All small-scale dissolution experiments were performed in triplicate.

#### 6.2.3.2.4 Biorelevant dissolution, mimicking rat physiological conditions

Biorelevant dissolution studies mimicking *in-vivo* conditions in rats were performed similar to Section 6.2.3.2.2 at 37 ± 0.5 °C under constant stirring, deviating in pH values of the dissolution media.

For $FaSSGF_{rat}$ and $FaSSIF_{rat}$, the pH values were adjusted to 3.2 and 5.0 respectively, by the addition of HCl 1M or NaOH 1M to FaSSGF and FaSSIF media.

For $FaSSIF_{conc., rat}$ preparation, the concentrations of FaSSIF components were increased by a factor of 1.5, taking into calculation the amount of NaCl and FaSSIF powder already dissolved in $FaSSGF_{rat}$. The experiments were performed in triplicate.

#### 6.2.3.2.5 Sampling procedure

Samples from all dissolution studies were taken as follows. By the use of a 10 mL syringe (Fisherbrand sterile 3 parts PP, fisher scientific, USA) and cannula (Sterican 20G, B. Braun Melsungen AG, Germany), a sample of 10 mL was taken from the dissolution system. No dissolution media was replaced. Via a syringe pump (LEGATO100, kdScience, USA), 9 mL were discarded over a syringe filter (PP 0.2 µm, VWR, USA) and a second cannula to avoid RGF loss due to filter adsorption. From the remaining dissolution fluid in the syringe, 750 µL were administered to HPLC brown glass vials with PP caps, already pre-filled with 750 µL methanol, and subsequently analyzed by HPLC.

### 6.2.3.3 RGF concentration determination by high-performance liquid chromatography (HPLC)

#### 6.2.3.3.1 HPLC method

RGF concentration analysis was performed via HPLC coupled with UV/Vis detector (HPLC/UV) using a Dionex P580 system, consisting of an ASI-100T autosampler, STH-585 column oven, p580-LPG pump, UVD-170U/340U UV/Vis detector, and UCI-50 interface (all Dionex, Germany). A YMC-Pack Pro C18 RS column (YMC Co. Ltd., Japan) was used at 40 °C, detection wavelength was set to 262 nm. The injection volume was set to 100 µL. A mixture of methanol and 0.2 % TFA in water was used as mobile phase at a flow rate of 1 mL/min with gradient mixing from 65/35 to 95/5 for 7 min, keeping the final ratio of 95/5 for additional 10 min before equilibration for the next run for 3 min. The retention time of the RGF peak was 6.8 min and clear peak separation was observed, as shown in Figure 74 (left).

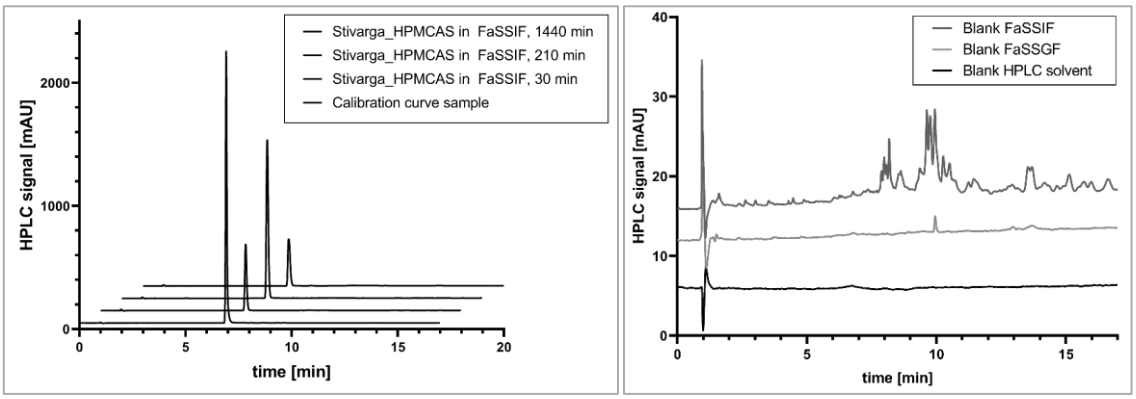


**Figure 74. Left: Regorafenib HPLC chromatogram of biorelevant dissolution samples and calibration curve. Chromatograms are nudged for clarity.**
**Right: HPLC chromatograms of biorelevant media and solvent blanks. Chromatograms are nudged for clarity.**

The matrix effects from biorelevant media components, shown in Figure 74 (right), did not interfere with RGF signals, due to the separation and strong differences in signal intensities. All samples were analyzed in triplicate. For device control and measurement analysis, Chromeleon version 6.80 (Dionex, USA) was used.

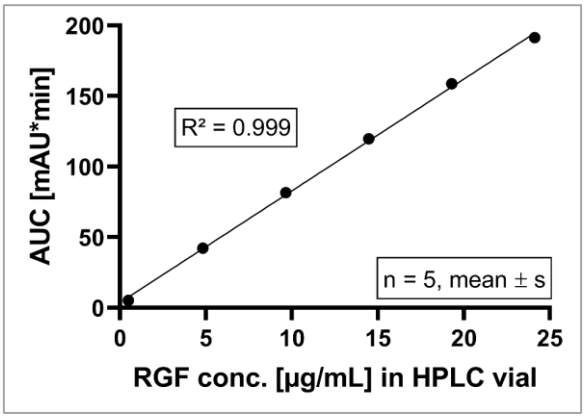


**Figure 75. HPLC calibration curve for Regorafenib concentration determination. Standard deviations are smaller than symbols.**

RGF concentration calibration was performed by precisely weighed and diluted RGF samples.

For the quantification of RGF, different calibration curves were recorded, depending on the target concentration (see Figure 75). At least five different RGF concentrations were prepared by dissolving RGF in MeOH/aq.dest. in a ratio of 50/50 (v/v).

HPLC sequences were created following a standard procedure. First, a solvent blank was injected, followed by media blank(s) and an RGF standard sample. Every 10$^{th}$ injection was

a solvent blank to detect for possible carry-over effects. Each sample was injected at least thrice.

#### 6.2.3.3.2 RGF content determination

To determine the RGF content of produced ASD batches or precipitates from biorelevant dissolution experiments, the sample to be investigated was dissolved in pure methanol und shortly ultra-sonicated. A sample of 65 mg ASD was dissolved in 100 mL methanol and further diluted until reaching the calibrated area. For the precipitates, a sample of 3-5 mg was dissolved in 50 mL methanol and further diluted.

The methanol solution was eventually diluted with distilled water by 1+1 parts (v/v) for HPLC analysis, as described in 6.2.3.3.1.

### 6.2.3.4 RGF physicochemical properties

#### 6.2.3.4.1 Sample preparation for off-line analysis

Since XRPD analysis required more precipitate sample material than obtained from the described dissolution methods, a concentrated dissolution was run. Here, a dose 30-fold to the daily dose of ASD was dissolved in FaSSIF for 48 h at 37 ± 0.5 °C under constant stirring at 75 rpm, centrifuged at 3000 rpm for 1 h to 2 h (Heraeus Multifuge 1, Thermo Fisher Scientific, USA) and freeze-dried (Christ Alpha 1-4 LDplus, Christ Gefriertrocknungsanlagen, Germany, with vacuum pump RZ-6, Vacuubrand, Germany). Samples investigated in FaSSGF were dissolved for 24 h prior to centrifugation and freeze-drying.

RGF Mod. I was prepared by dissolving RGF MH in a mixture of butanone and ethanol (80/20, v/v) and subsequent evaporation. The precipitate was investigated to match *Bayer* internal specifications for RGF Mod. I. Dried FaSSIF was prepared by water evaporation under maximum reduced atmospheric pressure conditions at 30 °C overnight (Heraeus vacutherm, Thermo Fisher Scientific, USA).

#### 6.2.3.4.2 X-ray powder diffraction (XRPD)

X-ray diffractograms of powder samples were obtained by using an X'Pert Pro MPD diffractometer (PANalytical, Netherlands) in the reflection or transmission mode. The samples were filled into a sample holder for reflection measurements, whereas extrudates were placed in between two polyester foils for transmission measurements. In the case of

needle-shaped particles, the sample was ground manually in a mortar to reduce orientation effects in the sample. For both measurement modes, a copper anode (30 mA, 30 kV) over Kα-radiation ($\lambda$ = 1.5406 Å) was used to determine diffractions from 10° to 50° $2\Theta$ with sampling steps of 0.033 ° $2\Theta$ and a scan speed of 0.0283 °/s by the use of the following slit assemblies, as listed in Table 27. The sample was rotating at 1 round per second. For data recording and export, X'Pert Data Collector (Version 2.2h) and X'Pert Data Viewer (Version 1.2f, both PANalytical, Netherlands) were used, respectively. Before experiments in reflection mode, once a day a silicon control standard sample was measured to ensure reliable thus comparable results. Each sample was measured at least twice.

**Table 27. XRPD measurement settings**

| XRPD mode | divergence slit | anti-scatter slit | mask | anti-scatter slit |
|---|---|---|---|---|
| | incident beam | | diffracted beam | incident beam |
| reflection | 1° | 2° | 10 mm | 6.6 mm |
| transmission | 1/8° | 1/4° | 15 mm | 5.0 mm |

#### 6.2.3.4.3 Wide-angle and small-angle X-ray diffraction (WAXS, SAXS)

For *in-situ* X-ray scattering of biorelevant media suspended samples, wide-angle (WAXS) and small-angle (SAXS) X-ray scattering experiments were performed in cooperation with Dr. Martin Dulle from JCNS-1/ICS-1 (Forschungszentrum Jülich, Germany). Samples were filled into glass capillaries and placed in the X-ray beam. The scattering patterns were recorded with the SAXS/WAXS system Ganesha-Air (SAXSLAB, Denmark). The X-ray source of this laboratory-based system is a D2-MetalJet (Excillum, Sweden) with a liquid metal anode operating at 70 kV and 3.57 mA with Ga-Kα radiation (wavelength $\lambda$ = 0.13414 nm) providing a brilliant and a small beam (<200 µm). The beam is slightly focused with a focal length of 55 cm using a specially made X-ray optic (Xenocs, Denmark) to provide a small and intense beam at the sample position. The X-ray path was evacuated, except at the position where the sample cell was set. Two pairs of scatterless slits are used to adjust the beam size depending on the detector distance. A Pilatus 300K (Dectris Ltd., Switzerland) was used to record the 2D scattering patterns. The sample to detector distance was set to be 0.159 m ($q$ = 0.8 – 22.6 $nm^{-1}$) for WAXS and to 0.507 m ($q$ = 0.18 – 7.8 $nm^{-1}$) for SAXS. The two-dimensional patterns were radially averaged to obtain 1D intensity profiles. These were normalized to measurement time and transmission after this a

suitable background subtracted. Silver behenate with d-spacing of 58.38 Å was used as a standard to calibrate.
Scattering patterns were recorded and accumulated for 10 min or 30 min for WAXS or SAXS, respectively.

A small-scale dissolution setup, as described in Section 6.2.3.2.3, was installed next to the SAXS / WAXS apparatus. Samples were drawn by the use of a pipette, filled into glass capillaries with an outer diameter of 0.1 mm and 0.01 mm wall thickness (Hilgenberg, Germany), centrifuged if necessary, and subjected to the autosampler.

#### 6.2.3.4.4 Polarized light microscopy (PLM)

The samples were investigated by a polarized microscope DM LB (Leica Microsystems, Germany). Optionally, a sample holder equipped with a heating device was used (THMS 600 and TMS 94, both Linkam Scientific Instruments, UK). Images were acquired by a digital microscope camera setup DFC450 (Leica Microsystems, Germany). Leica Application Suite V4.6.2 (Leica Microsystems, Germany) was used for image processing and particle size determination.

#### 6.2.3.4.5 (Confocal) Raman microscopy (CRM)

Raman spectroscopic investigations were performed using a confocal Raman microscope alpha300 R (WITec, Germany). A fiber-coupled single-mode diode laser with 785 nm excitation wavelength was used. The laser power on the samples was set to 75 mW. As microscope objectives, a Zeiss EC Epiplan-Neofluar DIC 100x/0.9 NA and Zeiss EC Epiplan-Neofluar DIC 50x/0.8 NA were selected. The spectrometer used was a WITec UHTS 300 in combination with an Andor iDus Deep Depletion CCD detector, which was cooled to -60 °C. The Raman scattered light was spectrally dispersed at a reflection grating with 300 lines/mm. An average spectral resolution of about 3.3 $\mu m^{-1}$/pixel was achieved.
Powder samples were placed on a glass slide and directly analyzed with an accumulated measurement time of 30 s. Samples of the dissolution experiments were placed on glass slides, covered by a cover slide against media evaporation and analyzed immediately. The time delay between sampling and measurement was around 2 min. Amorphous RGF was measured by heating RGF MH on a heating plate to > 200 °C and cooling on a lab bench

at ambient conditions before Raman analysis. All samples were measured at least twice and at several positions.

The evaluation of the measurement data and creation of the Raman images was performed using the software WITec FIVE Version 5.2.4.81, including a cosmic ray removal, background subtraction by the implemented shape function and Raman intensity normalization. The standard procedure for dissolution samples was as follows: background correction by the shape function, normalization to the maximum glass signal, subtraction of background signal, and normalization of the maximum signal intensity. For powder samples, no background subtraction was performed.

The Raman spectra of different RGF modifications showed clear differences in the regions of 80 – 300 $cm^{-1}$ and 400 – 800 $cm^{-1}$. For data interpretation and RGF modification assignment, the latter region was preferred, as the more homogeneous signal intensities allow for better illustration in one graph, therefore for more convenience for the reader. Since the obtained spectra from dissolution experiments were background corrected and signal intensities differed, more emphasis shall be given to the position of a Raman bond than to its absolute or relative intensity. These deviations in signal intensities can be explained by different sample densities. While powder samples exhibited strong Raman signals, the measurement of fine needles or thin platelet particles in dissolution media was more challenging as less scattered photons were collected. For the Raman mapping experiments, the laser exposure time was to 0.05 s – 0.5 s per spectrum, leading to less intense spectra. In this case, the full spectrum was considered for RGF modification assignment, with special emphasis on characteristic signals.

The dissolution media environment, as well as the cover glass slide, led to a background Raman signal, which was subtracted from every measurement after normalization. This Raman background spectrum is presented in Figure 76, the dominant signal around 1380 $cm^{-1}$ was caused by the cover glass slide.

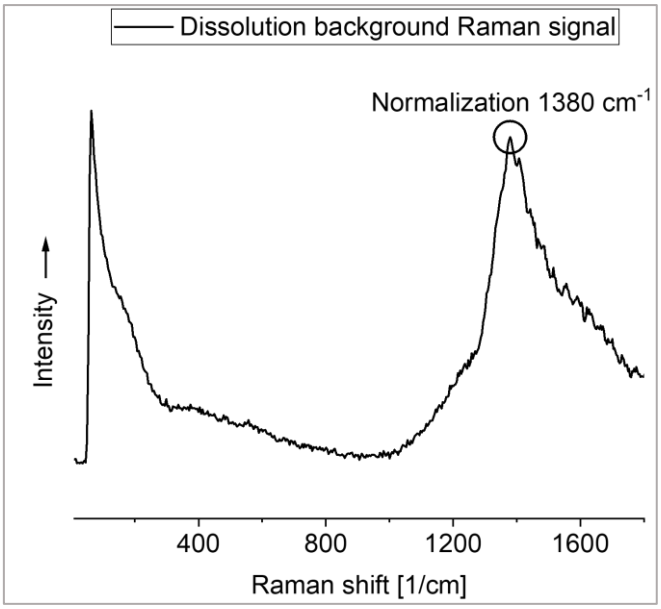


Figure 76. Raman background spectrum used for background correction in biorelevant dissolution studies.

#### 6.2.3.4.6 Thermoanalytical measurements

Thermoanalytical experiments were performed using dynamic scanning analysis (DSC, DSC-1, Mettler Toledo, USA). Up to 5 mg sample was weighed precisely (XP56, Mettler-Toledo, Germany) into perforated aluminum pans before being loaded into the DSC autosampler. The performed heating cycles are listed in Table 28. For determination of endo- or exothermic events, STARe software (Version 9.2 and 16.10, Mettler Toledo, USA) was used. Each sample was heated up twice and cooled in between. All samples were measured in duplicate.

Table 28. Temperature profiles of DSC measurements

| Profile name | Temperature range [°C] | Heating rate 1st heating [K/min] | Cooling rate [K/min] | Heating rate 2nd heating [K/min] |
|---|---|---|---|---|
| 2K | 20 – 220 – 20 – 220 | 2 | - 2 | 2 |
| 5K | 20 – 220 – 20 – 220 | 5 | - 5 | 5 |
| 10K | 20 – 220 – 20 – 220 | 10 | - 10 | 10 |
| 20K | 20 – 220 – 20 – 220 | 20 | - 20 | 20 |
| iso60 | isothermal at 60 °C for 60 min<br>60 – -20<br>-20 – 250 | <br><br>20 | <br>-20 | |

#### 6.2.3.4.7 Scanning electron microscopy (SEM)

SEM images were acquired using a G2pro (Phenom-World, Netherlands) at an acceleration voltage of 5 to 10 kV. In some cases, the samples were sputtered with a gold layer (MSC1T, LOT-Quantum Design, Germany).

For image generation and particle size measurements, the integrated software ProSuite (Phenom-World, Netherlands) was used.

#### 6.2.3.4.8 X-ray micro-computed tomography

The film thickness of HPMCAS-coated *Stivarga* tablets was determined by X-ray micro-computed tomography (µCT) by the use of a CT alpha setup (ProCon X-ray, Germany). The measurement settings were adjusted to 1600 projections at 8.5 µm voxel resolution, 80 kV acceleration voltage, and 110 µA currency. Exposure time was 500 ms per image, a mean from 5 images was calculated. For image reconstruction, the software VG Studio 3.0.1 (Volume Graphics, Germany) was applied. Image processing was performed by ImageJ 1.52p (Wayne Rasband, NIH, USA) using Java 1.8.0_172 (Sun Microsystems, USA). From reconstructed images, regions of interest were cut out manually and processed by the *enhance contrast* function to a level of 0.3 % saturated pixels by use of stack histogram and linear normalization. For coating thickness determination, the scale was set to 8.5 µm and the *measurement* function was used. Experiments were performed as n = 1.

#### 6.2.3.4.9 Viscosity measurements

To determine the rheological properties of dissolution media containing polymers, a rheometer (Kinexus pro KX2100, Malvern Panalytical, Germany) was equipped with a cone (1°, diameter 60 mm) and plate geometry (diameter 65 mm). Measurement conditions were kept constant at 37 °C at a shear rate of 20 $s^{-1}$ and a gap height of 0.053 mm. For each measurement, 60 values were recorded over 300 s, from which mean and standard deviation were calculated. Each sample was measured at least in triplicate.

#### 6.2.3.4.10 Isothermal titration calorimetric measurements (ITC)

To monitor the heat signal of precipitating RGF in FaSSIF an isothermal titration calorimeter (ITC, VP ITC, MicroCal, USA) was used. The temperature was set to 37 °C and the stirrer unit to 310 rpm. The calorimeter consisted of two identical cells of 1.41 mL volume each, a sample cell and a reference cell. The reference cell was filled with purified

water with a minimum resistivity of 18 MΩ cm and reference power was set to 2 µcal/s or 5 µcal/s, depending on the sample behavior. The differential power between the two cells was measured over time. To keep the same ratio ASD to FaSSIF as in the dissolution experiments, 0.37 mg ASD, with or without co-administration of HPMCAS, was vortexed for 15 s with 1.4 mL FaSSIF before injection into the measurement cell. The dissolution media was tempered to 37 °C before use.

One limitation in the ITC setup used in this work is the equilibration time of 40 min after ITC dissolution sample loading. During this period, no signal is recorded and no statement about the heat impact of the dissolution process can be made. In this work, solely ITC curves with a clear beginning of an endothermic event are presented, resulting in an unequal number of replicates per formulation.

#### 6.2.3.4.11 Particle size distribution (PSD)

To determine the particle size distribution of prepared ASDs, a Haver CPA 2-1 (Haver & Boecker, Germany) was used, based on a LED light source and CCD line scan camera. The pixel frequency was 50 MHz and evaluated in real-time. An optical density of 0.5 – 1.5 was chosen. A symmetry factor correction (min. SY of 0.5) was applied to avoid measurement of particles that were not sufficiently dispersed.

#### 6.2.3.4.12 Disintegration time

The tablets were examined using a disintegration test device (ZT 32, Erweka, Germany) according to the monograph “Disintegration of tablets and capsules” (European Pharmacopoeia 10.0, monograph 2.9.1, 2019). The specific test conditions for gastro-resistant tablets are stated in the monograph “Gastro-resistant tablets” (European Pharmacopoeia 10.0, monograph Tablets, 2019). As test media, 0.1 M hydrochloric acid, and phosphate buffer solution pH 6.8 were prepared from demineralized water and tested for 120 min and 60 min, respectively. Before media transfer, the tablets were examined for disintegration or coating cracks.

### 6.2.4 Permeation

#### 6.2.4.1 Dynamic light scattering (DLS)

To determine the presence or absence of BSA in permeation experiments, dynamic light scattering (DLS) was conducted. The nanoparticle analyzer nanoPartica SZ-100 (Horiba

Scientific, Germany) was used with disposable macro polystyrene cuvettes (VWR, Belgium). Scattered light was detected at 173° angle. Before measurements, if necessary, the samples were filtrated through a 0.45 µm pore size PP syringe filter (VWR, Belgium) to remove dust particles. As the size determination of dissolved BSA was not of interest, the z-average calculated by the device was used for the detection of the presence or absence of BSA in the sample.

#### 6.2.4.2 *In-vitro* dissolution-permeation setup

Permeation of RGF across an artificial membrane was investigated by the use of a self-assembled permeation cell setup, shown in Figure 68, which is described in Section 3.6.2. The whole setup was placed in an oven (Binder Cooling Incubator, Binder, Germany) at 37 °C on a digital magnetic stirring plate (MIXcontrol 20, 2mag, Germany) and connected with an external autosampler (Vision Autoplus, Teledyne Hanson Research, USA). In accordance with the small-scale dissolution setup (Section 6.2.3.2.3), 13.3 mg ASD were dissolved in 50.0 mL FaSSIF media. As acceptor media, 10.0 mL BSA 4 % in FaSSIF was used. PermeaPad and PermeaPlain membranes were clamped in between donor and acceptor compartments. The diameter of the non-covered membrane for permeation was 15 mm. The donor compartment was stirred at 200 rpm, whereas the acceptor compartment was agitated by the autosampler using the ‘transfer’ program mode for 3 mL every 14 min. After 6 h and 18 h, samples of ca. 2.5 mL were drawn from acceptor media using a syringe and cannula and 2.0 mL of the sample was mixed with 4.0 mL ACN to precipitate BSA, vortexed, and centrifuged for 10 min at maximum power (Minispin plus, Eppendorf, Germany). The supernatant was injected into the HPLC system for RGF concentration determination and the program from Method 6.2.3.3.1. was applied.

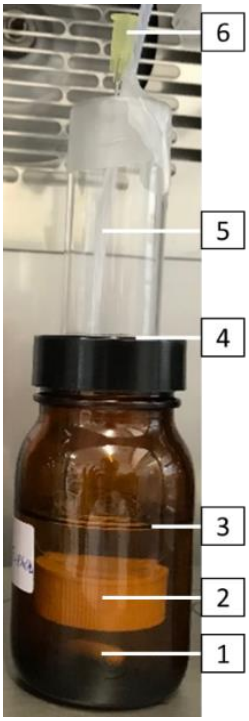


Figure 77. Self-assembled dissolution-permeation setup.

Table 29. Explanation of dissolution-permeation setup shown in Figure 77.

| No | Explanation |
|---|---|
| 1 | Stirring bar, 200 rpm |
| 2 | Permeation membrane clamped between the inner glass cylinder and its screw lid, membrane surface diameter 15.1 mm |
| 3 | Donor and acceptor media levels on same height to avoid hydrostatic pressure on the membrane |
| 4 | Tight connection between outer and inner glass |
| 5 | Autosampler capillary for acceptor media circulation |
| 6 | Cannula for venting |

## 6.3 *In-vivo* PK study in rats

### 6.3.1 Experiment

*In-vivo* pharmacokinetic (PK) studies were performed in cooperation with *Bayer* at the department Research Pharmacokinetics in Wuppertal (Germany) under supervision of Dr. Jan Stampfuss. For each study group, four male Wistar rats were used (supplier Charles River, Germany). The experiment followed the study protocol by *Bayer*, which is approved by the relevant authorities and an ethic committee. Before and during the experiment, the rats had free access to water and food and were only restricted for 4 h after sample administration.

At Day 1, the rats were narcotized and underwent surgery to insert a catheter for pain-free blood sampling during the experiment. At Day 2, the ASD formulations were suspended in tap water and the calculated volume was taken with a 10 mL syringe and applied via stomach tube to ensure a complete intake of the samples. The dose was adjusted individually to 50 mg RGF per kg body weight, which is known from previous *in-vivo* studies to allow for differentiation in PK behavior between RGF formulations. The sampling volume was adjusted to 5 mL per kg body weight.

Blood samples were drawn via the catheter over 48 h and analyzed for RGF concentration by a *Bayer* in-house Liquid chromatography–mass spectrometry (LC/MS) method. *Bayer* describes the sample preparation and analytics as follows:

A volume of 50 µL of the plasma samples was mixed with 250 µL acetonitrile including a method specific internal standard substance. The samples were vortexed for seconds and left at room temperature for at least 5 min. The samples were further mixed with 500 µL ammonium acetate buffer (10 mM, pH 3) and centrifuged for 10 min at 3000 rpm (no further information about the centrifuge model are provided).

From each sample, 25 µL were injected into the LC/MS system (Agilent 1260/1290 LC system, Agilent Technologies, USA), equipped with a Phenomenex Gemini 5µ C18 110A column (Phenomenex Deutschland, Germany) and a Sciex API 6500 MS device (AB Sciex, Singapore). A gradient elution was performed with ammonium acetate buffer (10 mM, pH 3) and acetonitrile with an acetonitrile ratio of 20 % to 90 % to 20 % over 5 min. The pump rate was 1000 µL/min and column oven was set to 22 °C. The MS device was operated at 400 °C and in multiple-reaction monitoring (MRM) mode.

The sampling time points were predetermined by the study design. Samples were drawn at 0.083 h (5 min), 0.25 h (15 min), 0.5 h (30 min), 1 h, 2 h, 3 h, 5 h, 7 h, 24 h, 26 h and 48 h. After the experiment, the rats were sacrificed.

### 6.3.2 Data evaluation and PK calculations

Several PK parameters were calculated from the obtained RGF plasma concentrations.

1) Elimination rate ($k_e$)

Before the calculation of the RGF elimination rate, the RGF plasma concentrations were transformed to its *ln* values and plotted against the time after administration to rats. A trend line was fitted through the descending part of the curve. The positive absolute amount of the slope is defined to be $k_e$ while the intercept is named $n$.

2) Area under the curve (AUC)

The AUC was calculated by applying the “linear-log method”. A linear trapezoidal method was used until $c_{max}$ was reached. For the following descending part of the plasma curve a logarithmic trapezoidal method as used.

*Linear method:* $AUC = \sum \frac{1}{2} (C_1 + C_2)(t_2 - t_1)$ Equation 11a

*Logarithmic model:* $AUC = \sum \frac{C_1 - C_2}{ln(C_1) - ln(C_2)} (t_2 - t_1)$ Equation 11b

$C_x$ = RGF plasma concentration at $t_x$

The terminal AUC $(AUC_{term})$ after the last determined RGF concentration was calculated by:

$$AUC_{term} = \frac{C_{final}}{k_e}$$ Equation 12

$C_{final}$ = last determined RGF plasma concentration at $t_{48h}$

$k_e$ = elimination constant

The total AUC ($AUC_{total}$) was calculated by addition of Equation 11a + Equation 11b + Equation 12.

3) Plasma half-life ($t_{1/2}$)

The plasma half-life of RGF in rat was calculated as follows:

$$t_{1/2} = ln(2)/k_e$$ Equation 13

# 7 Bibliography

Al-Obaidi, H., M. J. Lawrence, N. Al-Saden, and P. Ke (2013): *Investigation of griseofulvin and hydroxypropylmethyl cellulose acetate succinate miscibility in ball milled solid dispersions.* International Journal of Pharmaceutics, 443, pp. 95-102. DOI: 10.1016/j.ijpharm.2012.12.045

Alhayali, A., S. Tavellin, and S. Velaga (2017): *Dissolution and precipitation behavior of ternary solid dispersions of ezetimibe in biorelevant media.* Drug Development and Industrial Pharmacy, 43, pp. 79-88. DOI: 10.1080/03639045.2016.1220566

Alonzo, D. E., Y. Gao, D. Zhou, H. Mo, G. G. Z. Zhang, and L. S. Taylor (2011): *Dissolution and precipitation behavior of amorphous solid dispersions.* Journal of Pharmaceutical Sciences, 100, pp. 3316-3331. DOI: 10.1002/jps.22579

Alonzo, D. E., G. G. Zhang, D. Zhou, Y. Gao, and L. S. Taylor (2010): *Understanding the behavior of amorphous pharmaceutical systems during dissolution.* Pharmaceutical Research, 27, pp. 608-618. DOI: 10.1007/s11095-009-0021-1

Alonzo, D. E., S. Raina, D. Zhou, Y. Gao, G. G. Z. Zhang, and L. S. Taylor (2012): *Characterizing the impact of hydroxypropylmethyl cellulose on the growth and nucleation kinetics of felodipine from supersaturated solutions.* Crystal Growth & Design, 12, pp. 1538-1547. DOI: 10.1021/cg201590j

Amidon, G. L., H. Lennernäs, V. P. Shah, and J. R. Crison (1995): *A theoretical basis for a biopharmaceutic drug classification: The correlation of in vitro drug product dissolution and in vivo bioavailability.* Pharmaceutical Research, 12, pp. 413-420. DOI: 10.1023/A:1016212804288

Araújo, R. R., C. C. C. Teixeira, and L. A. P. Freitas (2010): *The preparation of ternary solid dispersions of an herbal drug via spray drying of liquid feed.* Drying Technology, 28, pp. 412-421. DOI: 10.1080/07373931003648540

Arnold, Y. E., G. Imanidis, and M. T. Kuentz (2011): *Advancing in-vitro drug precipitation testing: New process monitoring tools and a kinetic nucleation and growth model.* Journal of Pharmacy and Pharmacology, 63, pp. 333-341. DOI: 10.1111/j.2042-7158.2010.01228.x

Augustijns, P., and M. E. Brewster (2012): *Supersaturating drug delivery systems: Fast is not necessarily good enough.* Journal of Pharmaceutical Sciences, 101, pp. 7-9. DOI: 10.1002/jps.22750

Aulton, M. E., and K. Taylor (2017): "Aulton's pharmaceutics: The design and manufacture of medicines." Edition 5, Edinburgh, Churchill Livingstone/Elsevier.

Baghel, S., H. Cathcart, and N. J. O'Reilly (2016): *Polymeric amorphous solid dispersions: A review of amorphization, crystallization, stabilization, solid-state characterization, and aqueous solubilization of biopharmaceutical classification system class II drugs.* Journal of Pharmaceutical Sciences, 105, pp. 2527-2544. DOI: 10.1016/j.xphs.2015.10.008

Baghel, S., H. Cathcart, and N. J. O'Reilly (2018a): *Investigation into the solid-state properties and dissolution profile of spray-dried ternary amorphous solid dispersions: A rational step toward the design and development of a multicomponent amorphous system.* Molecular Pharmaceutics, 15, pp. 3796-3812. DOI: 10.1021/acs.molpharmaceut.8b00306

Baghel, S., H. Cathcart, and N. J. O'Reilly (2018b): *Understanding the generation and maintenance of supersaturation during the dissolution of amorphous solid dispersions using modulated DSC and 1H NMR.* International Journal of Pharmaceutics, 536, pp. 414-425. DOI: 10.1016/j.ijpharm.2017.11.056

Baird, J. A., and L. S. Taylor (2012): *Evaluation of amorphous solid dispersion properties using thermal analysis techniques.* Advanced Drug Delivery Reviews, 64, pp. 396-421. DOI: 10.1016/j.addr.2011.07.009

Batchelor, H. K., N. Fotaki, and S. Klein (2014): *Paediatric oral biopharmaceutics: Key considerations and current challenges.* Advanced Drug Delivery Reviews, 73, pp. 102-126. DOI: 10.1016/j.addr.2013.10.006

Berben, P., A. Bauer-Brandl, M. Brandl, B. Faller, G. E. Flaten, A. C. Jacobsen, J. Brouwers, and P. Augustijns (2018): *Drug permeability profiling using cell-free permeation tools: Overview and applications.* European Journal of Pharmaceutical Sciences, 119, pp. 219-233. DOI: 10.1016/j.ejps.2018.04.016

Berlin, M., K. H. Przyklenk, A. Richtberg, W. Baumann, and J. B. Dressman (2014): *Prediction of oral absorption of cinnarizine-a highly supersaturating poorly soluble weak base with borderline permeability.* European Journal of Pharmaceutics and Biopharmaceutics, 88, pp. 795-806. DOI: 10.1016/j.ejpb.2014.08.011

Bevernage, J., T. Forier, J. Brouwers, J. Tack, P. Annaert, and P. Augustijns (2011): *Excipient-mediated supersaturation stabilization in human intestinal fluids.* Molecular Pharmaceutics, 8, pp. 564-570. DOI: 10.1021/mp100377m

Bevernage, J., J. Brouwers, P. Annaert, and P. Augustijns (2012a): *Drug precipitation-permeation interplay: Supersaturation in an absorptive environment.* European Journal of Pharmaceutics and Biopharmaceutics, 82, pp. 424-428. DOI: 10.1016/j.ejpb.2012.07.009

Bevernage, J., B. Hens, J. Brouwers, J. Tack, P. Annaert, and P. Augustijns (2012b): *Supersaturation in human gastric fluids.* European Journal of Pharmaceutics and Biopharmaceutics, 81, pp. 184-189. DOI: 10.1016/j.ejpb.2012.01.017

Bevernage, J., J. Brouwers, M. E. Brewster, and P. Augustijns (2013): *Evaluation of gastrointestinal drug supersaturation and precipitation: Strategies and issues.* International Journal of Pharmaceutics, 453, pp. 25-35. DOI: 10.1016/j.ijpharm.2012.11.026

Bhugra, C., R. Shmeis, S. L. Krill, and M. J. Pikal (2006): *Predictions of onset of crystallization from experimental relaxation times i-correlation of molecular mobility from temperatures above the glass transition to temperatures below the glass transition.* Pharmaceutical Research, 23, pp. 2277-2290. DOI: 10.1007/s11095-006-9079-1

Bibi, H. A., R. Holm, and A. Bauer-Brandl (2016): *Use of permeapad(r) for prediction of buccal absorption: A comparison to in vitro, ex vivo and in vivo method.* European Journal of Pharmaceutical Sciences, 93, pp. 399-404. DOI: 10.1016/j.ejps.2016.08.041

Blanquet, S., E. Zeijdner, E. Beyssac, J. Meunier, S. Denis, R. Havenaar, and M. Alric (2004): *A dynamic artificial gastrointestinal system for studying the behavior of orally administered drug dosage forms under various physiological conditions.* Pharmaceutical Research, 21, pp. 585-591. DOI: 10.1023/B:PHAM.0000022404.70478.4b

Boetker, J. P., J. Rantanen, L. Arnfast, M. Doreth, D. Raijada, K. Loebmann, C. Madsen, J. Khan, T. Rades, A. Mullertz, A. Hawley, D. Thomas, and B. J. Boyd (2016): *Anhydrate to hydrate solid-state transformations of carbamazepine and nitrofurantoin in biorelevant media studied in situ using time-resolved synchrotron X-ray diffraction.* European Journal of Pharmaceutics and Biopharmaceutics, 100, pp. 119-127. DOI: 10.1016/j.ejpb.2016.01.004

Boetker, J., T. Rades, J. Rantanen, A. Hawley, and B. J. Boyd (2012): *Structural elucidation of rapid solution-mediated phase transitions in pharmaceutical solids using in situ synchrotron SAXS/WAXS.* Molecular Pharmaceutics, 9, pp. 2787-2791. DOI: 10.1021/mp3003072

Breitenbach, J., and M. Mägerlein (2003): "Pharmaceutical extrusion technology." New York, Marcel Dekker Inc.

Breitkreutz, J., F. El-Saleh, C. Kiera, P. Kleinebudde, and W. Wiedey (2003): *Pediatric drug formulations of sodium benzoate.* European Journal of Pharmaceutics and Biopharmaceutics, 56, pp. 255-260. DOI: 10.1016/s0939-6411(03)00090-0

Brough, C., and R. O. Williams, 3rd (2013): *Amorphous solid dispersions and nano-crystal technologies for poorly water-soluble drug delivery.* International Journal of Pharmaceutics, 453, pp. 157-166. DOI: 10.1016/j.ijpharm.2013.05.061

Brouwers, J., M. E. Brewster, and P. Augustijns (2009): *Supersaturating drug delivery systems: The answer to solubility-limited oral bioavailability?* Journal of Pharmaceutical Sciences, 98, pp. 2549-2572. DOI: 10.1002/jps.21650

Brouwers, J., S. Geboers, R. Mols, J. Tack, and P. Augustijns (2017): *Gastrointestinal behavior of itraconazole in humans - part 1: Supersaturation from a solid dispersion and a cyclodextrin-based solution.* International Journal of Pharmaceutics, 525, pp. 211-217. DOI: 10.1016/j.ijpharm.2017.04.029

Brunner, E. (1904): *Reaktionsgeschwindigkeit in heterogenen Systemen.* Zeitschrift für Physikalische Chemie, 47, pp. 56-102. DOI: 10.1515/zpch-1904-4705

Buckley, S. T., S. M. Fischer, G. Fricker, and M. Brandl (2012): *In vitro models to evaluate the permeability of poorly soluble drug entities: Challenges and perspectives.* European Journal of Pharmaceutical Sciences, 45, pp. 235-250. DOI: 10.1016/j.ejps.2011.12.007

Buckley, S. T., K. J. Frank, G. Fricker, and M. Brandl (2013): *Biopharmaceutical classification of poorly soluble drugs with respect to "enabling formulations".* European Journal of Pharmaceutical Sciences, 50, pp. 8-16. DOI: 10.1016/j.ejps.2013.04.002

Butler, J. M., and J. B. Dressman (2010): *The developability classification system: Application of biopharmaceutics concepts to formulation development.* Journal of Pharmaceutical Sciences, 99, pp. 4940-4954. DOI: 10.1002/jps.22217

Camp Jr., C. H., Y. J. Lee, J. M. Heddleston, C. M. Hartshorn, A. R. H. Walker, J. N. Rich, J. D. Lathia, and M. T. Cicerone (2014): *High-speed coherent raman fingerprint imaging of biological tissues.* Nature Photonics, 8, pp. 627-634. DOI: 10.1038/nphoton.2014.145

Carino, S. R., D. C. Sperry, and M. Hawley (2010): *Relative bioavailability of three different solid forms of pnu-141659 as determined with the artificial stomach-duodenum model.* Journal of Pharmaceutical Sciences, 99, pp. 3923-3930. DOI: 10.1002/jps.22236

Carlert, S., A. Palsson, G. Hanisch, C. von Corswant, C. Nilsson, L. Lindfors, H. Lennernas, and B. Abrahamsson (2010): *Predicting intestinal precipitation-a case example for a basic BCS class II drug.* Pharmaceutical Research, 27, pp. 2119-2130. DOI: 10.1007/s11095-010-0213-8

Chauhan, A. (2014): *Powder XRD technique and its applications in science and technology.* Journal of Analytical & Bioanalytical Techniques, 5, DOI: 10.4172/2155-9872.1000212

Chavan, R. B., S. Rathi, Vgss Jyothi, and N. R. Shastri (2019): *Cellulose based polymers in development of amorphous solid dispersions.* Asian Journal of Pharmaceutical Sciences, 14, pp. 248-264. DOI: 10.1016/j.ajps.2018.09.003

Chen, R., N. Ilasi, and S. S. Sekulic (2011): *Absolute molecular weight determination of hypromellose acetate succinate by size exclusion chromatography: Use of a multi angle laser light scattering detector and a mixed solvent.* Journal of Pharmaceutical and Biomedical Analysis, 56, pp. 743-748. DOI: 10.1016/j.jpba.2011.07.035

Chen, J., J. D. Ormes, J. D. Higgins, and L. S. Taylor (2015a): *Impact of surfactants on the crystallization of aqueous suspensions of celecoxib amorphous solid dispersion spray dried particles.* Molecular Pharmaceutics, 12, pp. 533-541. DOI: 10.1021/mp5006245

Chen, J., L. I. Mosquera-Giraldo, J. D. Ormes, J. D. Higgins, and L. S. Taylor (2015b): *Bile salts as crystallization inhibitors of supersaturated solutions of poorly water-soluble compounds.* Crystal Growth & Design, 15, pp. 2593-2597. DOI: 10.1021/acs.cgd.5b00392

Chen, X., J. Schroder, S. Hauschild, S. Rosenfeldt, M. Dulle, and S. Forster (2015c): *Simultaneous saxs/waxs/uv-vis study of the nucleation and growth of nanoparticles: A test of classical nucleation theory.* Langmuir, 31, pp. 11678-11691. DOI: 10.1021/acs.langmuir.5b02759

Chen, Y., C. Liu, Z. Chen, C. Su, M. Hageman, M. Hussain, R. Haskell, K. Stefanski, and F. Qian (2015d): *Drug-polymer-water interaction and its implication for the dissolution performance of amorphous solid dispersions.* Molecular Pharmaceutics, 12, pp. 576-589. DOI: 10.1021/mp500660m

Chen, Y., S. Wang, S. Wang, C. Liu, C. Su, M. Hageman, M. Hussain, R. Haskell, K. Stefanski, and F. Qian (2016): *Sodium lauryl sulfate competitively interacts with hpmc-as and consequently reduces oral bioavailability of posaconazole/hpmc-as amorphous solid dispersion.* Molecular Pharmaceutics, 13, pp. 2787-2795. DOI: 10.1021/acs.molpharmaceut.6b00391

Chen, Y., Y. Pui, H. Chen, S. Wang, P. Serno, W. Tonnis, L. Chen, and F. Qian (2018): *Polymer-mediated drug supersaturation controlled by drug − polymer interactions persisting in an aqueous environment.* Molecular Pharmaceutics, 16, pp. 205-213. DOI: 10.1021/acs.molpharmaceut.8b00947

Chiou, W. L., and S. Riegelman (1971): *Pharmaceutical applications of solid dispersion systems.* Journal of Pharmaceutical Sciences, 60, pp. 1281-1302. DOI: 10.1002/jps.2600600902

Chokshi, R. J., N. H. Shah, H. K. Sandhu, A. W. Malick, and H. Zia (2008): *Stabilization of low glass transition temperature indomethacin formulations: Impact of polymer-type and its concentration.* Journal of Pharmaceutical Sciences, 97, pp. 2286-2298. DOI: 10.1002/jps.21174

Clarysse, S., J. Tack, F. Lammert, G. Duchateau, C. Reppas, and P. Augustijns (2009): *Postprandial evolution in composition and characteristics of human duodenal fluids in different nutritional states.* Journal of Pharmaceutical Sciences, 98, pp. 1177-1192. DOI: 10.1002/jps.21502

Code, C. F. (1979): *The interdigestive housekeeper of the gastrointestinal tract.* Perspectives in Biology and Medicine, 22, pp. S49-55. DOI: 10.1353/pbm.1979.0050

Coombes, S. R., L. P. Hughes, A. R. Phillips, and S. A. Wren (2014): *Proton NMR: A new tool for understanding dissolution.* Analytical Chemistry, 86, pp. 2474-2480. DOI: 10.1021/ac403418w

Craig, D. Q. M. (2002): *The mechanisms of drug release from solid dispersions in water-soluble polymers.* International Journal of Pharmaceutics, 231, pp. 131-144. DOI: 10.1016/S0378-5173(01)00891-2

Curatolo, W., J. A. Nightingale, and S. M. Herbig (2009): *Utility of hydroxypropylmethylcellulose acetate succinate (hpmcas) for initiation and maintenance of drug supersaturation in the GI milieu.* Pharmaceutical Research, 26, pp. 1419-1431. DOI: 10.1007/s11095-009-9852-z

Curatolo, W. (1998): *Physical chemical properties of oral drug candidates in the discovery and exploratory development settings.* Pharmaceutical Science & Technology Today, 1, pp. 387-393. DOI: 10.1016/S1461-5347(98)00097-2

Darcy, P. A., Wiencek, J. M. 1988. E*stimating lysozyme crystallization growth rates and solubility from isothermal microcalorimetry*. Acta Crystallographica D 54, pp. 1387-1394. DOI: 10.1107/S0907444998006052

de Man, F. M., K.G.A.M. Hussaarts, M. de With, E. Oomen-de Hoop, P. de Bruijn, H. K. van Halteren, N.C.H.P. van der Burg-de Graauw, F.A.L.M. Eskens, T. van Gelder, R.W.F. van Leeuwen, and R.H.J. Mathijssen (2019): *Influence of the proton pump inhibitor esomeprazole on the bioavailability of regorafenib: A randomized crossover pharmacokinetic study.* Clinical Pharmacology and Therapeutics, 105, pp. 1456-1461. DOI: 10.1002/cpt.1331

Dereymaker, A., G. Cinghia, and G. Van den Mooter (2017): *Eudragit(r) RL as a stabilizer for supersaturation and a substrate for nanocrystal formation.* European Journal of Pharmaceutics and Biopharmaceutics, 114, pp. 250-262. DOI: 10.1016/j.ejpb.2017.02.002

DeSesso, J. M., and C. F. Jacobson (2001): *Anatomical and physiological parameters affecting gastrointestinal absorption in humans and rats.* Food and Chemical Toxicology, 39, pp. 209-228. DOI: 10.1016/S0278-6915(00)00136-8

di Cagno, M., H. A. Bibi, and A. Bauer-Brandl (2015): *New biomimetic barrier permeapad for efficient investigation of passive permeability of drugs.* European Journal of Pharmaceutical Sciences, 73, pp. 29-34. DOI: 10.1016/j.ejps.2015.03.019

Dressman, J. B., G. L. Amidon, C. Reppas, and V. Shah (1998): *Dissolution testing as a prognostic tool for oral drug absorption: Immediate release dosage forms.* Pharmaceutical Research, 15, pp. 11-22. DOI: 10.1023/a:1011984216775

Dressman, J. B., P. Bass, W. Ritschel, D. R. Friend, A. Rubinstein, and E. Ziv (1993): *Gastrointestinal parameters that influence oral medications.* Journal of Pharmaceutical Sciences, 82, pp. 857-872. DOI: 10.1002/jps.2600820902

Edward, J. T. (1970): *Molecular volumes and the stokes-einstein equation.* Journal of Chemical Education, 47, pp. 261-270. DOI: 10.1021/ed047p261

Elkhabaz, A., S. Sarkar, J. K. Dinh, G. J. Simpson, and L. S. Taylor (2018): *Variation in supersaturation and phase behavior of ezetimibe amorphous solid dispersions upon dissolution in different biorelevant media.* Molecular Pharmaceutics, 15, pp. 193-206. DOI: 10.1021/acs.molpharmaceut.7b00814

Ellenberger, D. J., D. A. Miller, and R. O. Williams, 3rd (2018): *Expanding the application and formulation space of amorphous solid dispersions with kinetisol(r): A review.* AAPS PharmSciTech, 19, pp. 1933-1956. DOI: 10.1208/s12249-018-1007-2

Engers, D., J. Teng, J. Jimenez-Novoa, P. Gent, S. Hossack, C. Campbell, J. Thomson, I. Ivanisevic, A. Templeton, S. Byrn, and A. Newman (2010): *A solid-state approach to enable early development compounds: Selection and animal bioavailability studies of an itraconazole amorphous solid dispersion.* Journal of Pharmaceutical Sciences, 99, pp. 3901-3922. DOI: 10.1002/jps.22233

European Pharmacopoeia 10.0 (Ph. Eur.) (2019a). *Monograph 2.9.1: Disintegration of tablets and capsules*. Directorate for the Quality of Medicines of the Council of Europe, Strasbourg.

European Pharmacopoeia 10.0 (Ph. Eur.) (2019b). *Monograph 2.9.3: Dissolution test for solid dosage forms*. Directorate for the Quality of Medicines of the Council of Europe, Strasbourg.

European Pharmacopoeia 10.0 (Ph. Eur.) (2019c). *Tablets*. Directorate for the Quality of Medicines of the Council of Europe, Strasbourg.

Feng, D., T. Peng, Z. Huang, V. Singh, Y. Shi, T. Wen, M. Lu, G. Quan, X. Pan, and C. Wu (2018): *Polymer-surfactant system based amorphous solid dispersion: Precipitation inhibition and bioavailability enhancement of itraconazole.* Pharmaceutics, 10, DOI: 10.3390/pharmaceutics10020053

Fong, S. Y. K., S. M. Martins, M. Brandl, and A. Bauer-Brandl (2016): *Solid phospholipid dispersions for oral delivery of poorly soluble drugs: Investigation into celecoxib incorporation and solubility-in vitro permeability enhancement.* Journal of Pharmaceutical Sciences, 105, pp. 1113-1123. DOI: 10.1016/s0022-3549(15)00186-0

Fong, S. Y., A. Bauer-Brandl, and M. Brandl (2017): *Oral bioavailability enhancement through supersaturation: An update and meta-analysis.* Expert Opinion on Drug Delivery, 14, pp. 403-426. DOI: 10.1080/17425247.2016.1218465

Food and Drug Administration (FDA). 2000. *Waiver of in vivo bioavailability and bioequivalence studies for immediate-release solid oral dosage forms based on a biopharmaceutics classification system: Guidance for industry.* Edited by Center for Drug Evaluation and Research at U.S. Department of Health and Human Services. USA.

Franca, M. T., R. N. Pereira, M. K. Riekes, J. M. O. Pinto, and H. K. Stulzer (2018): *Investigation of novel supersaturating drug delivery systems of chlorthalidone: The use of polymer-surfactant complex as an effective carrier in solid dispersions.* European Journal of Pharmaceutical Sciences, 111, pp. 142-152. DOI: 10.1016/j.ejps.2017.09.043

Frank, K. J., K. M. Rosenblatt, U. Westedt, P. Holig, J. Rosenberg, M. Magerlein, G. Fricker, and M. Brandl (2012a): *Amorphous solid dispersion enhances permeation of poorly soluble abt-102: True supersaturation vs. Apparent solubility enhancement.*

International Journal of Pharmaceutics, 437, pp. 288-293. DOI: 10.1016/j.ijpharm.2012.08.014

Frank, K. J., U. Westedt, K. M. Rosenblatt, P. Holig, J. Rosenberg, M. Magerlein, G. Fricker, and M. Brandl (2012b): *The amorphous solid dispersion of the poorly soluble abt-102 forms nano/microparticulate structures in aqueous medium: Impact on solubility.* International Journal of Nanomedicine, 7, pp. 5757-5768. DOI: 10.2147/IJN.S36571

Frank, K. J., U. Westedt, K. M. Rosenblatt, P. Holig, J. Rosenberg, M. Magerlein, G. Fricker, and M. Brandl (2014): *What is the mechanism behind increased permeation rate of a poorly soluble drug from aqueous dispersions of an amorphous solid dispersion?* Journal of Pharmaceutical Sciences, 103, pp. 1779-1786. DOI: 10.1002/jps.23979

Freyer, M. W., and E. A. Lewis (2008): "Isothermal titration calorimetry: Experimental design, data analysis, and probing macromolecule/ligand binding and kinetic interactions", Chapter 4. Edited by M. W. Freyer and E. A. Lewis. Vol. 84, *Methods in cell biology*. Flagstaff, USA, Elsevier Inc.

Friesen, D. T., R. Shanker, M. Crew, D. T. Smithey, W. J. Curatolo, and J. A. Nightingale (2008): *Hydroxypropyl methylcellulose acetate succinate-based spray-dried dispersions: An overview.* Molecular Pharmaceutics, 5, pp. 1003-1019. DOI: 10.1021/mp8000793

Fuchs, A., M. Leigh, B. Kloefer, and J. B. Dressman (2015): *Advances in the design of fasted state simulating intestinal fluids: Fassif-v3.* European Journal of Pharmaceutics and Biopharmaceutics, 94, pp. 229-240. DOI: 10.1016/j.ejpb.2015.05.015

Fujisawaa, M., T. Kimuraa, and S. Takagia (1990): *Enthalpy and entropy changes on molecular inclusion of 1-butanol into α- and β-cyclodextrin cavities in aqueous solutions.* Netsu Sokutei, 18, pp. 71-76. DOI: 10.11311/jscta1974.18.71

Gala, U. H., D. A. Miller, and R. O. Williams, 3rd (2020): *Harnessing the therapeutic potential of anticancer drugs through amorphous solid dispersions.* Biochimica et Biophysica Acta Reviews on Cancer, 1873, pp. 188319. DOI: 10.1016/j.bbcan.2019.188319

Garbacz, G., R. S. Wedemeyer, S. Nagel, T. Giessmann, H. Monnikes, C. G. Wilson, W. Siegmund, and W. Weitschies (2008): *Irregular absorption profiles observed from diclofenac extended release tablets can be predicted using a dissolution test apparatus that mimics in vivo physical stresses.* European Journal of Pharmaceutics and Biopharmaceutics, 70, pp. 421-428. DOI: 10.1016/j.ejpb.2008.05.029

Garbacz, G., S. Klein, and W. Weitschies (2010): *A biorelevant dissolution stress test device - background and experiences.* Expert Opinion, 7, pp. 1251-1261. DOI: 10.1517/17425247.2010.527943

Glatter, O. (1980): *Determination of particle-size distribution functions from small-angle scattering data by means of the indirect transformation method.* Journal of Applied Crystallography, 13, pp. 7-11. DOI: 10.1107/S0021889880011429

Goel, G. (2018): *Evolution of regorafenib from bench to bedside in colorectal cancer: Is it an attractive option or merely a "me too" drug?* Cancer Management and Research, 10, pp. 425-437. DOI: 10.2147/CMAR.S88825

Goldberg, A. H., M. Gibaldi, and J. L. Kanig (1965): *Increasing dissolution rates and gastrointestinal absorption of drugs via solid solutions and eutectic mixtures I: Theoretical considerations and discussion of the literature.* Journal of Pharmaceutical Sciences, 54, pp. 1145-1148. DOI: 10.1002/jps.2600540810

Goldberg, A. H., M. Gibaldi, and J. L. Kanig (1966a): *Increasing dissolution rates and gastrointestinal absorption of drugs via solid solutions and eutectic mixtures II: Experimental evaluation of a eutectic mixture: Urea-acetaminophen system.* Journal of Pharmaceutical Sciences, 55, pp. 482-487. DOI: 10.1002/jps.2600550507

Goldberg, A. H., M. Gibaldi, and J. L. Kanig (1966b): *Increasing dissolution rates and gastrointestinal absorption of drugs via solid solutions and eutectic mixtures III: Experimental evaluation of griseofulvin—succinic acid solid solution* Journal of Pharmaceutical Sciences, 55, pp. 487-492. DOI: 10.1002/jps.2600550508

Goldberg, A. H., M. Gibaldi, and J. L. Kanig (1966c): *Increasing dissolution rates and gastrointestinal absorption of drugs via solid solutions and eutectic mixtures IV: Chloramphenicol—urea system* Journal of Pharmaceutical Sciences, 55, pp. 581-583. DOI: 10.1002/jps.2600550610

Gordon, M., and J. S. Taylor (1952): *Ideal copolymers and the second-order transitions of synthetic rubbers. I. Non-crystalline copolymers.* Journal of Applied Chemistry, 2, pp. 493-500. DOI: 10.1002/jctb.5010020901

Grabowski, T., J. J. Jaroszewski, W. Piotrowski, and M. Sasinowska-Motyl (2014): *Method of variability optimization in pharmacokinetic data analysis.* European Journal of Drug Metabolism and Pharmacokinetics, 39, pp. 111-119. DOI: 10.1007/s13318-013-0145-x

Griffin, B. T., M. Kuentz, M. Vertzoni, E. S. Kostewicz, Y. Fei, W. Faisal, C. Stillhart, C. M. O'Driscoll, C. Reppas, and J. B. Dressman (2014): *Comparison of in vitro tests at various levels of complexity for the prediction of in vivo performance of lipid-based formulations: Case studies with fenofibrate.* European Journal of Pharmaceutics and Biopharmaceutics, 86, pp. 427-437. DOI: 10.1016/j.ejpb.2013.10.016

Grignard, E., R. Taylor, M. McAllister, K. Box, and N. Fotaki (2017): *Considerations for the development of in vitro dissolution tests to reduce or replace preclinical oral absorption studies.* European Journal of Pharmaceutical Sciences, 99, pp. 193-201. DOI: 10.1016/j.ejps.2016.12.004

Grimm, M., E. Scholz, M. Koziolek, J. P. Kuhn, and W. Weitschies (2017): *Gastric water emptying under fed state clinical trial conditions is as fast as under fasted conditions.*

Molecular Pharmaceutics, 14, pp. 4262-4271. DOI: 10.1021/acs.molpharmaceut.7b00623

Grothey, A., E. van Cutsem, A. Sobrero, S. Siena, A. Falcone, M. Ychou, Y. Humblet, O. Bouché, L. Mineur, C. Barone, A. Adenis, J. Tabernero, T. Yoshino, H. Lenz, R. M. Goldberg, D. J. Sargent, F. Cihon, L. Cupit, A. Wagner, and D. Laurent (2013): *Regorafenib monotherapy for previously treated metastatic colorectal cancer CORRECT): An international, multicentre, randomised, placebo-controlled, phase 3 trial.* Lancet, 381, pp. 303-312. DOI: 10.1016/s0140-6736(12)61900-x

Gu, C. H., D. Rao, R. B. Gandhi, J. Hilden, and K. Raghavan (2005): *Using a novel multicompartment dissolution system to predict the effect of gastric ph on the oral absorption of weak bases with poor intrinsic solubility.* Journal of Pharmaceutical Sciences, 94, pp. 199-208. DOI: 10.1002/jps.20242

Guzman, H. R., M. Tawa, Z. Zhang, P. Ratanabanangkoon, P. Shaw, C. R. Gardner, H. Chen, J. P. Moreau, O. Almarsson, and J. F. Remenar (2007): *Combined use of crystalline salt forms and precipitation inhibitors to improve oral absorption of celecoxib from solid oral formulations.* Journal of Pharmaceutical Sciences, 96, pp. 2686-2702. DOI: 10.1002/jps.20906

Haaser, M., M. Windbergs, C. M. McGoverin, P. Kleinebudde, T. Rades, K. C. Gordon, and C. J. Strachan (2011): *Analysis of matrix dosage forms during dissolution testing using raman microscopy.* Journal of Pharmaceutical Sciences, 100, pp. 4452-4459. DOI: 10.1002/jps.22609

Hallouard, F., L. Mehenni, M. Lahiani-Skiba, Y. Anouar, and M. Skiba (2016): *Solid dispersions for oral administration: An overview of the methods for their preparation.* Current Pharmaceutical Design, 22, pp. 1-17. DOI: 10.2174/1381612822666160726095916

Han, Y. R., and P. I. Lee (2017): *Effect of extent of supersaturation on the evolution of kinetic solubility profiles.* Molecular Pharmaceutics, 14, pp. 206-220. DOI: 10.1021/acs.molpharmaceut.6b00788

Hancock, B. C., S. L. Shamblin, and G. Zografi (1995): *Molecular mobility of amorphous pharmaceutical solids below their glass transition temperatures.* Pharmaceutical Research, 12, pp. 799-806. DOI: 10.1023/A:1016292416526

Haralampiev, I., H. A. Scheidt, T. Abel, M. Luckner, A. Herrmann, D. Huster, and P. Muller (2016): *The interaction of sorafenib and regorafenib with membranes is modulated by their lipid composition.* Biochimica et Biophysica Acta, 1858, pp. 2871-2881. DOI: 10.1016/j.bbamem.2016.08.014

Haser, A., and F. Zhang (2018): *New strategies for improving the development and performance of amorphous solid dispersions.* AAPS PharmSciTech, 19, pp. 978-990. DOI: 10.1208/s12249-018-0953-z

He, Y., and C. Ho (2015): *Amorphous solid dispersions: Utilization and challenges in drug discovery and development.* Journal of Pharmaceutical Sciences, 104, pp. 3237-3258. DOI: 10.1002/jps.24541

Hoffman, J. D. (1958): *Thermodynamic driving force in nucleation and growth processes.* Journal of Chemical Physics, 29, pp. 1192-1193. DOI: 10.1063/1.1744688

Hua, L., G. Wanga, R. Caob, C. Yanga, and X. Chen (2014): *Fabrication and surface properties of hydrophobic barium sulfate aggregates based on sodium cocoate modification.* Applied Surface Science, 315, pp. 184-189. DOI: 10.1016/j.apsusc.2014.07.068

Hunter, E., J. T. Fell, and H. Sharma (1982): *The gastric emptying of pellets contained in hard gelatin capsules.* Drug Development and Industrial Pharmacy, 8, pp. 751-757. DOI: 10.3109/03639048209042700

Ibekwe, V. C., H. M. Fadda, E. L. McConnell, M. K. Khela, D. F. Evans, and A. W. Basit (2008): *Interplay between intestinal pH, transit time and feed status on the in vivo performance of ph responsive ileo-colonic release systems.* Pharmaceutical Research, 25, pp. 1828-1835. DOI: 0.1007/s11095-008-9580-9

Ilevbare, G. A., H. Liu, K. J. Edgar, and L. S. Taylor (2012): *Effect of binary additive combinations on solution crystal growth of the poorly water-soluble drug, ritonavir.* Crystal Growth & Design, 12, pp. 6050-6060. DOI: 10.1021/cg301169t

Ilevbare, G. A., and L. S. Taylor (2013): *Liquid−liquid phase separation in highly supersaturated aqueous solutions of poorly water-soluble drugs: Implications for solubility enhancing formulations.* Crystal Growth & Design, 13, pp. 1497−1509. DOI: 10.1021/cg301679h

Ilevbare, G. A., H. Liu, K. J. Edgar, and L. S. Taylor (2013): *Impact of polymers on crystal growth rate of structurally diverse compounds from aqueous solution.* Molecular Pharmaceutics, 10, pp. 2381-2393. DOI: 10.1021/mp400029v

Indulkar, A. S., Y. Gao, S. A. Raina, G. G. Zhang, and L. S. Taylor (2016): *Exploiting the phenomenon of liquid-liquid phase separation for enhanced and sustained membrane transport of a poorly water-soluble drug.* Molecular Pharmaceutics, 13, pp. 2059-2069. DOI: 10.1021/acs.molpharmaceut.6b00202

Indulkar, A. S., J. E. Waters, H. Mo, Y. Gao, S. A. Raina, G. G. Z. Zhang, and L. S. Taylor (2017): *Origin of nanodroplet formation upon dissolution of an amorphous solid dispersion: A mechanistic isotope scrambling study.* Journal of Pharmaceutical Sciences, 106, pp. 1998-2008. DOI: 10.1016/j.xphs.2017.04.015

InnoME GmbH. 2018. *Permeapad barrier manual*. Link: https://permeapad.com/wp-content/uploads/2018/10/Manual_PermeaPad_Barrier_EN_.pdf [Last accessed: 2020-10-10].

Jackson, M. J., U. S. Kestur, M. A. Hussain, and L. S. Taylor (2016): *Dissolution of danazol amorphous solid dispersions: Supersaturation and phase behavior as a function of drug loading and polymer type.* Molecular Pharmaceutics, 13, pp. 223-231. DOI: 10.1021/acs.molpharmaceut.5b00652

Jacob, J., C. Krafft, K. Welfle, H. Welfle, and W. Saenger (1998): *Melting points of lysozyme and ribonuclease a crystals correlated with protein unfolding: A raman spectroscopic study.* Acta Crystallographica Section D, 54, pp. 74-80. DOI: 10.1107/s0907444997010603

Jacobsen, A. C., P. A. Elvang, A. Bauer-Brandl, and M. Brandl (2019): *A dynamic in vitro permeation study on solid mono- and diacyl-phospholipid dispersions of celecoxib.* European Journal of Pharmaceutical Sciences, 127, pp. 199-207. DOI: 10.1016/j.ejps.2018.11.003

Jankovic, S., P. J. O'Dwyer, K. J. Box, G. Imanidis, C. Reppas, and M. Kuentz (2019): *Biphasic drug release testing coupled with diffusing wave spectroscopy for mechanistic understanding of solid dispersion performance.* European Journal of Pharmaceutical Sciences, 137, pp. 105001. DOI: 10.1016/j.ejps.2019.105001

Jede, C., C. Wagner, H. Kubas, M. Weigandt, C. Weber, M. Lecomte, L. Badolo, M. Koziolek, and W. Weitschies (2019): *Improved prediction of in vivo supersaturation and precipitation of poorly soluble weakly basic drugs using a biorelevant bicarbonate buffer in a gastrointestinal transfer model.* Molecular Pharmaceutics, 16, pp. 3938-3947. DOI: 10.1021/acs.molpharmaceut.9b00534

Jermain, S. V., C. Brough, and R. O. Williams, 3rd (2018): *Amorphous solid dispersions and nanocrystal technologies for poorly water-soluble drug delivery - an update.*

International Journal of Pharmaceutics, 535, pp. 379-392. DOI: 10.1016/j.ijpharm.2017.10.051

Kalantzi, L., K. Goumas, V. Kalioras, B. Abrahamsson, J. B. Dressman, and C. Reppas (2006): *Characterization of the human upper gastrointestinal contents under conditions simulating bioavailability/bioequivalence studies.* Pharmaceutical Research, 23, pp. 165-176. DOI: 10.1007/s11095-005-8476-1

Kambayashi, A., T. Yasuji, and J. B. Dressman (2016): *Prediction of the precipitation profiles of weak base drugs in the small intestine using a simplified transfer ("dumping") model coupled with in silico modeling and simulation approach.* European Journal of Pharmaceutics and Biopharmaceutics, 103, pp. 95-103. DOI: 10.1016/j.ejpb.2016.03.020

Kanzer, J., S. Hupfeld, T. Vasskog, I. Tho, P. Holig, M. Magerlein, G. Fricker, and M. Brandl (2010): *In situ formation of nanoparticles upon dispersion of melt extrudate formulations in aqueous medium assessed by asymmetrical flow field-flow fractionation.* Journal of Pharmaceutical and Biomedical Analysis, 53, pp. 359-365. DOI: 10.1016/j.jpba.2010.04.012

Kerlin, P., A. Zinsmeister, and S. Phillips (1982): *Relationship of motility to flow of contents in the human small intestine.* Gastroenterology, 82, pp. 701-706. DOI: 10.1016/0016-5085(82)90314-6

Khan, J., A. Hawley, T. Rades, and B. J. Boyd (2016a): *In situ lipolysis and synchrotron small-angle x-ray scattering for the direct determination of the precipitation and solid-state form of a poorly water-soluble drug during digestion of a lipid-based formulation.* Journal of Pharmaceutical Sciences, 105, pp. 2631-2639. DOI: 10.1002/jps.24634

Khan, J., T. Rades, and B. J. Boyd (2016b): *Lipid-based formulations can enable the model poorly water-soluble weakly basic drug cinnarizine to precipitate in an amorphous-salt*

*form during in vitro digestion.* Molecular Pharmaceutics, 13, pp. 3783-3793. DOI: 10.1021/acs.molpharmaceut.6b00594

Khan, J., T. Rades, and B. J. Boyd (2016c): *The precipitation behavior of poorly water-soluble drugs with an emphasis on the digestion of lipid based formulations.* Pharmaceutical Research, 33, pp. 548-562. DOI: 10.1007/s11095-015-1829-5

Klein, S. (2010): *The use of biorelevant dissolution media to forecast the in vivo performance of a drug.* The AAPS Journal, 12, pp. 397-406. DOI: 10.1208/s12248-010-9203-3

Klein, S. (2016): *Anwendung und Vergleich unterschiedlicher Dissolutionmethoden - Teil 2.* Techno Pharm, 6, pp. 166-171.

Klein, S. (2019): *Advancements in dissolution testing of oral and non-oral formulations.* AAPS PharmSciTech, 20, pp. 266. DOI: 10.1208/s12249-019-1479-8

Knopp, M. M., J. H. Nguyen, H. Mu, P. Langguth, T. Rades, and R. Holm (2016): *Influence of copolymer composition on in vitro and in vivo performance of celecoxib-pvp/va amorphous solid dispersions.* The AAPS Journal, 18, pp. 416-423. DOI: 10.1208/s12248-016-9865-6

Koch, M. H., P. Vachette, and D. I. Svergun (2003): *Small-angle scattering: A view on the properties, structures and structural changes of biological macromolecules in solution.* Q Rev Biophys, 36, pp. 147-227. DOI: 10.1017/s0033583503003871

Kojima, T., K. Higashi, T. Suzuki, K. Tomono, K. Moribe, and K. Yamamoto (2012): *Stabilization of a supersaturated solution of mefenamic acid from a solid dispersion with eudragit EPO.* Pharmaceutical Research, 29, pp. 2777-2791. DOI: 10.1007/s11095-011-0655-7

Kostewicz, E. S., M. Wunderlich, U. Brauns, R. Becker, T. Bock, and J. B. Dressman (2004): *Predicting the precipitation of poorly soluble weak bases upon entry in the small intestine.* Journal of Pharmacy and Pharmacology, 56, pp. 43-51. DOI: 10.1211/0022357022511

Kostewicz, E. S., B. Abrahamsson, M. Brewster, J. Brouwers, J. Butler, S. Carlert, P. A. Dickinson, J. Dressman, R. Holm, S. Klein, J. Mann, M. McAllister, M. Minekus, U. Muenster, A. Mullertz, M. Verwei, M. Vertzoni, W. Weitschies, and P. Augustijns (2014): *In vitro models for the prediction of in vivo performance of oral dosage forms.* European Journal of Pharmaceutical Sciences, 57, pp. 342-366. DOI: 10.1016/j.ejps.2013.08.024

Koziolek, M., K. Gorke, M. Neumann, G. Garbacz, and W. Weitschies (2014): *Development of a bio-relevant dissolution test device simulating mechanical aspects present in the fed stomach.* European Journal of Pharmaceutical Sciences, 57, pp. 250-256. DOI: 10.1016/j.ejps.2013.09.004

Krasser, W., P. S. Bechthold, and U. Kettler (1983): *Enhanced raman scattering from small metallic particles and metallic films.* Fresenius Zeitschrift für Analytische Chemie, 314, pp. 319-323. DOI: 10.1007/BF00516830

Lang, B., S. Liu, J. W. McGinity, and R. O. Williams, 3rd (2016): *Effect of hydrophilic additives on the dissolution and pharmacokinetic properties of itraconazole-enteric polymer hot-melt extruded amorphous solid dispersions.* Drug Development and Industrial Pharmacy, 42, pp. 429-445. DOI: 10.3109/03639045.2015.1075031

Li, N., and L. S. Taylor (2018): *Tailoring supersaturation from amorphous solid dispersions.* Journal of Controlled Release, 279, pp. 114-125. DOI: 10.1016/j.jconrel.2018.04.014

Lindfors, L., S. Forssen, J. Westergren, and U. Olsson (2008): *Nucleation and crystal growth in supersaturated solutions of a model drug.* Journal of Colloid and Interface Science, 325, pp. 404-413. DOI: 10.1016/j.jcis.2008.05.034

Lipinski, C. A., F. Lombardo, B. W. Dominy, and P. J. Feeney (1997): *Experimental and computational approaches to estimate solubility and permeability in drug discovery and development settings.* Advanced Drug Delivery Reviews, 23, pp. 3−25. DOI: 10.1016/S0169-409X(96)00423-1

Liu, H., L. S. Taylor, and K. J. Edgar (2015): *The role of polymers in oral bioavailability enhancement; a review.* Polymer, 77, pp. 399-415. DOI: 10.1016/j.polymer.2015.09.026

Loftsson, T., and M. E. Brewster (2010): *Pharmaceutical applications of cyclodextrins: Basic science and product development.* Journal of Pharmacy and Pharmacology, 62, pp. 1607-1621. DOI: 10.1111/j.2042-7158.2010.01030.x

Lu, J., J. D. Ormes, M. Lowinger, W. Xu, A. Mitra, A. K. P. Mann, J. D. Litster, and L. S. Taylor (2017): *Impact of endogenous bile salts on the thermodynamics of supersaturated active pharmaceutical ingredient solutions.* Crystal Growth & Design, 17, pp. 1264−1275. DOI: 10.1021/acs.cgd.6b01664

Ma, X., and R. O. Williams (2019): *Characterization of amorphous solid dispersions: An update.* Journal of Drug Delivery Science and Technology, 50, pp. 113-124. DOI: 10.1016/j.jddst.2019.01.017

Maderuelo, C., J. M. Lanao, and A. Zarzuelo (2019): *Enteric coating of oral solid dosage forms as a tool to improve drug bioavailability.* European Journal of Pharmaceutical Sciences, 138, pp. 105019. DOI: 10.1016/j.ejps.2019.105019

McConnell, E. L., A. W. Basit, and S. Murdan (2008): *Measurements of rat and mouse gastrointestinal pH, fluid and lymphoid tissue, and implications for in-vivo experiments.* Journal of Pharmacy and Pharmacology, 60, pp. 63-70. DOI: 10.1211/jpp.60.1.0008

Mendonsa, N., B. Almutairy, V. R. Kallakunta, S. Sarabu, P. Thipsay, S. Bandari, and M. A. Repka (2020): *Manufacturing strategies to develop amorphous solid dispersions: An overview.* Journal of Drug Delivery Science and Technology, 55, pp. 101459. DOI: 10.1016/j.jddst.2019.101459

Meyer, J. H., J. Elashoff, V. Porter-Fink, J. Dressman, and G. L. Amidon (1988): *Human postprandial gastric emptying of 1-3-millimeter spheres.* Gastroenterology, 94, pp. 1315-1325. DOI: 10.1016/0016-5085(88)90669-5

Miller, J. M., A. Beig, R. A. Carr, J. K. Spence, and A. Dahan (2012): *A win-win solution in oral delivery of lipophilic drugs: Supersaturation via amorphous solid dispersions increases apparent solubility without sacrifice of intestinal membrane permeability.* Molecular Pharmaceutics, 9, pp. 2009-2016. DOI: 10.1021/mp300104s

Minekus, M., M. Smeets-Peeters, A. Bernalier, S. Marol-Bonnin, R. Havenaar, P. Marteau, M. Alric, G. Fonty, and J. H. J. Huis in't Veld (1999): *A computer-controlled system to simulate conditionsof the large intestine with peristaltic mixing, water absorptionand absorption of fermentation products.* Applied Microbiology and Biotechnology, 53, pp. 108-114. DOI: 10.1007/s002530051622

Moes, J., S. Koolen, A. Huitema, J. Schellens, J. Beijnen, and B. Nuijen (2013): *Development of an oral solid dispersion formulation for use in low-dose metronomic chemotherapy of paclitaxel.* European Journal of Pharmaceutics and Biopharmaceutics, 83, pp. 87-94. DOI: 10.1016/j.ejpb.2012.09.016

Moore, J. W., and H. H. Flanner (1996): *Mathematical comparison of dissolution profiles.* Pharmaceutical Technology, 20, pp. 64-74. ISSN: 0147-8087

Van den Mooter, G., M. Wuyts, N. Blaton, R. Busson, P. Grobet, P. Augustijns, and R. Kinget (2001): *Physical stabilisation of amorphous ketoconazole in solid dispersions with polyvinylpyrrolidone k25.* European Journal of Pharmaceutical Sciences, 12, pp. 261-269. DOI: 10.1016/S0928-0987(00)00173-1

Motz, S. A., U. F. Schaefer, S. Balbach, T. Eichinger, and C. M. Lehr (2007): *Permeability assessment for solid oral drug formulations based on caco-2 monolayer in combination with a flow through dissolution cell.* European Journal of Pharmaceutics and Biopharmaceutics, 66, pp. 286-295. DOI: 10.1016/j.ejpb.2006.10.015

Mross, K., A. Frost, S. Steinbild, S. Hedbom, M. Buchert, U. Fasol, C. Unger, J. Kratzschmar, R. Heinig, O. Boix, and O. Christensen (2012): *A phase I dose-escalation study of regorafenib (bay 73-4506), an inhibitor of oncogenic, angiogenic, and stromal kinases, in patients with advanced solid tumors.* Clinical Cancer Research, 18, pp. 2658-2667. DOI: 10.1158/1078-0432.CCR-11-1900

Mudie, D. M., G. L. Amidon, and G. E. Amidon (2010): *Physiological parameters for oral delivery and in vitro testing.* Molecular Pharmaceutics, 7, pp. 1388-1405. DOI: 10.1021/mp100149j

Nakamoto, K., T. Urasaki, S. Hondo, N. Murahashi, E. Yonemochi, and K. Terada (2013): *Evaluation of the crystalline and amorphous states of drug products by nanothermal analysis and raman imaging.* Journal of Pharmaceutical and Biomedical Analysis, 75, pp. 105-111. DOI: 10.1016/j.jpba.2012.11.020

Nernst, W. (1904): *Theorie der Reaktionsgeschwindigkeit in heterogenen Systemen.* Zeitschrift für Physikalische Chemie, 47, pp. 52-55. DOI: 10.1515/zpch-1904-4704

Noyes, A. A., and W. R. Whitney (1897): *The rate of solution of solid substances in their own solutions.* Journal of the American Chemical Society, 19, pp. 930-934. DOI: 10.1021/ja02086a003

Nunes, R., C. Silva, and L. Chaves (2015): "Tissue-based in vitro and ex vivo models for intestinal permeability studies", Chapter 4.2. Edited by B. Sarmento. Edition 1, *Concepts and models for drug permeability studies*. Woodhead Publishing.

O'Neill, M. A., and S. Gaisford (2011): *Application and use of isothermal calorimetry in pharmaceutical development.* International Journal of Pharmaceutics, 417, pp. 83-93. DOI: 10.1016/j.ijpharm.2011.01.038

Oberle, R. L., T. Chen, C. Lloyd, J. L. Barnett, C. Owyang, J. Meyer, and G. L. Amidon (1990): *The influence of the interdigestive migrating myoelectric complex on the gastric emptying of liquids.* Gastroenterology, 99, pp. 1275-1282. DOI: 10.1016/0016-5085(90)91150-5

Park, H. M., S. M. Chernish, B. D. Rosenek, R. L. Brunelle, B. Hargrove, and H. N. Wellman (1984): *Gastric emptying of enteric-coated tablets.* Digestive Diseases and Sciences, 29, pp. 207-212. DOI: 10.1007/BF01296253

Patel, A. R., and V. Y. Joshi (2008): *Evaluation of sls: Apg mixed surfactant systems as carrier for solid dispersion.* AAPS PharmSciTech, 9, pp. 583-590. DOI: 10.1208/s12249-008-9093-1

Patil, H., R. V. Tiwari, and M. A. Repka (2016): *Hot-melt extrusion: From theory to application in pharmaceutical formulation.* AAPS PharmSciTech, 17, pp. 20-42. DOI: 10.1208/s12249-015-0360-7

Paudel, A., J. Meeus, and G. Van den Mooter (2014): *Structural characterization of amorphous solid dispersions.* Advances in Delivery Science and Technology, pp. 421-485. DOI: 10.1007/978-1-4939-1598-9_14

Pedersen, P. B., P. Vilmann, D. Bar-Shalom, A. Müllertz, and S. G. Baldursdottir (2013): *Polymer selection for simulation of rheological properties of human gastric fluid.* Annual Transactions of the Nordic Rheology Society, 21, pp. 241-248.

Price, D. J., F. Ditzinger, N. J. Koehl, S. Jankovic, G. Tsakiridou, A. Nair, R. Holm, M. Kuentz, J. B. Dressman, and C. Saal (2019): *Approaches to increase mechanistic understanding and aid in the selection of precipitation inhibitors for supersaturating formulations - a pearrl review.* Journal of Pharmacy and Pharmacology, 71, pp. 483-509. DOI: 10.1111/jphp.12927

Prozeller, D., S. Morsbach, and K. Landfester (2019): *Isothermal titration calorimetry as a complementary method for investigating nanoparticle-protein interactions.* Nanoscale, 11, pp. 19265-19273. DOI: 10.1039/c9nr05790k

Psachoulias, D., M. Vertzoni, J. Butler, D. Busby, M. Symillides, J. Dressman, and C. Reppas (2012): *An in vitro methodology for forecasting luminal concentrations and precipitation of highly permeable lipophilic weak bases in the fasted upper small intestine.* Pharmaceutical Research, 29, pp. 3486-3498. DOI: 10.1007/s11095-012-0844-z

Psachoulias, D., M. Vertzoni, K. Goumas, V. Kalioras, S. Beato, J. Butler, and C. Reppas (2011): *Precipitation in and supersaturation of contents of the upper small intestine after administration of two weak bases to fasted adults.* Pharmaceutical Research, 28, pp. 3145-3158. DOI: 10.1007/s11095-011-0506-6

Pudipeddi, M., T. D. Sokoloski, S. P. Duddu, and J. T. Carstensen (1995): *Calorimetric determination of the heat of precipitation of pseudsephedrine racemic compound - its*

*agreement with the heat of solution.* Journal of Pharmaceutical Sciences, 84, pp. 1236-1239. DOI: 10.1002/jps.2600841017

Purohit, H. S., and L. S. Taylor (2015): *Phase separation kinetics in amorphous solid dispersions upon exposure to water.* Molecular Pharmaceutics, 12, pp. 1623-1635. DOI: 10.1021/acs.molpharmaceut.5b00041

Que, C., Y. Gao, S. A. Raina, G. G. Z. Zhang, and L. S. Taylor (2018): *Paclitaxel crystal seeds with different intrinsic properties and their impact on dissolution of paclitaxel-hpmcas amorphous solid dispersions.* Crystal Growth & Design, 18, pp. 1548-1559. DOI: 10.1021/acs.cgd.7b01521

Rahman, A., and C. W. Brown (1983): *Effect of ph on the critical micelle concentration of sodium dodecyl sulphate.* Journal of Applied Polymer Science, 28, pp. 1331-1334. DOI: 10.1002/app.1983.070280407

Rahman, M. A., A. Hussain, M. S. Hussain, M. A. Mirza, and Z. Iqbal (2013): *Role of excipients in successful development of self-emulsifying/microemulsifying drug delivery system (sedds/smedds).* Drug Development and Industrial Pharmacy, 39, pp. 1-19. DOI: 10.3109/03639045.2012.660949

Raina, S. A., D. E. Alonzo, G. G. Zhang, Y. Gao, and L. S. Taylor (2014): *Impact of polymers on the crystallization and phase transition kinetics of amorphous nifedipine during dissolution in aqueous media.* Molecular Pharmaceutics, 11, pp. 3565-3576. DOI: 10.1021/mp500333v

Raina, S. A., B. Van Eerdenbrugh, D. E. Alonzo, H. Mo, G. G. Z. Zhang, Y. Gao, and L. S. Taylor (2015): *Trends in the precipitation and crystallization behavior of supersaturated aqueous solutions of poorly water-soluble drugs assessed using synchrotron radiation.* Journal of Pharmaceutical Sciences, 104, pp. 1981-1992. DOI: 10.1002/jps.24423

Raman, C., and K. Krishnan (1928): *A new type of secondary radiation.* Nature, 121, pp. 501-502. DOI: 10.1038/121501c0

Repka, M. A., S. K. Battu, S. B. Upadhye, S. Thumma, M. M. Crowley, F. Zhang, C. Martin, and J. W. McGinity (2007): *Pharmaceutical applications of hot-melt extrusion: Part II.* Drug Development and Industrial Pharmacy, 33, pp. 1043-1057. DOI: 10.1080/03639040701525627

Rodgers, A. L., and G. E. Jackson (2017): *Determination of thermodynamic parameters for complexation of calcium and magnesium with chondroitin sulfate isomers using isothermal titration calorimetry: Implications for calcium kidney-stone research.* Journal of Crystal Growth, 463, pp. 14-18. DOI: 10.1016/j.jcrysgro.2017.01.056

Rowe, R. C. (1980): *The molecular weight and molecular weight distribution of hydroxypropyl methylcellulose used in the film coating of tablets.* Journal of Pharmacy and Pharmacology, 32, pp. 116-119. DOI: 10.1111/j.2042-7158.1980.tb12865.x

Sassene, P. J., M. M. Knopp, J. Z. Hesselkilde, V. Koradia, A. Larsen, T. Rades, and A. Mullertz (2010): *Precipitation of a poorly soluble model drug during in vitro lipolysis: Characterization and dissolution of the precipitate.* Journal of Pharmaceutical Sciences, 99, pp. 4982-4991. DOI: 10.1002/jps.22226

Sassene, P., M. Mosgaard, K. L bmann, H. Mu, F. Larsen, T. Rades, and A. Müllertz (2015): *Elucidating the molecular interactions occurring during drug precipitation of weak bases from lipid-based formulations: A case study with cinnarizine and a long chain self-nanoemulsifying drug delivery system.* Molecular Pharmaceutics, 12, pp. 4067−4076. DOI: 10.1021/acs.molpharmaceut.5b00498

Sawicki, E., J. H. Schellens, J. H. Beijnen, and B. Nuijen (2016): *Inventory of oral anticancer agents: Pharmaceutical formulation aspects with focus on the solid dispersion*

*technique.* Cancer Treatment Reviews, 50, pp. 247-263. DOI: 10.1016/j.ctrv.2016.09.012

Schall, C. A., E. Arnold, and J. M. Wiencekc (1996): *Enthalpy of crystallization of hen egg-white lysozyme.* Journal of Crystal Growth, 165, pp. 293-298. DOI: 10.1016/0022-0248(96)00180-7

Schiller, C., C. P. Frohlich, T. Giessmann, W. Siegmund, H. Monnikes, N. Hosten, and W. Weitschies (2005): *Intestinal fluid volumes and transit of dosage forms as assessed by magnetic resonance imaging.* Alimentary Pharmacology & Therapeutics, 22, pp. 971-979. DOI: 10.1111/j.1365-2036.2005.02683.x

Schittny, A., J. Huwyler, and M. Puchkov (2020): *Mechanisms of increased bioavailability through amorphous solid dispersions: A review.* Drug Delivery, 27, pp. 110-127. DOI: 10.1080/10717544.2019.1704940

Scoutaris, N., K. Vithani, I. Slipper, B. Chowdhry, and D. Douroumis (2014): *SEM/EDX and confocal raman microscopy as complementary tools for the characterization of pharmaceutical tablets.* International Journal of Pharmaceutics, 470, pp. 88-98. DOI: 10.1016/j.ijpharm.2014.05.007

Sekiguchi, K., and N. Obi (1961): *Studies on absorption of eutectic mixture. I. A comparison of the behavior of eutectic mixture of sulfathiazole and that of ordinary sulfathiazole in man.* Chemical and Pharmaceutical Bulletin, 9, pp. 866-872. DOI: 10.1248/cpb.9.866

Serajuddin, A. T. (1999): *Solid dispersion of poorly water-soluble drugs: Early promises, subsequent problems, and recent breakthroughs.* Journal of Pharmaceutical Sciences, 10, pp. 1058-1066. DOI: 10.1021/js9804031

Sinclair, W., M. Leane, G. Clarke, A. Dennis, M. Tobyn, and P. Timmins (2011): *Physical stability and recrystallization kinetics of amorphous ibipinabant drug product by fourier transform raman spectroscopy.* Journal of Pharmaceutical Sciences, 100, pp. 4687-4699. DOI: 10.1002/jps.22658

Singh, H. D., S. Roychowdhury, P. Verma, and V. Bhandari (2012): *A review on recent advances of enteric coating.* IOSR Journal of Pharmacy, 2, pp. 5-11. e-ISSN: 2250-3013

Sjökvist, Eva, Christer Nyström, Maggie Aldén, and Ninus Caram-Lelham (1992): *Physicochemical aspects of drug release. XIV. The effects of some ionic and non-ionic surfactants on properties of a sparingly soluble drug in solid dispersions.* International Journal of Pharmaceutics, 79, pp. 123-133. DOI: 10.1016/0378-5173(92)90103-9

Srinarong, P., H. de Waard, H. W. Frijlink, and W. L. Hinrichs (2011): *Improved dissolution behavior of lipophilic drugs by solid dispersions: The production process as starting point for formulation considerations.* Expert Opinion on Drug Delivery, 8, pp. 1121-1140. DOI: 10.1517/17425247.2011.598147

Stegemann, S., F. Leveiller, D. Franchi, H. de Jong, and H. Linden (2007): *When poor solubility becomes an issue: From early stage to proof of concept.* European Journal of Pharmaceutical Sciences, 31, pp. 249-261. DOI: 10.1016/j.ejps.2007.05.110

Stillhart, C., D. Durr, and M. Kuentz (2014): *Toward an improved understanding of the precipitation behavior of weakly basic drugs from oral lipid-based formulations.* Journal of Pharmaceutical Sciences, 103, pp. 1194-1203. DOI: 10.1002/jps.23892

Stivarga 40 mg Filmtabletten Gebrauchsinformation (2019): *Information für Anwender.* Bayer AG, Leverkusen, Germany.

Stivarga product monograph (2020): *Part I: Health professional information.* Bayer Inc., Canada. Link: www.bayer.ca/omr/online/stivarga-pm-en.pdf [last accessed: 2020-09-04].

Strumberg, D., M. E. Scheulen, B. Schultheis, H. Richly, A. Frost, M. Buchert, O. Christensen, M. Jeffers, R. Heinig, O. Boix, and K. Mross (2012): *Regorafenib (bay 73-4506) in advanced colorectal cancer: A phase I study.* British Journal of Cancer, 106, pp. 1722-1727. DOI: 10.1038/bjc.2012.153

Sugawara, M., S. Kadomura, X. He, Y. Takekuma, N. Kohri, and K. Miyazaki (2005): *The use of an in vitro dissolution and absorption system to evaluate oral absorption of two weak bases in pH-independent controlled-release formulations.* European Journal of Pharmaceutical Sciences, 26, pp. 1-8. DOI: 10.1016/j.ejps.2005.02.017

Sun, D. D., and P. I. Lee (2013): *Evolution of supersaturation of amorphous pharmaceuticals: The effect of rate of supersaturation generation.* Molecular Pharmaceutics, 10, pp. 4330-4346. DOI: 10.1021/mp400439q

Sun, D. D., and P. I. Lee (2015a): *Evolution of supersaturation of amorphous pharmaceuticals: Nonlinear rate of supersaturation generation regulated by matrix diffusion.* Molecular Pharmaceutics, 12, pp. 1203-1215. DOI: 10.1021/mp500711c

Sun, D. D., and P. I. Lee (2015b): *Haste makes waste: The interplay between dissolution and precipitation of supersaturating formulations.* The AAPS Journal, 17, pp. 1317-1326. DOI: 10.1208/s12248-015-9825-6

Sun, D. D., and P. I. Lee (2015c): *Probing the mechanisms of drug release from amorphous solid dispersions in medium-soluble and medium-insoluble carriers.* Journal of Controlled Release, 211, pp. 85-93. DOI: 10.1016/j.jconrel.2015.06.004

Sun, M. Y., S. X. Wu, X. B. Zhou, J. M. Gu, and X. R. Hu (2016): *Comparison of the crystal structures of the potent anticancer and anti-angiogenic agent regorafenib and its monohydrate.* Acta Crystallographica Section C, 72, pp. 291-296. DOI: 10.1107/S2053229616003727

Surwase, S. A., L. Itkonen, J. Aaltonen, D. Saville, T. Rades, L. Peltonen, and C. J. Strachan (2015): *Polymer incorporation method affects the physical stability of amorphous indomethacin in aqueous suspension.* European Journal of Pharmaceutics and Biopharmaceutics, 96, pp. 32-43. DOI: 10.1016/j.ejpb.2015.06.005

Suzuki, T., and H. Nakagami (1998): *Effect of crystallinity of microcrystalline cellulose on the compactability and dissolution of tablets.* European Journal of Pharmaceutics and Biopharmaceutics, 47, pp. 225-230. DOI: 10.1016/S0939-6411(98)00102-7

Svergun, D. I, and M. H. J. Koch (2003): *Small-angle scattering studies of biological macromolecules in solution.* Reports on Progress in Physics, 66, pp. 1735-1782. DOI: 10.1088/0034-4885/66/10/R05

Taevernier, L., E. Wynendaele, M. D'Hondt, and B. De Spiegeleer (2015): *Analytical quality-by-design approach for sample treatment of bsa-containing solutions.* Journal of Pharmaceutical Analysis, 5, pp. 27-32. DOI: 10.1016/j.jpha.2014.06.001

Takano, R., M. Kataoka, and S. Yamashita (2012): *Integrating drug permeability with dissolution profile to develop IVIVC.* Biopharmaceutics & Drug Disposition, 33, pp. 354-365. DOI: 10.1002/bdd.1792

Tanaka, Y., M. Sugihara, A. Kawakami, S. Imai, T. Itou, H. Murase, K. Saiki, S. Kasaoka, and H. Yoshikawa (2017): *In vivo analysis of supersaturation/precipitation/absorption behavior after oral administration of pioglitazone hydrochloride salt; determinant site of oral absorption.* European Journal of Pharmaceutical Sciences, 106, pp. 431-438. DOI: 10.1016/j.ejps.2017.06.011

Tanno, F. K., S. Sakuma, Y. Masaoka, M. Kataoka, T. Kozaki, R. Kamaguchi, Y. Ikeda, H. Kokubo, and S. Yamashita (2008): *Site-specific drug delivery to the middle region of the small intestine by application of enteric coating with hypromellose acetate succinate (hpmcas).* Journal of Pharmaceutical Sciences, 97, pp. 2665-2679. DOI: 10.1002/jps.21172

Taylor, L. S., and G. G. Z. Zhang (2016): *Physical chemistry of supersaturated solutions and implications for oral absorption.* Advanced Drug Delivery Reviews, 101, pp. 122-142. DOI: 10.1016/j.addr.2016.03.006

Teckoe, J., T. Mascaro, T. P. Farrell, and A. R. Rajabi-Siahboomi (2013): *Process optimization of a novel immediate release film coating system using qbd principles.* AAPS PharmSciTech, 14, pp. 531-540. DOI: 10.1208/s12249-013-9935-3

Thommes, M., D. R. Ely, M. T. Carvajal, and R. Pinal (2011): *Improvement of the dissolution rate of poorly soluble drugs by solid crystal suspensions.* Molecular Pharmaceutics, 8, pp. 727-735. DOI: 10.1021/mp1003493

Tres, F., M. M. Posada, S. D. Hall, M. A. Mohutsky, and L. S. Taylor (2018): *Mechanistic understanding of the phase behavior of supersaturated solutions of poorly water-soluble drugs.* International Journal of Pharmaceutics, 543, pp. 29-37. DOI: 10.1016/j.ijpharm.2018.03.038

Tsume, Y., N. Igawa, A. J. Drelich, G. E. Amidon, and G. L. Amidon (2018): *The combination of gis and biphasic to better predict in vivo dissolution of BCS class IIb drugs, ketoconazole and raloxifene.* Journal of Pharmaceutical Sciences, 107, pp. 307-316. DOI: 10.1016/j.xphs.2017.09.002

Ueda, H., Y. Ida, K. Kadota, and Y. Tozuka (2014): *Raman mapping for kinetic analysis of crystallization of amorphous drug based on distributional images.* International Journal of Pharmaceutics, 462, pp. 115-122. DOI: 10.1016/j.ijpharm.2013.12.025

Ueda, K., K. Higashi, and K. Moribe (2017): *Direct NMR monitoring of phase separation behavior of highly supersaturated nifedipine solution stabilized with hypromellose derivatives.* Molecular Pharmaceutics, 14, pp. 2314-2322. DOI: 10.1021/acs.molpharmaceut.7b00178

Ueda, K., K. Higashi, and K. Moribe (2019): *Mechanistic elucidation of formation of drug-rich amorphous nanodroplets by dissolution of the solid dispersion formulation.* International Journal of Pharmaceutics, 561, pp. 82-92. DOI: 10.1016/j.ijpharm.2019.02.034

Vajna, B., H. Pataki, Z. Nagy, I. Farkas, and G. Marosi (2011): *Characterization of melt extruded and conventional isoptin formulations using raman chemical imaging and chemometrics.* International Journal of Pharmaceutics, 419, pp. 107-113. DOI: 10.1016/j.ijpharm.2011.07.023

Van Den Abeele, J., J. Brouwers, R. Mattheus, J. Tack, and P. Augustijns (2016): *Gastrointestinal behavior of weakly acidic BCS class II drugs in man-case study of diclofenac potassium.* Journal of Pharmaceutical Sciences, 105, pp. 687-696. DOI: 10.1002/jps.24647

Van Eerdenbrugh, B., S. Raina, Y. L. Hsieh, P. Augustijns, and L. S. Taylor (2014): *Classification of the crystallization behavior of amorphous active pharmaceutical ingredients in aqueous environments.* Pharmaceutical Research, 31, pp. 969-982. DOI: 10.1007/s11095-013-1216-z

Vardakou, M., A. Mercuri, S. A. Barker, D. Q. Craig, R. M. Faulks, and M. S. Wickham (2011): *Achieving antral grinding forces in biorelevant in vitro models: Comparing the USP dissolution apparatus II and the dynamic gastric model with human in vivo data.* AAPS PharmSciTech, 12, pp. 620-626. DOI: 10.1208/s12249-011-9616-z

Vasconcelos, T., S. Marques, J. das Neves, and B. Sarmento (2016): *Amorphous solid dispersions: Rational selection of a manufacturing process.* Advanced Drug Delivery Reviews, 100, pp. 85-101. DOI: 10.1016/j.addr.2016.01.012

Versantvoort, C. H. M., E. van de Kamp, and C. J. M. Rompelberg (2004): *RIVM report 320102002/2004. Development and applicability of an in vitro digestion model in assessing the bioaccessibility of contaminants from food.* Inspectorate for Health Protection, Netherlands.

Vo, C. L., C. Park, and B. J. Lee (2013): *Current trends and future perspectives of solid dispersions containing poorly water-soluble drugs.* European Journal of Pharmaceutics and Biopharmaceutics, 85, pp. 799-813. DOI: 10.1016/j.ejpb.2013.09.007

Wanapun, D., U. S. Kestur, D. J. Kissick, G. J. Simpson, and L. S. Taylor (2010): *Selective detection and quantitation of organicmolecule crystallization by second harmonic generation microscopy.* Analytical Chemistry, 82, pp. 5425-5432. DOI: 10.1021/ac100564f

Wang, S., C. Liu, Y. Chen, Z. Zhang, A. Zhu, and F. Qian (2018a): *A high-sensitivity HPLC-ELSD method for hpmc-as quantification and its application in elucidating the release mechanism of hpmc-as based amorphous solid dispersions.* European Journal of Pharmaceutical Sciences, 122, pp. 303-310. DOI: 10.1016/j.ejps.2018.07.007

Wang, S., C. Liu, Y. Chen, A. D. Zhu, and F. Qian (2018b): *Aggregation of hydroxypropyl methylcellulose acetate succinate under its dissolving pH and the impact on drug supersaturation.* Molecular Pharmaceutics, 15, pp. 4643-4653. DOI: 10.1021/acs.molpharmaceut.8b00633

Warren, B. E. (1990): "X-ray diffraction." Series *Addison-wesley series in metallurgy and materials engineering*, New York, USA, Dover Publications, Addison-Wesley.

Warren, D. B., H. Benameur, C. J. Porter, and C. W. Pouton (2010): *Using polymeric precipitation inhibitors to improve the absorption of poorly water-soluble drugs: A mechanistic basis for utility.* Journal of Drug Targeting, 18, pp. 704-731. DOI: 10.3109/1061186X.2010.525652

Wilson, C. G., and P. J. Crowley (2011): "Controlled release in oral drug delivery." Edition 1, Series *Advances in delivery science and technology*, Springer US.

Wright, A. K., and M. R. Thompson (1975): *Hydrodynamic structure of bovine serum albumin determined by transient electric birefringence.* Biophysical Journal, 15, pp. 137-141. DOI: 10.1016/S0006-3495(75)85797-3

Xie, F., S. Ji, and Z. Cheng (2015): *In vitro dissolution similarity factor (f2) and in vivo bioequivalence criteria, how and when do they match? Using a BCS class II drug as a simulation example.* European Journal of Pharmaceutical Sciences, 66, pp. 163-172. DOI: 10.1016/j.ejps.2014.10.002

Xie, T., and L. S. Taylor (2016a): *Dissolution performance of high drug loading celecoxib amorphous solid dispersions formulated with polymer combinations.* Pharmaceutical Research, 33, pp. 739-750. DOI: 10.1007/s11095-015-1823-y

Xie, T., and L. S. Taylor (2016b): *Improved release of celecoxib from high drug loading amorphous solid dispersions formulated with polyacrylic acid and cellulose derivatives.* Molecular Pharmaceutics, 13, pp. 873-884. DOI: 10.1021/acs.molpharmaceut.5b00798

Xie, T., W. Gao, and L. S. Taylor (2017): *Impact of eudragit EPO and hydroxypropyl methylcellulose on drug release rate, supersaturation, precipitation outcome and redissolution rate of indomethacin amorphous solid dispersions.* International Journal of Pharmaceutics, 531, pp. 313-323. DOI: 10.1016/j.ijpharm.2017.08.099

Xu, S., and W. G. Dai (2013): *Drug precipitation inhibitors in supersaturable formulations.* International Journal of Pharmaceutics, 453, pp. 36-43. DOI: 10.1016/j.ijpharm.2013.05.013

Yamashita, S., A. Fukunishi., H. Higashino, M. Kataoka, and K. Wada (2017): *Design of supersaturable formulation of telmisartan with pH modifier: In vitro study on dissolution and precipitation.* Journal of Pharmaceutical Investigation. DOI: 10.1007/s40005-017-0310-3

Zhang, J., R. Han, W. Chen, W. Zhang, Y. Li, Y. Ji, L. Chen, H. Pan, X. Yang, W. Pan, and D. Ouyang (2018): *Analysis of the literature and patents on solid dispersions from 1980 to 2015.* Molecules, 23, pp. 1-19. DOI: 10.3390/molecules23071697

Zhang, W., S. S. Hate, D. J. Russell, H. H. Hou, and K. Nagapudi (2019): *Impact of surfactant and surfactant-polymer interaction on desupersaturation of clotrimazole.* Journal of Pharmaceutical Sciences, 108, pp. 3262-3271. DOI: 10.1016/j.xphs.2019.05.035

Zhao, Y., T. Xin, T. Ye, X. Yang, and W. Pan (2014): *Solid dispersion in the development of a nimodipine delayed-release tablet formulation.* Asian Journal of Pharmaceutical Sciences, 9, pp. 35-41. DOI: 10.1016/j.ajps.2013.11.006

Zhu, Q., S. J. Toth, G. J. Simpson, H. Y. Hsu, L. S. Taylor, and M. T. Harris (2013): *Crystallization and dissolution behavior of naproxen/polyethylene glycol solid dispersions.* Journal of Physical Chemistry B, 117, pp. 1494-1500. DOI: 10.1021/jp3106716

Zopf, D., I. Fichtner, A. Bhargava, W. Steinke, K. H. Thierauch, K. Diefenbach, S. Wilhelm, F. T. Hafner, and M. Gerisch (2016): *Pharmacologic activity and pharmacokinetics of metabolites of regorafenib in preclinical models.* Cancer Medicine, 5, pp. 3176-3185. DOI: 10.1002/cam4.883

# 8 Appendix

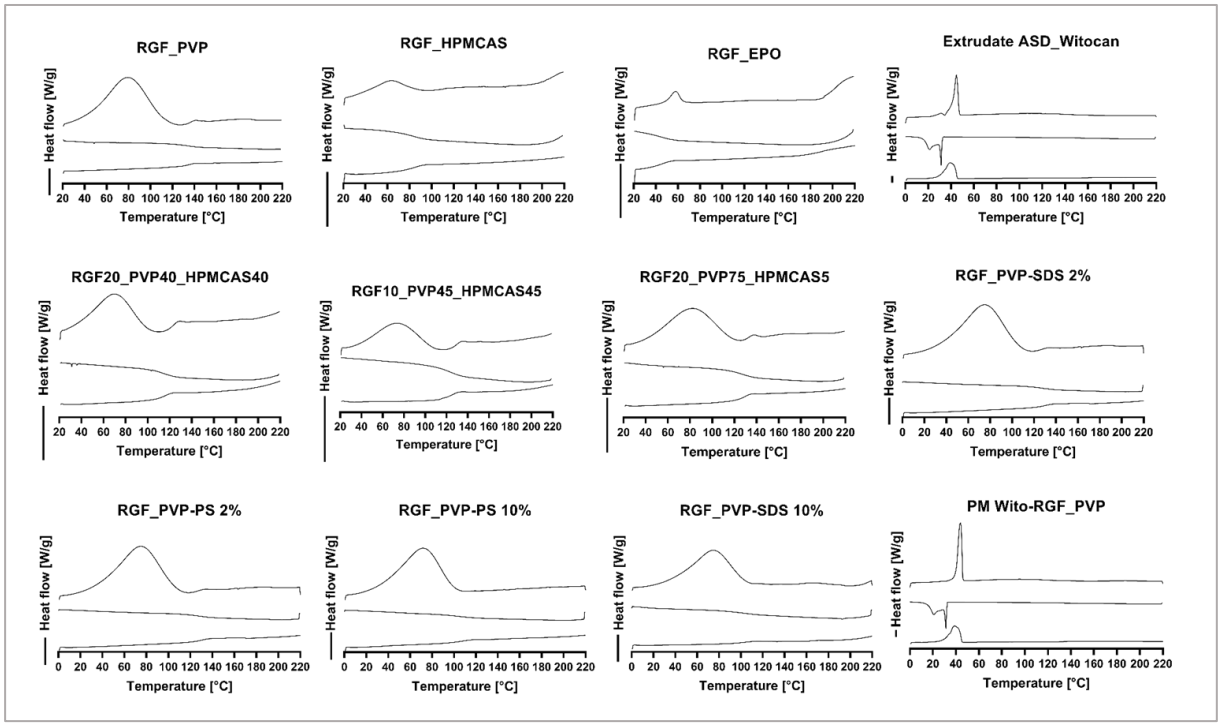


**Figure 78. DSC curves of all prepared formulations. From top to bottom 1st heating, cooling and 2nd heating are shown. Heating rate was set to 5 K/min. The scale bar on the left of each graph indicates 0.2 W/g.**

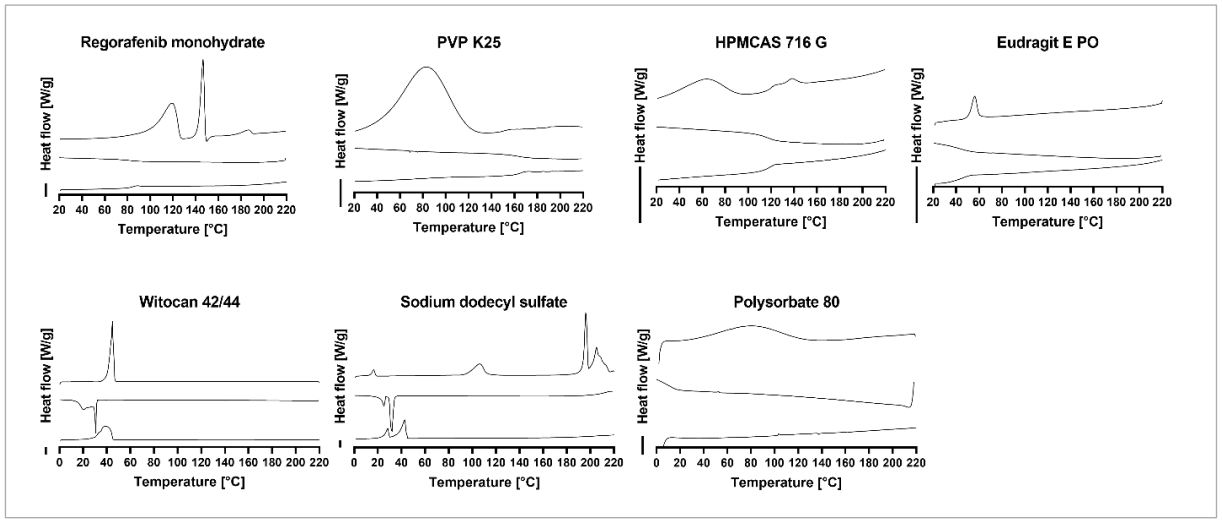


**Figure 79. DSC curves of all materials used for RGF formulations. From top to bottom 1st heating, cooling and 2nd heating are shown. Heating rate was set to 5 K/min. The scale bar on the left of each graph indicates 0.2 W/g.**

**Table 30. Reported thermoanalytical properties of different RGF modifications by *Bayer*.**

| RGF Modification | T [°C]<br>*ΔH [J/g]* | T [°C]<br>*ΔH [J/g]* | T [°C]<br>*ΔH [J/g]* |
|---|---|---|---|
| I, case a | - | - | 206<br>*92* |
| I, case b | - | - | 186<br>*77* |
| II | - | 181<br>*78* | - |
| III | - | 141<br>+ transition to Mod. I | 207 |
| MH, case a | ca. 109 | - | 208 |
| MH, case b | ca. 77 | ca. 144<br>+ transition to Mod. I | 209 |

Thermoanalytical properties of different RGF polymorphs (reported internally from *Bayer*):
Depending on the heating rate in DSC experiments and the preparation method of the investigated modifications, differences in DSC melting events are stated. RGF MH is reported to undergo one of two different transitions after monohydrate release, either to RGF Mod. I or RGF Mod III. With the first possibility (case a), after water release, RGF is present in the amorphous state and crystallizes directly into Mod. I. With the second possibility (case b), a solid-liquid-solid transformation to Mod. III was observed after water release.
In addition, for RGF Mod. I two different melting behaviors were described, case a and case b. The RGF MH batch used in this study always followed RGF MH case b, by means of water release and subsequent melting as Mod. III, solid-liquid-solid transformation, and finally melting to some extent as Mod. I case a. Deviating from the data reported from *Bayer*, the final melting after monohydrate release occurred at the temperature of Mod. I case b, a depressed melting temperature of RGF Mod. I case a (see Figure 79).

Table 31. DSC results of investigated ASD precipitates and references. Onset temperatures are given.

| Precipitate | Temperature [°C] | Enthalpy [J/g] | Explanation |
|---|---|---|---|
| RGF_PVP / FaSSIF | 134 | | glass transition PVP |
| | 175 | 33.6 | melting |
| RGF_HPMCAS / FaSSIF | 168 | 18.8 | melting, two species |
| | 192 | 15.6 | |
| RGF_PVP + 10% HPMCAS / FaSSIF | 146 | -18.0 | two step crystallization |
| | 168 | 11.3 | melting |
| | 189 | 38.9 | melting |
| RGF_PVP / FaSSGF | 139 | 8.9 | melting, two species |
| | 155 | 14.1 | |
| | 169 | -8.3 | crystallization |
| | 183.5 | 11.3 | melting |
| FaSSIF dried | 106 – 165 | 45.3 | bubbling/boiling |
| | 176 | 23.3 | melting |
| | 195 | 4.0 | melting |
| PVP K25 | 145 | | glass transition |

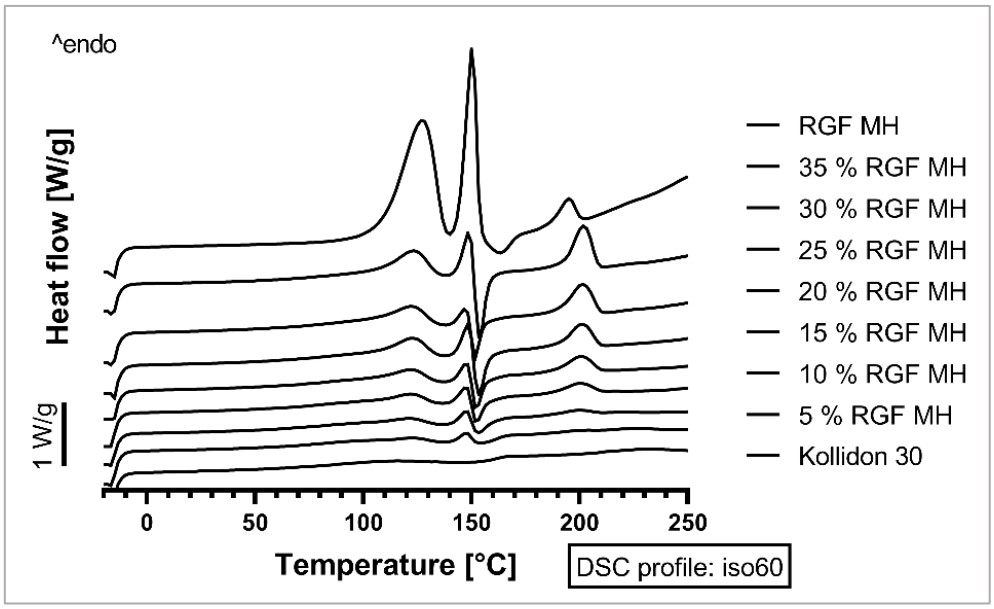


**Figure 80. DSC limit of detection for RGF MH in PVP K30 (Kollidon 30) physical mixtures. RGF MH content in the physical mixtures is given in % (m/m).**

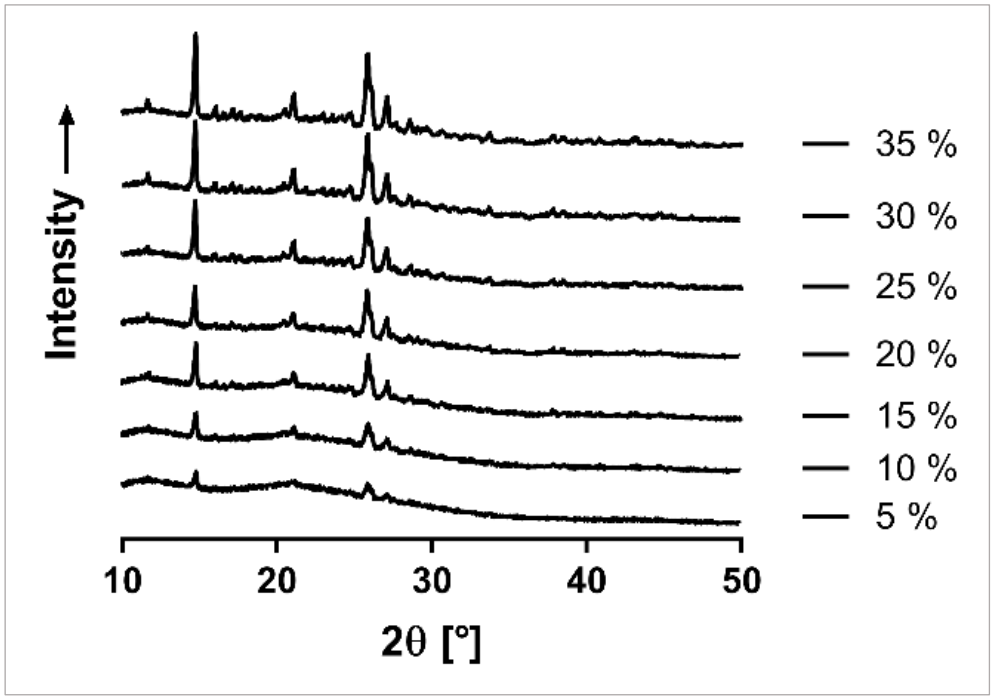


**Figure 81. XRPD limit of detection for RGF MH in PVP K30 physical mixtures. RGF MH content in the physical mixtures is given in % (m/m).**

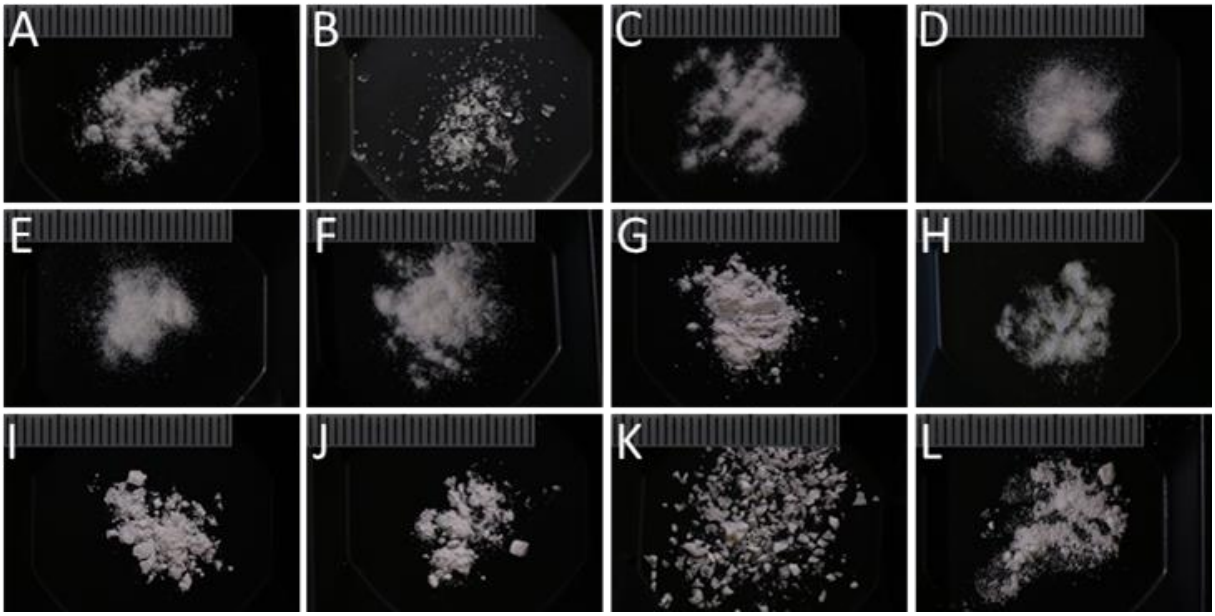


**Figure 82. Images of API, prepared ASD formulations and precipitates: RGF_PVP (A), RGF_HPMCAS (B), RGF_EPO (C), RGF20_PVP40_HPMCAS40 (D), RGF10_PVP45_HPMCAS45 (E), RGF20_PVP75_HPMCAS5 (F), RGF Mod. I (G), RGF MH (H), Prec. RGF_PVP$_{FaSSIF}$ (I), Prec. RGF_PVP+HPMCAS10%$_{FaSSIF}$ (J), Prec. RGF_HPMCAS$_{FaSSIF}$ (K), Prec. RGF_PVP$_{FaSSGF}$ (L). The scale bar is in steps of 1 mm.**

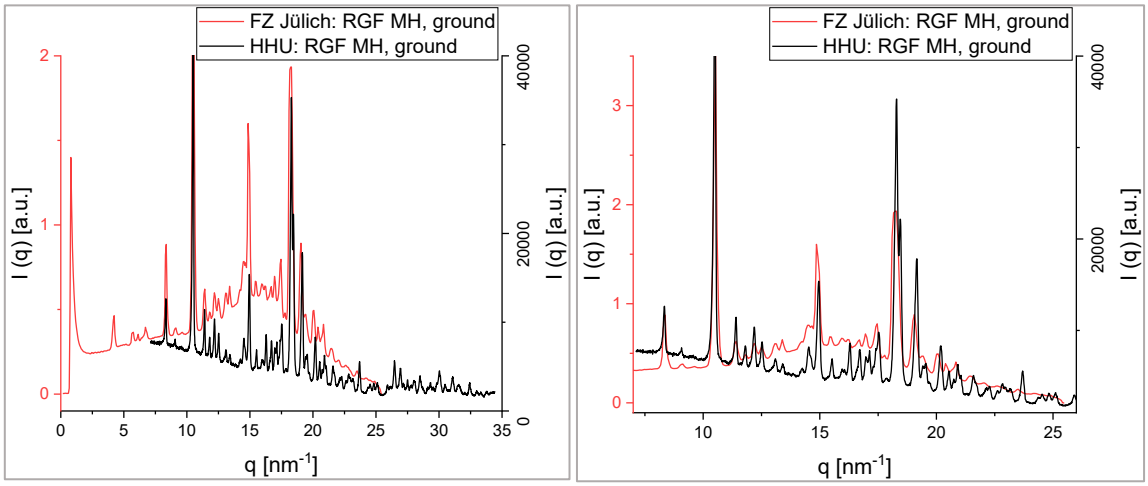


**Figure 83. Comparison of RGF MH X-ray diffraction spectra, obtained at HHU and FZ Jülich. A full overview (left) and overlapping q values (right) are shown.**

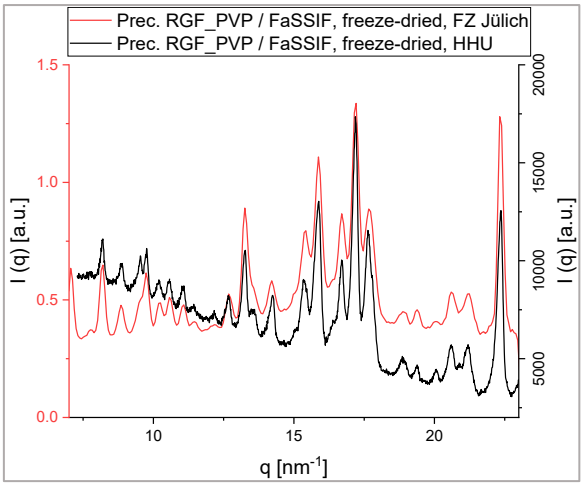


**Figure 84. Comparison of X-ray diffraction spectra of the freeze-dried precipitate from RGF_PVP dissolution in FaSSIF, obtained at HHU and at FZ Jülich. Overlapping *q* values are shown.**

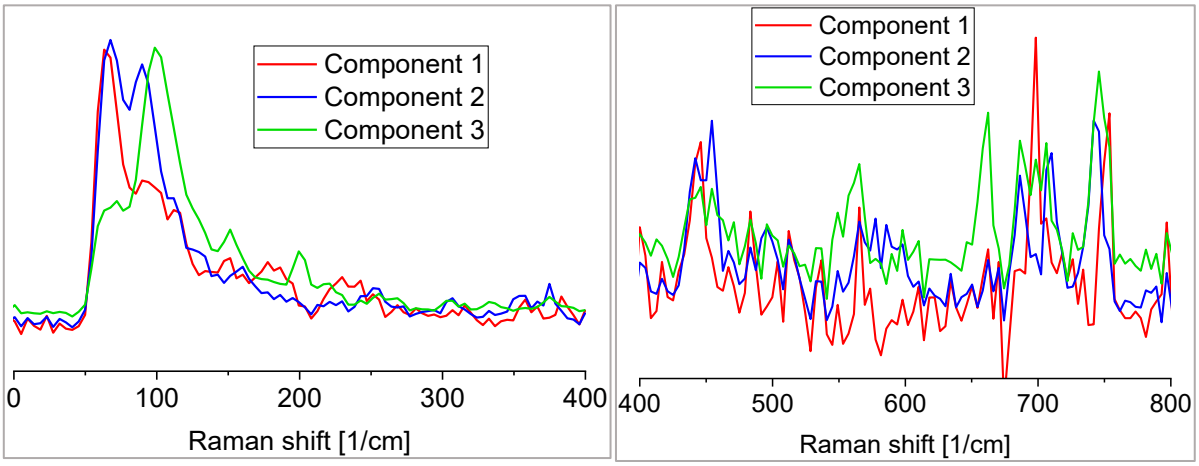


Figure 85. Raman spectra of color-coded components in Raman mapping of particle 3 in Figure 57.

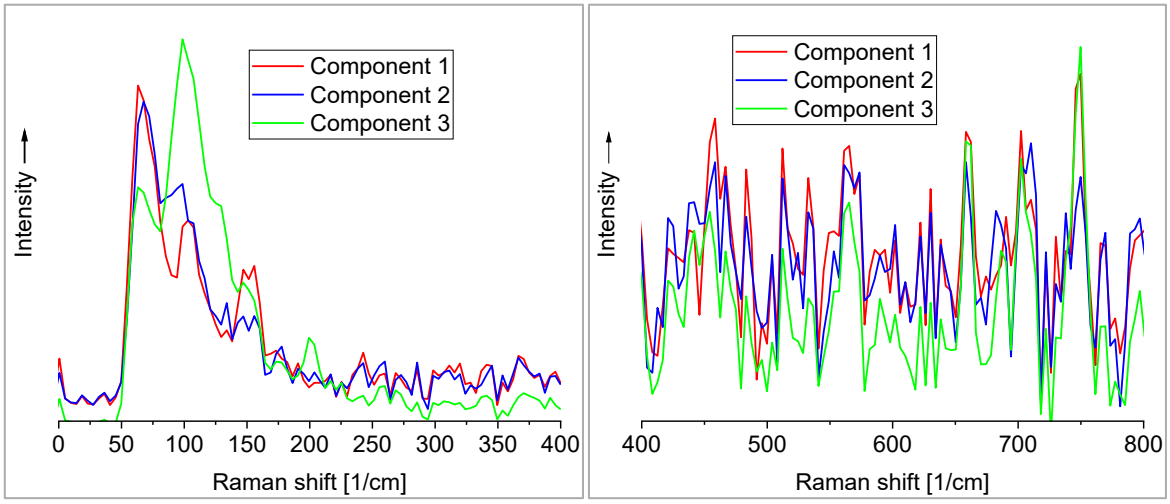


Figure 86. Single component spectra of Raman mapping of RGF_HPMCAs in FaSSIF after 48h, see Section 3.5.3.2.

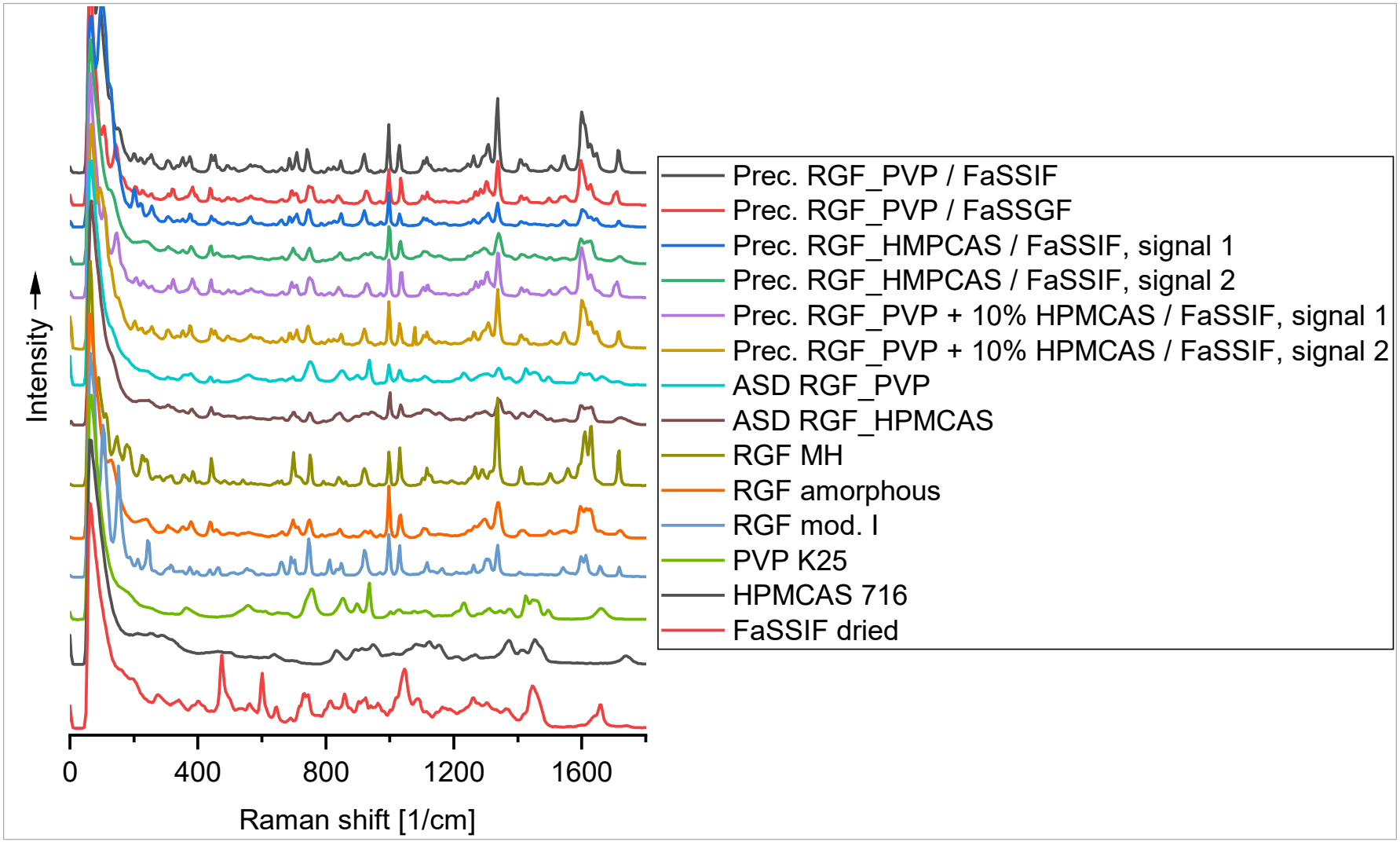


Figure 87. CRM spectra of freeze-dried RGF precipitates and reference substances.

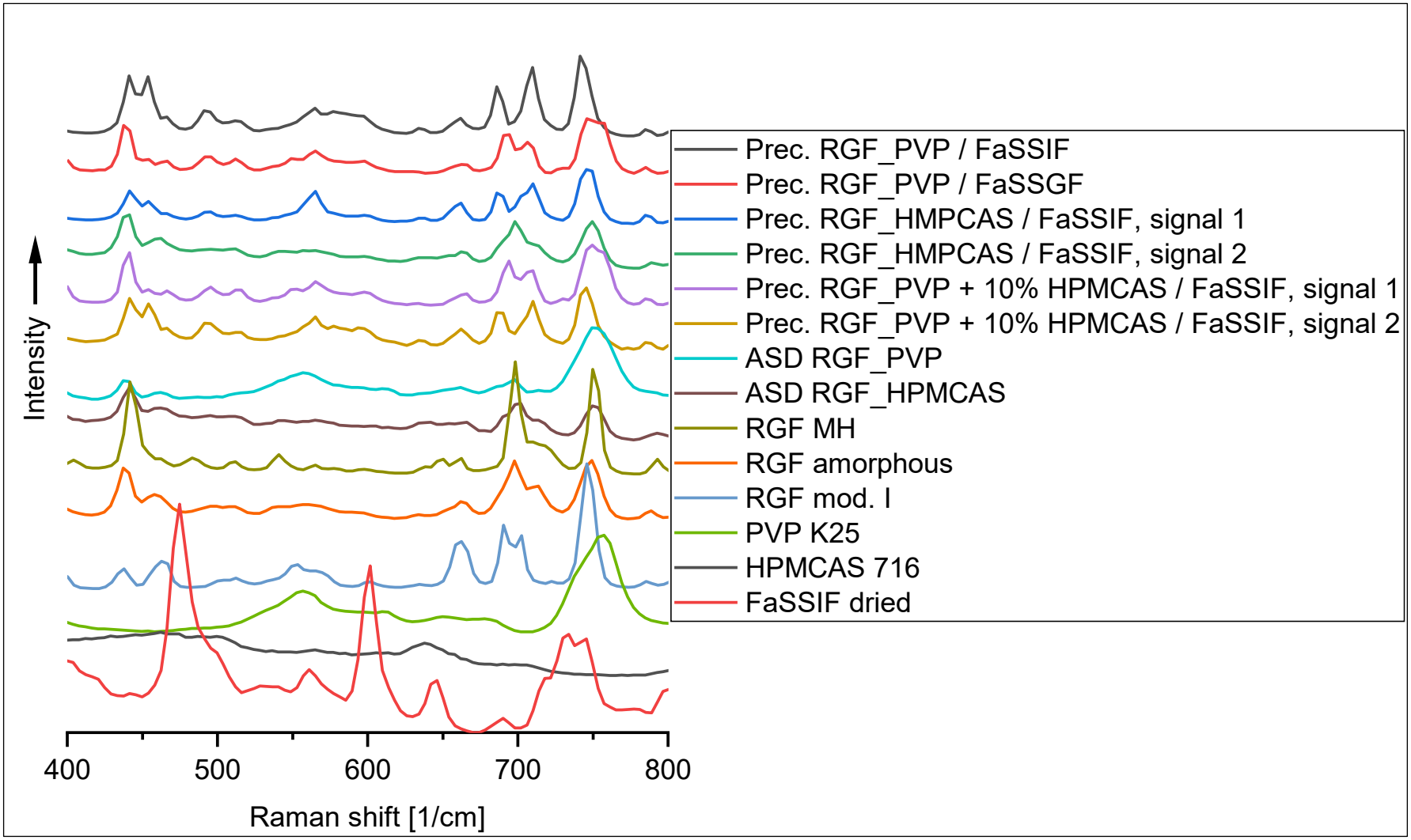


Figure 88. CRM spectra at region of interest of freeze-dried RGF precipitates and reference substances.

**Table 32. Process parameters during HPMCAS coating of *Stivarga* tablets.**

| Process time [min] | Sprayed mass [g] | Spay rate [g/min] | Air flow [$Nm^3/h$] | Inlet air temperature [°C] | Outlet air temperature [°C] | Spraying pressure [bar] | Forming pressure [bar] | Drum speed [rpm] | Comment |
|---|---|---|---|---|---|---|---|---|---|
| 0-4 | - | - | 94 | 52.5 | 34.6 | - | - | 5 | Warm-up |
| 5 | 158 | 31.6 | 161 | 37.2 | 33.7 | 0.5 | 0.3 | 19 | Spaying start |
| 10 | 234 | 15.2 | 160 | 39.7 | 34.9 | 0.5 | 0.3 | 19 | Decrease pump rate |
| 22 | 418 | 15.3 | 160 | 40.0 | 36.0 | 0.5 | 0.3 | 19 | Decrease pump rate |
| 30 | 532 | 12.6 | 160 | 40.3 | 36.5 | 0.5 | 0.3 | 19 | |
| 40 | 645.5 | 11.4 | 159 | 40.0 | 36.6 | 0.5 | 0.3 | 19 | |
| 53 | 789 | 12.0 | 160 | 39.9 | 36.6 | 0.5 | 0.3 | 19 | Spraying stop |
| 0-10 | | | 151 | 37.1 | 37.9 | - | - | 5 | Drying |
| 0-10 | | | 150 | 31.8 | - | - | - | 5 | Cooling |

**Table 33. Parameters of *in-vivo* PK study for RGF_PVP study group**

| Parameter | Rat A | Rat B | Rat C | Rat D | Mean (arithmetic) | SD | RSD [%] |
|---|---|---|---|---|---|---|---|
| Bodyweight [g] | 271 | 266 | 246 | 269 | 263 | 11.5 | 4.4 |
| RGF dose equivalent [mg/kg] | 50 | 50 | 50 | 50 | | | |
| $AUC_{total}$ [µg·h/L] | 165826.5 | 154861.7 | 88573.7 | 257922.2 | 166796.0 | 69680.4 | 41.8 |
| $AUC_{0-24h}$ [µg·h/L] | 149020.9 | 119811.5 | 76687.9 | 218243.6 | 140941.0 | 59486.4 | 42.2 |
| $AUC_{0-48h}$ [µg·h/L] | 164531.9 | 147814.6 | 87250.3 | 253696.1 | 163323.2 | 68790.3 | 42.1 |
| $AUC_{0-7h}$ [µg·h/L] | 71612.7 | 51883.5 | 37015.5 | 92987.7 | 63374.8 | 24301.3 | 38.3 |
| $AUC_{7h-\infty}$ [µg·h/L] | 94213.8 | 102978.2 | 51558.2 | 164934.5 | 103421.2 | 46756.9 | 45.2 |
| $c_{max}$ [µg/L] | 13429.0 | 10610.0 | 7717.0 | 17631.0 | 12346.8 | 4224.8 | 34.2 |
| $t_{max}$ [h] | 2 | 2 | 2 | 3 | 2.25 | 0.50 | 22.2 |
| $t_{1/2}$ [h] | 6.70 | 10.50 | 7.84 | 8.13 | 8.29 | 1.60 | 19.2 |
| $k_e$ [1/h] | 0.1034 | 0.066 | 0.0884 | 0.0853 | 0.08578 | 0.02 | 17.9 |

**Table 34. Parameters of *in-vivo* PK study for the RGF_PVP + 10% HPMCAS study group.**

| Parameter | Rat A | Rat B | Rat C | Rat D | Mean (arithmetic) | SD | RSD [%] |
|---|---|---|---|---|---|---|---|
| Bodyweight [g] | 279 | 269 | 263 | 260 | 267.8 | 8.4 | 3.1 |
| RGF dose equivalent [mg/kg] | 50 | 50 | 50 | 50 | | | |
| $AUC_{total}$ [µg·h/L] | 403362.4 | 290432.7 | 120128.1 | 151989.6 | 241478.2 | 130814.2 | 54.2 |
| $AUC_{0-24h}$ [µg·h/L] | 306244.4 | 234356.8 | 89090.9 | 133071.4 | 190690.9 | 98152.7 | 51.5 |
| $AUC_{0-48h}$ [µg·h/L] | 385291.3 | 281356.5 | 112629.0 | 149973.2 | 232312.5 | 125049.0 | 53.8 |
| $AUC_{0-7h}$ [µg·h/L] | 123757.1 | 102557.3 | 35319.1 | 59899.0 | 80383.1 | 40097.2 | 49.9 |
| $AUC_{7h-\infty}$ [µg·h/L] | 279605.3 | 187875.3 | 84809.0 | 92090.7 | 161095.1 | 91911.2 | 57.1 |
| $c_{max}$ [µg/L] | 22722.0 | 18508.0 | 6450.0 | 11589.0 | 14817.3 | 7223.6 | 48.8 |
| $t_{max}$ [h] | 2 | 3 | 3 | 2 | 2.5 | 0.6 | 23.1 |
| $t_{1/2}$ [h] | 11.02 | 9.42 | 11.69 | 7.75 | 10.0 | 1.8 | 17.6 |
| $k_e$ [1/h] | 0.0629 | 0.0736 | 0.0593 | 0.0894 | 0.0713 | 0.0135 | 18.9 |

**Table 35. RGF plasma concentrations from *in-vivo* PK study for the RGF_PVP study group.**

| | RGF_PVP group | | | |
|---|---|---|---|---|
| Time after administration [h] | Rat A [µg/mL] | Rat B [µg/mL] | Rat C [µg/mL] | Rat D [µg/mL] |
| 0 | no value | no value | no value | no value |
| 0.083 | 39.4 | 39.3 | 31.6 | 14.7 |
| 0.25 | 829.7 | 306.4 | 563.3 | 27.9 |
| 0.5 | 3658.3 | 1387.8 | 2626.6 | 4199.4 |
| 1 | 9863.8 | 4622.6 | 5085.6 | 7086.1 |
| 2 | 13429.3 | 10610.0 | 7716.6 | 15022.3 |
| 3 | 13158.1 | 9942.1 | 6283.4 | 17630.9 |
| 5 | 10254.9 | 8090.3 | 5242.3 | 15817.6 |
| 7 | 9131.6 | 6268.2 | 4541.4 | 13104.7 |
| 24 | 1842.0 | 2352.8 | 992.5 | 3614.4 |
| 26 | 1462.0 | 2062.4 | 931.8 | 3205.2 |
| 48 | 133.9 | 465.1 | 117.0 | 360.5 |

**Table 36. RGF plasma concentrations from *in-vivo* PK study for RGF_PVP + 10% HPMCAS study group**

| | RGF_PVP + 10% HPMCAS group | | | |
|---|---|---|---|---|
| Time after administration [h] | Rat A [µg/mL] | Rat B [µg/mL] | Rat C [µg/mL] | Rat D [µg/mL] |
| 0 | no value | no value | no value | no value |
| 0.083 | 159.0 | 126.4 | 10.2 | 76.4 |
| 0.25 | 3343.2 | 1592.2 | 237.0 | 997.3 |
| 0.5 | 8375.3 | 5994.3 | 1219.1 | 4600.9 |
| 1 | 15278.7 | 11754.9 | 3391.0 | 8635.2 |
| 2 | 22721.9 | 16302.3 | 6422.7 | 11589.4 |
| 3 | 22683.9 | 18507.9 | 6450.1 | 10557.6 |
| 5 | 18280.8 | 16895.8 | 5565.2 | 7790.9 |
| 7 | 15373.2 | 13445.5 | 5069.2 | 8634.4 |
| 24 | 7138.6 | 3951.3 | 1807.7 | 1740.3 |
| 26 | 6208.7 | 3749.8 | 1633.3 | 1495.0 |
| 48 | 1136.7 | 668.0 | 444.7 | 180.3 |

# 9 Danksagung

Die vorliegende Arbeit entstand unter der Leitung von Herrn Prof. Dr. Breitkreutz und der Betreuung von Herrn Prof. Dr. Dr. h.c. Kleinebudde, Herrn Dr. Serno und Herrn Dr. Hoheisel im Rahmen meiner Tätigkeit als Doktorand bei der Firma INVITE GmbH in Leverkusen in Kooperation mit der Firma Bayer AG in Leverkusen, sowie als wissenschaftlicher Mitarbeiter am Institut für Pharmazeutische Technologie und Biopharmazie der Heinrich-Heine-Universität Düsseldorf.

Mein besonderer Dank gilt zunächst meinem Doktorvater Herrn Prof. Dr. Breitkreutz für die Aufnahme in seinen Arbeitskreis und die mir dadurch gegebene Möglichkeit, an einem aktuellen und spannenden Promotionsthema zu arbeiten. Ich möchte mich bei Ihnen für die gute Betreuung, die Unterstützung bei jeglichen Problemen und Fragen und dafür, dass Sie stets ein offenes Ohr hatten, ganz herzlich bedanken.
Herrn Prof. Dr. Kleinebudde danke ich für die Übernahme des Koreferats und die vielen hilfreichen Vorschläge und kritischen Fragen, die Sie mir während der vielen Fokus-Gruppen und Doktorandenseminare mitgegeben haben.
Beiden Professoren möchte ich für die Schaffung einer außerordentlich kollegialen Arbeitsatmosphäre am Institut und die Förderung der gemeinsamen zahlreichen Besuche internationaler Konferenzen danken.

Ich möchte Herrn Dr. Serno für die Bereitstellung des Themas durch Bayer und sein Feedback bei den regelmäßigen JF Treffen bedanken. Durch Ihre Unterstützung konnte ich bei Bayer Versuche durchführen, die einem Doktoranden sonst nicht zugänglich sind. Ganz besonders danke ich Ihnen für Ihr Vertrauen während des ersten Teils der Promotionszeit, als wegen vieler Methodenentwicklungen noch wenig „greifbar“ war.

Ein besonderer Dank geht an Herrn Dr. Schweiger und das ganze INVITE Team für die herzliche Aufnahme und gute Zusammenarbeit. Nicht zuletzt beim legendären Business Lauf.
Bei Herrn Dr. Werner Hoheisel möchte ich mich für die zahlreichen konstruktiven Diskussionen und Denkanstöße bedanken. Dein stetiges Nachbohren hat wesentlich zum Erfolg dieser Arbeit beigetragen.

Mit Herrn Dr. Björn Fischer verbrachte ich unzählige Stunden in seinem „Darkroom“ des Herren-WC an HPLC- und Raman-Messungen, wobei ich auch für die große Unterstützung bei den Messungen am konfokalen Ramanmikroskop in seiner Firma danken möchte. Vielen Dank auch an deine wettkampfqualifizierte Dartscheibe und deine Geduld bei Niederlagen.

Einen besonderen Dank möchte ich Herrn Prof. Dr. Stefan Egelhaaf und Herrn Dr. Florian Platten aussprechen. Eine große Bereicherung waren die vielen Diskussionen und deine mehrfachen Erklärungen für mich als SAXS/WAXS und ITC-Anfänger, die uns auch vier spannende Tage am Forschungszentrum Jülich beschert haben.

Vielen herzlichen Dank an Herrn Dr. Raphael Wiedey für seine vielen Ideen, seine Unterstützung in Praxis und Statistik, sowie schlussendlich das Korrekturlesen der Arbeit.

Die große Unterstützung bei der Einarbeitung durch Frau Dr. Yasmin Thabet war zu Beginn eine große Hilfe und hat mir den Einstieg in die Arbeit sehr erleichtert, vielen Dank dafür. Ebenso danke für die vielen Kletterausflüge.

Ich möchte Herrn Dr. Martin Dulle für die große Hilfsbereitschaft bei der Planung der SAXS/WAXS Messungen und deren unkomplizierte Durchführung mit anschließendem Support danken.

Für die Planung und Durchführung der Tierstudie bei Bayer möchte ich mich bei Herrn Dr. Jan Stampfuss bedanken. Danke auch dafür, dass ich bei der Studienvorbereitung am Tier anwesend sein durfte.

Ich danke Frau Dr. Anke Stroyer und Herrn Dr. Markus Albers für die Unterstützung und zahlreichen Erläuterungen, die schlussendlich zur Einreichung des Patents geführt haben.

Herrn Ataklti Himmelmann möchte ich für seine Unterstützung bei den organischen Lackierungsversuchen bei Bayer danken – ganz besonders seinem Optimismus trotz streikender Technik.

Bei Dorothee Eikeler, Andrea Michels und Karin Mathée möchte ich mich nicht nur für drei volle Ordner an DSC Ausdrucken bedanken, ebenfalls nicht nur für die unzähligen praktischen

Hilfestellungen bei den Freisetzungen. Ganz besonders jedoch für die vielen Gespräche und Aufmunterungen.

Herrn Dr. Klaus Knop gilt mein Dank für vielerlei Hilfestellungen und die freundlichen Hinweise, dass das Labor ein wenig Sauberkeit vertragen dürfe.

Meinen WPP-Studentinnen Frau Isra Atalla and Frau Pinar Bozkurt danke ich für die gute Zusammenarbeit und ihren Fleiß.

Für die zuverlässige und kreative Anfertigung von Spezialaufbauten und die Organisation von Aufträgen an die Feinmechanik danke ich Herrn Stefan Stich.

Mit Herrn Philipp Kiefer, Herrn Bastian Hahn und Herrn Marcel Kokott durfte ich lange Zeit zusammen ein Büro teilen, wir haben alle Phasen unserer Promotionsarbeiten gemeinsam erlebt. Vielen herzlichen Dank für eure Unterstützung, auch in nichtwissenschaftlichen Fragen und die unzähligen, unzähligen, unzähligen, … Diskussionen. Und was in einem Fotostudio passiert bleibt auch dort.

Ich danke ganz herzlich allen Kolleginnen und Kollegen des Instituts für die freundliche Aufnahme und die besondere Zeit, die ich mit Euch verbringen durfte. Den Institut-„BoyZ“ danke ich für zahlreiche FIFA Abende, Altstadtabende, Grillabende, Fahrradtouren und nicht zuletzt den legendären Holland-Trip. Den wackeren Helden des *MudMasters 2019* danke ich für die großartige Teamarbeit, die diese Matschschlacht für mich zu etwas ganz Besonderem gemacht haben.

Meiner Familie danke ich für den stetigen Zuspruch, ihren stetigen Rückhalt und ihr Vertrauen in mich. Und auch für all die Erinnerungen an Geburtstage oder Events, die wohl sonst vergessen worden wären.
Meiner Partnerin Carmen danke ich von ganzen Herzen, dass sie mit mir für diese Zeit nach Düsseldorf gekommen ist, auf vieles verzichtet hat, sowie für ihre fortwährende liebevolle Unterstützung und Geduld.

# 10 Eidesstattliche Erklärung

Ich versichere an Eides Statt, dass die vorliegende Dissertation von mir selbständig und ohne unzulässige fremde Hilfe unter Beachtung der „Grundsätze zur Sicherung guter wissenschaftlicher Praxis an der Heinrich-Heine-Universität Düsseldorf“ erstellt worden ist. Die vorliegende Dissertation wurde bisher bei keiner anderen Fakultät vorgelegt.

_____

Martin Günter Müller